Report No. UCB/SEMM-2018/05	Structural Engineering Mechanics and Materials
	Anchored Nonstructural Component Response to Seismic Loading – Shaking Table Tests Report By Tal Feinstein, Jack P. Moehle and Stephen A. Mahin
October 2018	Department of Civil and Environmental Engineering University of California, Berkeley

ANCHORED NONSTRUCTURAL COMPONENT RESPONSE TO SEISMIC LOADING – SHAKING TABLE TESTS REPORT

Tal Feinstein, Jack P. Moehle and Stephen A. Mahin

ABSTRACT

Research attention to nonstructural damage has been awakened in recent years, as performance-based earthquake engineering has advanced and loss estimations have shown that more than fifty percent of the damage following an earthquake is due to nonstructural components. Seismic codes are focused on life safety, for nonstructural design it mainly means preventing shifting or toppling of large components during a seismic event. The codes have one approach suggested to protect important components, that are required to operate after the earthquake, which includes amplifying the force demand on the component. This approach is good to protect the component from detaching from its origin place but doesn't necessarily help mitigating the response of the component during the seismic event. Some components may contain valuable content that could be damaged under a design level event or even at lower intensity ground motions, such as a medical freezer containing hazardous material or research samples.

Available methodologies for seismic design of nonstructural components anchorage are based on very simplistic equations. Using constant values for generalized sub-groups of components, together with a basic dynamic approach of spectral acceleration distribution throughout the structure height. Current design equations and variables are considered to lead to very conservative results, due to the simplicity and over-strength incorporated in anchorage design. Previous testing of nonstructural component anchorage has been performed without considering the contribution of the structural system of the component itself.

In order to deepen the understanding of the seismic loading of nonstructural components, shaking table tests were conducted with floor mounted components anchored to concrete and steel, using instrumented anchors. The shaking table was subjected to input motions based on several ground motions and floor accelerations based on numerical models of a few building types, including mid-rise structure, low-rise and an isolated low-rise structure. The input motion was based on real

recordings and broadband spectrum matching and included different excitation directions allowing the comparison of 1 vs 2 and 3 components of motion.

This report focuses on the components responses and anchor loads, comparing test results to results obtained using design equations and first principles. The goal of the tests is to identify key parameters that control the response of the components and evaluate the parameters that are used in current code provisions.

CONTENTS

LIST OF FIGURES

LIST OF TABLES

1 INTRODUCTION

1.1 OVERVIEW

Research of nonstructural components has mainly focused on life safety concerns. Code provisions for nonstructural lateral force design were introduced to help prevent shifting or toppling of nonstructural component during a seismic event. The anchorage design is generally based on seismic lateral force equations given in the different code provisions. The seismic design calculation considers the contribution of a few parameters, that are believed to be the controlling factors of the dynamic response of the nonstructural components. Different provisions adopted a similar set of key parameters with minor changes. However, the final equations that appear in the provisions vary a lot from one to the other. The common controlling factors include a location based seismic hazard, elevation in the structure, importance of the component and component specific properties. Some additional parameters are the ratio between the component's and the structure's periods and the components ductility. The code provisions provide an equivalent static load and don't specify guidelines to the direct calculation of the anchor forces. As a result, most calculations of the anchor forces are based on simple assumptions of symmetry in the force flow through the component. ASCE-7-10 (ASCE, 2013) does encourage to design the anchor to have ductile failure by introducing an overstrength factor Ω_0 that has to be added when a non-ductile failure might occur (Johnson et al., 2016).

Recent development in the lateral force equations for anchored components has focused on approximating floor acceleration (Miranda and Taghavi, 2005), and effects of inelastic structure behavior on the nonstructural demands (Ricardo et al. 2009). In addition, research on the dynamic effects of a brittle failure has been carried out, to evaluate the nature of the factor Ω_0 and its value (Johnson et al., 2017(b)). Most analyses and experiments are based on an idealized Single Degree Of Freedom (SDOF) system, based on a single mass located at the top of a column. Analytical models sometime incorporate a more complicated force displacement relation for the component, while maintaining the SDOF system (Anjafi, 2018).

Research on nonstructural component seismic response has been growing in recent years, as the methodology of performance-based earthquake engineering (PBEE) has become more popular. PBEE has shed a new light on the importance of nonstructural components for calculations of expected losses and downtime for a structure. losses to buildings from nonstructural components

can get to 80% of the total damage after a seismic event (Taghavi and Miranda, 2003). Nonstructural damage to the structure could also prevent the use of a building even if the structural system is unharmed. Evaluation of anchored nonstructural components performance in recent earthquakes suggests that improvements in the design are required as many failures in anchorage and bracing systems have been observed (Miranda et al. 2012). Moreover, current code provisions concentrate on life safety and don't provide any guidelines for component protection. Some components could contain valuable content that might be vulnerable under a design level earthquake or even in lower levels of ground motion. One example is a medical research freezer that is only designed to stay in place and contains hazardous materials or research samples collected over a decade that could be damaged.

Base isolated structures are not addressed in present nonstructural code provisions. The dynamic behavior of isolated structures has different characteristics than a fixed based structure, resulting in a modified spectral acceleration distribution along the height of the structure, which constitutes a main parameter in the lateral force design. However, the failure mode of the isolation needs to be considered for the design of the nonstructural components, such as using a moat wall of stiffening bearing that would introduce larger loads or impact loads into the structure.

1.2 OBJECTIVES

The objectives of the test program were to obtain quantitative data through shaking table testing regarding the seismic performance of actual anchored nonstructural components. The components were subjected to recorded and spectrally-matched in-structure seismic excitations. Moreover, the tests were designed to provide information on key parameters that control the current design procedures, as appears in the American and European seismic codes. Two companion papers address the contribution of a few of the key parameters to the dynamic response of the nonstructural component based on the test results (Feinstein and Mahin, 2018a,2018b).

In addition, the contribution of the attachment design was investigated based on several different designs for the connection of the component to the shaking table during the tests. The connection that were chosen for the tests were aimed to represent realistic designs and were based on ASCE7-10 guidelines and professional advice from practicing engineers.

1.3 RESEARCH SCOPE

The study includes analyses of the response of anchored nonstructural component, including two types of components attached to a concrete slab or to a metal plate. The input motion for the shaking table was based on floor response computed according to computer simulations of three structures excited with a real recorded ground motion, and on prequalifying spectral matched ground motion.

Excitation used:

1. Ground motions used for prequalifying tests according to IEEE standard (IEEE Std 693, 2005).
2. Floor response computed for the 16-story tall Health Sciences Institute building at UCSF:
    a. Computer simulated motions based on a ground motion used in a recent seismic evaluation of this building at the ground level, mid-height, and roof.
    b. These motions made to be spectrum compatible with the smooth AC156 (AC156, 2010) spectral requirements for the assumed location in the building.
3. Floor response computed for a 3-story steel braced frame that was either fixed based or seismically isolated. These motions were computed for the base level and for the roof.

The tests allowed comparison of the dynamic response of nonstructural components considering:

1. Two different types of anchored components.
2. Components that are located at different elevations in a building.
3. Floor motions from three structure types (Mid-rise, Low-rise and Isolated low rise).
4. Different intensities of floor shaking.
5. Equipment subjected to building-specific floor motions and spectrum compatible floor motions according to AC156.
6. Equipment subjected to prequalification motions according to IEEE.
7. Multidirectional input motion in one horizontal direction, two directions and with added vertical direction.
8. Connection to a concrete slab and a steel plate.
9. Connection using two thicknesses of brackets to a concrete slab.

2 LITERATURE REVIEW

2.1 NONSTRUCTURAL CODE – ASCE-7

Significant damage to nonstructural components was observed after Loma Prieta in 1989 and Northridge Earthquakes. That inspired a program for the development of a detailed and rational basis for nonstructural seismic design, that was supported by the National Hazard Reduction Program (Johnson et al. 2016).

From an early stage the seismic force design equation has taken into account a few influences that are believed to be most crucial for determining the force transferred to the nonstructural component. Those key performance parameters include component mass distribution, location within the structure, hazard risk and importance of post-earthquake operation. The anchorage of the component was not considered directly in the force equation for simplicity and was encouraged to have a ductile behavior with a non-ductile overstrength factor.

Since the first component force demand equation formulated, there haven't been major changes in the concepts, but rather small modification of the factors themselves. The efforts in developing the design considerations are built on limited knowledge from laboratory tests, simplified structural analyses and field observations and, as such, are hampered by the paucity of research results that addresses gaps in the behavior of anchored equipment during seismic events, or validates the adequacy of current and proposed design equations. Development in recent years focuses on the properties of the components to determine the ductility and flexibility of different components.

The force equation in ASCE-7 chapter 13 of is given in equation 1 (ASCE7, 2010).

$$F_p = \frac{0.4 \cdot a_p S_{DS} W_p}{\frac{R_p}{I_p}} \left(1 + 2 \cdot \left(\frac{z}{h}\right)\right) \quad (1)$$

Where a_p, R_p, W_p, I_p are component properties, S_{DS} is the peak ground motion for the imposed hazard level, and $1 + 2 \cdot \left(\frac{z}{h}\right)$ is to account for the position of the component in the structure, z accounts for the height of the component in the structure and h is the overall height of the structure. W_p is the component weight. I_p is the component importance factor, that accounts for the functionality expected post-earthquake. a_p accounts for component flexibility that can produce a

magnification of the floor acceleration throughout the component, a_p is taken as 1 for a rigid component, or 2.5 for a flexible one. R_p accounts for the ductility and inelastic behavior of the structure, and is taken as a value between 1 to 6. The component factors a_p, R_p are given in tables according to component type. Incorporated in the code are an upper bound and lower bound that should be considered using the force equation in equation 1, and are given in equation 2 and 3.

$$F_{p,min} = 0.3 S_{DS} I_p W_p \tag{2}$$

$$F_{p,max} = 1.6 S_{DS} I_p W_p \tag{3}$$

Demand forces are calculated using LRFD with an additional multiplier for the component force F_p. That multiplier is the over strength factor Ω_0, which is used when the anchor failure is assuming to have a non-ductile failure. The values of many factors of the equation factor has been based mostly on expert opinions and with limited research to substantiate the values. There is ongoing research to evaluate a more realistic value for Ω_0 (Johnson and Dowel, 2017), and the present research tries to produce quantitative data to help validate the recommended component factors.

2.2 NONSTRUCTURAL CODE – EUROCODE 8

The seismic design force calculation for nonstructural components as appears in Eurocode-8-1 (Eurocode 8, 2004) is defined in Equations 4 and 5.

$$F_a = (S_a \cdot W_a \cdot \gamma_a)/q_a \tag{4}$$

$$S_a = \alpha \cdot S \left[\frac{3(1+z/H)}{1+(1-T_a/T_1)^2} - 0.5\right] \tag{5}$$

where S_a and α represents the local peak ground acceleration for a site. Floor acceleration amplification throughout the height is considered linear in the term $3 \cdot (1 + z/H)$, with z as the component height in the structure divided by the total height H. This term is then adjusted based on the proximity between the component period, T_a and the first fundamental period of the structure, T_1. The decreasing term $1 + (1 - T_a/T_1)^2$ will equal 2.0 when the periods are highly

separated and decreased to 1.0 when in full resonance. W_a is the component weight. γ_a is the component importance factor, that accounts for the functionality expected post-earthquake. q_a accounts for component behavior and is chosen as one or two, according to the type of component.

One issue that arises from this form of the equations is that prior information regarding the component and structure natural periods is needed to calculate the design force. The structure natural period is usually estimated for design purposes and is not verified once the construction is completed. Moreover, the designer of the component's anchorage most often has relatively small amount of information regarding the structure in which the component is installed.

Once the demand force F_a is obtained, the designer decides on the force flow between the component and the anchors. Due to lack of information, the component is usually considered symmetrical and the only factors contributing to the calculation are the location of the component's center of gravity, the number of anchors used and the distance between the anchors.

2.3 QUALIFICATION OF EQUIPMENT

Qualification of equipment is intended to determine the ability of the piece of equipment to function after a seismic event of a certain magnitude based onS_{DS}, or smaller. There are two main guidelines that are used to evaluate the components. Acceptance criteria for seismic certification by shaking table testing of nonstructural components (AC156, 2010) and IEEE recommended practice for seismic design of substations (IEEE 693, 2005). The IEEE standard is applicable for electrical equipment only, while AC156 is used to certify all types of nonstructural components. The general guidelines of the two documents are similar and the details given in this document are based on AC156.

The qualification of the equipment is achieved based on shaking table tests, the component is attached to a steel plate on the shaking table using machine bolts. If the equipment will be attached using a different support system between the component and the anchors there is a need for additional tests or supporting analysis. Mass distribution in the component should be greater than or equal to the typical weight of the equipment.

The seismic parameters are given as a required broadband response spectrum, based on site specific ground motion acceleration parameter S_{DS}. The shaking table input motion is than

designed to match the required spectrum in all the three principal axes of the component. However, there are a high and lower limits for the spectrum that are based on ASCE-7 chapter 13, given in Equations 2 and 3. The lateral force design equation is based on Equation 1, with a change in the component parameters. The value of a_p is determined according to the frequency of the component, the component is considered flexible if the frequency is lower than 16.7Hz demanding an $a_p = 2.5$. The component factor R_p is taken as 1 to account for unreduced response.

Components with an importance factor $I_p = 1.5$ must satisfy functionality requirements after the seismic tests. Minor repairs are permitted, and some structural damage is acceptable in the members and joints that are not part of the force-resisting system of the component.

3 TEST PROPERTIES

The test program leveraged efforts by a manufacturer to qualify a heavy battery cabinet. In the preliminary tests, the manufacturer, as is common industry practice, anchored their cabinet to a steel plate mounted on the UC Berkeley 6DOF shaking table. The cabinet was to be qualified for an on-ground location using the IEEE standard, with an S_{DS} value of 2.5, thus certifying it for every location within the state of California.

3.1 SHAKING TABLE PROPERTIES

The test was performed using the PEER earthquake shaking table, located in Richmond, California. The reinforced concrete platform dimensions are 20' X 20' with a thickness of 1'. Table weight is about 100,000 pounds.

The shaking table is driven by 12 hydraulic actuators, Capable of producing 6 degrees of motion in two horizontal, vertical and three rotational degrees of freedom.

Maximum allowable horizontal displacement is 5'' in each direction, and 2'' in the vertical direction.

Velocity limit of the table is 30 in/sec.

3.2 COMPONENTS

A total of three components were tested, consisting of a medical freezer and two battery cabinets with the same design, but with varying mass and centers of mass, as one cabinet had one battery missing on the top rack. For consistency of notation cabinet 1 is the heavier cabinet, and cabinet 2 is the lighter cabinet. The cabinets configuration during the tests is presented in Figure 1.

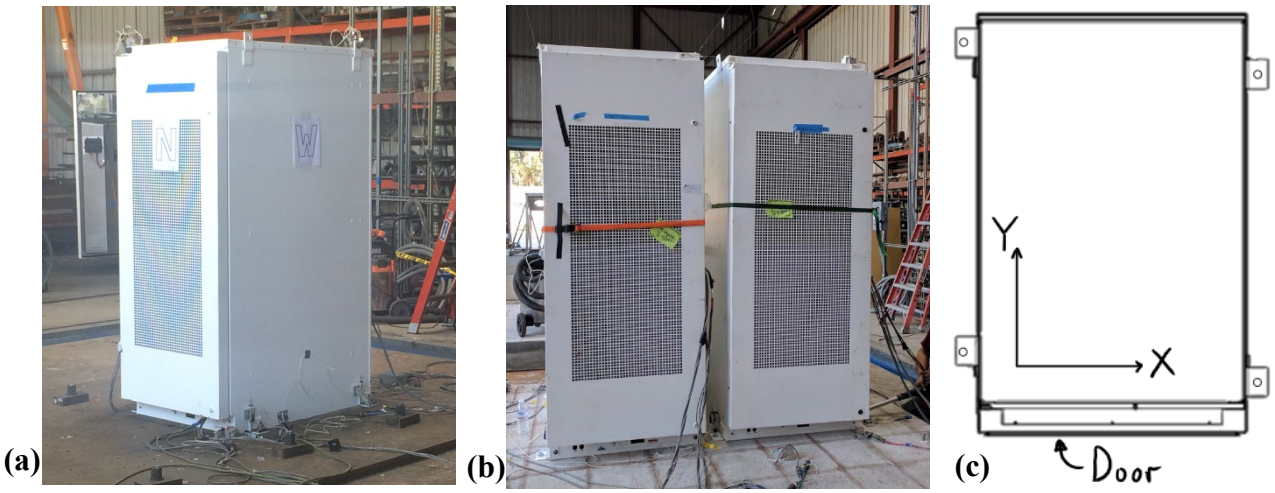

Figure 1. Battery cabinets configuration during the tests. (a) Steel mounted Cabinet 1, (b) Concrete anchored Cabinet 1 (right cabinet) and Cabinet 2. (c) Component axis

The medical freezer that was used in the tests is a commercial off-the-shelf product, manufactured by Thermo Fisher Scientific, model number SLT-25V-85A48. The freezer capacity is 24.4 ft^3. The freezer was connected to the concrete using post-expansion instrumented HSL-G M16, as seen in Figure 2. The cabinet weight is 726 lb and was filled with 484 lb of gravel bags. Wooden supports were added between the shelves to support the loose bags. Two bags were positioned at each of the 5 drawers of the freezer, one at each side as illustrated in Figure 2. The medical freezer was connected using two angle brackets that were located in the two sides of the freezer. The brackets were designed with 11'' distance between the two anchors in Y direction.

(a)  (b)  (c) 

Figure 2. Medical freezer configuration (a) Side view (b) Front view (c) Inside view

All the component measurements are listed in Table 1, including their total weight and location of their center of gravity in the Z axis.

Table 1. Components measurements

Component	Height [Inch]	Depth [Inch]	Length [Inch]	Weight [lbs]	C.G. [Inch]
Cabinet 1	84.2	50	32.4	4330	41
Cabinet 2	84.2	50	32.4	4213	40
Freezer	77.5	44.5	33.3	1210	37

3.3 SLABS

Most tests were performed with the specimens anchored to a concrete slab. The concrete slab with the dimensions of 124'x88'x12' was constructed of concrete that was assumed to reach f'c of 3 ksi. The actual concrete strength on test week was measured with in compression tests and split tension tests of concrete cylinders from the same concrete batch that was used to cast the slabs. The average compressive test f'c from the tests was 4.7 ksi, and the tension strength was measured as about a tenth of the compressive strength, with an average of 0.45 ksi.

Anchoring of the specimen was done with Hilti HSL-G post expansion anchors according to Hilti ESR-1545 with a minimum edge distance of $5\frac{7}{8}''$, and a minimum distance between two holes of $3h_{ef}$.

4 TEST DESIGN

4.1 INPUT MOTION

Input motions for the test plan were based on a medical research facility, the Health Sciences Instruction and Research (HSIR) complex. The HSIR consists of two 16-story steel moment frame structures, made of large built-up sections. Floor accelerations at various heights were recorded from a simulated realistic numerical model of the structure, which was developed using the Open System for Earthquake Engineering Simulation (OpenSees) (Mckenna, 2000). The input ground motion for the simulation, shown in Figure 3, was chosen to fit the site specific hazard spectrum.

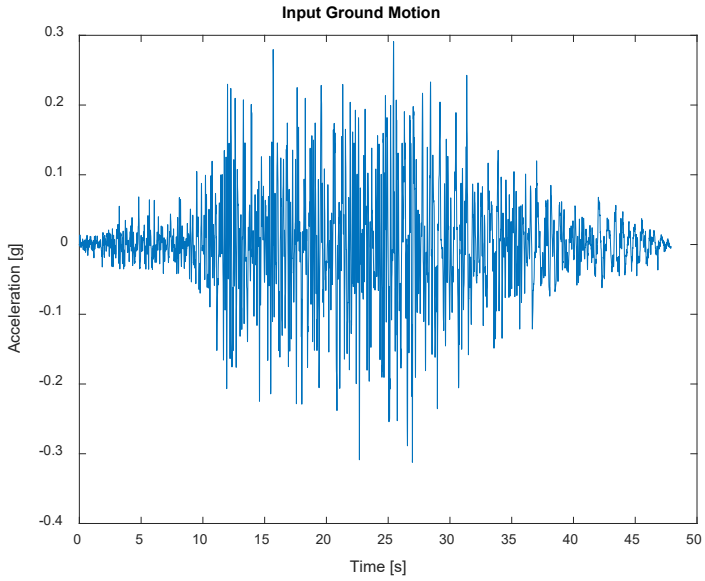

Figure 3. Ground motion acceleration record used in the test plan

Two additional structures were analyzed to allow for comparison between different types of structures, including low-rise and isolated models. The low-rise consist of a three stories archetype steel structure, with a lateral load resisting system of a special concentric braced frame. The structure was designed as a typical steel structure with a ductile response, using an R value of 6.0

according to ASCE 7-10 (ASCE 7, 2013). For the isolated model, the same archetype structure was considered, the lateral resisting frame was modified to an ordinary concentric braced frame, which is not expected to reach the same ductility demand and was designed with a ductility factor R set to one. The same ground motion from the HSIR location was used as the input motion for all models. Floor acceleration at the first floor, mid-height and roof levels were used as shaking table input.

The shake table accelerations during the test program were based on seven different input motion were used for the shaking table test plan, their corresponding response spectra are given in Figure 4. The input motion also included broadband spectrum matching of some of the input motions, based on qualification requirements based on AC156 (AC156, 2010). Figure 5 provides an example of a broadband motion that was matched to the target spectrum required by AC156, based HSIR mid-level simulated motion. Input motions were applied in the two principal directions of the cabinet and in the vertical direction. Some tests included only one horizontal direction of motion, while others had included two horizontal directions and the vertical accelerations as well.

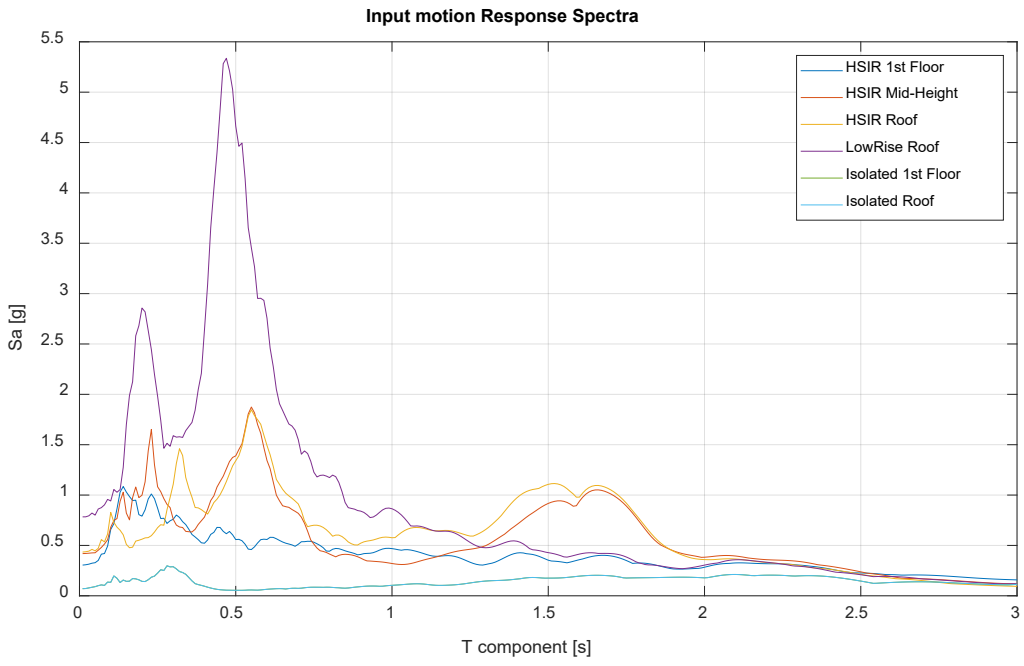

Figure 4. Response spectra of the different input floor accelerations

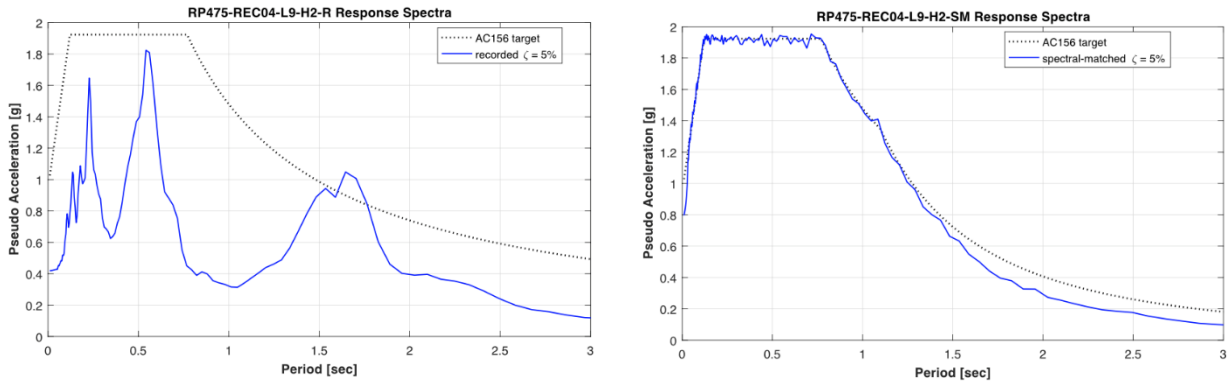

Figure 5. Input floor spectra extracted from HSIR simulation. (a) recorded, (b) broadband

The general response spectrum for the HSIR structure was based on a shear wave velocity over the top thirty meters (vS30) of approximately 1900 ft/sec, and was classified as class C. This was used to define the site specific hazard spectrum that guided the selection of ground motion recording. The HSIR periods from the numerical simulation were calculated as: T1=1.55sec, T2=0.481sec, T3=0.315sec and T4=0.216sec.

4.2 INSTRUMENTATION

Instrumentation during the shaking table tests were designed to measure the dynamic behavior of the components during seismic loading. A total amount of 34 channels were used to record each component response, including 12 displacements, 4 instrumented anchor rods and 18 accelerometers.

Component acceleration was recorded in three locations along the height of the component, positioned at the bottom, center of gravity and on the top of the component, thus allowing an observation of dynamic response shape of the structure throughout the tests. Two accelerometers were used at each location, to provide the ability to evaluate the torsional effects of the component, the location of the accelerometers can be observed in Figure6 (d). In addition, the slab and shaking table accelerations were also measured to give the exact floor response during the test.

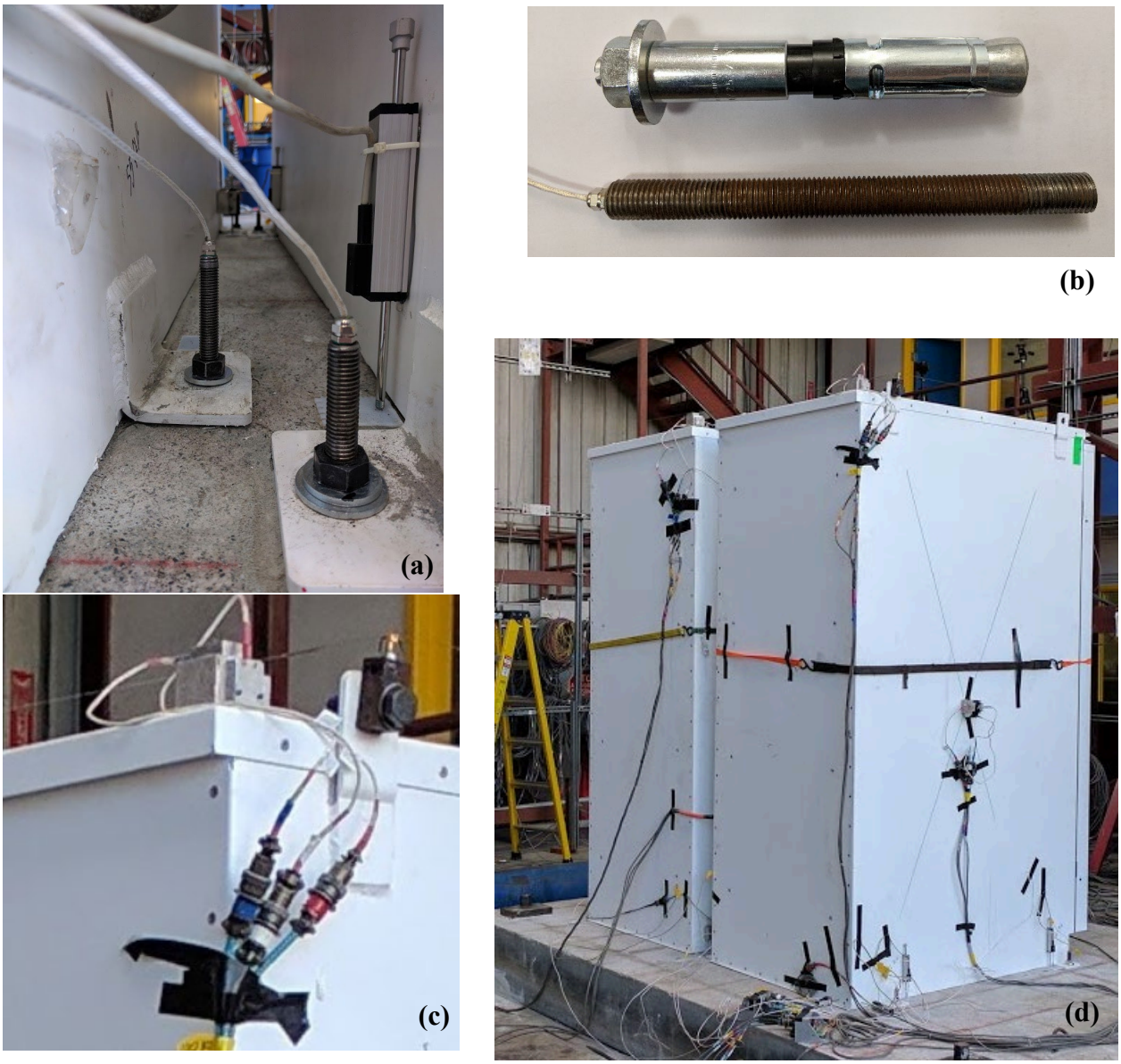

Figure 6. Instrumentation used during the test (a) LVDT, (b) Instrumented rods, (c) Accelerometers and wire pots connection, (d) Overall view from NE.

Similarly, the component displacements were recorded in order to provide quantitative data to determine the component response in sliding, rocking and elastic deformations. Sliding was measured with the use of linear variable differential transformers (LVDT) that were located at the bottom of the component at two corners. To determine the rocking mechanism of the component LVDTs were positioned at the bottom of the component near the anchor location, at four corners

of the component, as can be seen in Figure6 (a). Top displacements were measured using wire pods at two corners of the component roof. The displacement measures, together with the accelerations throughout the height of the component were used to calculate the dynamic response of the component.

In addition, the anchor tension forces were measured during the tests. The component was anchored using instrumented anchors, as shown in Figure6 (b). Post expansion anchors were used to anchor the component in the concrete slab with a simple modification that included replacing the inner rod of the anchor with an instrumented rod. The instrumented rod was 12.9 steel with 4 strain gauges inserted in the core in a full gauge configuration.

4.3 ANCHOR DESIGN

Attachment of the cabinets to the shaking table during the test were done using two designs, for the preliminary tests cabinet 1 was mounted to a steel plate using 25mm instrumented bolts, as usually done in qualifying tests. In the second set of tests all the components were anchored to a 124 in x 88 in x 12 in concrete slab that was attached to the shaking table, concrete strength at time of testing was measured to be 4.7 ksi. Specimen configurations are presented in Figure7. Attachment of the components to the slab was done via instrumented Hilti HSL-3-G M12 and M16 post expansion anchors, the HSL-3-G design allows the replacement of the original threaded rod with an instrumented threaded rod, which allow measurements of individual anchor tension force throughout the test.

The HSL-3-G installation was done according to the instruction manual in appendix 10.4. First a hole is drilled using a 18mm and 24mm drill bits for the M12 and M16 respectively. The hole depth needs to be larger than the required embedded length of the anchor. Than the anchor is placed in the hole through the bracket and hammered in gently until there is no additional gap between the bracket and the washer in the anchor. Finally, the anchor is torqued to the required installation torque, 59ft-lb and 89ft-lb for the M12 and M16 respectively, which measures to a tension force of about 4000lb and 5500lb respectively.

4.4 CONFIGURATION

The shaking table test set was separated to three stages, in the first, two battery cabinets were attached at the closest proximity to each other, while leaving enough space to install the post-expansion anchors in place between the cabinets. The second and third stages included testing of one medical freezer attached using thick and thin steel brackets. The specimens were positioned so the door of the component faces the control room which is positioned in the west of the building. The configuration of the two types of components is given in Figure 7.

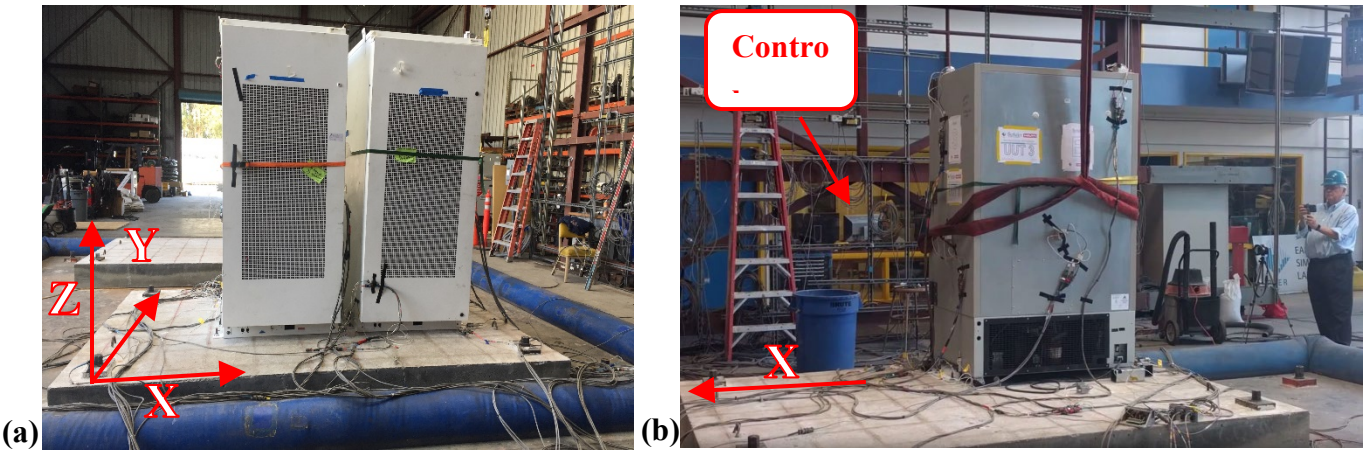

Figure 7. Test configuration (a) battery cabinets from the front, (b) Freezer from the back.

5 EXPERIMENTAL RESULTS

The experimental results for this set of tests were divided to individual test results and comparative analysis. The individual results are focused on understanding the dynamic behavior of the component, together with validation of the results based on basic principles.

5.1 LIST OF TESTS

A list of all the tests that were performed is given in Table 2, including a test number, which structure model the input motion was based on, the level from which the floor motion was taken, direction of input motion, if the input motion was spectral matched, what type of component was tested and additional notes.

Table 2. List of all tests included in the test plan

Test Number	Model	Height in Structure	Direction	S_{DS}	Spectral Matched	Component Type	Notes - Connection
2	HSIR	1st floor	Y	0.04	No	Battery Cabinets	72 return period
3	HSIR	1st floor	Y	1.2	No	Battery Cabinets	
4	HSIR	Mid-height	Y	1.2	No	Battery Cabinets	
5	HSIR	Roof	Y	1.2	No	Battery Cabinets	
6	HSIR	1st floor	X	1.2	No	Battery Cabinets	
7	HSIR	Mid-height	X	1.2	No	Battery Cabinets	
8	HSIR	Roof	X	1.2	No	Battery Cabinets	
9	HSIR	1st floor	XY	1.2	No	Battery Cabinets	
10	HSIR	Mid-height	XY	1.2	No	Battery Cabinets	
11	HSIR	Roof	XY	1.2	No	Battery Cabinets	
12	HSIR	1st floor	XYZ	1.2	No	Battery Cabinets	
13	HSIR	Mid-height	XYZ	1.2	No	Battery Cabinets	

14	HSIR	1st floor	X	1.2	Yes	Battery Cabinets	
15	HSIR	1st floor	Y	1.2	Yes	Battery Cabinets	
16	HSIR	Mid-height	Y	1.2	Yes	Battery Cabinets	
17	HSIR	Mid-height	X	1.2	Yes	Battery Cabinets	
18	HSIR	1st floor	X	1.2	Yes	Battery Cabinets	
19	HSIR	Mid-height	X	1.2	Yes	Battery Cabinets	
20	Isolated	1st floor	Y	1.2	No	Battery Cabinets	
21	Isolated	1st floor	Y	1.2	No	Battery Cabinets	
22	Isolated	Roof	Y	1.2	No	Battery Cabinets	
23	Low Rise	1st floor	Y	1.2	No	Battery Cabinets	
24	Low Rise	Roof	Y	1.2	No	Battery Cabinets	
25	Isolated	1st floor	X	1.2	No	Battery Cabinets	
26	Isolated	Roof	X	1.2	No	Battery Cabinets	
27	Low Rise	1st floor	X	1.2	No	Battery Cabinets	
28	Low Rise	Roof	X	1.2	No	Battery Cabinets	
29	IEEE	Ground	X	2.5	Yes	Battery Cabinets	
30	IEEE	Ground	XY	2.5	Yes	Battery Cabinets	
31	HSIR	Mid-height	XYZ	1.2	No	Battery Cabinets	Aftershock
32	HSIR	1st floor	X	1.2	No	Medical Freezer	
33	HSIR	1st floor	Y	1.2	No	Medical Freezer	
34	HSIR	1st floor	XY	1.2	No	Medical Freezer	
35	HSIR	1st floor	XYZ	1.2	No	Medical Freezer	

36	HSIR	Mid-height	X	1.2	No	Medical Freezer	
37	HSIR	Mid-height	Y	1.2	No	Medical Freezer	
38	HSIR	Mid-height	XY	1.2	No	Medical Freezer	
39	HSIR	Mid-height	XYZ	1.2	No	Medical Freezer	
40	HSIR	Roof	X	1.2	No	Medical Freezer	
41	HSIR	Roof	Y	1.2	No	Medical Freezer	
42	HSIR	Roof	XY	1.2	No	Medical Freezer	
43	HSIR	Roof	XYZ	1.2	No	Medical Freezer	
44	HSIR	1st floor	X	1.2	Yes	Medical Freezer	
45	HSIR	1st floor	Y	1.2	Yes	Medical Freezer	
46	HSIR	1st floor	XY	1.2	Yes	Medical Freezer	
47	HSIR	Mid-height	X	1.2	Yes	Medical Freezer	
48	HSIR	Mid-height	Y	1.2	Yes	Medical Freezer	
49	HSIR	Mid-height	XY	1.2	Yes	Medical Freezer	
50	Isolated	1st floor	X	1.2	No	Medical Freezer	
51	Low Rise	Roof	X	1.2	No	Medical Freezer	
52	Low Rise	Roof	Y	1.2	No	Medical Freezer	
53	IEEE	Ground	XY	2.5	Yes	Medical Freezer	
54	IEEE	Ground	XYZ	2.5	Yes	Medical Freezer	
55	HSIR	Mid-height	X	1.2	No	Medical Freezer	Thin Brackets
56	HSIR	Mid-height	Y	1.2	No	Medical Freezer	Thin Brackets

57	HSIR	Mid-height	XYZ	1.2	No	Medical Freezer	Thin Brackets
58	IEEE	Ground	XYZ	2.5	Yes	Medical Freezer	Thin Brackets
59	IEEE	Ground	XYZ	2.5	Yes	Battery Cabinet	Mounted to steel plate
60	IEEE	Ground	Y	2.5	Yes	Battery Cabinet	Mounted to steel plate
61	IEEE	Ground	X	2.5	Yes	Battery Cabinet	Mounted to steel plate
62	IEEE	Ground	XY	2.5	Yes	Battery Cabinet	Mounted to steel plate

5.2 DATA POST PROCESSING

Recorded data from the tests have been post-processed using MATLAB scripts. All the acceleration and displacement data are filtered using a bandpass filter with cutoffs at 0.9 Hz and 35Hz. The goal of the filter is to get rid of high frequencies which cannot be measured by the data acquisition system used. LVDT's and wire pots were initialized to zero at the location of the components before the beginning of the tests. The Anchor forces data contained very low frequency content, which is the reason the anchor forces were not filtered. Anchor forces were initialized according to manufacturer's instructions for each instrumented rod.

5.3 RESULTS VALIDATION

Validation of the experiment measurements was done through basic principles, using simple equilibrium equations, based on the results of the 1D tests. A SDOF equivalent system was used for calculation, based on the component weight and height of the center of gravity, as shown in Figure 8 (a). The equivalent force (F_p) was calculated based on the acceleration measurements in the component's center of gravity, as calculated in equation 6. The tension force (F_t) at the bottom

was taken as the sum of the two anchors acting in tension, and the validation was done based on a simple moment equilibrium calculated with equation 7. The equilibrium equation assumes that the weight of the component acts in the center and neglects the horizontal displacement.

$$F_p = a_{cg}[g] \cdot W_c \tag{6}$$

$$F_p \cdot H = F_t \cdot L + W_c \cdot \frac{L}{2} \rightarrow F_t = \frac{F_p H}{L} + 0.5 W_c \tag{7}$$

An example for the comparison of anchor forces with the forces calculated from equilibrium is given in Figure 8 (b) for 1D test in Y direction, for roof level in the three-stories fix-based structure.

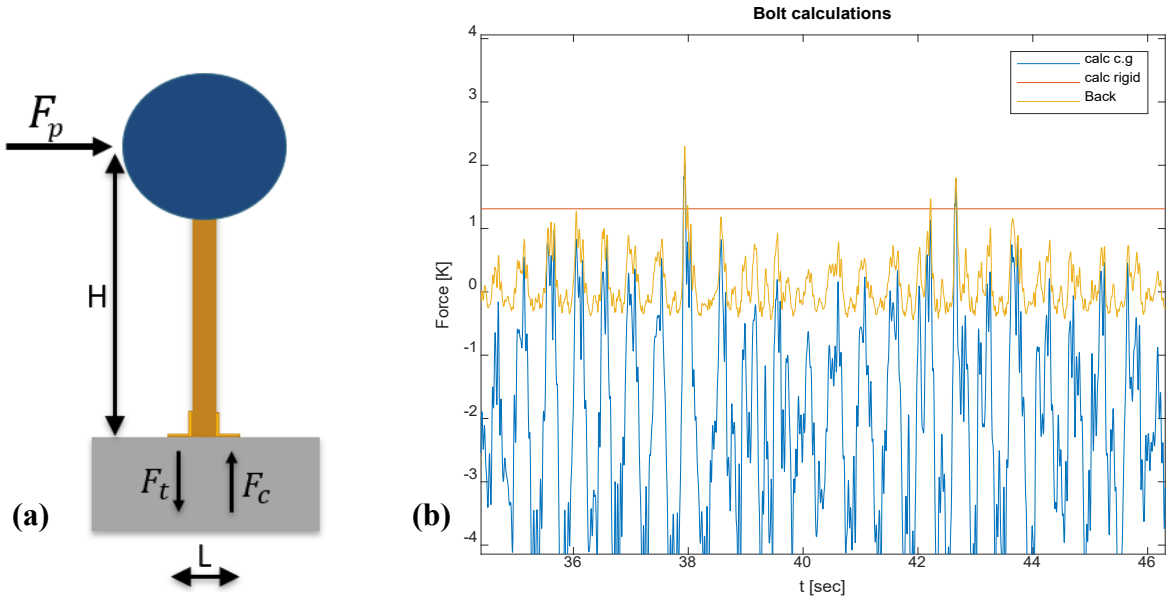

Figure 8. (a) Equivalent SDOF system (b) validation of anchor forces measurements during the dynamic test.

5.4 GENERAL COMPONENT BEHAVIOR

The test program included 61 different tests, including different input motion parameters and nonstructural component properties. During the tests there were a few interesting responses that are worth mentioning and would be elaborated in other sections of the report.

The nonstructural inner structure has a large effect on the force flow in the component, acting more like a scaled down structure than a simple symmetric box. For example, the door of the battery

cabinets was not contributing to the resistance of the cabinet, resulting in a C shaped structure with a highly asymmetric dynamic response.

The attachment of the nonstructural component has a large contribution to the overall response type. Flexible attachment allows uplift and results in combined rigid-rocking response and flexible fixed-based response.

Two failure modes were observed during the tests. One of the battery cabinet brackets fractured off the cabinet. The freezer buckled in the inner frame of the component base, resulting in some permanent deformation and change in component dynamic properties, such as the natural period and damping. The freezer was still stable after the buckling occurred and was tested further in a few tests after the failure.

5.5 INDIVIDUAL TEST RESULTS

Results summary page has been created for each test separately to provide insights on the component behavior under different input motion that simulate building type, height in the structure or added base isolation.

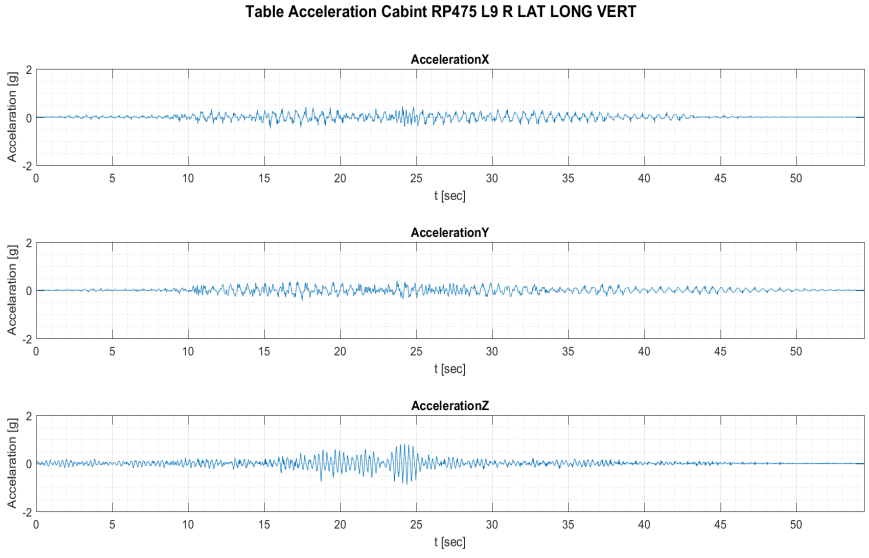

Figure 9. Acceleration input for mid-height HSIR 3D

Each summary page consists of five or six figures that provide the general results for that specific test. All figures will be presented in this section for one test as an example, while the summaries for all the tests done during this phase of test are given in the appendix of this report.

The top two figures in the summary page contains the input data for the specific test, including the acceleration history of the recorded floor motion in the three translational degrees of freedom, together with a response spectrum for that input time series. An example of the input motion information given in the data sheet is given in figure 9 and 10 for input from the mid floor of the HSIR structure, with input motion in three translational directions.

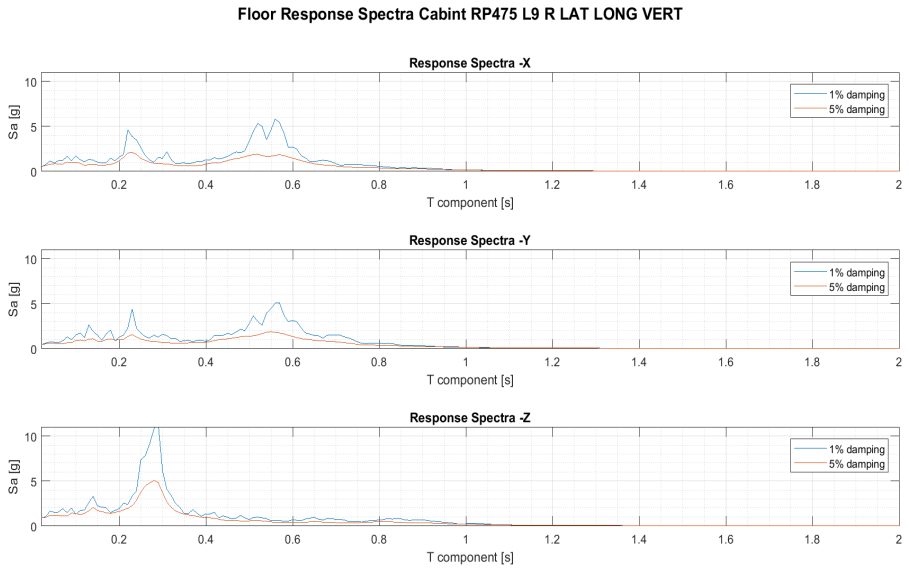

Figure 10. Acceleration response spectra for mid-height HSIR 3D

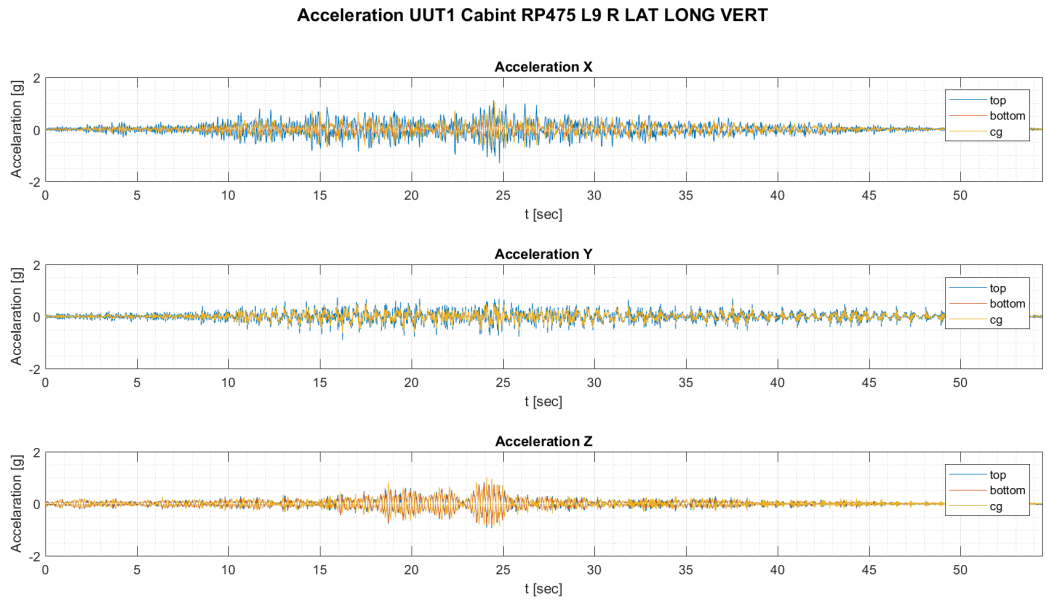

Figure 11. Cabinet 1 accelerations for mid-height HSIR 3D

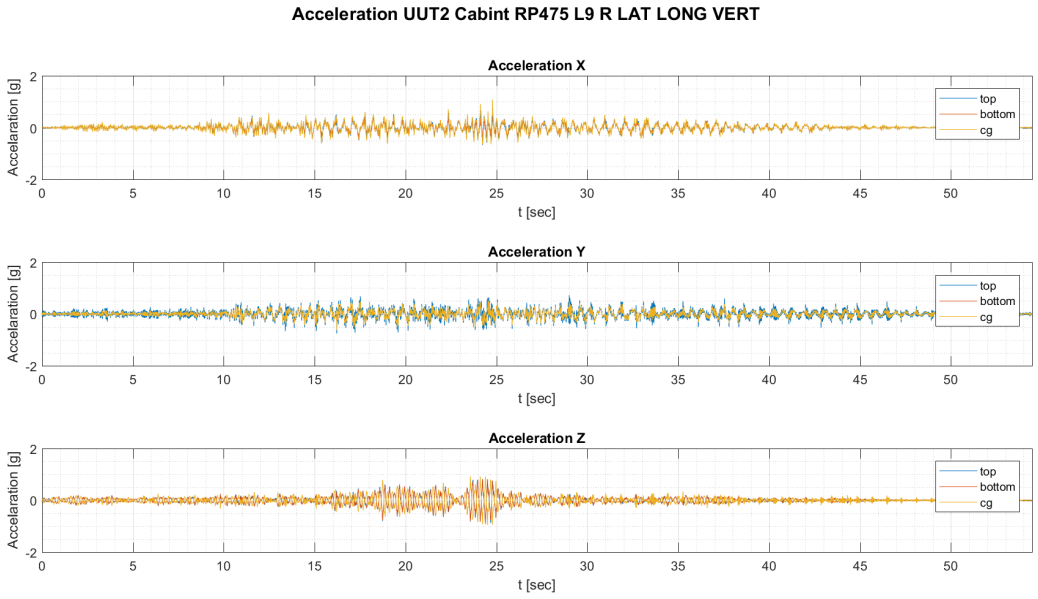

Figure 12. Cabinet 2 accelerations for mid-height HSIR 3D

In addition, the acceleration response at three positions along the height is given for the components that were on the shaking table during the test. The results with input motion from the mid floor of the HSIR structure are given in Figure 11 and Figure 12, the bottom acceleration is shown in red color, center of gravity is shown in yellow color and the top is shown in blue color in the figure. When comparing the two results we can see that cabinet 1 response is mainly in a first mode in the two horizontal directions. However, cabinet 2 exhibits higher mode response in the X direction, which results in similar accelerations in the top of the cabinet as in the center of gravity. This behavior was repeated in many of the tests and is apparent in cabinet 2 as a result of one missing battery at the top of the cabinet, causing the mass to be evenly distributed in all the cabinet except for the top part of it.

Displacements are shown in the top plane of the component, reflecting the displacements at the center of the roof of the component, by using the average recorded displacement from the top two corners of the component. An example of the top displacements for the two cabinets is given for the mid-height of HSIR in Figure 13, cabinet 1 displacements are in blue and cabinet 2 in red. The results suggest that while the dynamic properties of the two cabinets are not the same, the overall displacement trend is similar for the two cabinets with similar maximum displacement values.

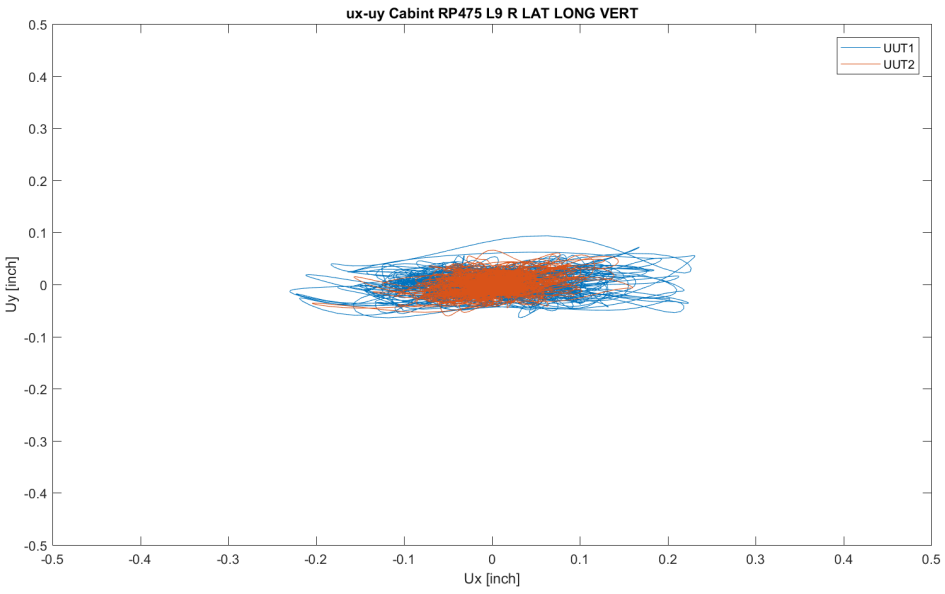

Figure 13. Top displacements for mid-height HSIR 3D

Lastly, the anchor forces for cabinet 2 are displayed, as in Figure 14. The anchors are pretensioned with 3000-4000 pound in the beginning of the tests. The forces in the figure are shifted to zero, to allow for easier observation of the added tension force from the tests themselves. Tension force is shown as negative in the figure. The forces are concentrating on a few anchors and don't distribute evenly between the four anchors, as observed in Figure 14 and also during other tests. This behavior is associated with the properties of the cabinet, the front door has limited capability to transfer shear forces and the whole cabinet has a structural system that is "C" shaped, and not a closed box. As a result of the irregular shape torsional effects are also recorded with accelerations in the transverse direction to the input motion.

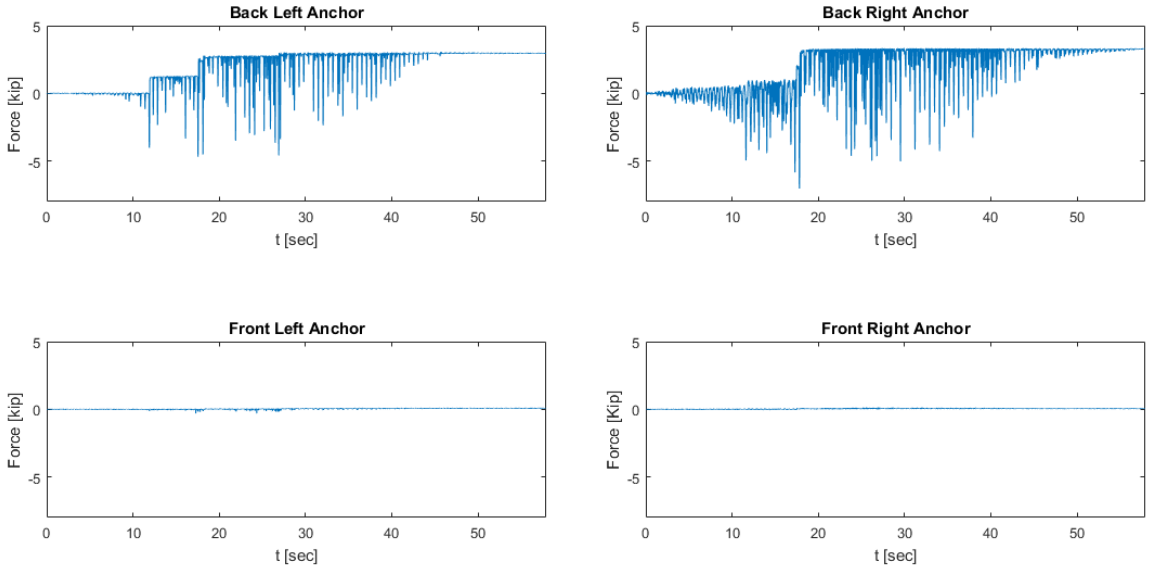

Figure 14. Anchor forces for Low rise structure at roof level with input motion in X direction

5.6 COMPONENT DISPLACEMENT DUCTILITY

The displacement ductility demand of a component generally originates from a combination of the component structural properties, the attachment design and the anchor properties. The experimental equivalent displacement ductility demand of the cabinets was calculated based on an equivalent SDOF system. The equivalent system properties are based on the measured response of the components during the tests with 1D input motion. The stiffness of the equivalent system was based on service level shaking test. Stiffness was taken as the maximum force divided by the maximum recorded displacement, according to equation 8.

$$K_{eq} = F_{p\_max}/\delta_{max} \cong 47 \ \ kip/inch \tag{8}$$

The equivalent systems, as presented in Figure 15, allows to measure the ductility demand for each test. First, the elastic displacement for the test is calculated based on the maximum force recorded during the test divided by the equivalent stiffness of the system, according to equations 9. Later the displacement ductility demand is calculated as the ratio between the maximum displacement and the elastic displacement for the maximum force as appears in equation 10.

$$\delta_{elastic} = F_{p\_\mathrm{max\_per\_test}}/K_{eq} \tag{9}$$

$$\mu = \delta_{max}/\delta_{elastic} \tag{10}$$

The values for the displacement ductility demand of the components under the 1D excitation used during the tests was calculated for the two cabinets. These results are summarized in Table 3 and provide quantitative data regarding the performance of the cabinets under several floor acceleration time series.

The latest recommendation for improved seismic performance of nonstructural components (ATC, 2018) suggest basing the design force equation for a nonstructural component on the assumed ductility of the component. The values that are considered for the component ductility in the suggestion are between 1.0, 1.25, 1.5 and 2.0. or larger. In the interest of comparing the experimental results to the new suggested equation, an average ductility was considered to determine the assumed ductility for the component tested. Cabinet 1 (HBC) assumed ductility was taken as 1.25, as the average value from the different tests was 1.23, and cabinet 2 (LBC) was considered with an assumed ductility of 1.5, with the average value 1.43, and ranging from 1.36 to 1.56.

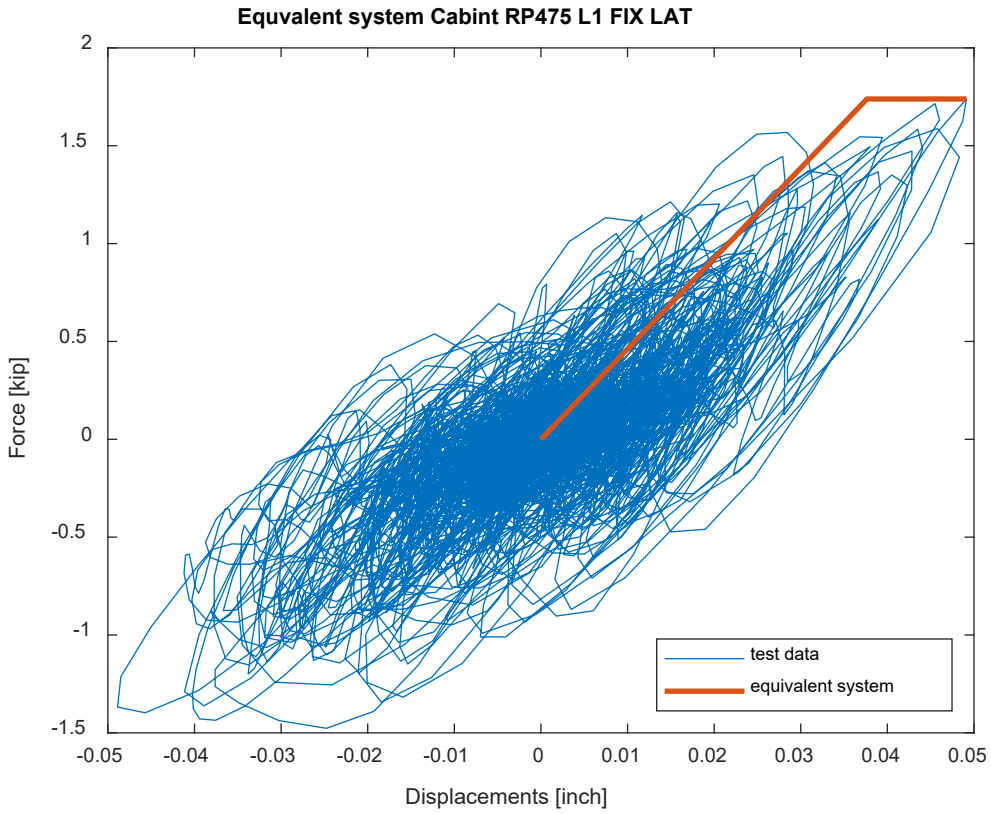

Figure 15. Equivalent force displacement relationship

Table 3. Displacement ductility demand values calculated using the equivalent system for the different input motions

Building	Floor	μ Cabinet 1	μ Cabinet 2
HSIR	Ground	1.09	1.56
HSIR	Mid-height	1.26	1.36
HSIR	Roof	1.23	1.37
Low-Rise	Ground	1.15	1.38
Low-Rise	Roof	1.43	1.5

5.7 DAMPING

The equivalent viscous damping in the components was measured from the free vibration at the end of the tests based on the logarithmic decrement after the end of the input motion. The measured damping values are summarized in Table 4. The results for the cabinets were 0.7%-1.5% in Y direction (The symmetric direction of the cabinet), and 1.4%-3% in X direction. For the freezer connected using ¼'' angles, measured damping was 2.8%-3.7% in Y direction and 1.4%-2.2% in X direction. After buckling occurred in the freezer, the damping in Y direction increased to about 5%. For the freezer connected using 16 gauge angles, the measured damping was 4%-5.5% in the Y direction and 3-4.5% in X direction. The damping measured in the two freezer attachment configurations suggest that the use of thin angles provides additional damping to the system in X direction.

Table 4. Equivalent viscous damping values

Component	Direction	Lower range [%]	Upper range [%]
Cabinet	Y	0.7	1.5
Cabinet	X	1.4	3
Freezer – ¼ ''	Y	3	5*
Freezer – ¼ ''	X	1.3	2.2
Freezer – 16 gauge	Y	4	5.5
Freezer – 16 gauge	X	3	4.5

* There was an increase in damping value after local buckling occurred in the freezer lower frame

5.8 FAILURE OF THE NONSTRUCTURAL COMPONENTS

Cabinet 1 which was the heavier battery cabinet failed on test number 30, with input motion in the two principal directions based on IEEE spectral matched ground motion with a S_{DS} of 2.5. The back right anchor had the largest measured forces and uplift in all the tests, as such it not surprising that the right back bracket was the one that failed first. The failure occurred near the end of the input motion, after the bracket experienced large plastic deformations. The bracket was made from cold rolled steel and failed in the corner, where the steel was bent and had the largest stresses from the manufacturing process. While cabinet 1 failed, cabinet 2 exhibited plastic deformations but remained intact. Figure 16 shows the cracked bracket in cabinet 1 compared with the bracket from cabinet 2 that is in the same location. Figure 16(b) shows that the back-right bracket of cabinet 2 experienced large deformations and has chipped paint and residual plastic deformations. Also, in Figure 16 (b) the back-left bracket of the failed cabinet is shown with plastic deformations and when the anchor is an apparent angle to the washer as the anchor lost the pretension and was lifted by the bracket.

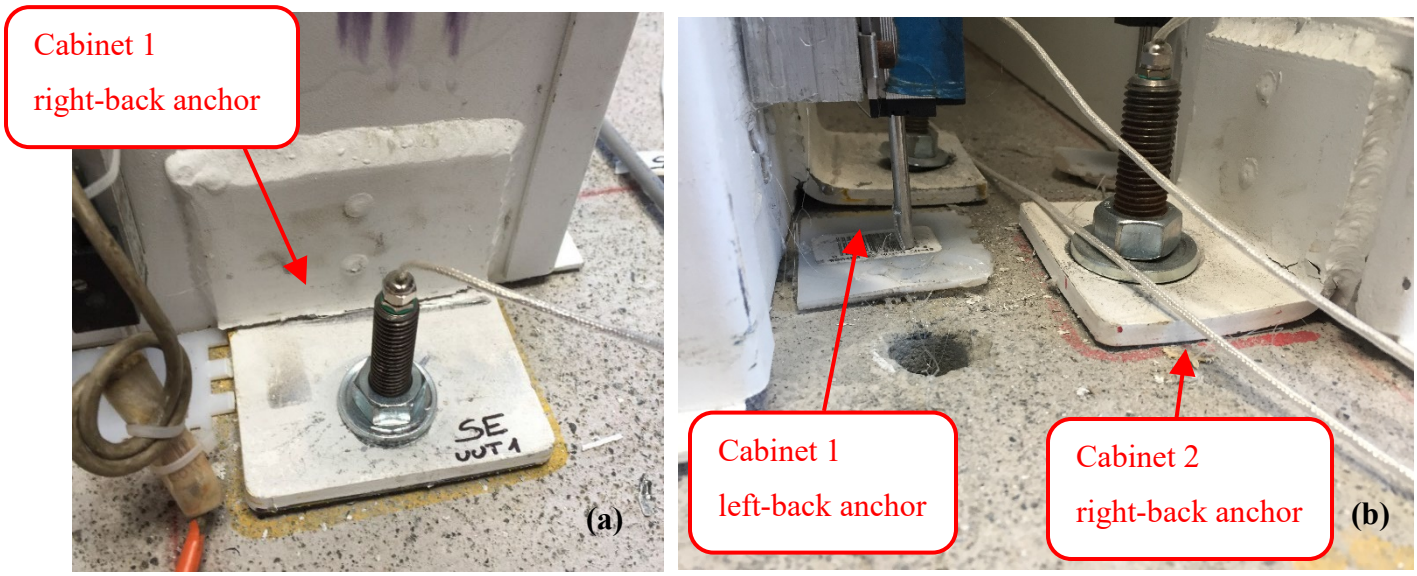

Figure 16. Bracket failure in the battery cabinet (a) cracked bracket (b) same bracket on the second cabinet

Following the cabinet 1 failure an additional input motion was tested in order to observe the behavior of the cabinet in an aftershock motion. The cabinet rocked and cracked two more brackets, including the back-left (still attached in Figure 16 (b)) and front-right brackets, the

cabinet had impacted the front-left anchor and sheared it off, allowing the bracket to deform and detach from the anchor. After all the brackets were either disconnected from the cabinet or from the anchor the cabinet started to move, ending in a new position located a few inches away. The final position of cabinet 1 can be seen in Figure 17, with a view of the first bracket that failed and the entire right side of the cabinet.

Figure 17. Cabinet location at the end of the aftershock motion

The Freezer is essentially built up of two parts, the base that is supported by a 12 gauge sheet metal frame and the top storage part. The Freezer experienced local buckling under the input motion number 46, that was spectral matched according to AC156 standard, based on the mid-height floor motions of the HSIR structure. The freezer base frame has six fabricated rectangular holes, as can be seen in Figure 18, creating locations with reduced sections that are more sensitive to failure. The local buckling occurred in the left side of the base frame of the freezer, at the location of the

reduced sections in the top of the frame columns, both locations buckled at the same time. Figure 19 shows the frame local buckling in the two locations that are shown in Figure 18.

Figure 18. Freezer base with the location of the failures

Figure 19. Freezer base after local failure at the two locations in the frame

6 ANALYSIS OF RESULTS

The main goal of the set of experimental tests was to obtain quantitative results from real equipment, that will allow to assess the contribution of different parameters on the dynamic behavior of the nonstructural component. The factors that were considered include:

- Amplification throughout the height of the structure
- Different types of structures
- Isolated structure compared with a fix-based structure
- Effects of spectral matching of the input motion
- Influence of multi directional input motion
- Influence of the connection between the component and the slab
- Different types of nonstructural components

The results of the comparison between the different tests have been analyzed to determine the contribution of the different factors.

6.1 STRUCTURE EFFECTS

A dozen tests were compared in order to identify structure effects, such as floor height, structure period and structure isolation. The results of the tests are listed in Table 5, including the test number, structure type, input motion direction, calculated design force according to ASCE7-10 (ASCE, 2010) and the maximum recorded anchor force.

Table 5. Test data set for structure effect comparison

Test Number	Model	Height in Structure	Direction	Design Force [lb]	Max Force [lb]	Test/Design
3	HSIR	1st floor	Y	1095	243	22%
4	HSIR	Mid-height	Y	1215	375	31%
5	HSIR	Roof	Y	2170	285	13%
6	HSIR	1st floor	X	1605	1314	82%

7	HSIR	Mid-height	X	1759	1481	84%
8	HSIR	Roof	X	2986	1274	43%
24	Low Rise	Roof	Y	2170	2244	103%
28	Low Rise	Roof	X	2986	7036	236%
21	Isolated	1st floor	Y	1095	165	15%
22	Isolated	Roof	Y	2170	169	8%
25	Isolated	1st floor	X	1605	514	32%
26	Isolated	Roof	X	2986	476	16%

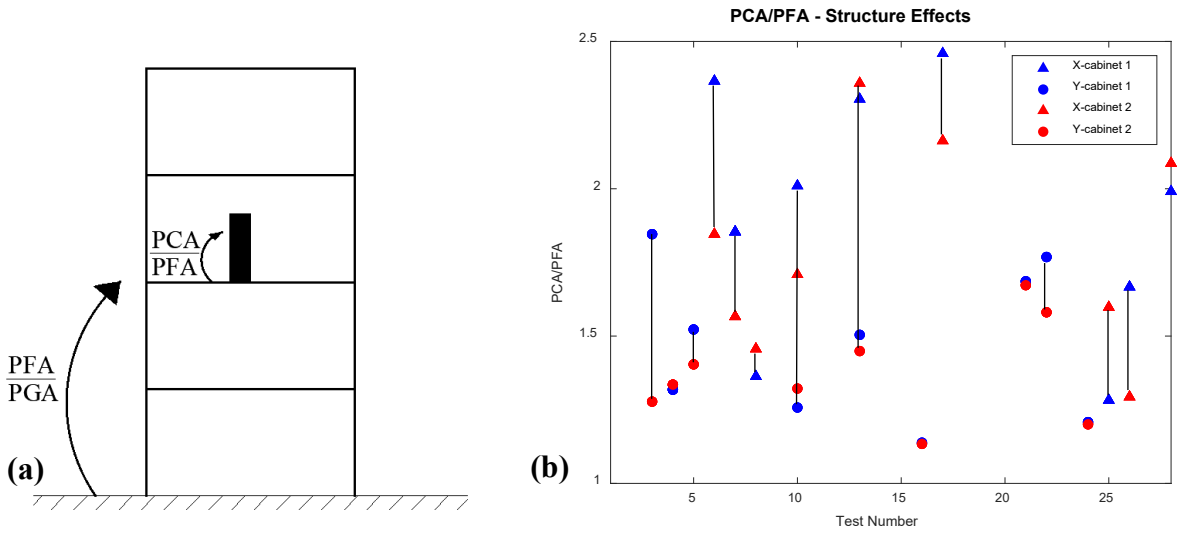

Figure 20. Acceleration amplification factors, (a) illustration of two contributions, (b) PCA/PFA from test set to study structure effects.

Note: Vertical lines connecting points identify data from a single test. Interconnected circles are for input in Y-direction only; interconnected triangles are for input motion in X-direction only; Interconnected circles and triangles are for bidirectional input motion in X and Y directions.

Acceleration amplification of a nonstructural component is considered as the ratio between the peak ground acceleration (PGA) and the peak component acceleration (PCA). This amplification can be broken into two contributions, as illustrated in Figure 20 (a). The first part is the amplification throughout the height of the structure, which considers the peak floor acceleration (PFA) relative to the PGA. The second part is the component acceleration amplification compared to the floor, which is calculated using the ratio of PCA to PFA. The component amplification may depend on many factors, such as component properties, attachment characteristics, and floor response spectrum

The results for the different floors and structure types are given in Figure 20 (b). The component amplifications for all tests are in the range of 1.2 to 2.4. The results are given for the two cabinets that were tested simultaneously and similarly attached with post expansion anchors to a rigid concrete slab.

6.1.1 FLOOR HEIGHT

In most codes, amplification of floor response throughout the height of the structure is considered as linear, conditioned only on the first mode. However, both present and past research show that consideration of additional information regarding inelastic behavior and additional modes of the structure provides improves approximations of floor demand (Miranda and Taghavi, 2005).

The component amplification ratio throughout the height of the structure is not consistent in the two principal directions of the component. Moreover, the two cabinets have different amplification factors for the same input motion, for example in test one and four there is a difference of 30-40 percent between the two cabinets. Results suggest that the component amplification factor has no simple dependence on floor height, as the amplification for the HSIR structure shows an increasing trend along the height in the Y direction and decreasing trend in the X direction. Furthermore, component amplification with input motion from the short fixed-based structure does not support the same trend.

6.1.2 STRUCTURE PROPERTIES

Structure properties are considered in the lateral force design in the ratio between the natural period of the structure and component first modes. Additional structure properties are not considered, such as building expected ductility and damping at a design level earthquake. The HSIR building, that was used for tests one through six, undergoes large inelastic deformations under design level earthquake. Thus, the floor amplification throughout the height of the structure is not linear, and the PFA of the roof is similar to mid-height. On the contrary, the short archetype structure amplifications are controlled almost entirely by first mode behavior, with a linear amplification of the ratio of PFA vs PGA up to a maximum of three.

Anchor forces recorded from the shaking table tests are given in Table 5. The maximum force recorded for the roof is smaller compared to the mid-height input motion from HSIR structure. However, the three-story structure showed a very large amplification of the anchor forces recorded at roof level, with anchor forces that are 2.36 times larger than their calculated design forces according to ASCE7-10 (ASCE, 2010).

6.1.3 ISOLATION EFFECTS

Present nonstructural design codes do not give special treatment to isolated buildings, even though the dynamic behavior of the building is extremely different. Isolated buildings act as a nearly rigid system above the isolation, resulting in a nearly constant floor amplification throughout the height of the building, as can be seen in Figure 20. The long period of the isolated building is considered in the Eurocode-8 lateral seismic force equations, and as a result the forces that are calculated based on the Eurocode equations give a good estimate for the base level. However, the building period accounts only for a small contribution compared to the height in the building. As a result, the design forces overestimate the forces at roof level by a large margin. As can be observed from Table 5, ASCE 7 is overestimating the forces throughout the entire building, with recorded forces that are between 8 to 32 percent of the design forces. This overestimation might be the result of not considering the effects of the ratio between the period of the building and the non-structural component. The anchor forces remain in a constant range as would be expected in an isolated low-height structure.

It is important to note that the failure mode of the isolation in the building should be considered when calculating the nonstructural demands, if considering above design level performance. For example, if the isolation design includes a moat wall, pounding would occur beyond the design level and would add additional demands on the nonstructural component.

6.2 INPUT MOTION EFFECTS

In this study the shaking table tests used either a single horizontal direction of shaking or three components of shaking. We also considered broadband motions that have been spectrum-matched to target response spectra. The following two subsections will examine effects of these parameters on the measured response. The comparison is based on six individual tests from the mid-height floor of the HSIR building that are listed in Table 6.

Table 6. Test data set for input motion comparison

Test Number	S_{DS}	Broadband	Direction	Design Force [lb]	Max Force [lb]	Test/Design
4	1.2	No	Y	1215	375	31%
7	1.2	No	X	1759	1481	84%
10	1.2	No	XY	1759	1907	108%
13	1.2	No	XYZ	1759	2068	118%
16	1.2	Yes	Y	1215	2981	245%
17	1.2	Yes	X	1759	6699	381%

6.2.1 SPECTRAL-MATCHING MOTIONS

Component dynamic response from broadband input motion was studied from the comparison between tests 4 and 7 vs 16 and 17 respectively. The maximum recorded anchor forces that are listed in Table 6, are consistently much larger for the broadband input motion. It seems that one main contribution for that is that the spectral matched input motion consisted of a much higher

PFA than the base real recording (1.05 g vs 0.42 g respectably), resulting in larger acceleration of the component. When considering the component amplification factor, we normalize the PCA by the PFA, this way we can compare the results from the broadband input and the real recording. Figure 21 shows that there is no general trend in the amplification factors for the broadband motion with higher amplification in X direction and lower in Y direction.

The main conclusion from the small amount of experimental test data is that the component response is highly sensitive to input motion parameters and spectral matching of the input motion doesn't necessarily result in the worst-case response for the component.

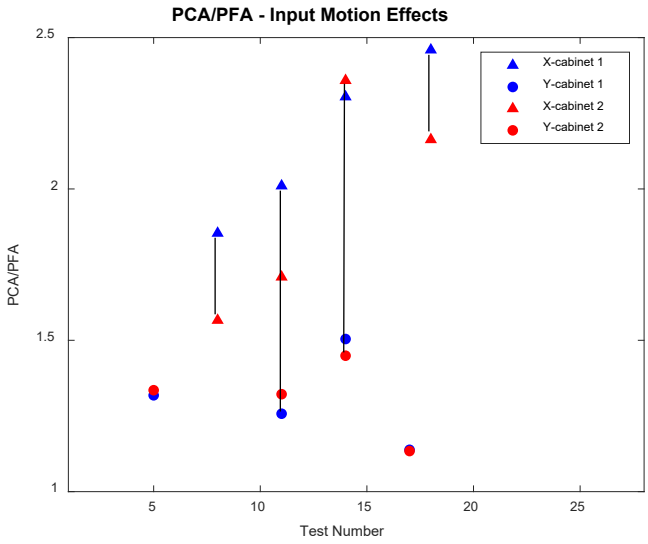

Figure 21. Acceleration amplification factor, PCA/PFA, for test set of different input motion

Note: Vertical lines connecting points identify data from a single test. Interconnected circles are for input in Y-direction only; interconnected triangles are for input motion in X-direction only; Interconnected circles and triangles are for bidirectional input motion in X and Y directions.

6.2.2 MULTIDIRECTIONAL INPUT MOTION

Effects of multidirectional excitations on anchored equipment were observed through a series of four shaking table tests repeating the same excitation in different combinations. In this test program, a unidirectional input motion was tested in the X direction and then in Y direction, following the same motions simultaneously in both direction and finally the same motions

simultaneously in 3D with the additional vertical motion. The maximum recorded anchor forces and design forces according to ASCE7-10 (ASCE, 2010) are listed for all the tests in Table 6.

Often codes simplify lateral force calculation by separating excitations into two horizontal directions. Consequently, the design forces calculated for the multidirectional tests were simply taken as the larger out of the two principal directions. Recorded forces shown in Table 6 suggest that anchor forces are larger when subjected to more than one direction of excitation, forces were amplified by almost 30 percent for the bi-directional excitation (1907 lb vs 1481 lb). An additional eight percent increase in the maximum force was recorded when vertical excitation was included.

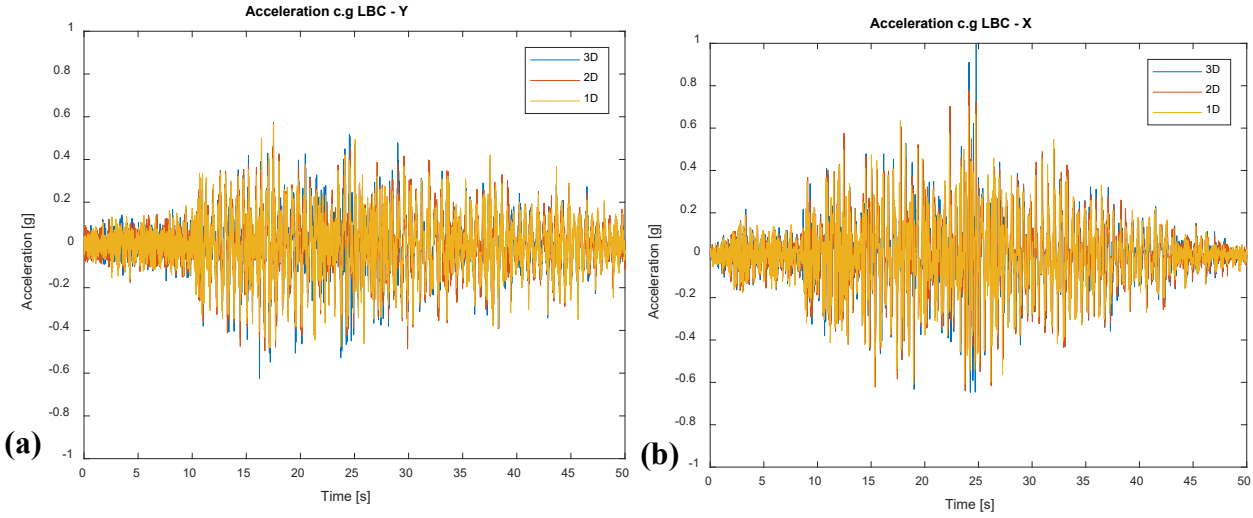

Figure 22. Acceleration of cabinet 2 center of gravity under multidirectional excitation, (a) Acceleration in Y direction, (b) Acceleration in X direction.

The cabinets acceleration and overall behavior in a given direction was nearly independent of the presence of motions in orthogonal directions. However, because an individual anchor is resisting forces from responses in all three directions, the multi-directional response results in increased design forces in the individual anchor. A typical comparison between the cabinet's center of gravity accelerations under the different input motions, as shown in Figure22, demonstrates that the 2D and 3D excitations track the accelerations recorded in the one-dimensional excitation test. The cabinet's response period remained unchanged, but there was an amplification of the values at the maximum response that contributed to the increase in the anchor forces. In many codes

appears a requirement to use a design force taken from 100% in X direction and an additional 30% in the Y direction. This method would produce reasonable design force of 2123 lb, which gives a 10% margin of safety based on the recorded force in the bidirectional test and a margin of 2.5% when the vertical accelerations are included.

The freezer response for the multidirectional input motion showed coupling of the two horizontal directions and a significant change in the component response. Figure 23 displays the freezer center of gravity's acceleration in the two principal directions. The response period of the freezer changed significantly between the uniaxial and multidirectional input motions, from Figure 23 it can be observed that the Y direction of input motion is the one that controls the freezer response. The response in the X direction is independent of the vertical direction, but the response in Y direction changes significantly when the vertical input motion is added.

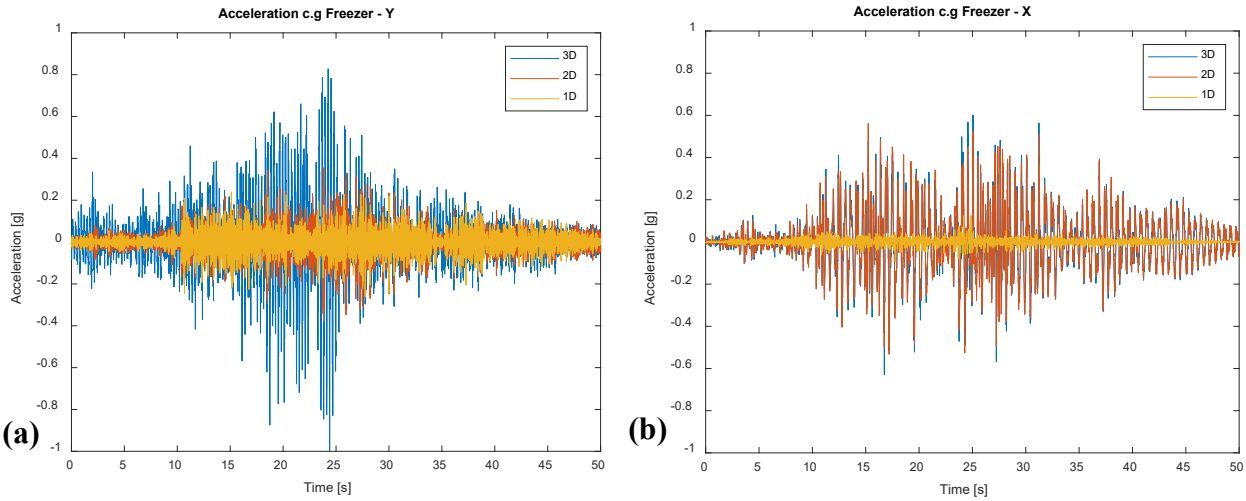

Figure 23. Acceleration of the freezer center of gravity under multidirectional excitation, (a) Acceleration in Y direction, (b) Acceleration in X direction

6.3 ATTACHMENT EFFECTS

Two different connections were used to attach the battery cabinets, one connection with post-tension anchors into a concrete slab, and the second mounted to a steel plate with large diameter steel bolts, as normally done in prequalifying tests of equipment. The post-expansion connection was tested with the recommended installation pretension, as detailed in the anchor design section, and without any pre-loading to simulate aftershock conditions.

The medical freezer was tested with two different connection designs that differed only in the thickness of the connection brackets. The medical freezer was first tested with the thick brackets and later installed and tested with the thin brackets with a some of the same input motions.

6.3.1 POST EXPANSION ANCHORS VS STEEL PLATE

Attachment design has a noteworthy influence on the component dynamic response resulting in modified component demands that are transferred from the floor through the anchors. Two designs were tested for the attachment of the battery cabinet, using bracket connection as shown in Figure 24. The first design consisted of an HSL-3-G post expansion anchor in a one-foot deep concrete slab. The second design, used in test number 61, is the commonly used connection in qualifying tests in which a quarter inch bracket was connected to a steel plate with 25mm instrumented machine bolts with an additional quarter inch washer.

Table 7. Test data set for input motion comparison

Test Number	**Connection**	**S_{DS}**	**Broadband**	**Direction**	**Design Force [lb]**	**Max Force [lb]**	**Test/ Design**	**PCA/PFA X**
29	Concrete slab	2.5	Yes	X	4371	11163	255%	1.64
61	Steel plate	2.5	Yes	X	4497	20570	457%	3.15

The most notable change between the two designs was the amplified response in the component attached to the steel plate. The accelerations of cabinet 1 were 38 percent higher with the steel connection, and the maximum anchor force was significantly higher compared to the concrete case. Two major reasons for the differences in the responses are that the brackets in the concrete connection did not have an additional washer which allowed the formation of a plastic hinge at the base of the angle in the concrete connection. Significant uplift was observed with the concrete connection, as shown in Figure 25, which eventually resulted in a fatigue failure of the cabinet in a later test. The second reason is that the anchor strength of the machine bolt is substantially higher than that of the post expansion anchor, though the forces in the test were not limited by this, as none of the anchors reached its strength capacity. In addition, the post expansion anchor allows for more slip in the anchor which adds to the flexibility of the entire concrete connection.

(a)  **(b)** 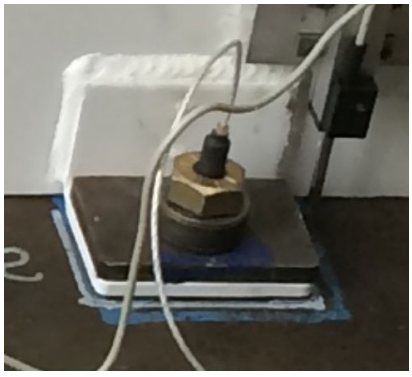

Figure 24. Attachment design for different floor types (a) concrete, (b) Steel plate.

Modifications in the component's overall stiffness were observed through a major change in the natural period of cabinet 1. The natural period in the X axis of the component shifted from 0.1 seconds in the stiff steel connection to 0.2 seconds when connected to concrete. Previous research supports that these changes seen in the dynamic response of components depends on the anchor characteristics (Johnson and Dowell, 2017).

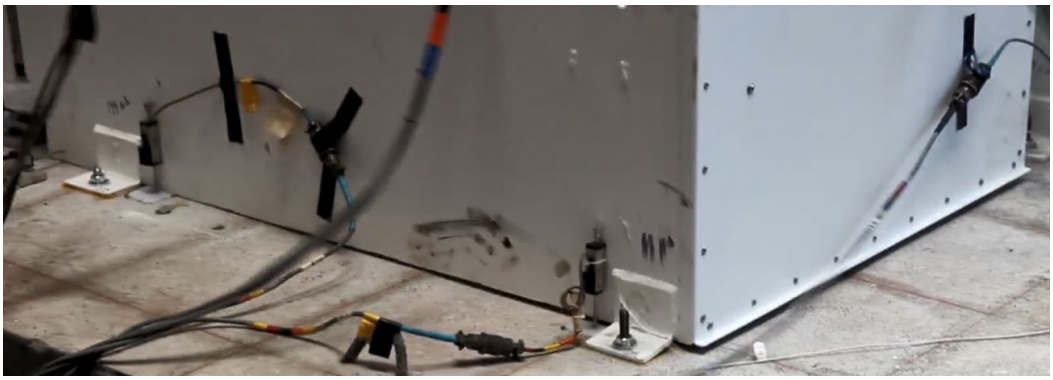

Figure 25. Uplift of the component attached to concrete.

6.3.2 AFTERSHOCK – LOSS OF PRETENSION IN THE ANCHORS

Loss of pretension in the post-expansion anchors was very common in the tests and was very easy to identify with the instrumented anchors. However, in a real component there will be no way to see if there was an extensive loss of prestress without measuring the torque on all the anchors. Therefore, it is believed that in the event of an aftershock some of the components might experience a loss of pretension in the anchors. For this reason, a test was conducted to measure the influence of the loss of prestress on the response of the component.

Table 8. Test data set for pretension comparison

Test Num	Height in Structure	S_{DS}	Direction	Design Force [lb]	Max Force [lb]	Test/ Design	PCA/ PFA X	PCA/ PFA Y	PCA/ PFA Z
13	Mid-height	1.2	XYZ	1759	2068	118%	2.36	1.44	1.12
31	Mid-height	1.2	XYZ	1759	11212	637%	1.71	1.62	2.8

The data set used to evaluate the effects of an aftershock are listed in Table 8, and is based on the same input motion before and after the anchors have lost all of their pre-loading. The test shows that there is a very large effect of the initial prestress of the anchors on the component response.

The component connection didn't fail under any of these tests. However, as expected, the battery cabinet experienced much more uplift and rocking behavior during the aftershock which resulted in much higher vertical acceleration amplification and the anchors experienced forces that were six time bigger than the equivalent test with pretension on the anchors.

6.3.3 THIN VS THICK BRACKETS

Two different connections were used for the connection of the medical freezer during the shaking table tests. One was using 1/4'' brackets and the other used a thinner 16 gauge bent sheet metal brackets. Figure 26 shows the two configurations for the freezer connections. Some practicing engineers have expressed the opinion that allowing for more ductility in the component or connection will provide a reduced response. Analytical models based on a SDOF models with a ductility larger than one provide smaller amplifications in the component compared to a component with no ductility. Based in part on such studies, the draft ATC-120 report (ATC, 2018) recommends using ductile angles in the connection of non-structural components.

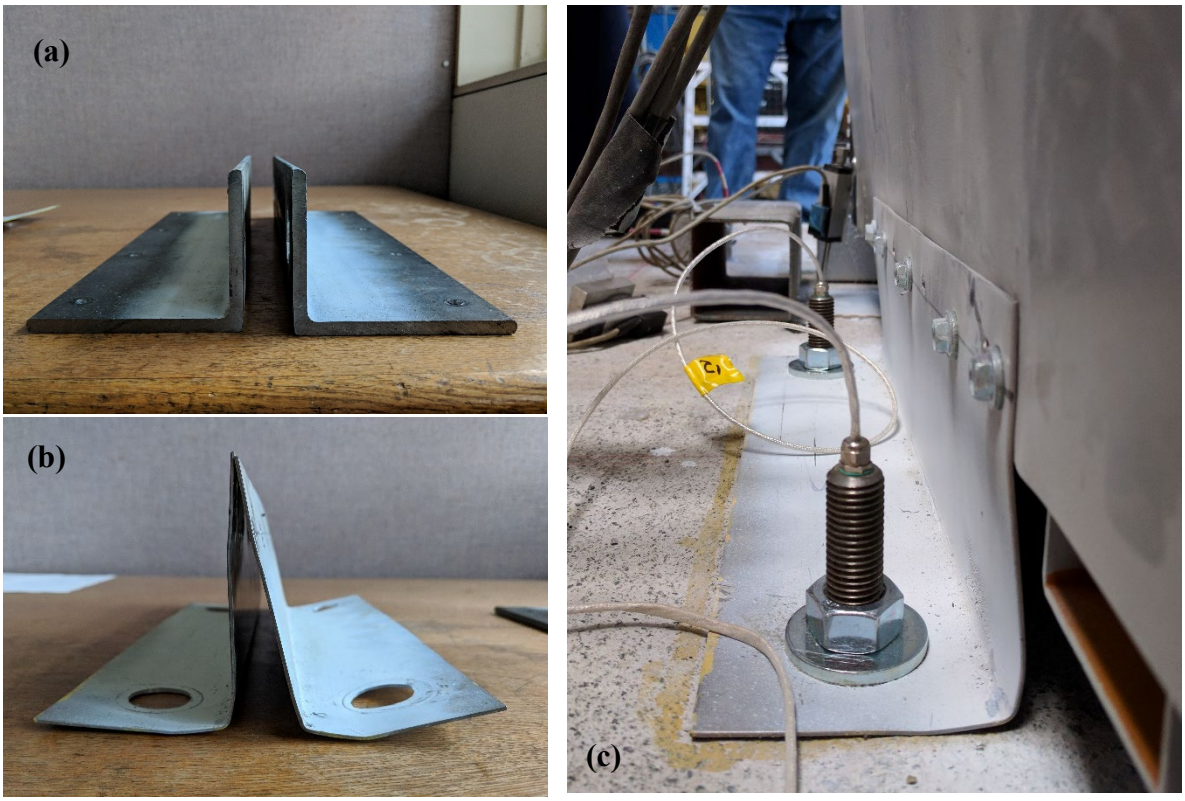

Figure 26. Different bracket connections for the medical freezer (a) ¼'' angle, (b) 16-gauge angle, (c) Thin angle installed

Four separate tests were done in both pairs of brackets and provide quantitative data to assess the effectiveness of the use of yielding brackets. Table 9 summarizes the data collected from the relevant tests and provides the anchor forces and the component amplifications (PCA/PFA).

Table 9. Test data set for thin vs thick bracket comparison

Test Number	**Height in Structure**	**S_{DS}**	**Direction**	**Design Force [lb]**	**Max Force [lb]**	**Test/Design**	**PCA/ PFA X**	**PCA/ PFA Y**	**PCA/ PFA Z**
36	Mid-height	1.2	X	445	77	17%	0.63		
37	Mid-height	1.2	Y	695	330	48%		0.56	
39	Mid-height	1.2	XYZ	695	274	39%	1.58	2.4	0.83
54	Ground - IEEE	2.5	XYZ	1620	1015	63%	1.06	1.33	1.78
55	Mid-height	1.2	X	445	198	45%	0.55		
56	Mid-height	1.2	Y	695	310	45%		0.5	
57	Mid-height	1.2	XYZ	695	343	49%	1.4	2.3	0.95
58	Ground - IEEE	2.5	XYZ	1620	1117	69%	0.9	1.06	1.68

The test results suggest that for the medical freezer experienced similar accelerations and anchor forces with the two different types of brackets. However, the response of the freezer was not the same in all the tests, as the thin brackets allowed sliding in the X direction. Figure 27 compares orbits at the top of the freezer for the mid-height 3D input motion, showing that the displacements in x direction are double with the thin brackets. The displacements in the transverse Y direction are in the same range for both tests.

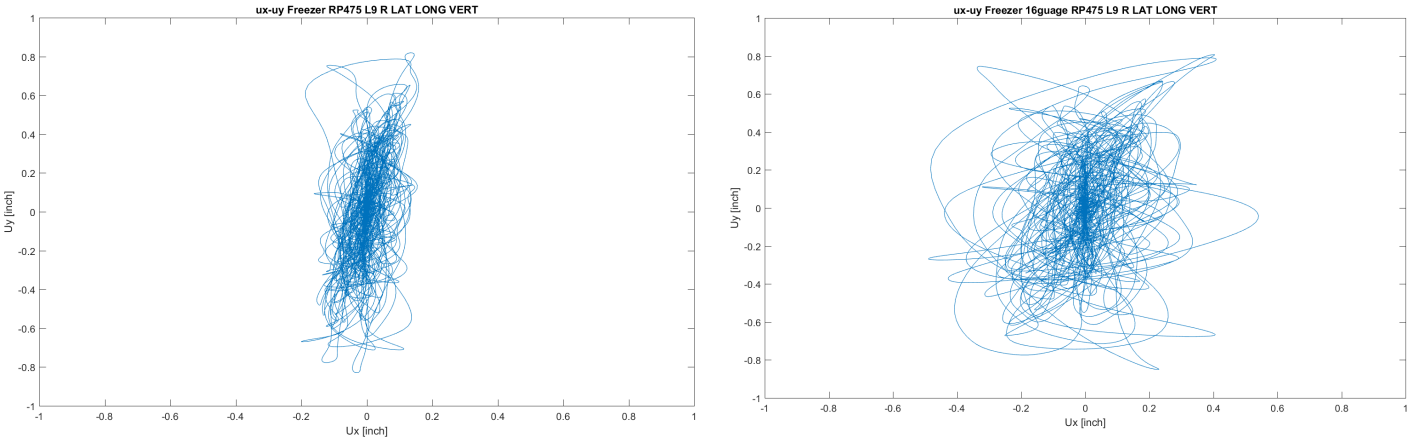

Figure 27. Freezer top displacements for two connection types (a) Thick ¼ ‘’ (b) 16-gauge brackets

6.4 DIFFERENT COMPONENTS

The two types of components that were used in this test program differed in a few ways that affected the dynamic response from the same input motions. The most notable difference between the components is their contact with the floor: the battery cabinet has full contact between the sheet metal at the base, whereas the freezer which sits on casters and has only 4 points of contact with the floor in addition to the brackets. The brackets design is another change, with two long angle brackets for the freezer compared with four individual brackets for each anchor in the connection of the battery cabinet. The mass of the components was around 4000 lb for the battery cabinets, while the freezer mass was 1200 lb, about a quarter of the battery cabinets, with periods of around 20 hz and 6 hz respectively.

The nonstructural component amplification was calculated as PCA/PFA, with the results shown in Figure 28 for the two component types. The results show that the freezer had amplifications smaller

than 1.0 in many of the tests. This result suggests that the casters may have acted as some form of isolation between the freezer and the floor. We can observe in Figure 28 (b), that for multidirectional input motions that included vertical acceleration the horizontal component amplifications were larger in the freezer, especially in Y direction.

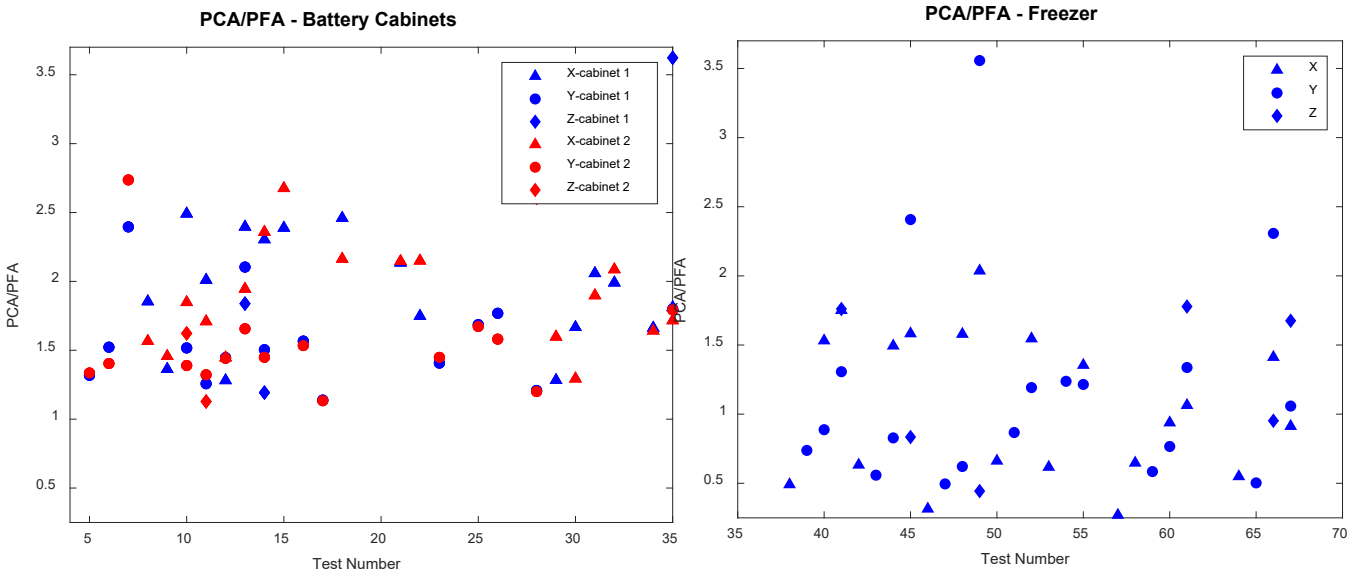

Figure 28. PCA/PFA for all tests according to the component type (a) Battery cabinet (b) Medical freezer

A comparison of the components acceleration across all the tests shows that the battery cabinet amplifications are concentrated in the range of 1 to 2.5, while the amplification of the freezer concentrate mostly between 0.5 to 1.5. However, it is important to note that while the casters generally decreased the horizontal acceleration of the freezer, it introduced vertical acceleration from the impact of the rocking response of the freezer. An example of this vertical acceleration effect is given in Figure 29, where the acceleration history for the uniaxial mid-height HSIR input in X direction. We can observe the introduced vertical accelerations and horizontal accelerations in the transverse direction, even though there is no input motion in those directions.

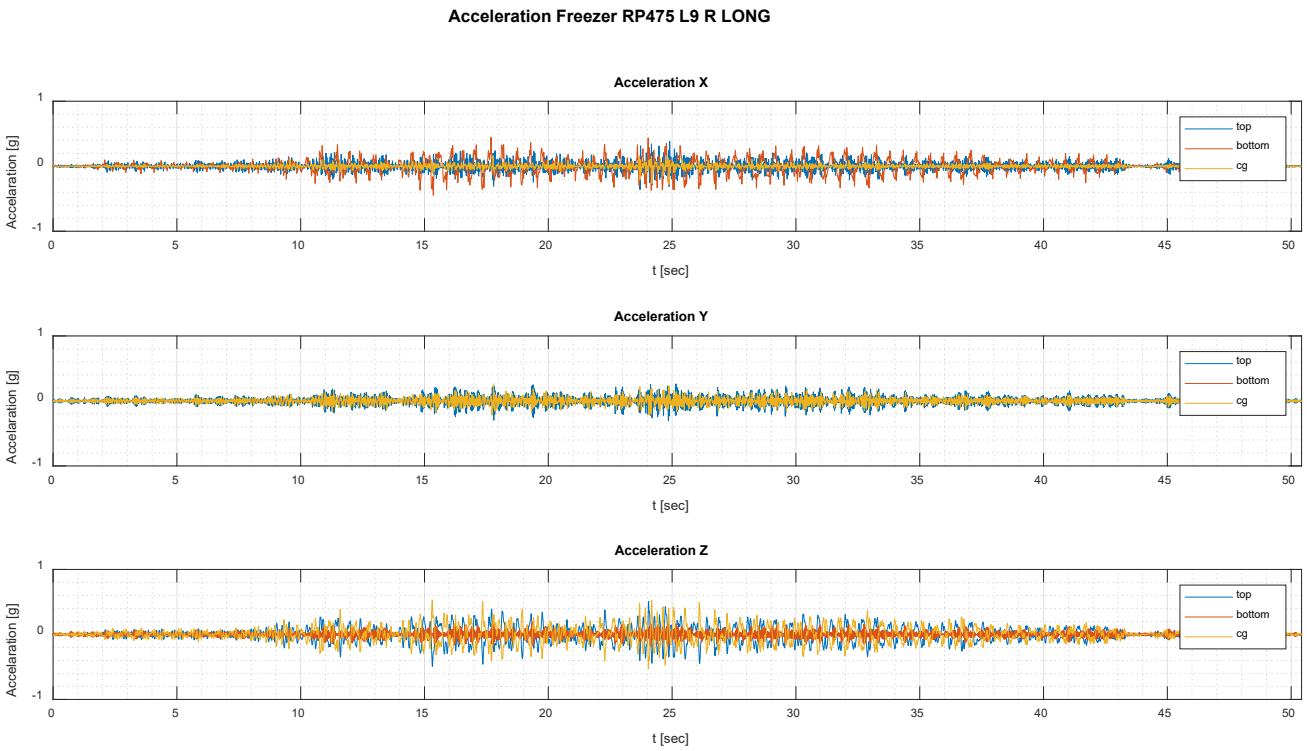

Figure 29. PCA/PFA for all tests according to the component type (a) Battery cabinet (b) Medical freezer

7 SUMMARY AND CONCLUSIONS

Multiple shaking table tests with anchored nonstructural components were performed to provide quantitative data that would improve the current understanding of the response of anchored nonstructural components under seismic loading. The current study focused on performance of actual anchored equipment subjected to seismic excitations. Data from the experimental program was used to evaluate current code design procedures.

Performance of the components was assessed under floor motions from several types of simulated structures, taken at several locations along the height of the structure. Test input motions were based on an actual site in San Francisco and were tested alongside spectral matched motion based on AC156 (AC156, 2010). The shaking table input motion was designed to assess a realistic scenario, thus included multidirectional floor motions, composed of two horizontal and the vertical components of motion. The components were tested using different attachment designs to provide insight into the role they take in determining the overall response of the component.

7.1 CODE DESIGN PROCEDURES

One of the test goals was to evaluate the current code design procedures. The variety of different parameters in the chosen input set enabled the assessment of the current lateral design load equations, especially of the component related factors.

Code lateral force equations are commonly believed to give conservative results. However, test results show that even with consideration of the overstrength factor Ω_0, the code equation gave unconservative values relative to measured anchor tension forces. Test results clearly show that component factors a_p and R_p do not predict actual component amplification.

Component dynamic response to broadband input motion was more severe, compared to the design level recorded floor motion. Interestingly the ratio of PCA to PFA wasn't consistently higher for the broadband motion, which suggests that broadband input motion does not always produce the largest amplification of responses.

Multidirectional input motion produces larger dynamic response compared to a unidirectional input motion. The amplified response was contained within the range that is considered by most

codes when considering a combined loading of 100% in X direction plus 30% in Y direction. The cabinets acceleration and overall behavior in a given direction was nearly independent of the presence of motions in orthogonal directions. However, the freezer with the casters experience a change in the dynamic properties when subjected to bi-directional input motion, compared to one direction excitation.

Amplification throughout the structure height at a design level is highly dependent on structure inelastic properties. Floor accelerations are filtered by the structure and result in narrowband motions. Component acceleration amplifications compared at different floors in highly dependent on the relation between the nonstructural component and building periods. Eurocode 8 bases the lateral force equation on this relationship and produces better predictions than ASCE 7.

Isolation of structures is not considered in present nonstructural lateral force design codes. The dynamic behavior of isolated structures is very different than fix-based structures. Using the same equations in both cases leads to overestimation of the lateral force, especially in the higher floors of the isolated structure. Nevertheless, the failure mode of the isolated structures needs to be considered for the maximum earthquake response of the nonstructural components. Impact with a moat wall or large stiffening of the isolation system results in accelerations and forces that transfer to the rest of the structure, where the nonstructural components are located.

7.2 DYNAMIC BEHAVIOR OF REALISTIC NONSTRUCTURAL COMPONENTS

The dynamic behavior of anchored nonstructural components is a combination of rigid body rocking and flexible dynamic response. It seems that the attachment design is one of the dominant elements that controls the overall dynamic behavior of the component. Flexible connections elongate the components period and allow for more uplift in the connection, this produces rocking behavior of the component that can be observed in the freezer behavior during the tests. Flexible attachments could potentially create a plastic hinge that could act as a fuse to control the maximum demand that can be transferred to the component and the anchors.

Additionally, the component internal structural system controls the force flow in the anchors, which results in a highly asymmetrical force distribution that is not usually considered in the anchor design process.

8 FUTURE WORK

This report is an interim data report, that is a part of a research program that will continue through additional laboratory and numerical work, including the work identified in the following subsections.

8.1 ANALYTICAL MODEL

Future work will focus on the influence of the connection on the overall dynamic response. An analytical model would be developed to model the component behavior under different connection conditions. The model would represent the flexible response of the component along with the rocking behavior that may occur and will be calibrated based on these test results and additional tests. Parametric studies will be done to provide the key parameters that affect the component response. As the component response is sensitive to the input motion, different types of input motions will be considered during the study.

8.2 ADDITIONAL TESTS

An additional test program to assess the effects of intense near-fault motion was carried out, with collaboration with the National Center for Earthquake Engineering in Taiwan. The nonstructural component in the test program was designed as a generic nonstructural component with a variety of attachment designs that could shed more light on the influence of the connection on the component dynamic response. The generic component was constructed in Taiwan and used in the collaborative shaking table test program with four different attachment designs.

8.3 IMPROVED DESIGN

An improve design method for the attachment of nonstructural components will be pursued based on the results of numerical and laboratory studies. The design may include methods to improve performance through detailing of the steel connection brackets.

8.4 INFLUENCE CODES

The quantitative data gained from laboratory and numerical studies would be used to calibrate design procedures of current provisions, such as qualification of equipment (AC156) and lateral force design equations in ASCE7 or new equation proposals (ATC, 2018).

9 REFERENCES

1. AC156, Acceptance Criteria for Seismic Certification by Shake-Table Testing of Nonstructural Components, International Code Council, 2010.
2. ATC, Recommendations for Improved Seismic Performance of Nonstructural Components – draft, NIST, 2018
3. Anajafi, H., 2018, Improved Seismic Design of Non-structural Components (NSCs) and Development of Innovative Control Approaches to Enhance the Seismic Performance of Buildings and NSCs, Ph.D. Thesis, University of New Hampshire.
4. ASCE/SEI-7-10, Minimum design loads for buildings and other structures, American Society of Civil Engineers, Reston, VA, 2013.
5. Eurocode 8. Design of structures for earthquake resistance—Part 1: general rules, seismic actions and rules for buildings. (2004) European Committee for Standardization (CEN), Brussels, EN 1998–1.
6. Feinstein T, Mahin S. Shake Table Tests to Evaluate Seismic Performance of Floor Mounted Nonstructural Components. Proceedings of the 16th European Conference on Earthquake Engineering, Thessaloniki, Greece. 2018.
7. Feinstein T, Mahin S. Experimental Performance of Floor Mounted Nonstructural Components Under Seismic Loading. Proceedings of the 11th National Conference in Earthquake Engineering, Earthquake Engineering Research Institute, Los Angeles, CA. 2018.
8. IEEE Std 693, IEEE Recommended Practice for Seismic Design Substations, IEEE Power Engineering Society, New York, 2005.
9. Johnson T.P., Dowell R.K., Silva J.F., A review of code seismic demands for anchorage of nonstructural components, J. of Building Engineering, 2016
10. Johnson T.P., Dowell R.K., Evaluation of the overstrength factor for nonstructural component anchorage into concrete via dynamic shaking table tests, J. of Building Engineering, 2017a; 11: 205-215.
11. Johnson, T.P., Dowell, R.K., Silva, J.F, Recommendations For Ω0 For Anchorage Into Concrete For Floor-Mounted Nonstructural Components, J. Struct. Eng., 2018; 144(2): 04017183.

12. Mckenna, F., Fenves, G.L., Open system for earthquake engineering simulation. University of California, Berkeley, CA, 2000.
13. Miranda, E. and S. Taghavi. Approximate floor acceleration demands in multistory buildings. I: Formulation. Journal of Structural Engineering, ASCE, 2005; 131(2): 203-211.
14. Miranda, E. and Taghavi, S., 2009, "A comprehensive study of floor acceleration demands in multi-story buildings," ATC & SEI 2009 Conference on Improving the Seismic Performance of Existing Buildings and Other Structures, San Francisco, California.
15. Miranda, E., Mosqueda G, Retamales, R, Pekcan, G. Performance of Nonstructural Components during the 27 February 2010 Chile Earthquake. Earthquake Spectra, 2012; 28 (1): 453-S471.
16. Ricardo, M.A, Clayton J, Sankaranarayanan R, Ferguson M, Seismic Acceleration Demands on Nonstructural Components Attached to Elastic and Inelastic Structures, ATC & SEI Conference on Improving the Seismic, 2009.
17. Taghavi S., Miranda E., Response assessment of nonstructural building elements, Pacific Earthquake Engineering Research Center, 2003.

10 APPENDIX

10.1 SLAB DESIGN

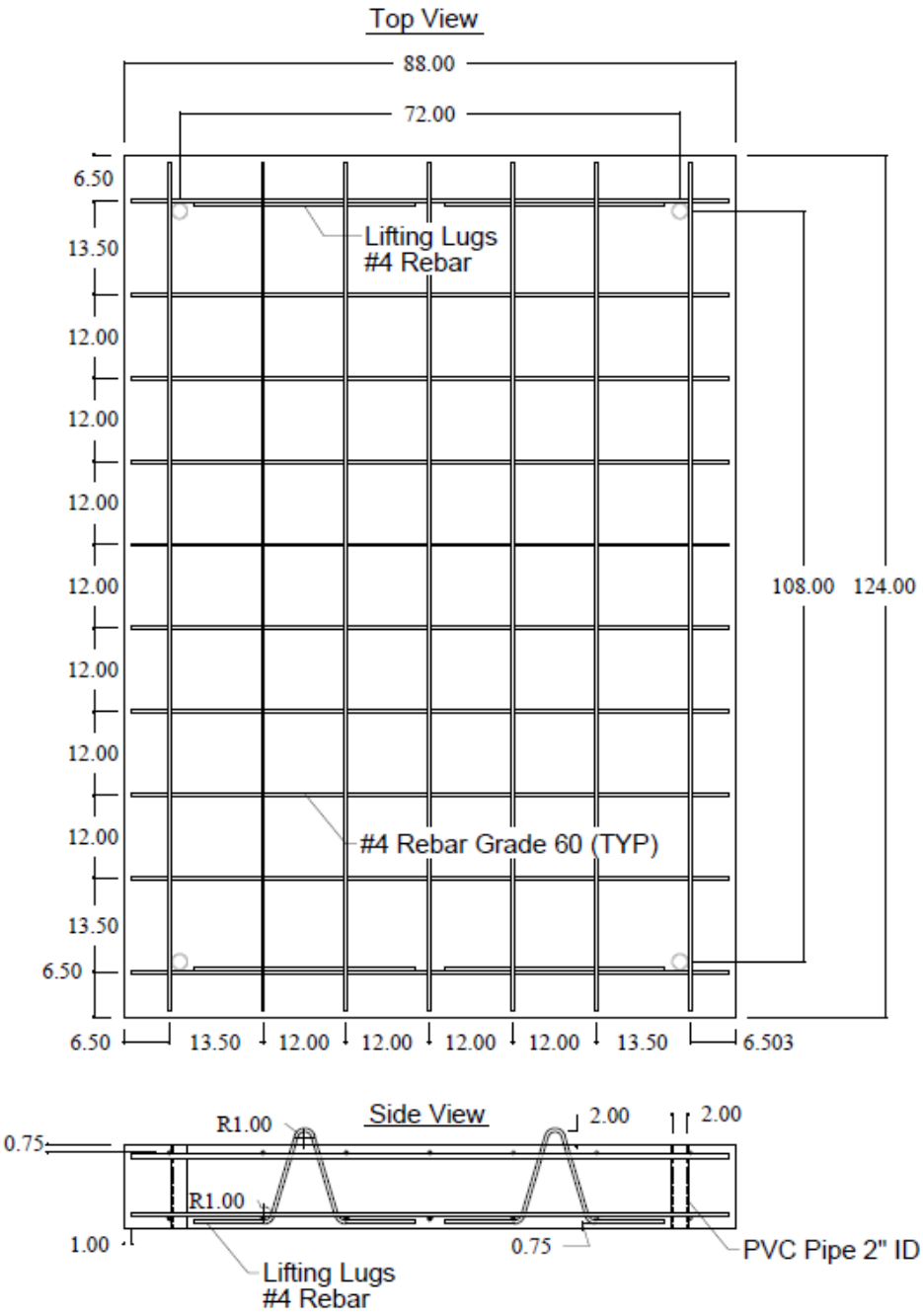

10.2 BRACKET DESIGN

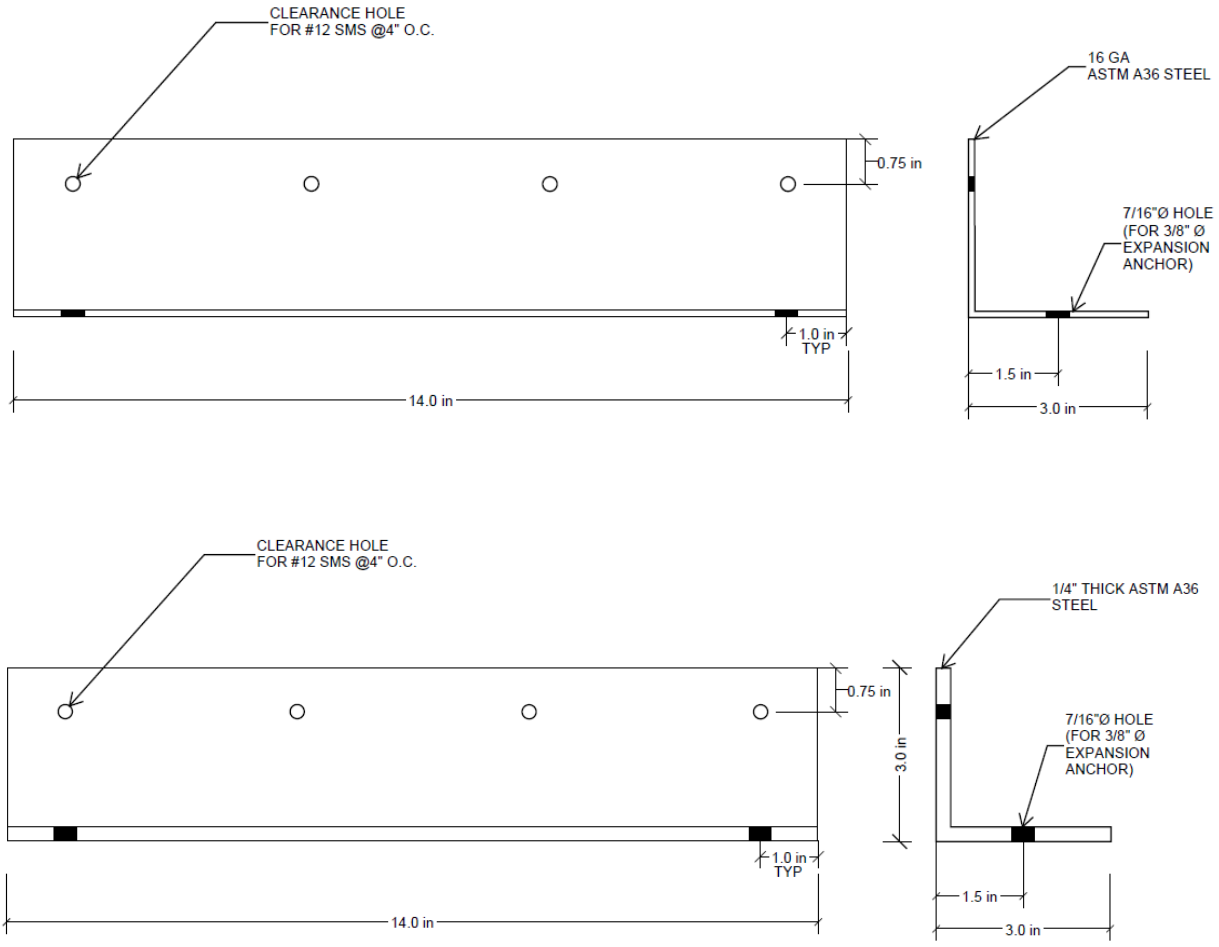

10.3 BATTERY RACK DIMENSIONS

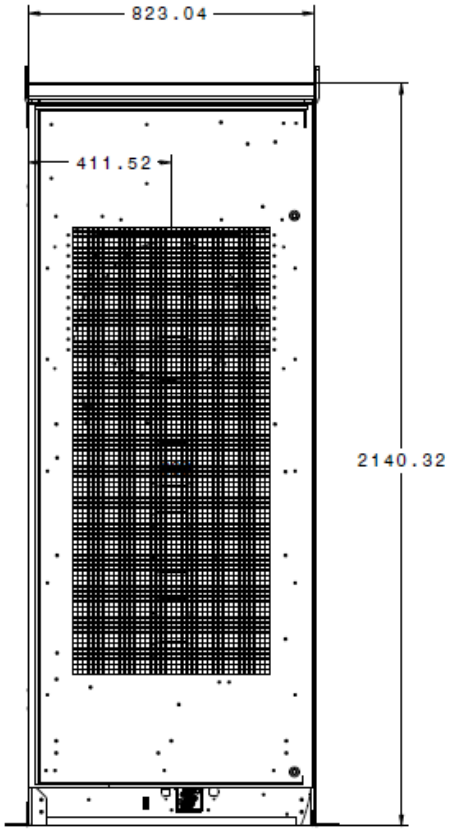

Front view
Scale: 1:10

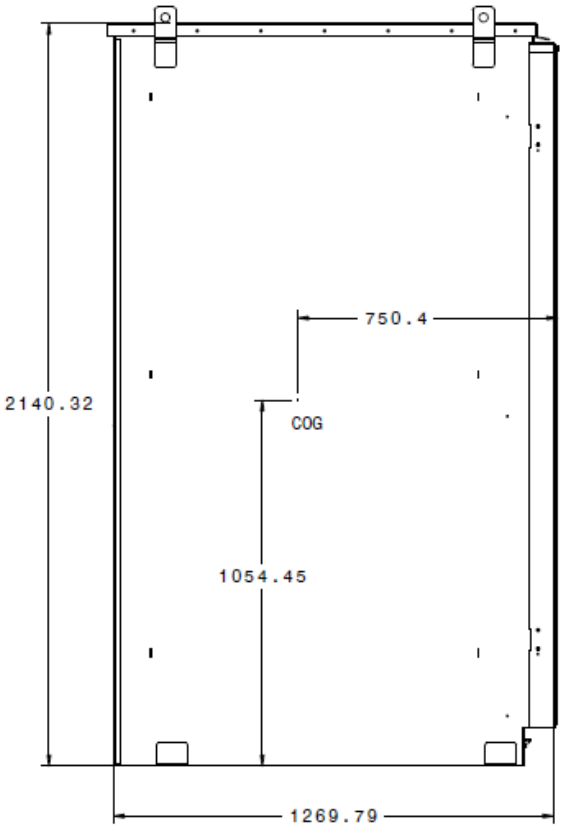

Left view
Scale: 1:10

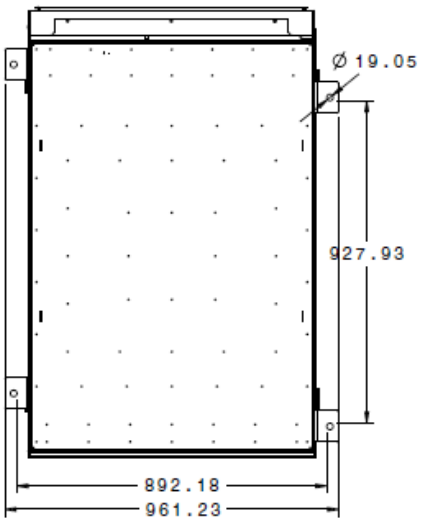

Bottom view
Scale: 1:10

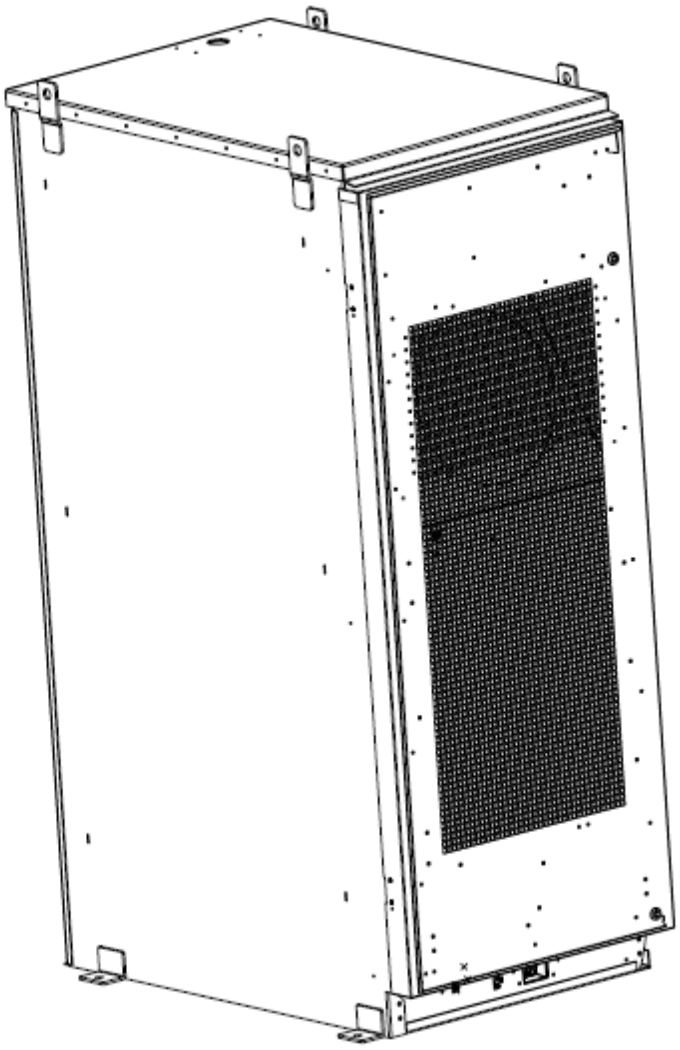

Isometric view
Scale: 1:10

10.4 ANCHOR INSTALLATION INSTRUCTIONS

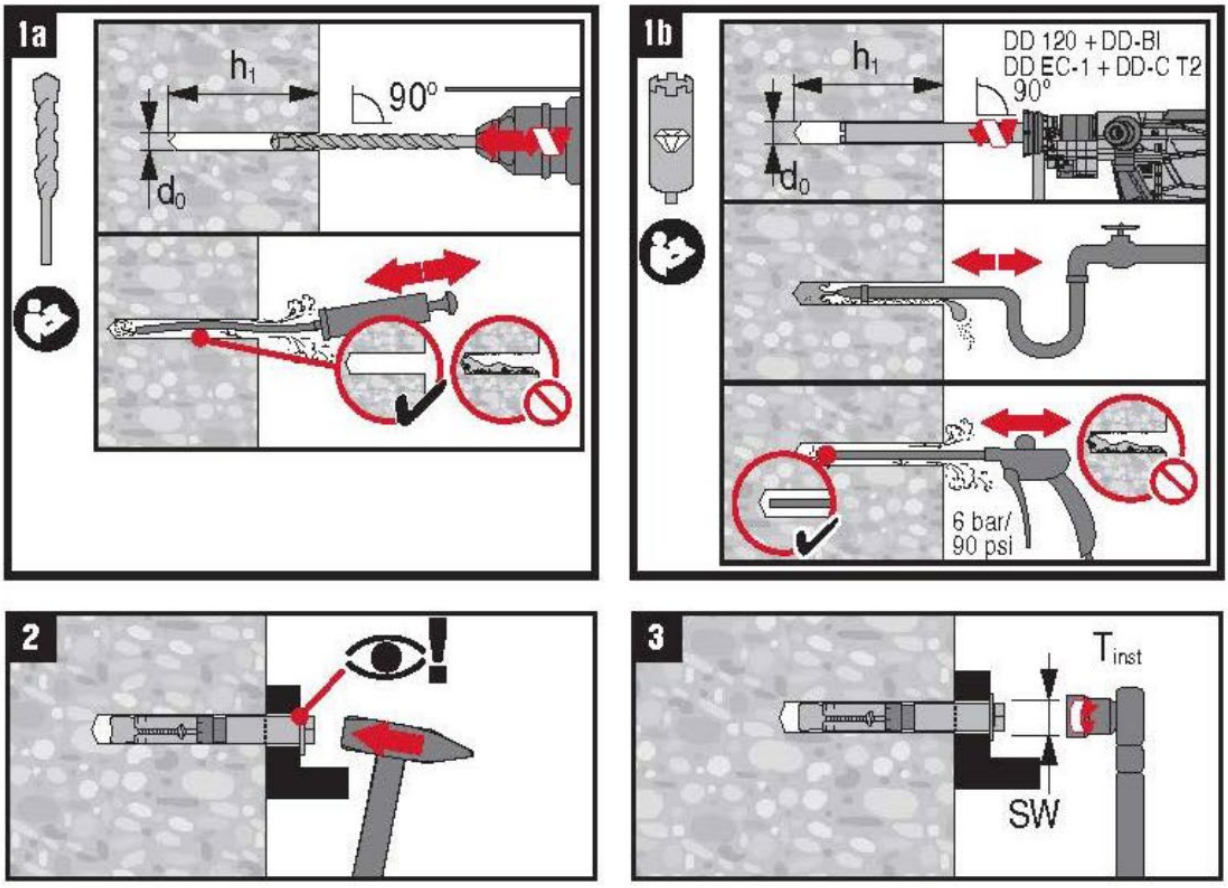

ICC-ES Report, ESR-1545 (Hilti, 2016) – "Hilti HSL-3 Carbon steel heavy duty expansion anchors for cracked and uncracked concrete.

10.5 INDIVIDUAL TEST SUMMARY PAGES

Testing Phase 2 – (2) Level 2 RP 72 Y direction

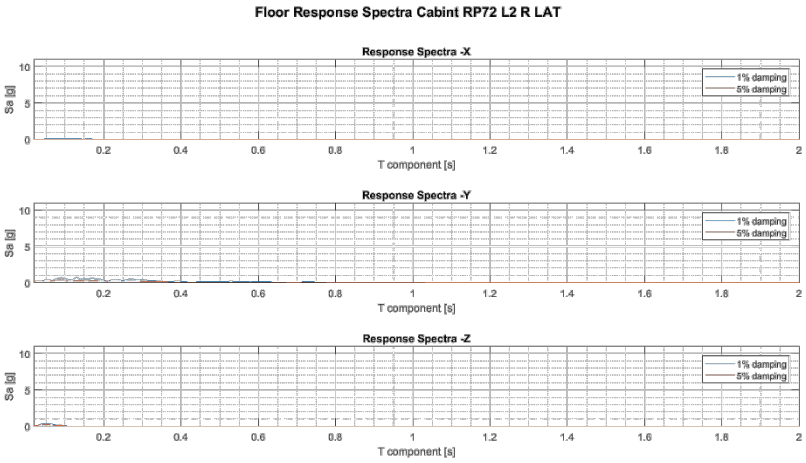

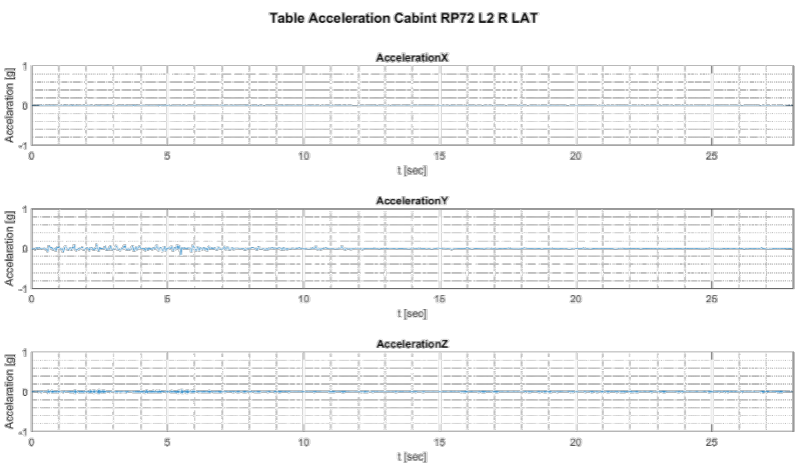

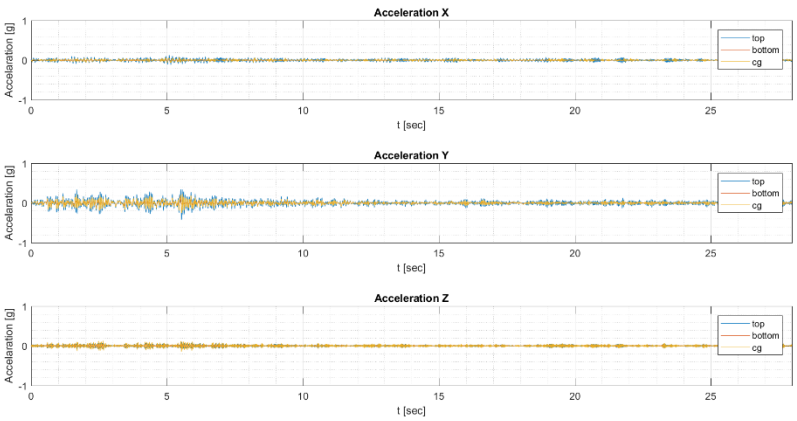

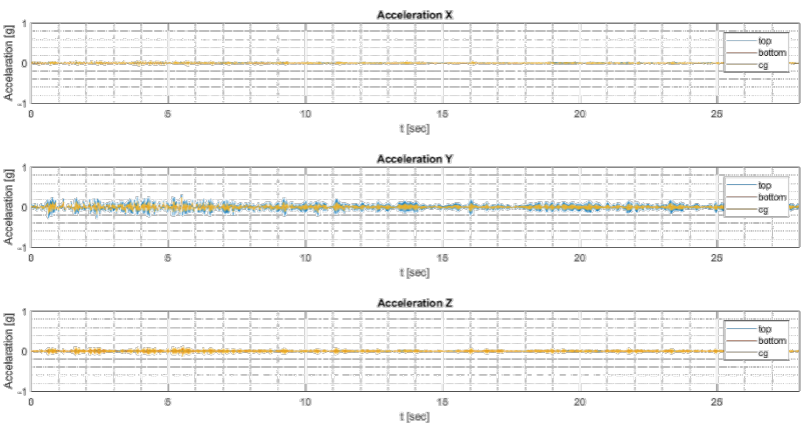

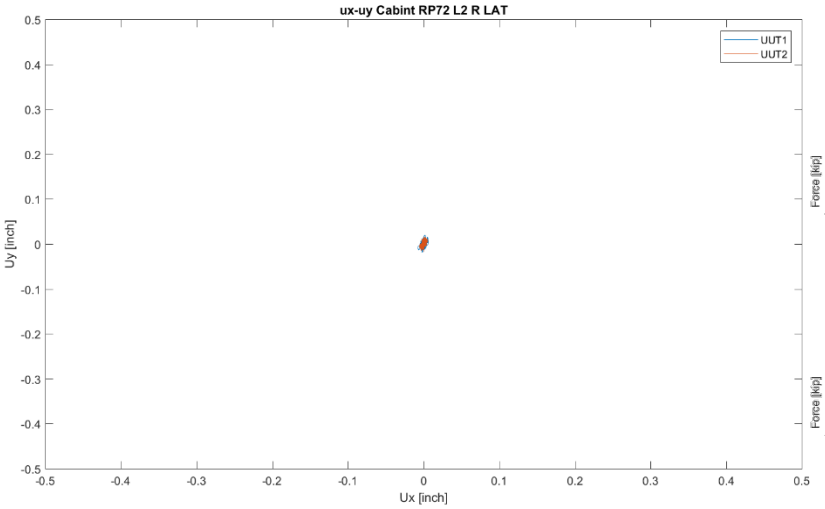

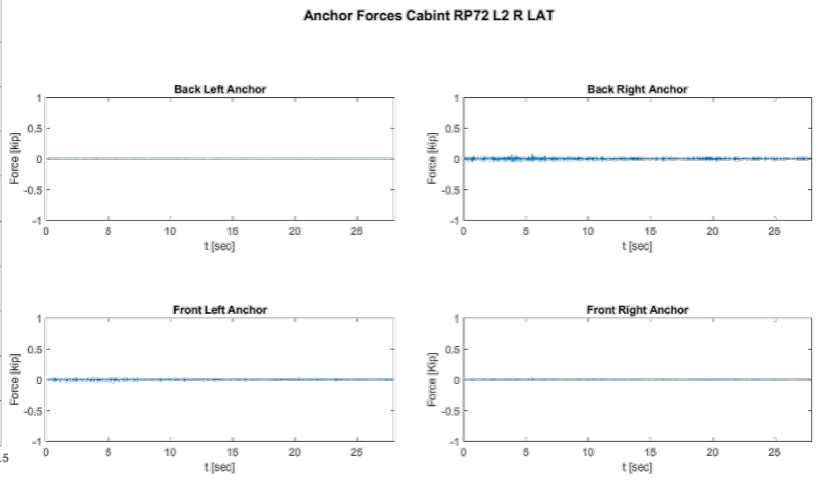

Testing Phase 2 – (3) Level 2 RP 475 Y direction

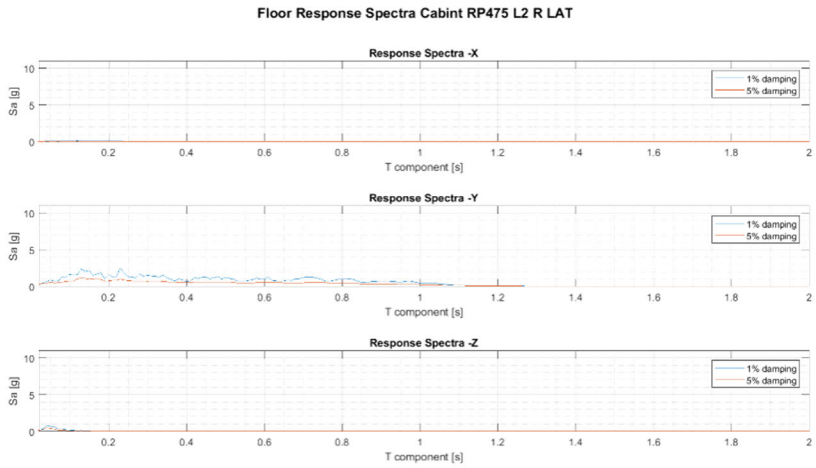

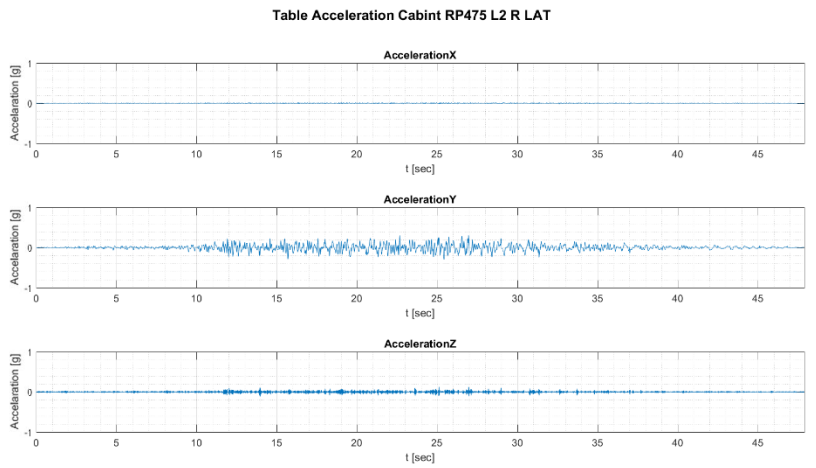

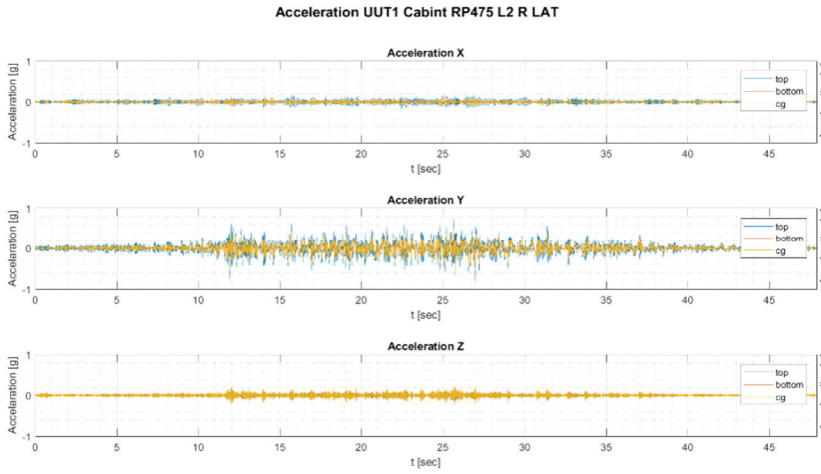

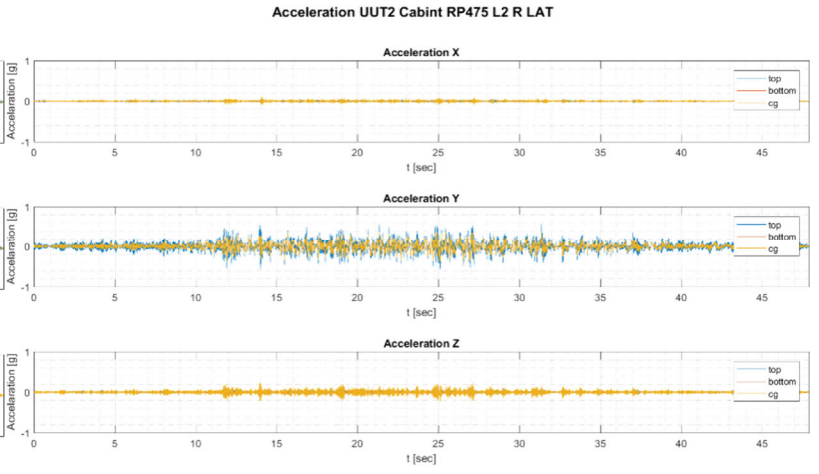

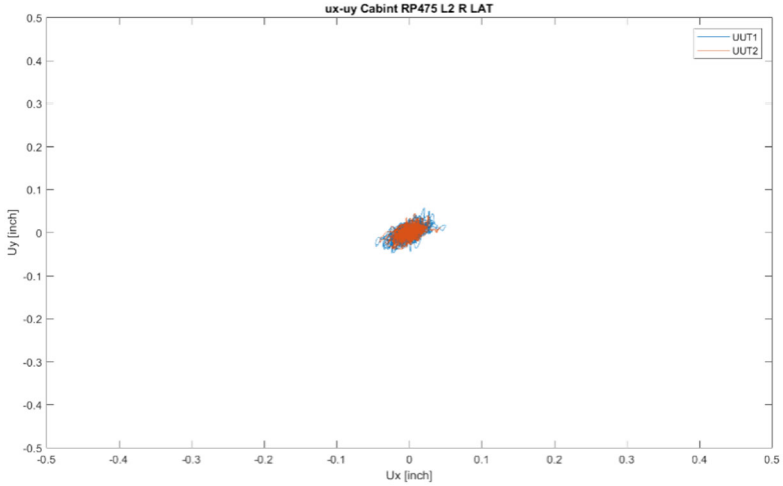

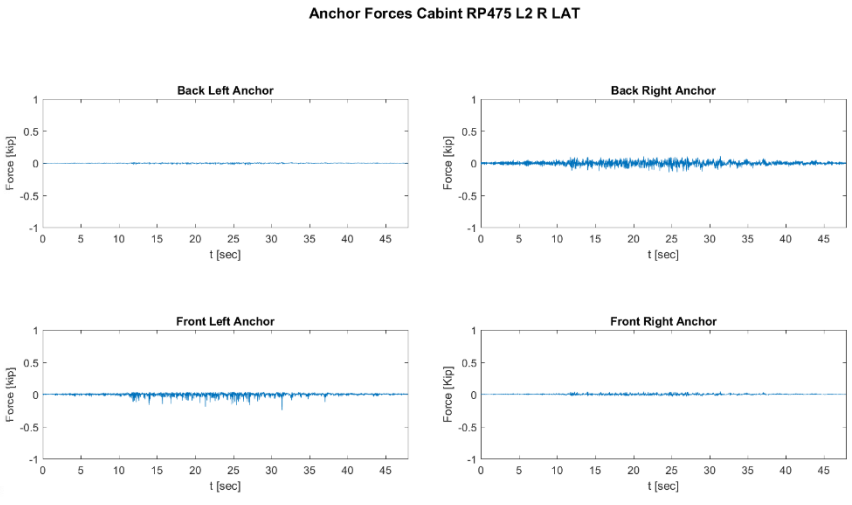

Testing Phase 2 – (4) Level 9 RP 475 Y direction

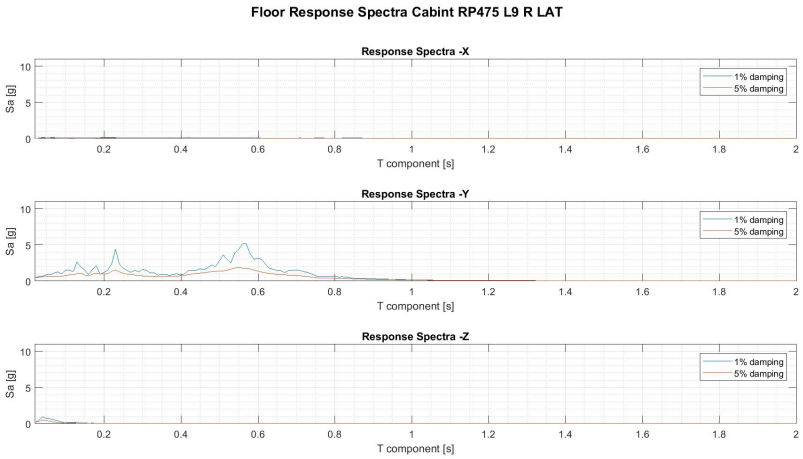

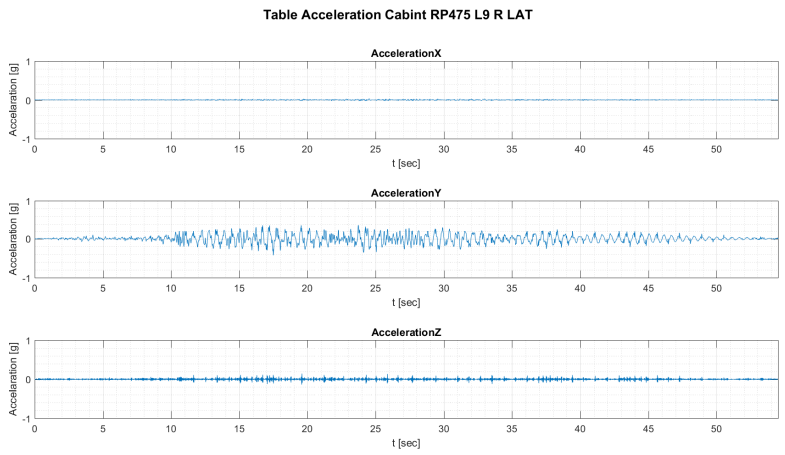

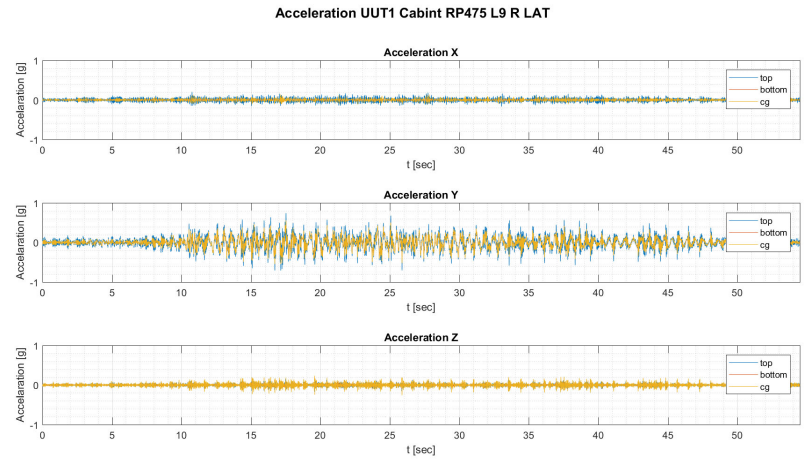

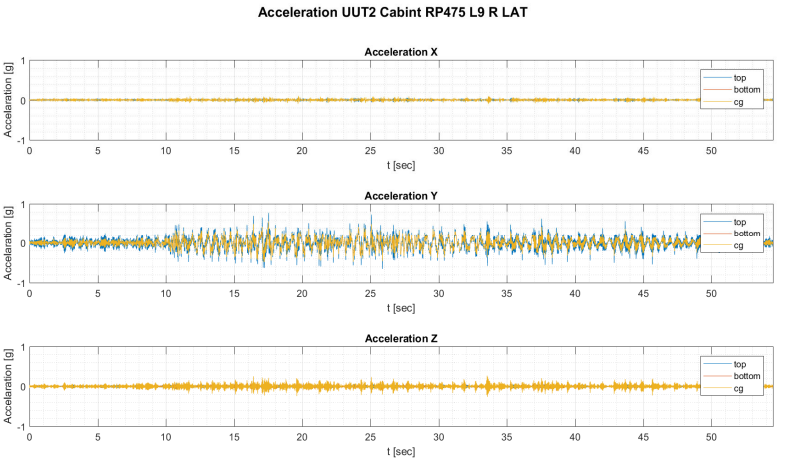

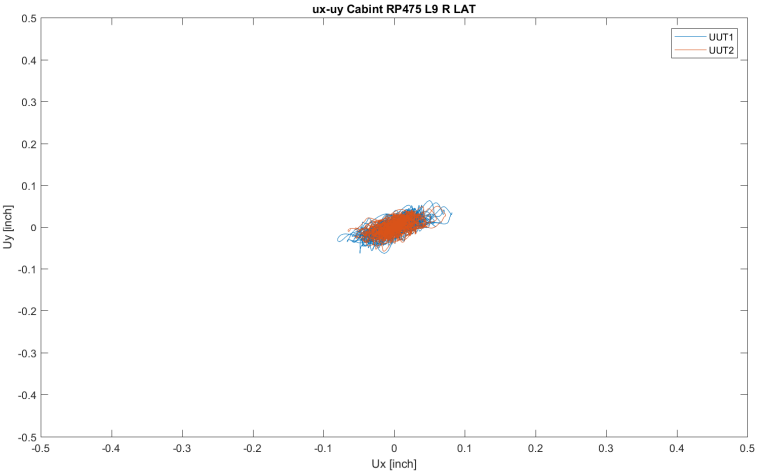

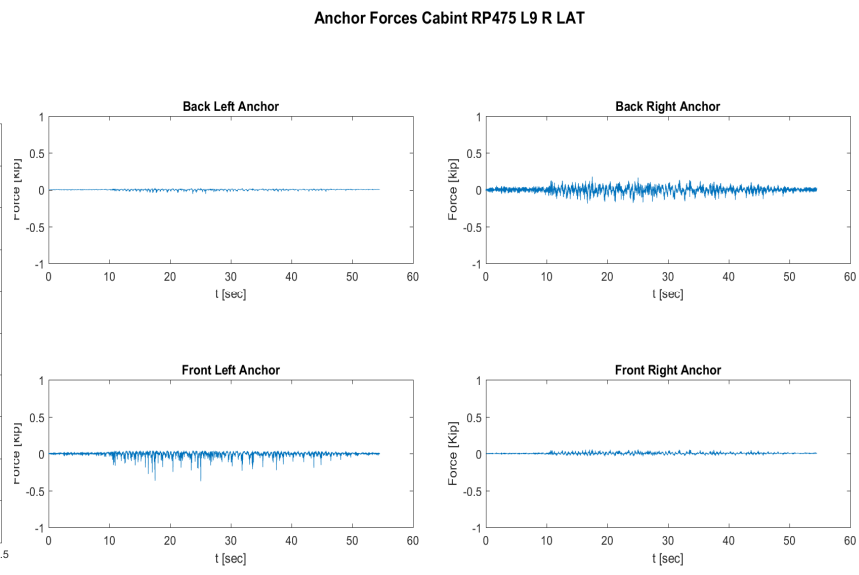

Testing Phase 2 – (5) Level 16 RP 475 Y direction

Floor Response Spectra Cabint RP475 L16 R LAT

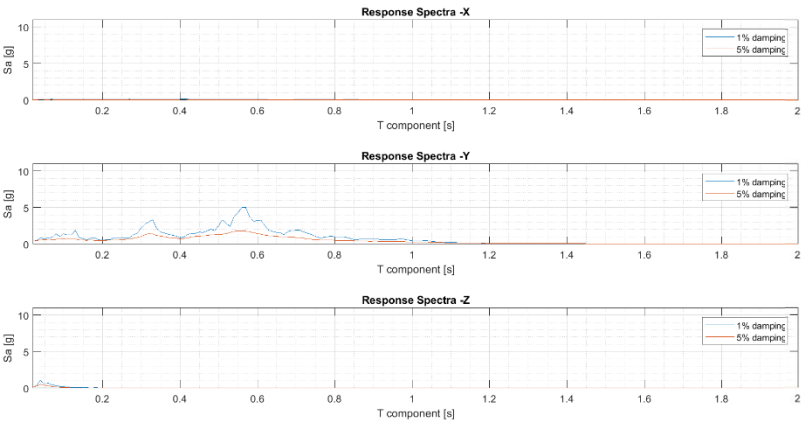

Table Acceleration Cabint RP475 L16 R LAT

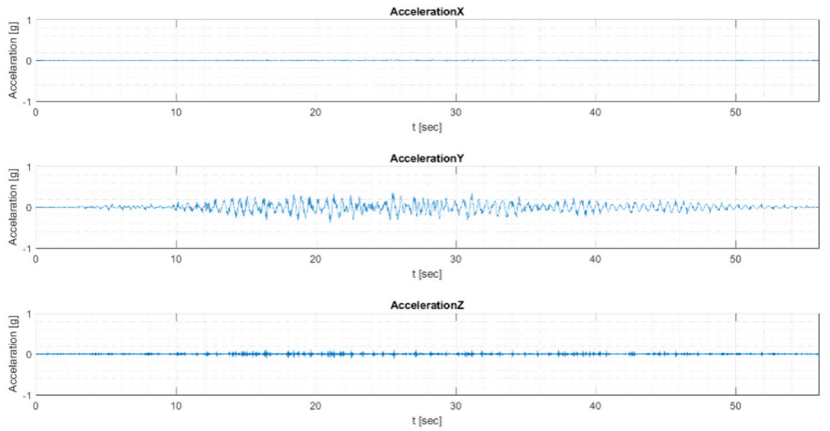

Acceleration UUT1 Cabint RP475 L16 R LAT

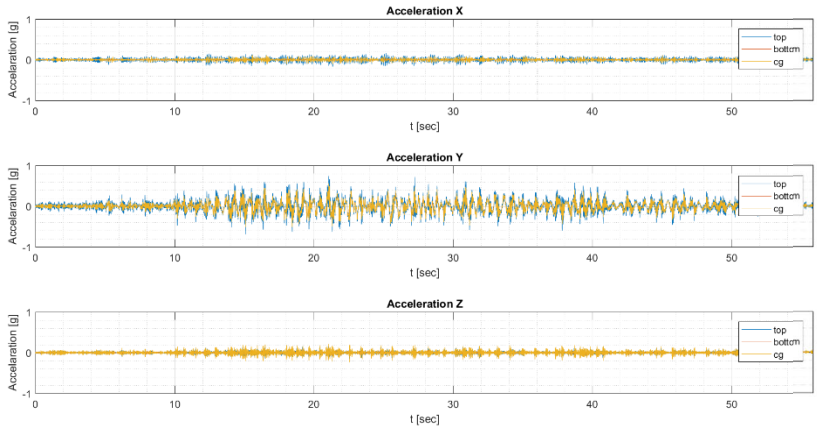

Acceleration UUT2 Cabint RP475 L16 R LAT

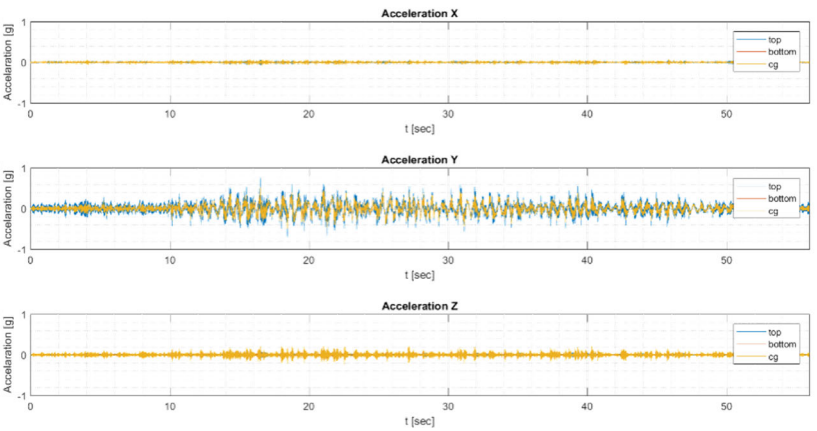

ux-uy Cabint RP475 L16 R LAT

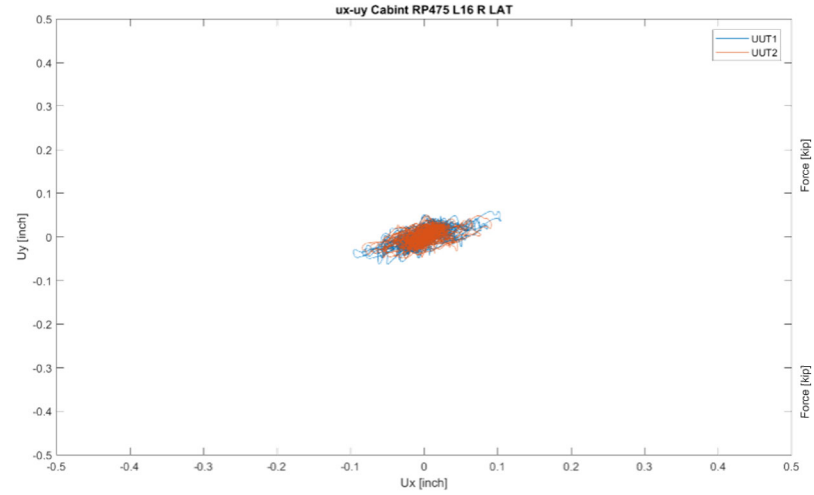

Anchor Forces Cabint RP475 L16 R LAT

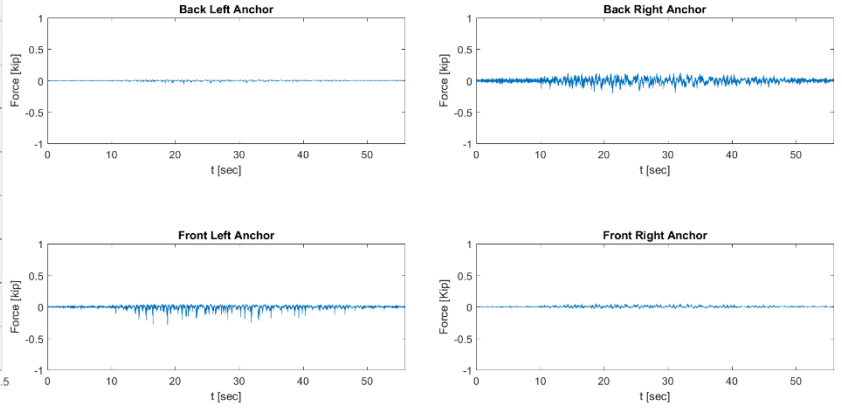

Testing Phase 2 – (6) Level 2 RP 475 X direction

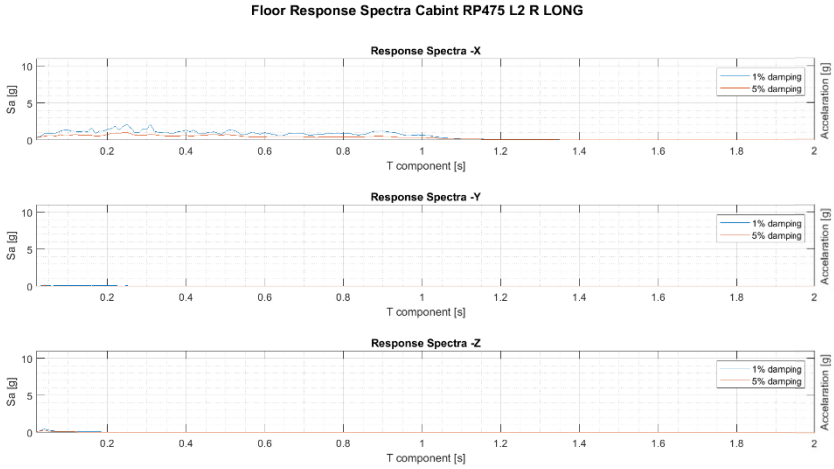

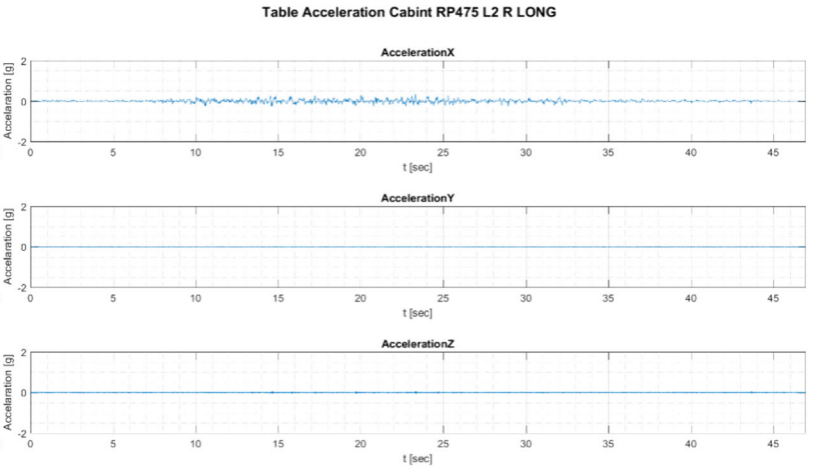

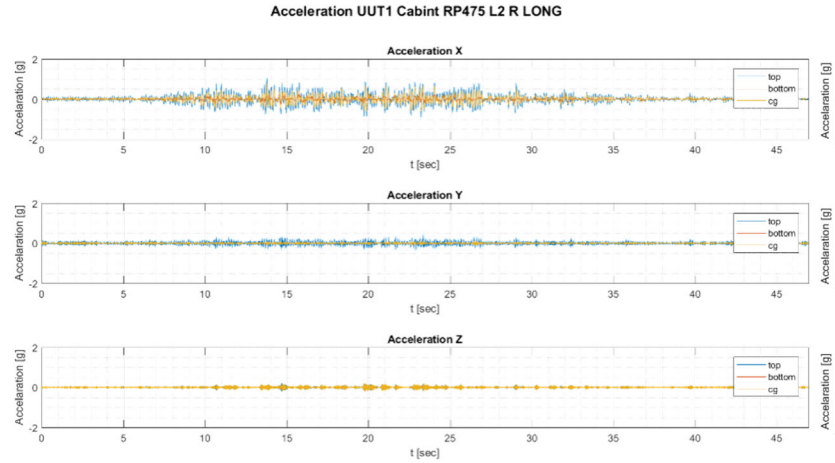

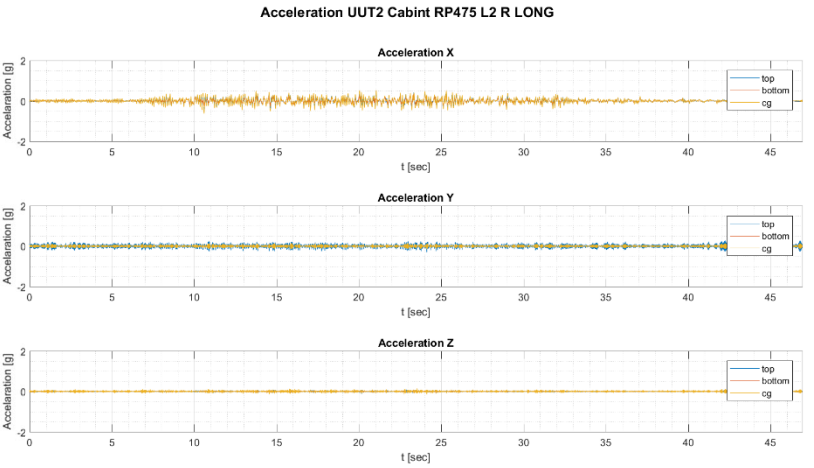

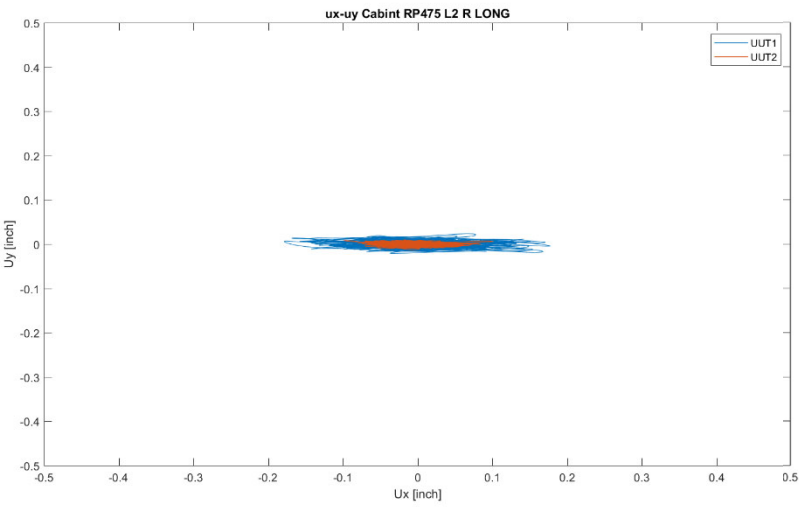

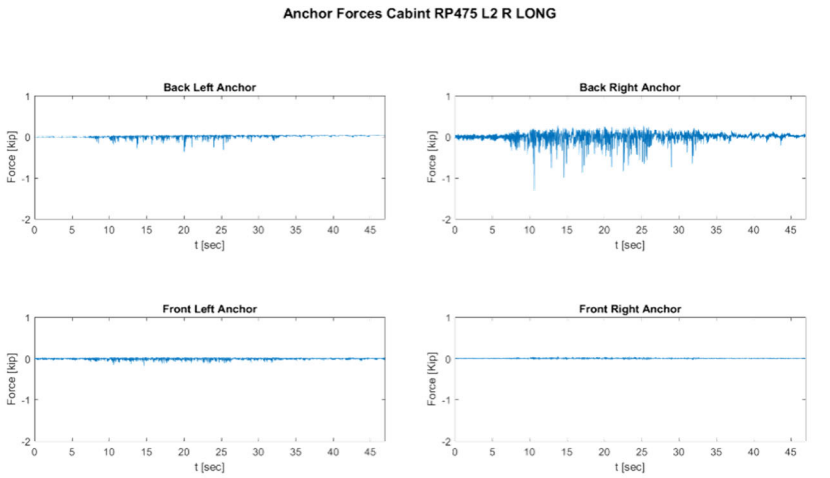

Testing Phase 2 – (7) Level 9 RP 475 X direction

Floor Response Spectra Cabint RP475 L9 R LONG

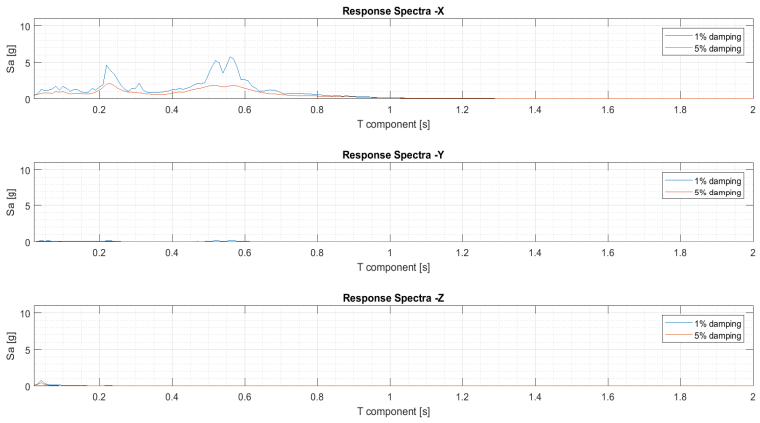

Table Acceleration Cabint RP475 L9 R LONG

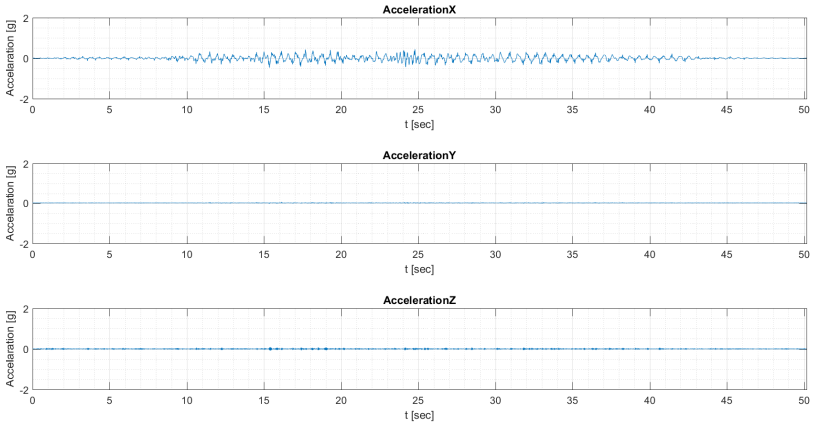

Acceleration UUT1 Cabint RP475 L9 R LONG

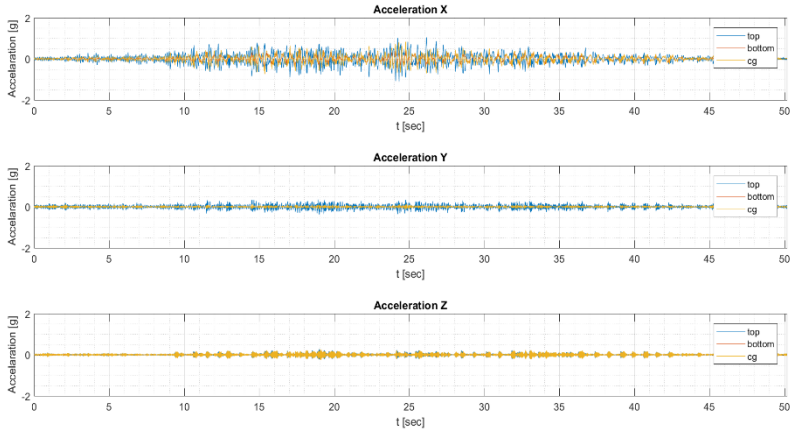

Acceleration UUT2 Cabint RP475 L9 R LONG

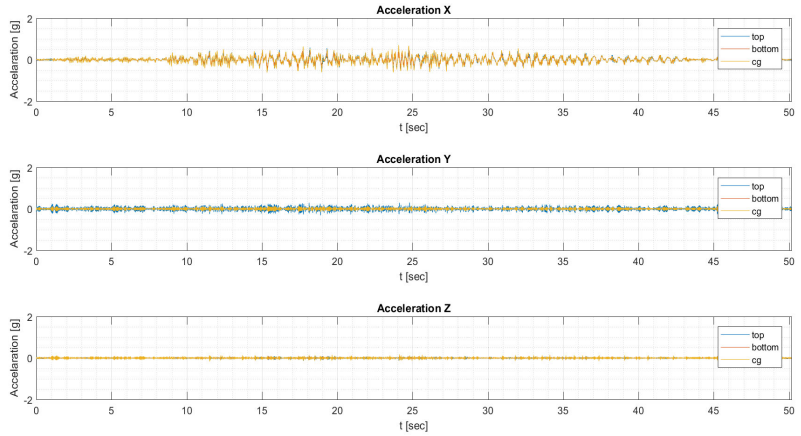

Anchor Forces Cabint RP475 L9 R LONG

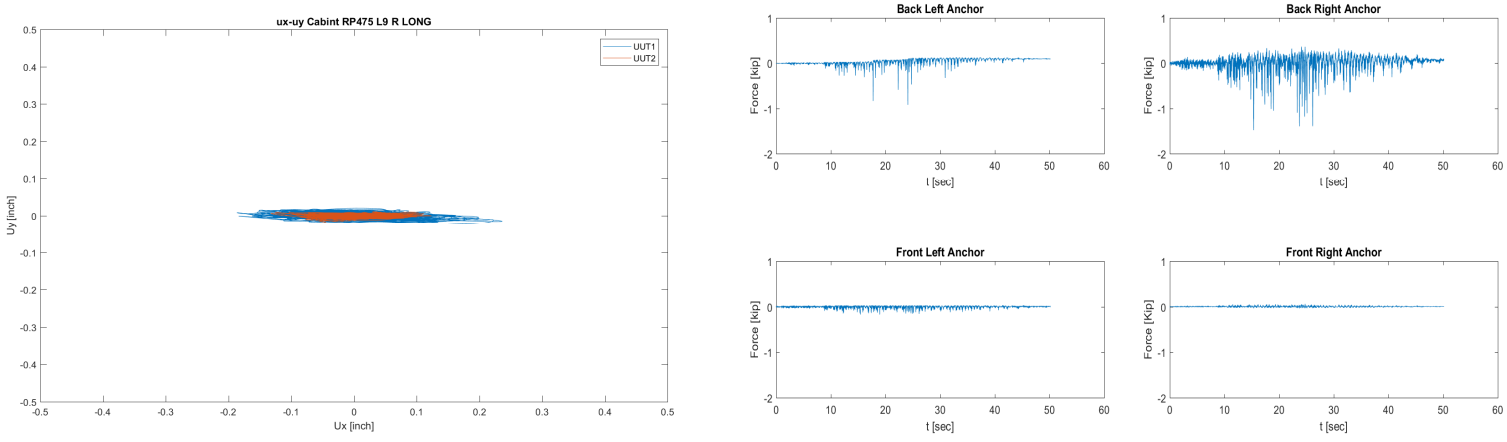

Testing Phase 2 – (8) Level 16 RP 475 X direction

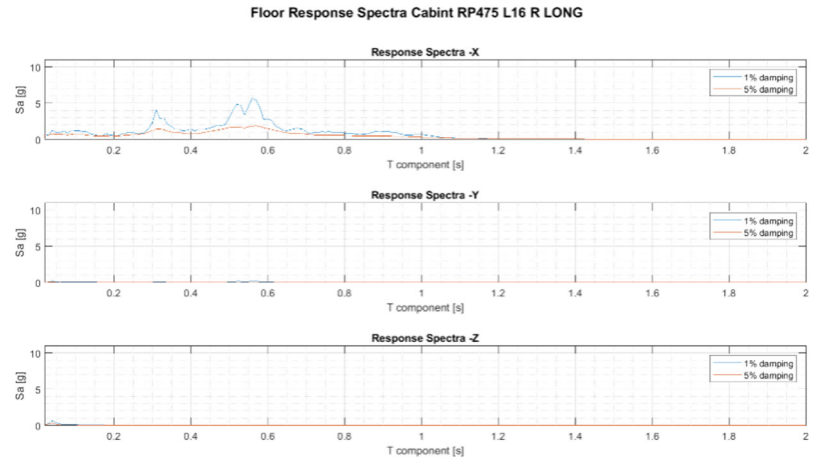

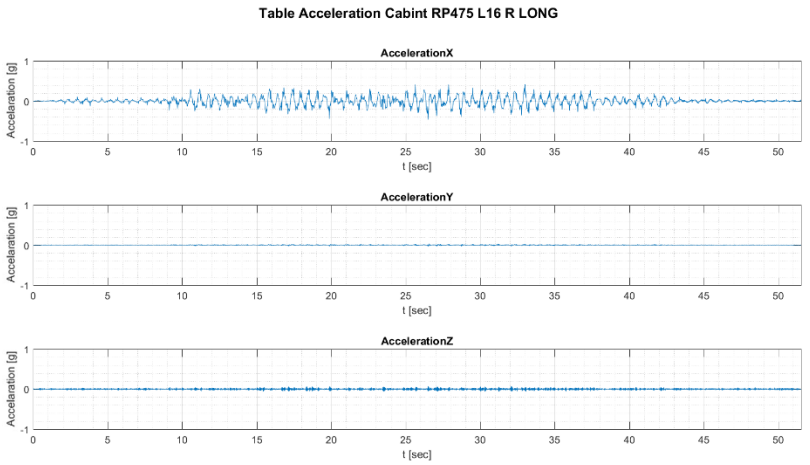

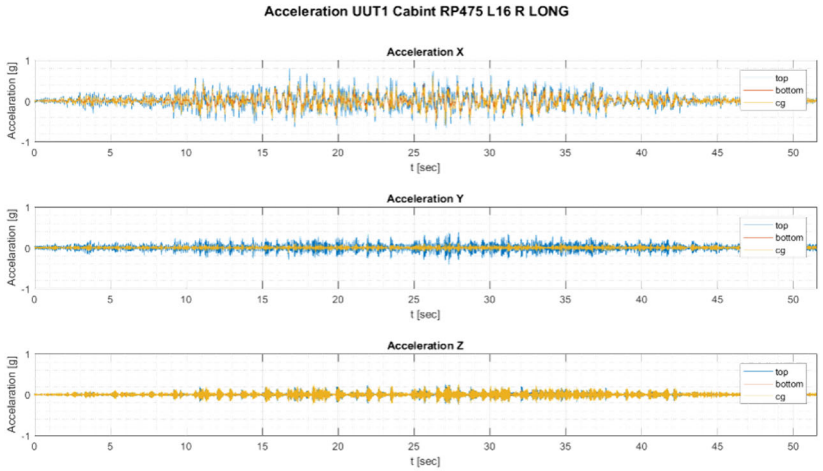

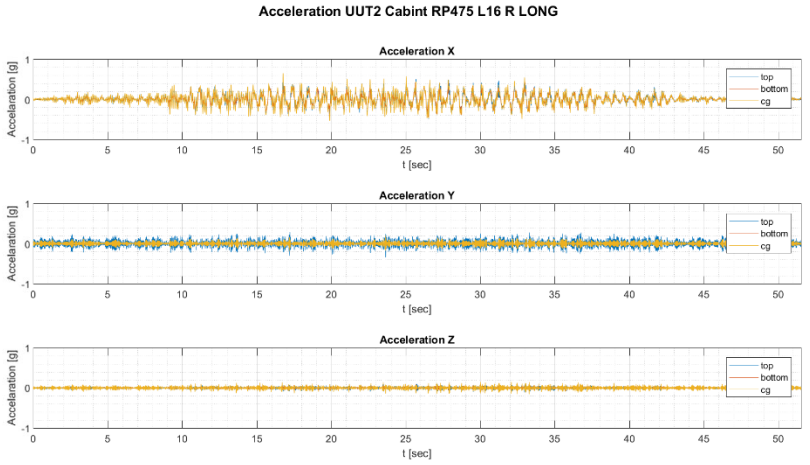

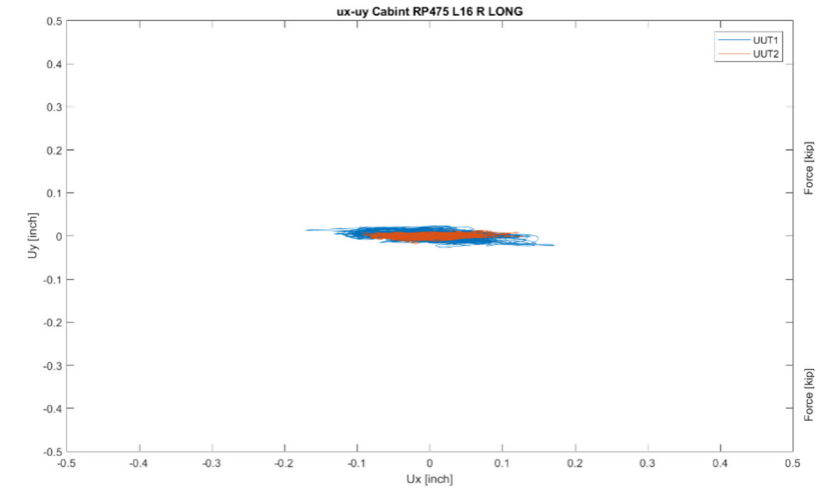

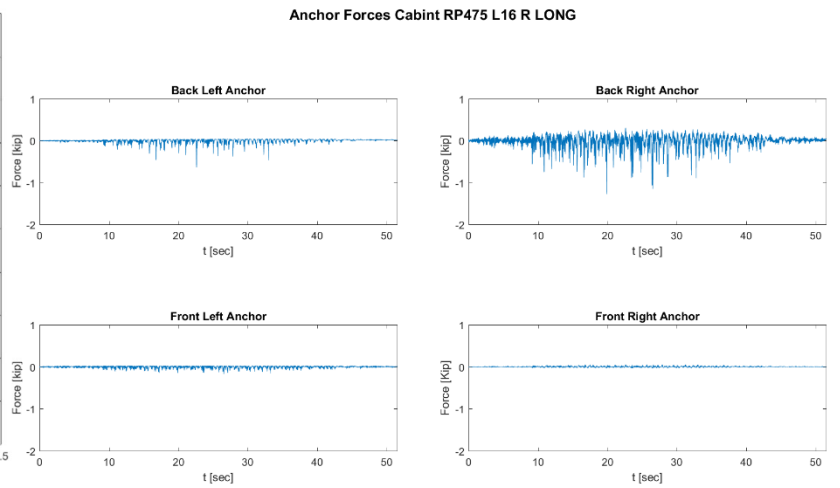

Testing Phase 2 – (9) Level 2 RP 475 XY direction

Floor Response Spectra Cabint RP475 L2 R LAT LONG

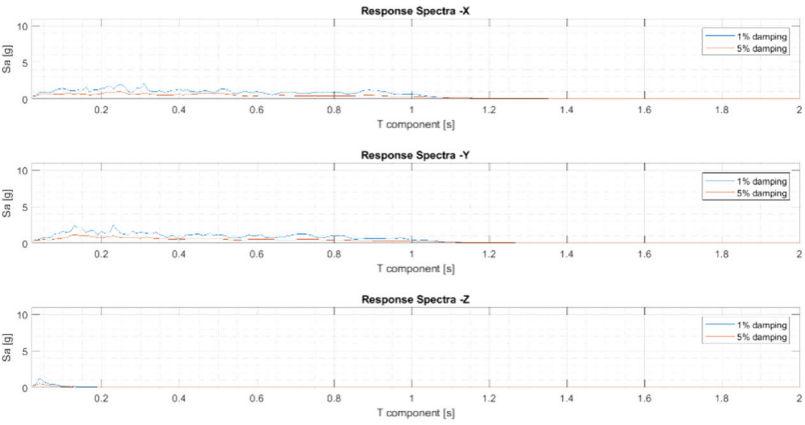

Table Acceleration Cabint RP475 L2 R LAT LONG

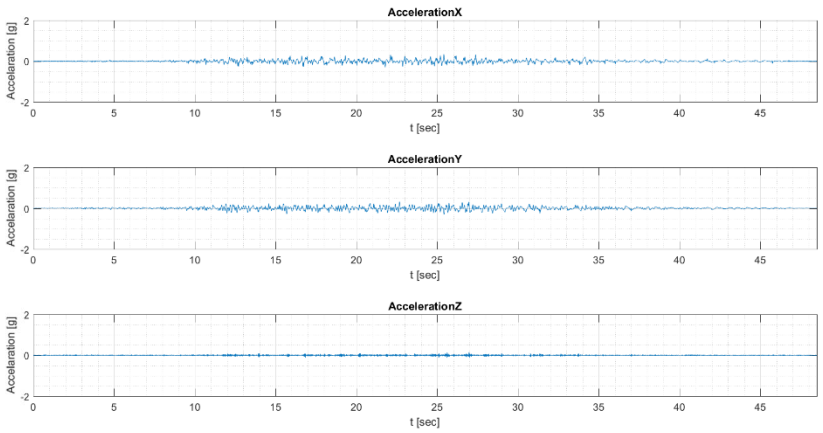

Acceleration UUT1 Cabint RP475 L2 R LAT LONG

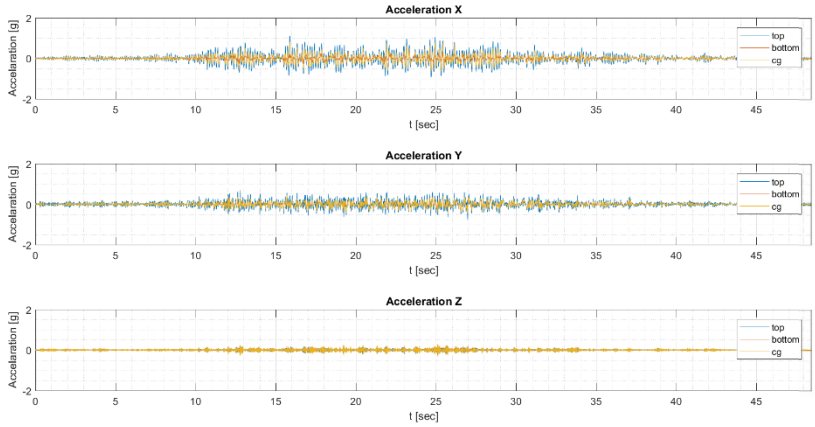

Acceleration UUT2 Cabint RP475 L2 R LAT LONG

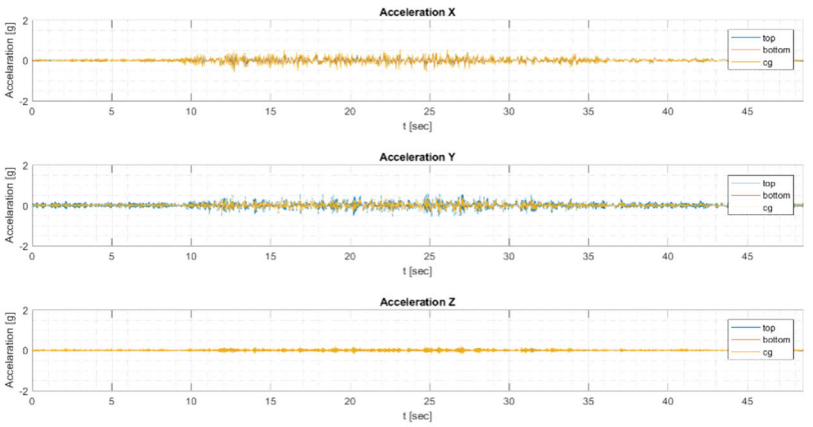

ux-uy Cabint RP475 L2 R LAT LONG

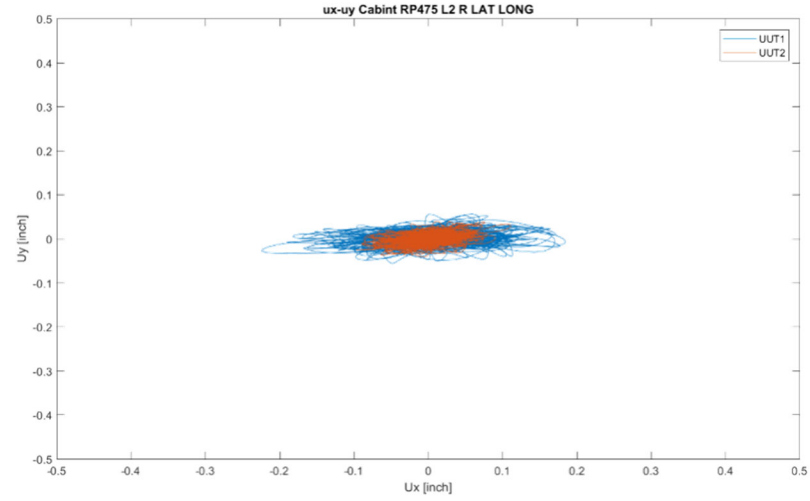

Anchor Forces Cabint RP475 L2 R LAT LONG

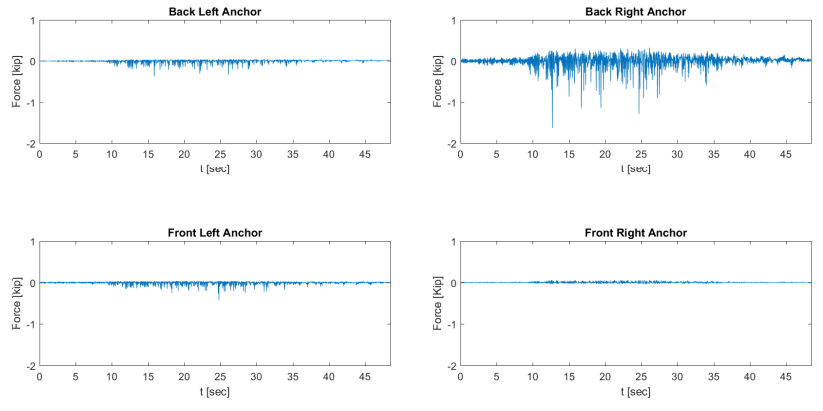

Testing Phase 2 – (10) Level 9 RP 475 XY direction

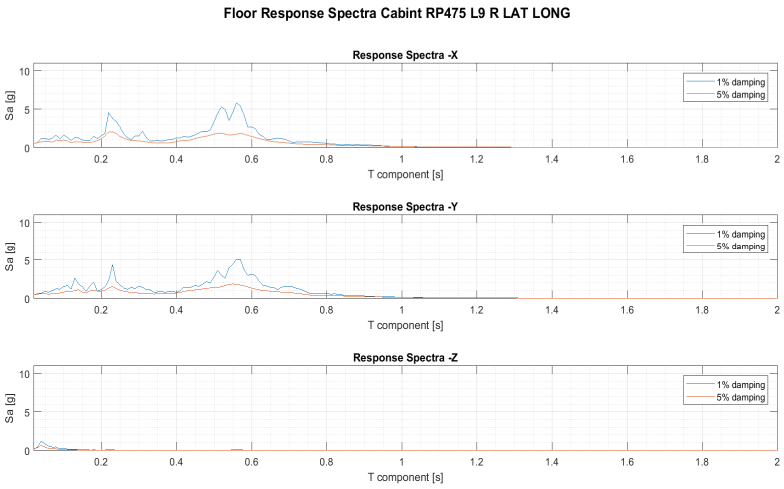

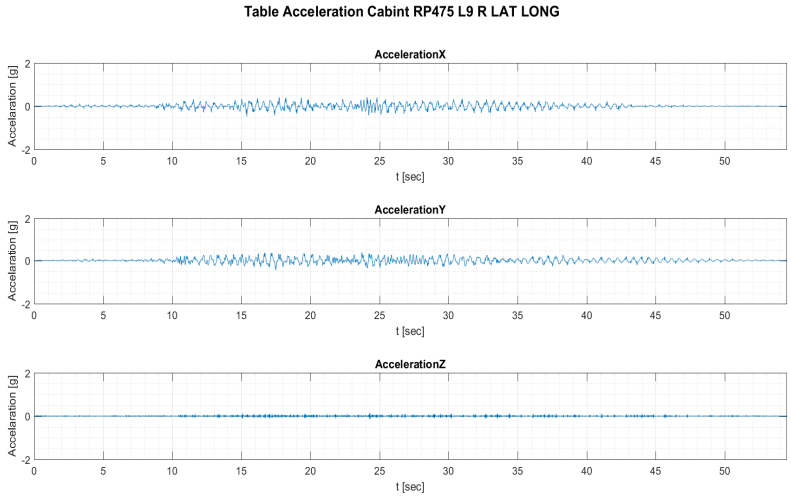

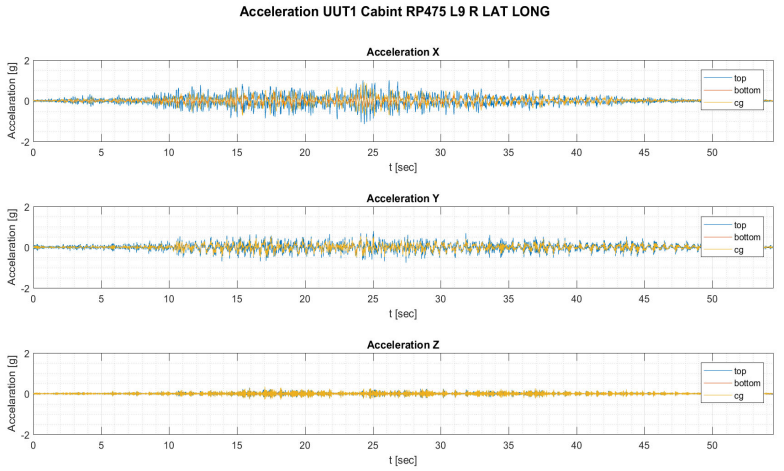

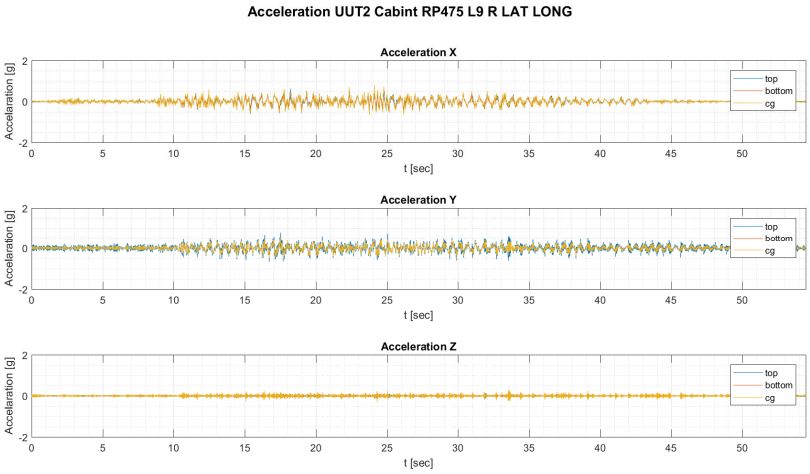

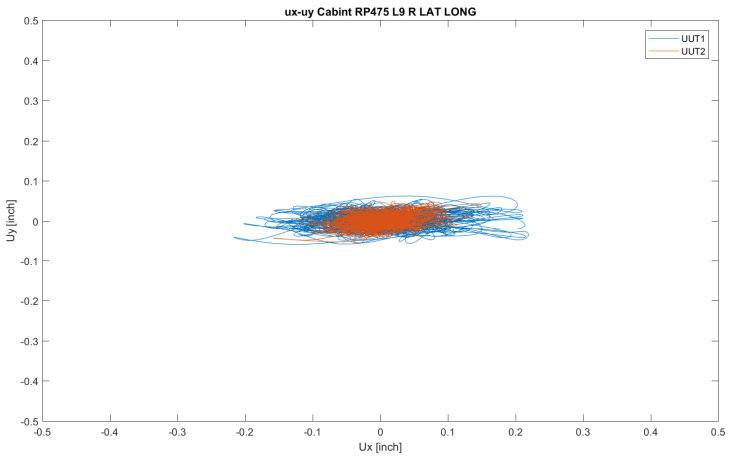

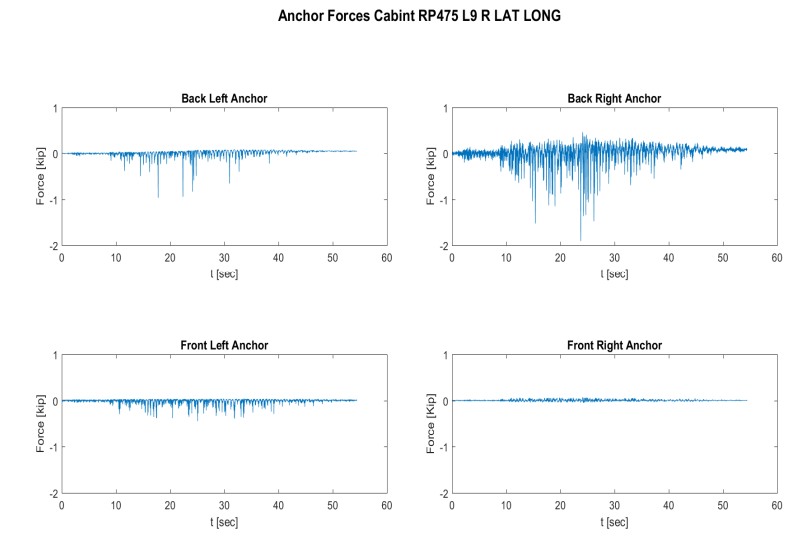

Testing Phase 2 – (11) Level 16 RP 475 XY direction

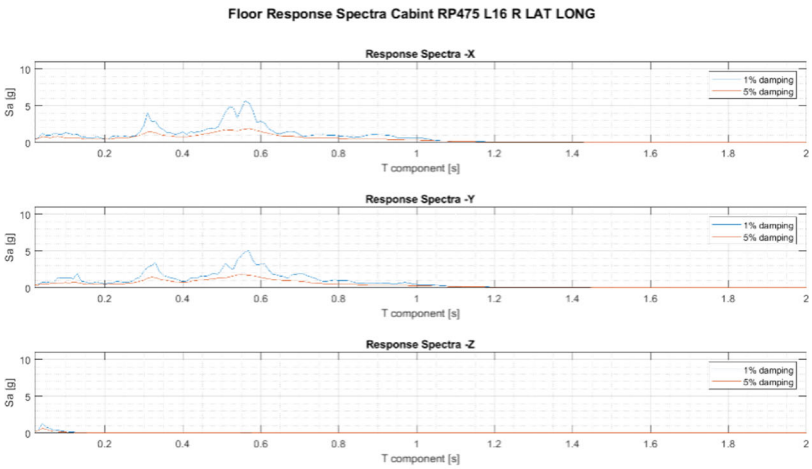

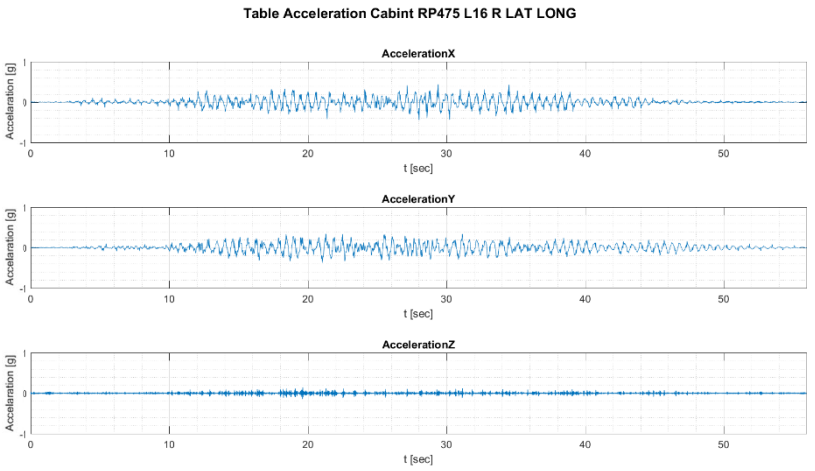

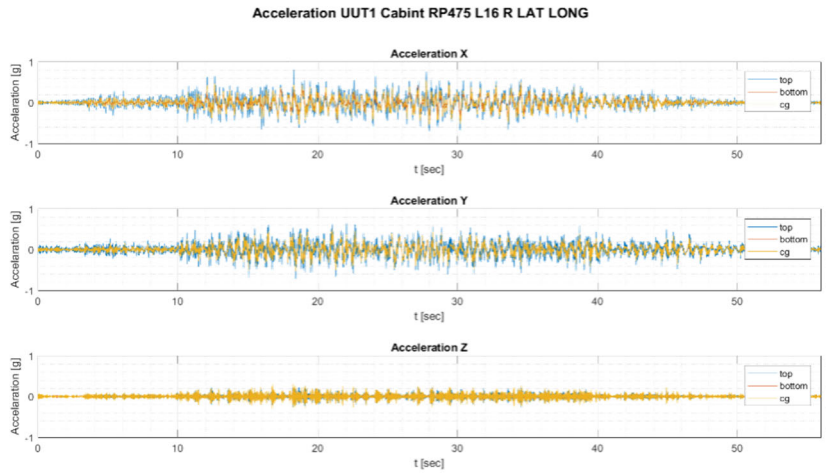

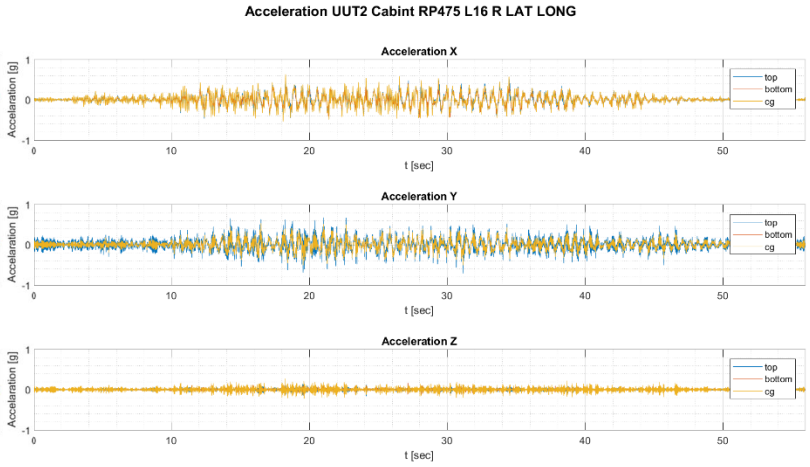

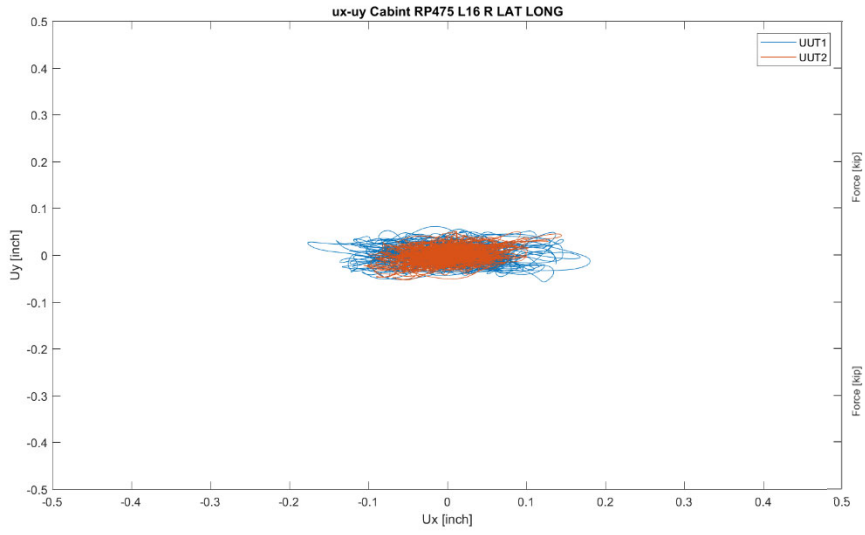

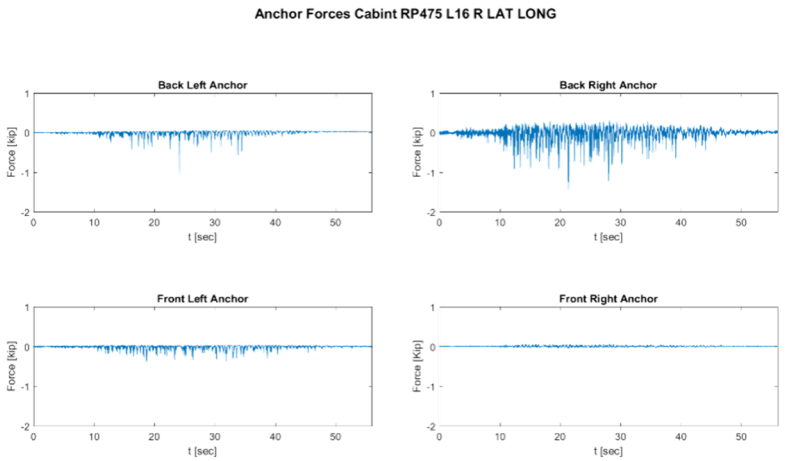

Testing Phase 2 – (12) Level 2 RP 475 XYZ direction

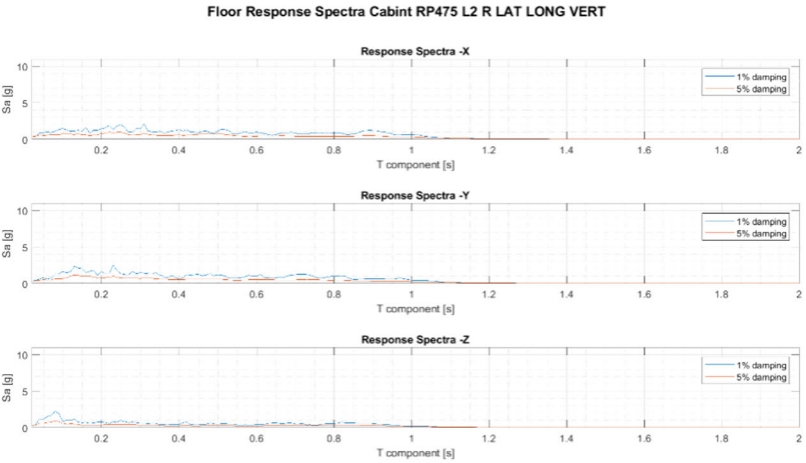

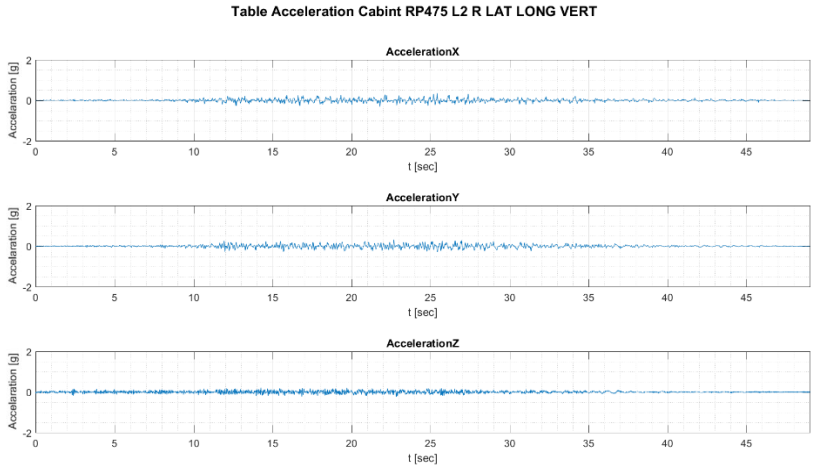

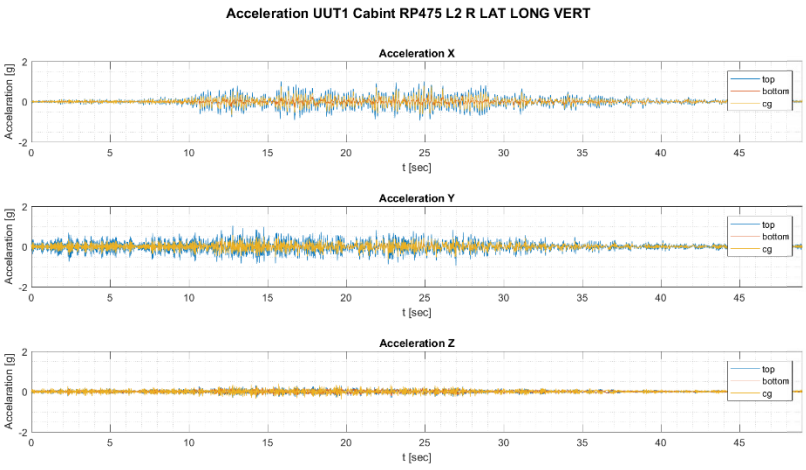

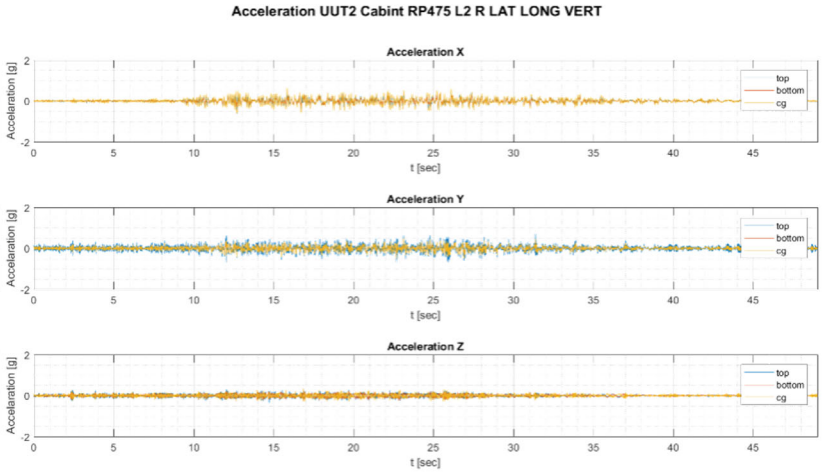

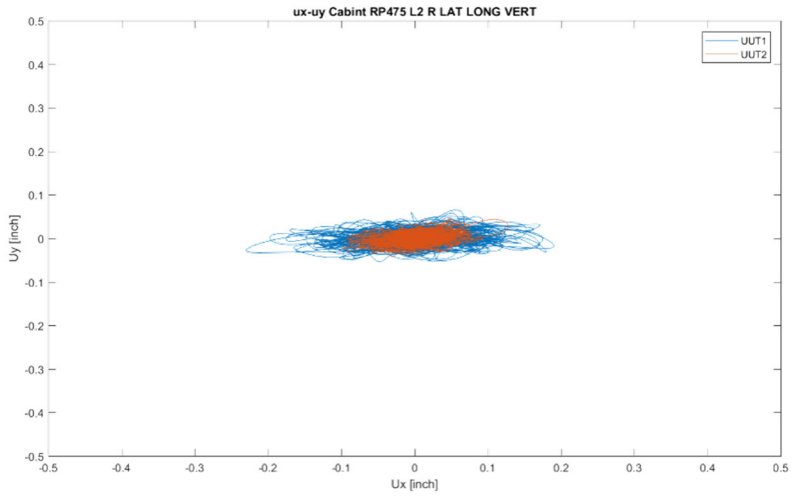

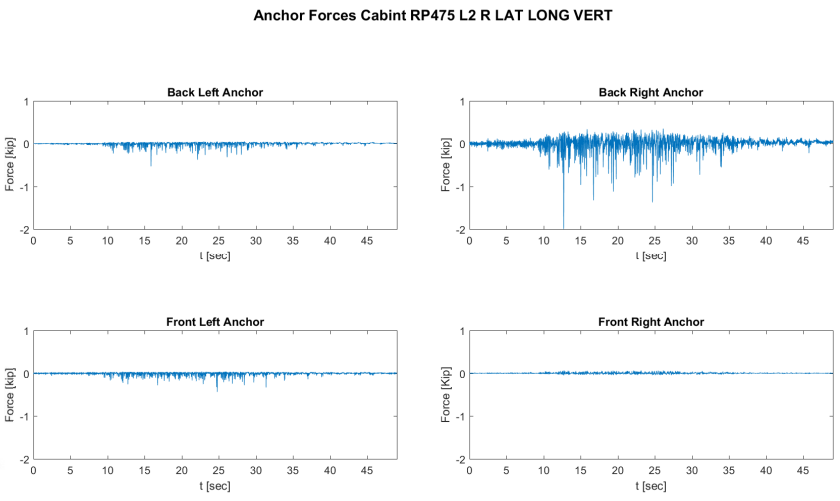

Testing Phase 2 – (13) Level 9 RP 475 XYZ direction

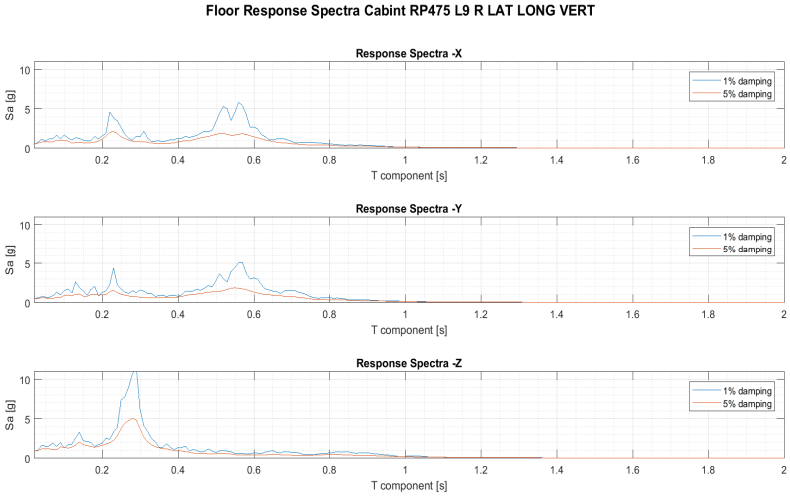

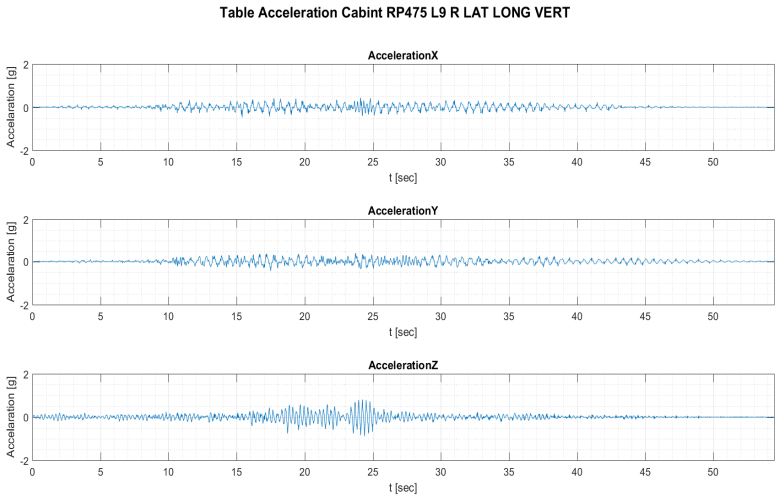

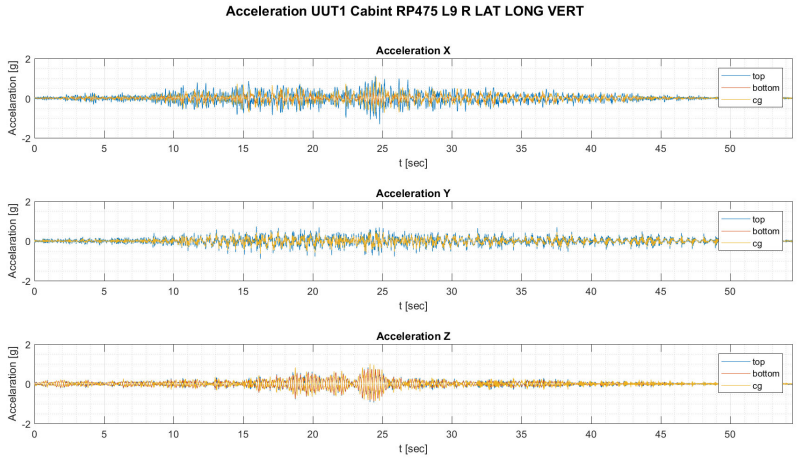

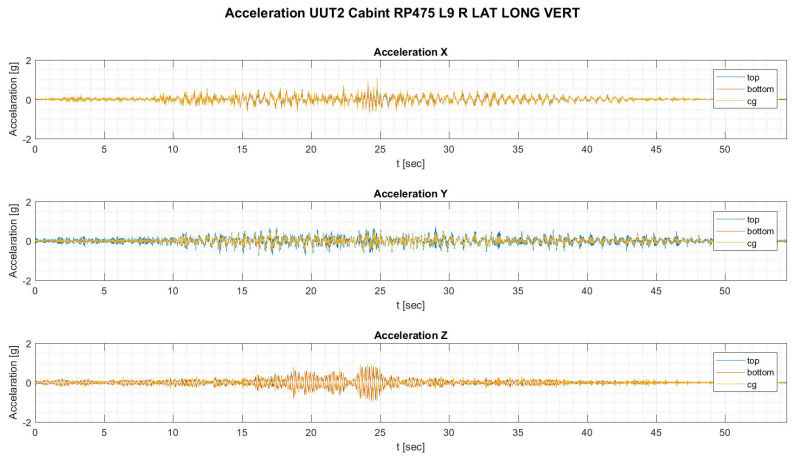

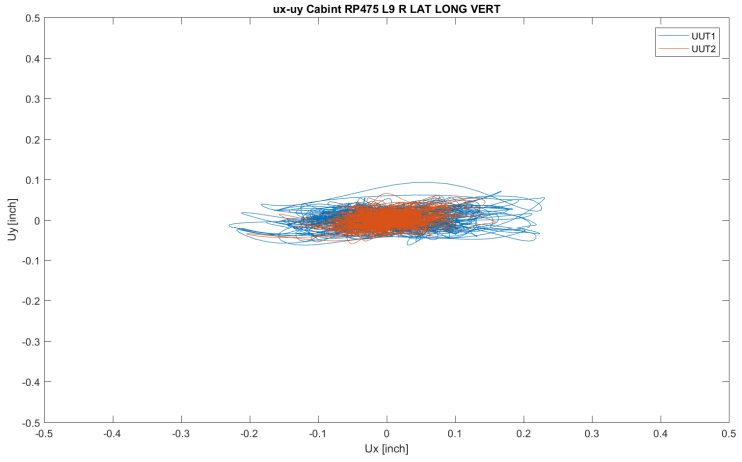

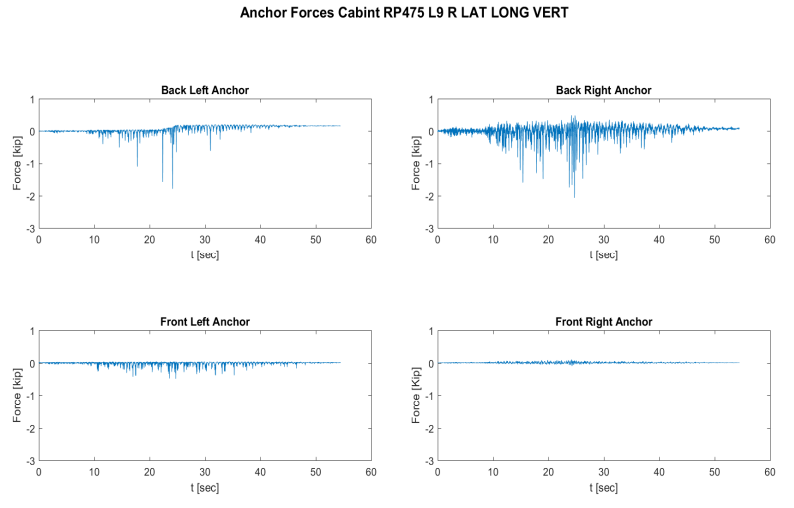

Testing Phase 2 – (14) Level 2 RP 475 X direction – SM

Floor Response Spectra Cabint RP475 L2 SM LONG 1

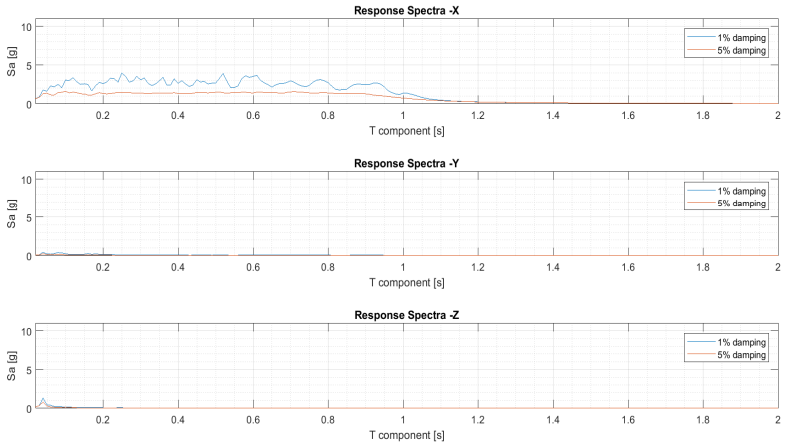

Table Acceleration Cabint RP475 L2 SM LONG 1

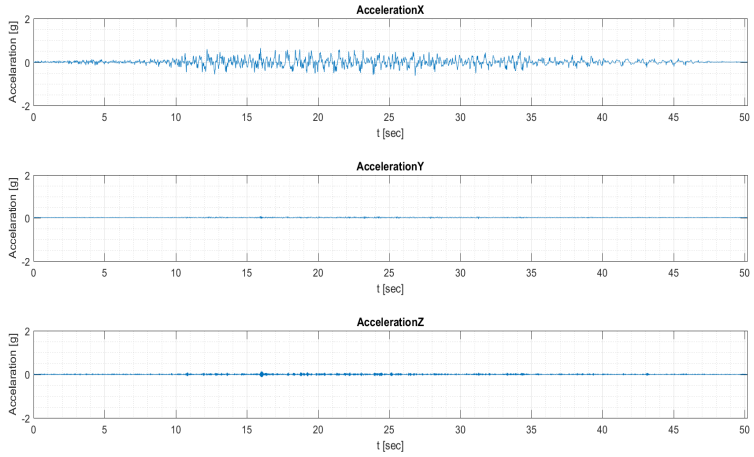

Acceleration UUT1 Cabint RP475 L2 SM LONG 1

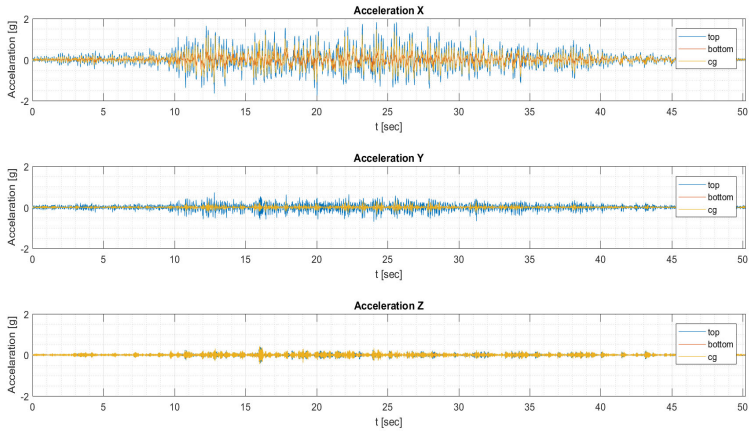

Acceleration UUT2 Cabint RP475 L2 SM LONG 1

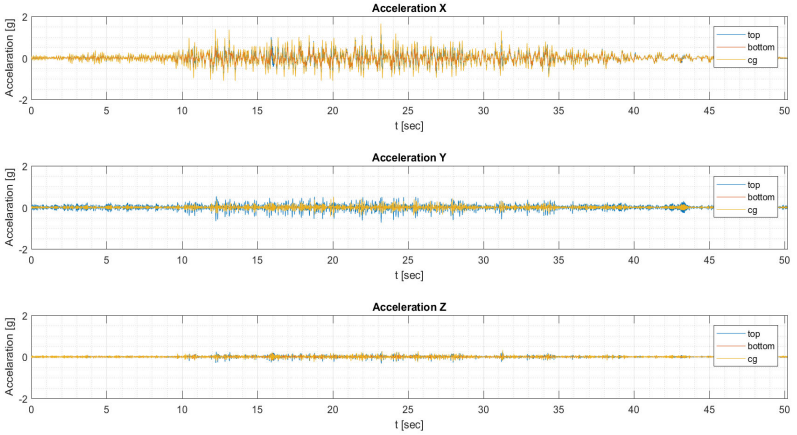

ux-uy Cabint RP475 L2 SM LONG 1

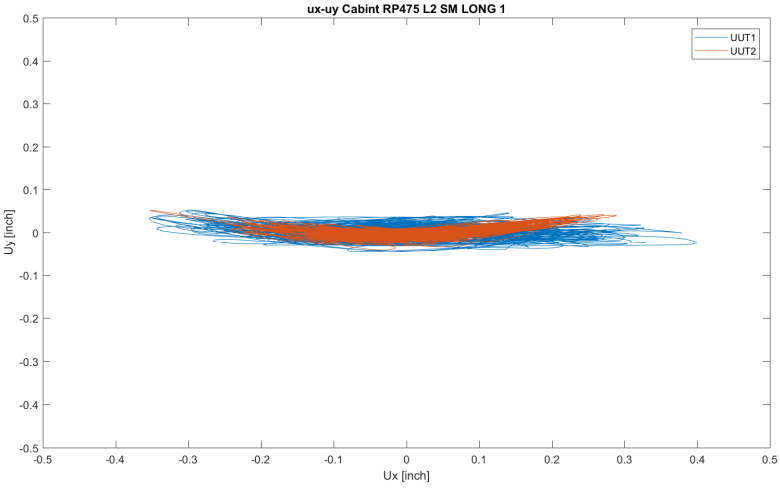

Anchor Forces Cabint RP475 L2 SM LONG 1

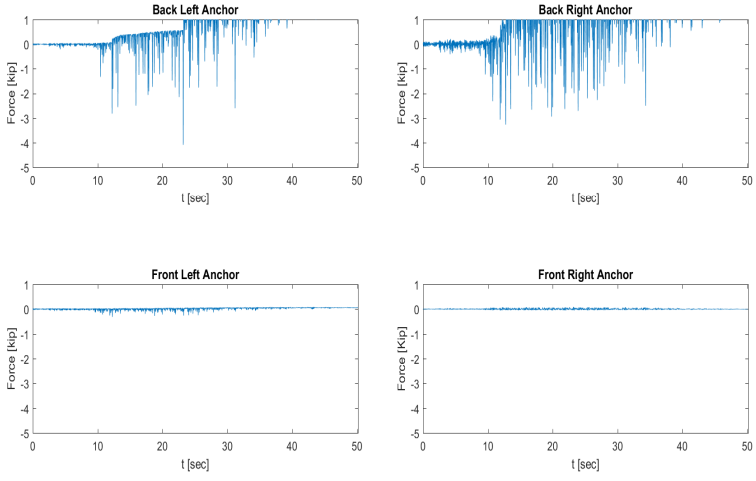

Testing Phase 2 – (15) Level 2 RP 475 Y direction – SM

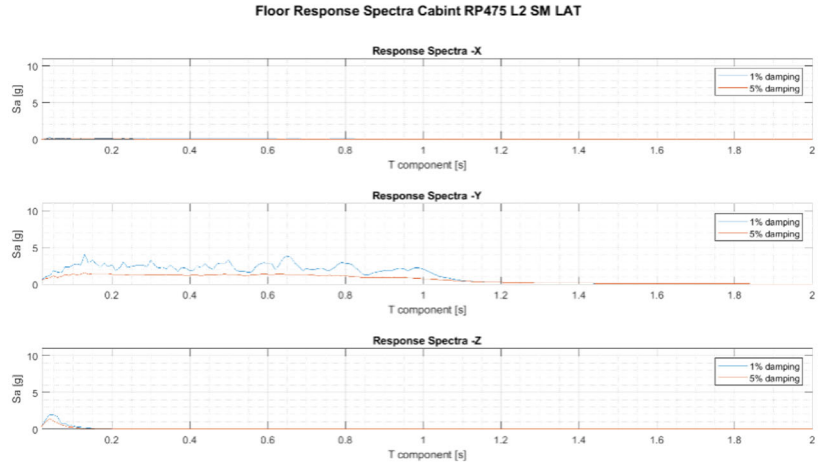

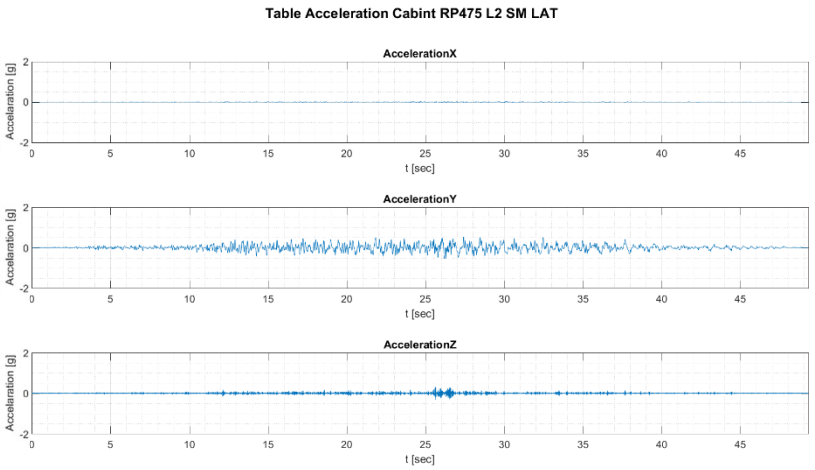

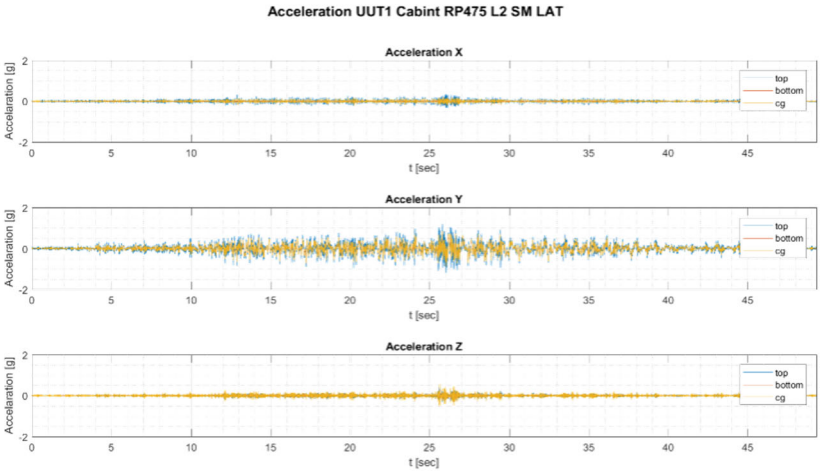

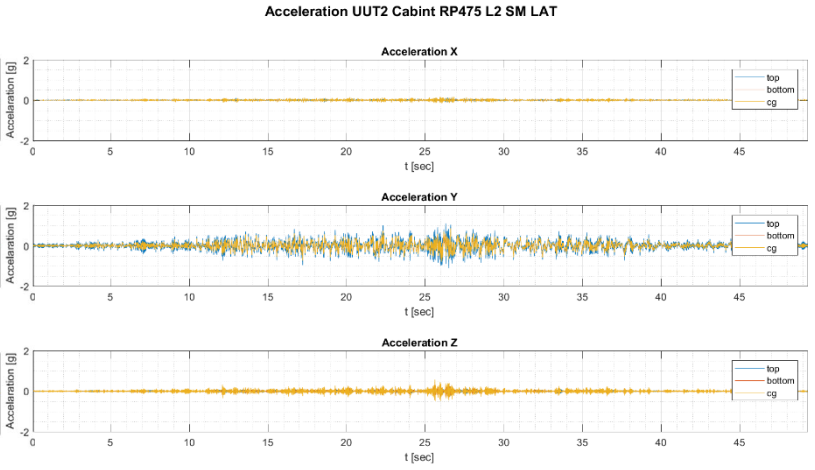

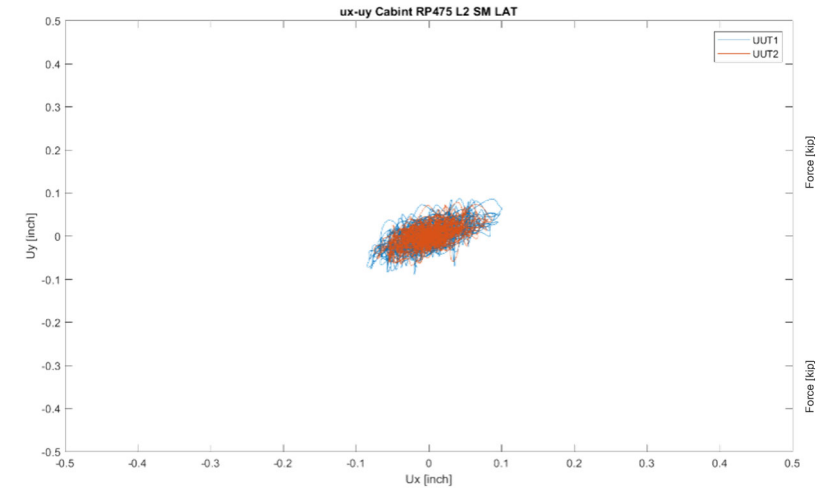

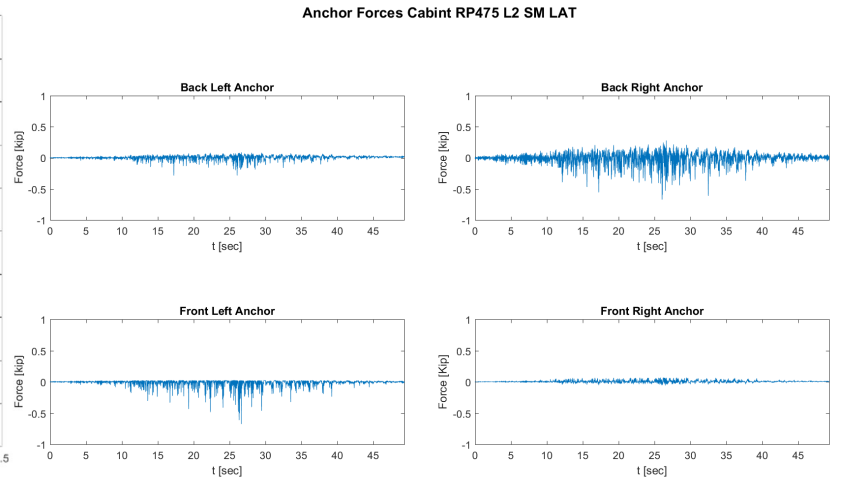

Testing Phase 2 – (16) Level 9 RP 475 Y direction – SM

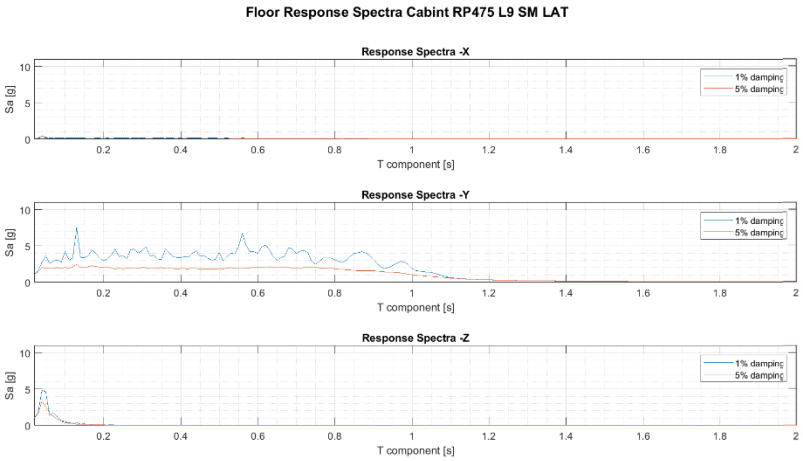

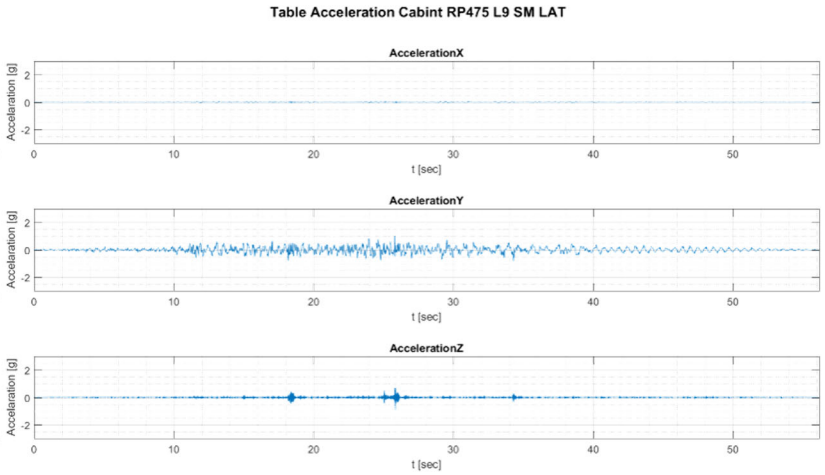

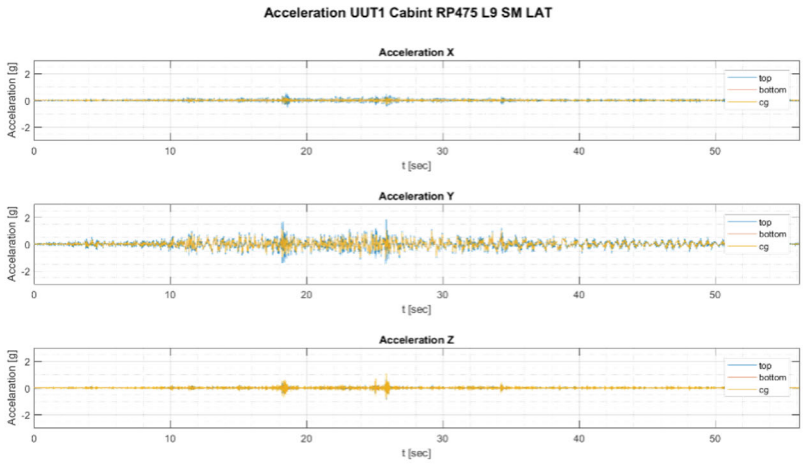

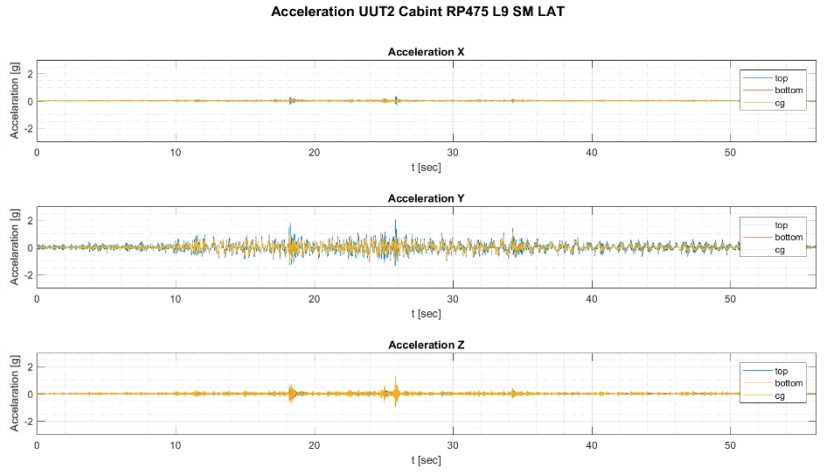

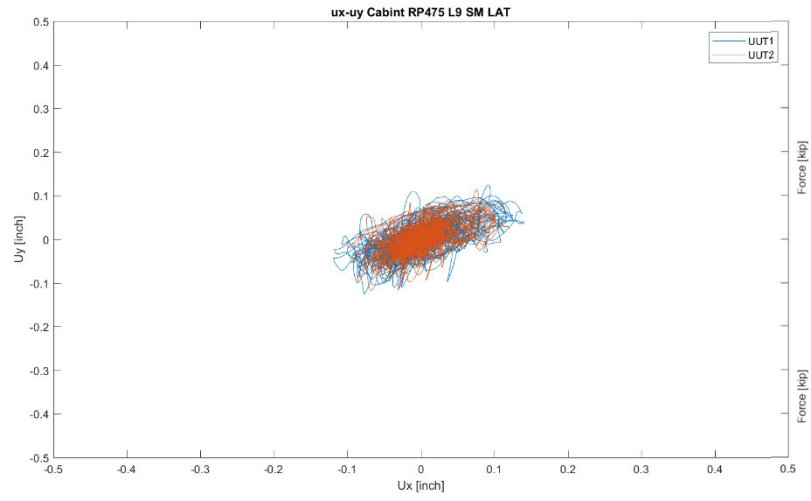

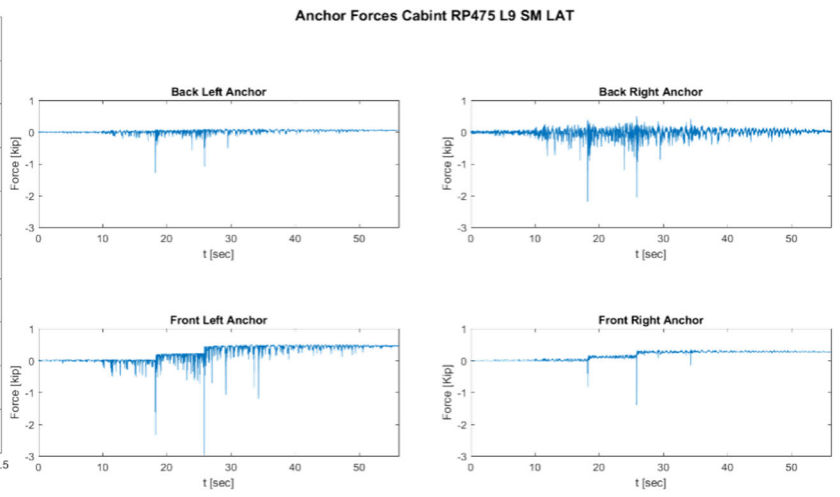

Testing Phase 2 – (17) Level 9 RP 475 X direction - SM

Floor Response Spectra Cabint RP475 L9 SM LONG 1

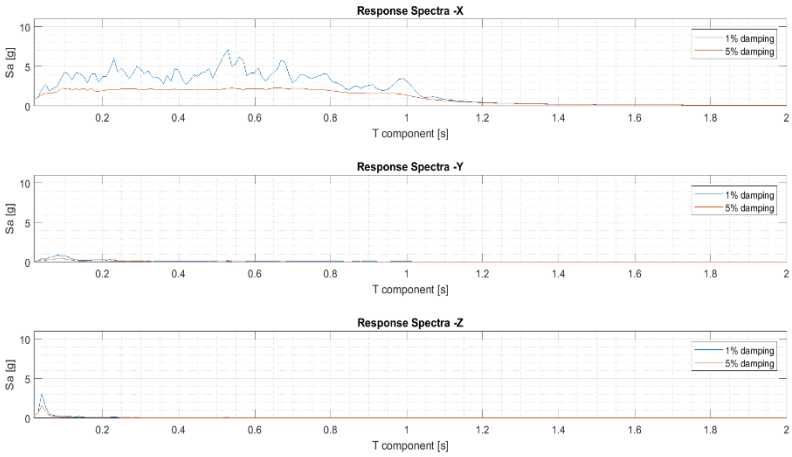

Table Acceleration Cabint RP475 L9 SM LONG 1

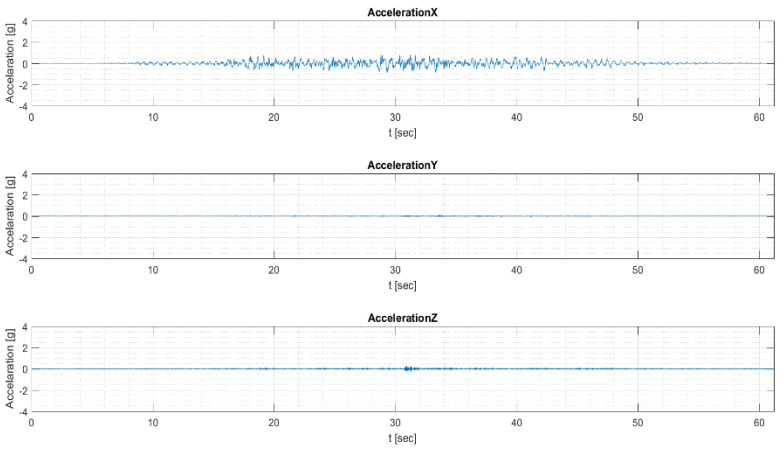

Acceleration UUT1 Cabint RP475 L9 SM LONG 1

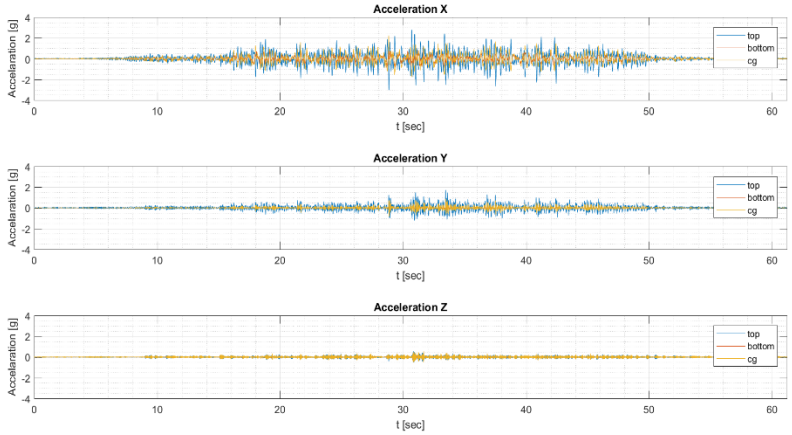

Acceleration UUT2 Cabint RP475 L9 SM LONG 1

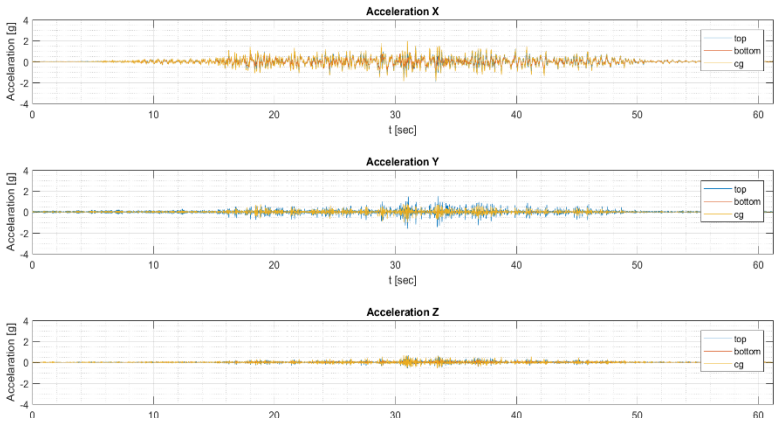

ux-uy Cabint RP475 L9 SM LONG 1

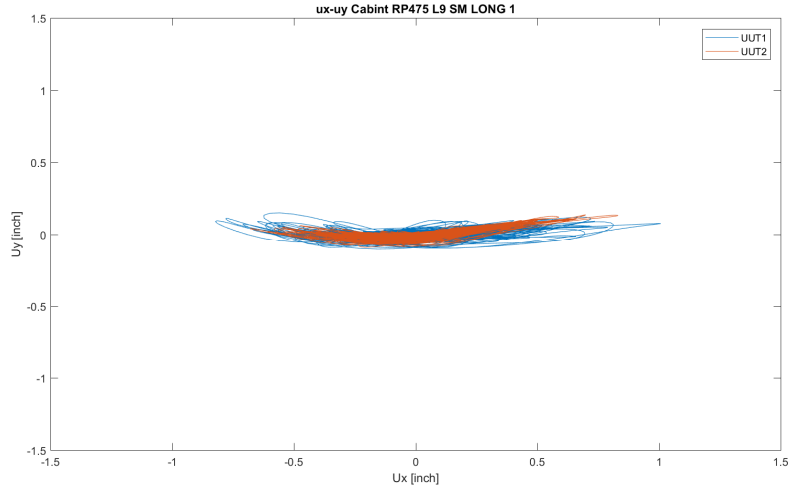

Anchor Forces Cabint RP475 L9 SM LONG 1

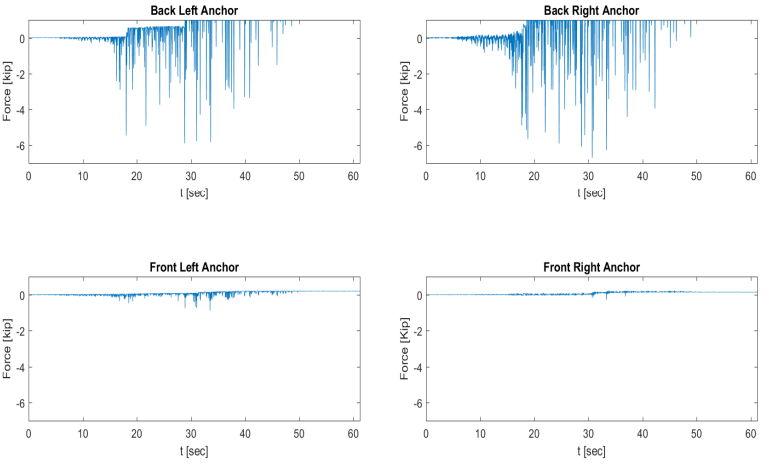

Testing Phase 2 – (18) Level 2 RP 475 X direction – SM – After retorqueing

Floor Response Spectra Cabint RP475 L2 SM LONG 2

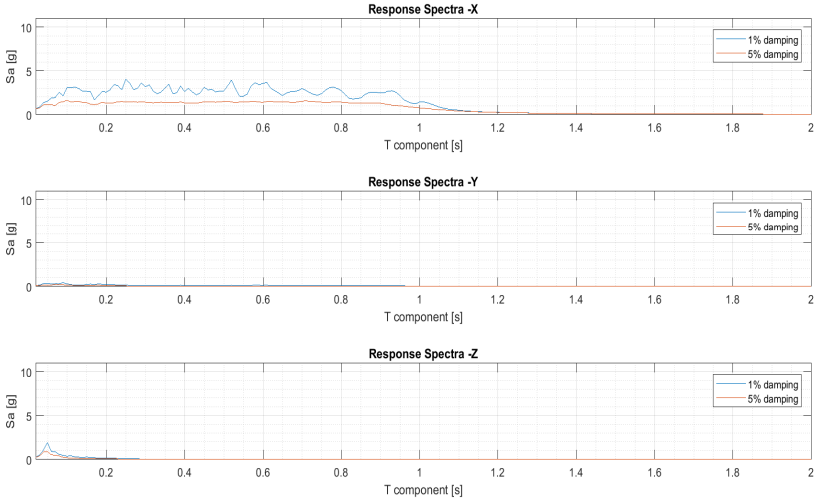

Table Acceleration Cabint RP475 L2 SM LONG 2

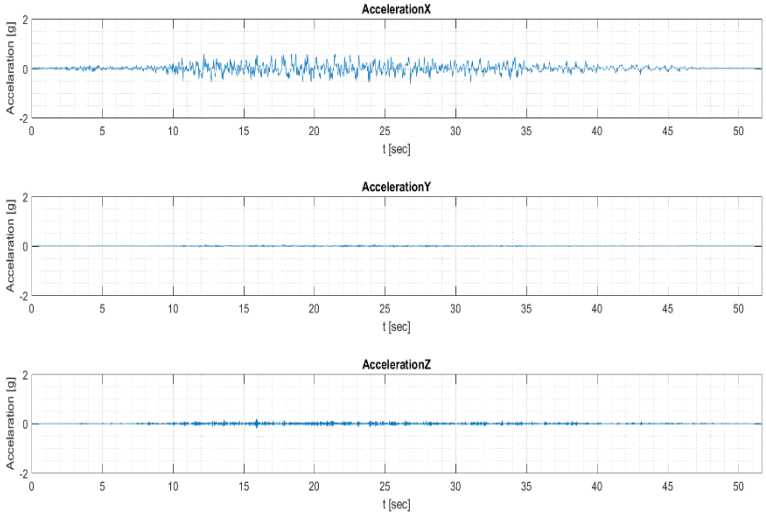

Acceleration UUT1 Cabint RP475 L2 SM LONG 2

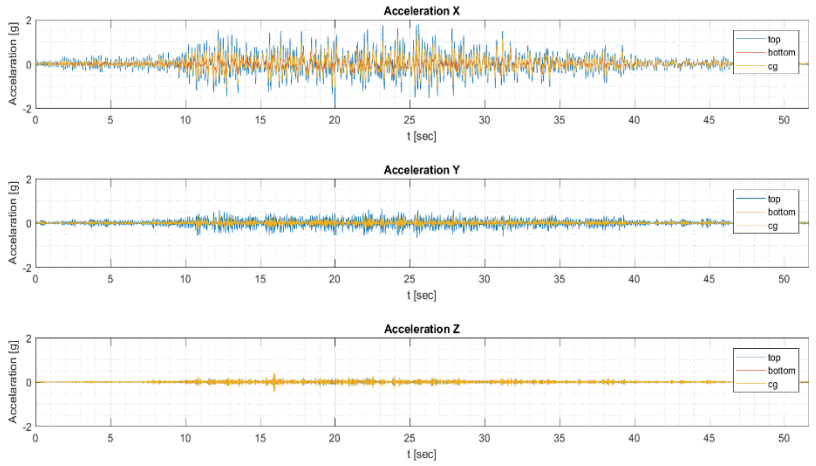

Acceleration UUT2 Cabint RP475 L2 SM LONG 2

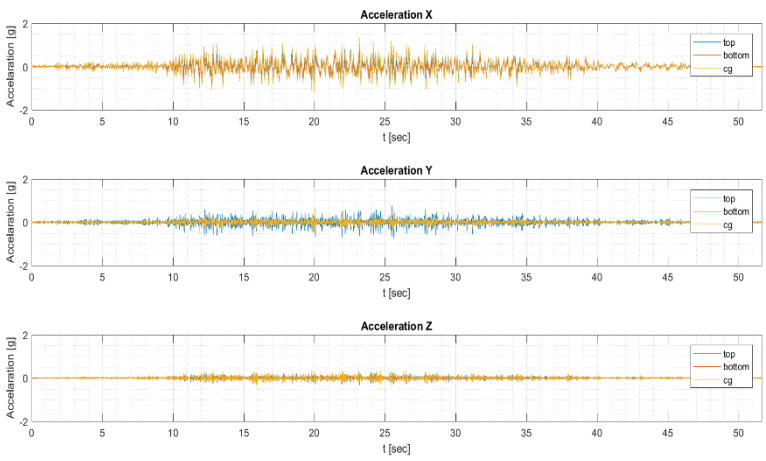

ux-uy Cabint RP475 L2 SM LONG 2

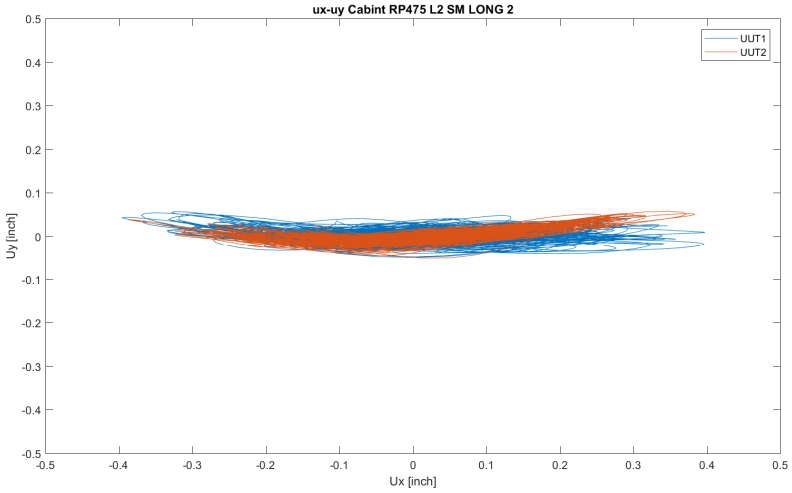

Anchor Forces Cabint RP475 L2 SM LONG 2

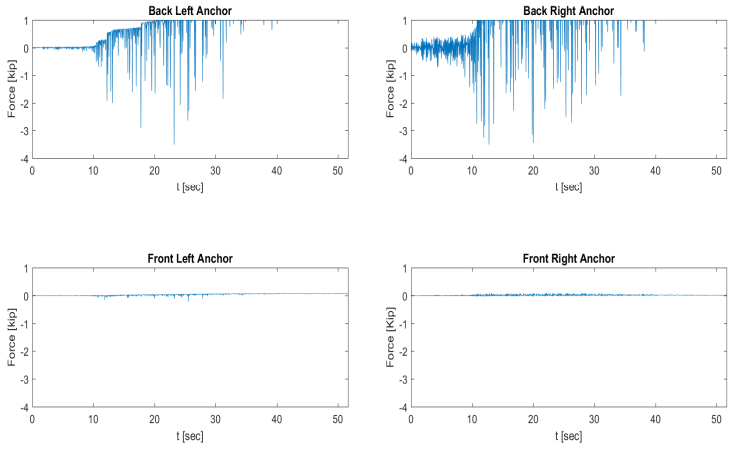

Testing Phase 2 – (19) Level 9 RP 475 X direction – SM – After retorqueing

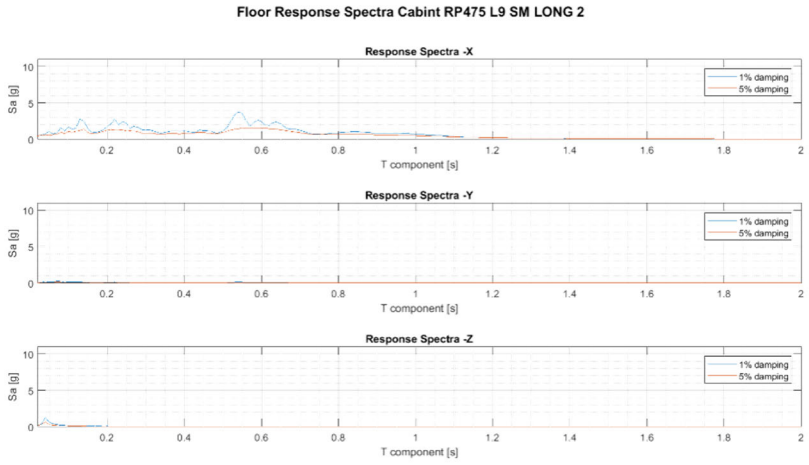

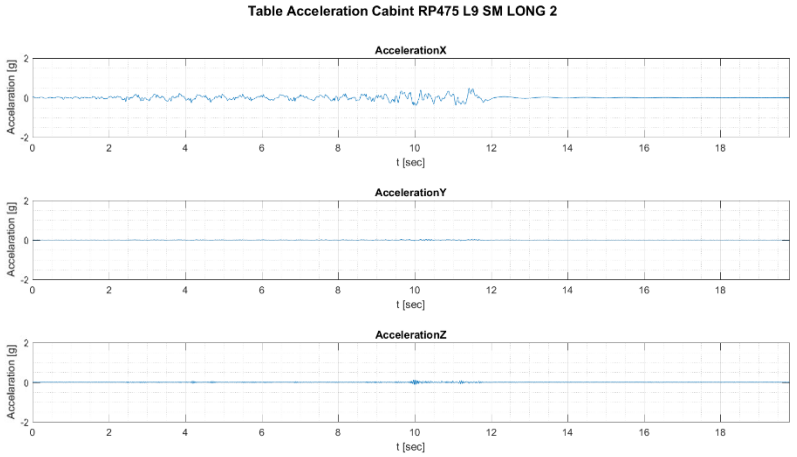

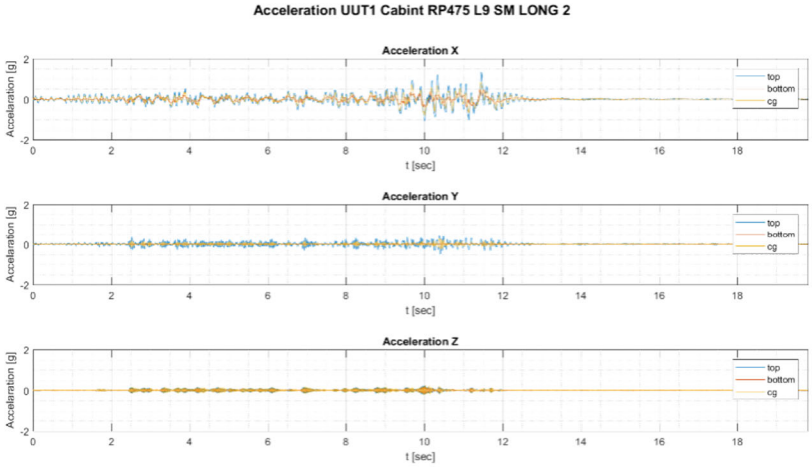

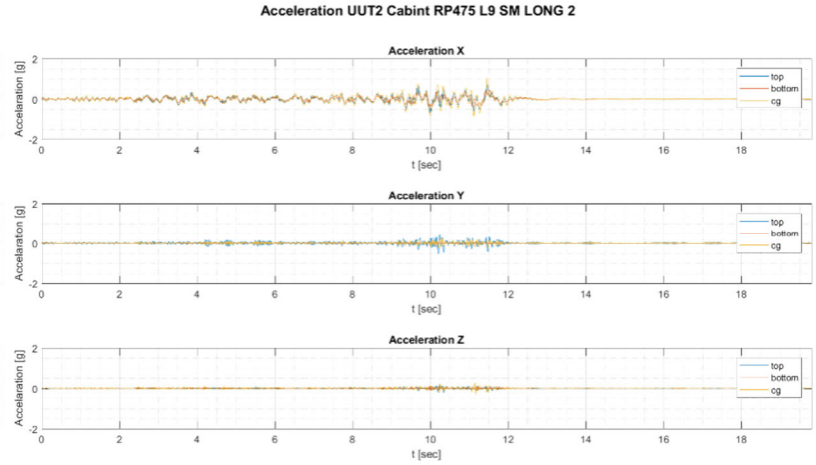

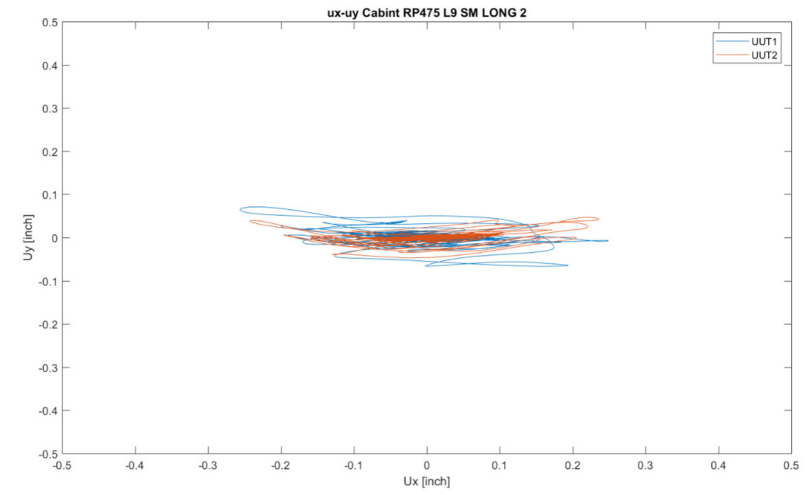

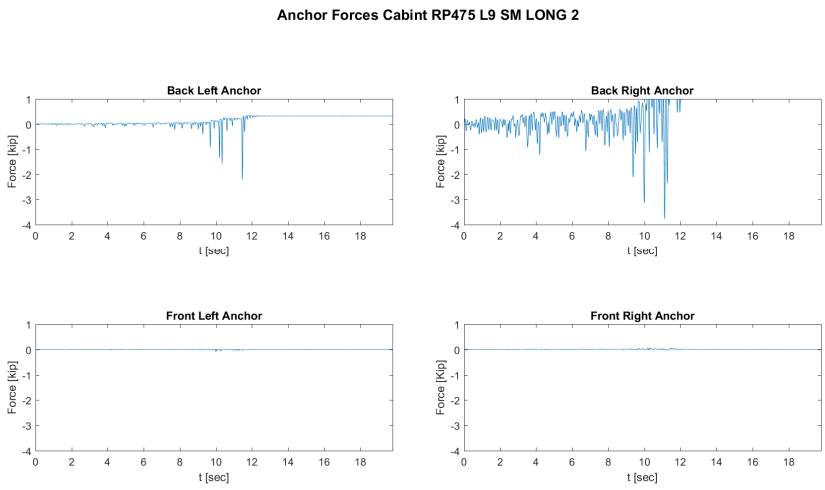

Testing Phase 2 – (20) Level 1 RP 475 Y direction – Isolated

Floor Response Spectra Cabint RP475 L1 ISO LAT

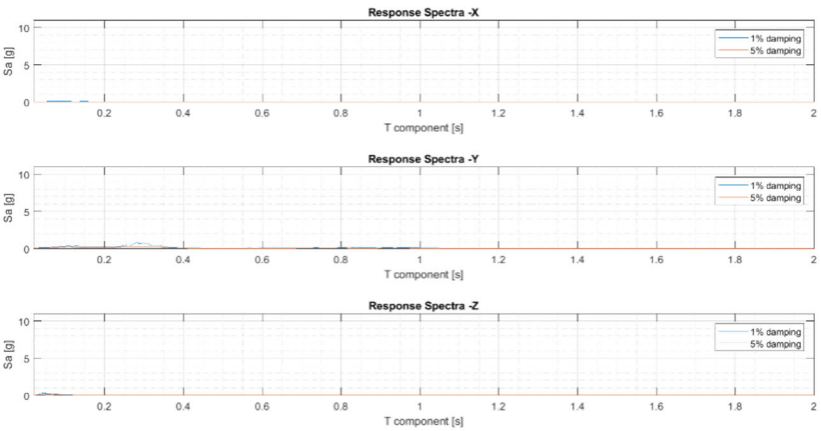

Table Acceleration Cabint RP475 L1 ISO LAT

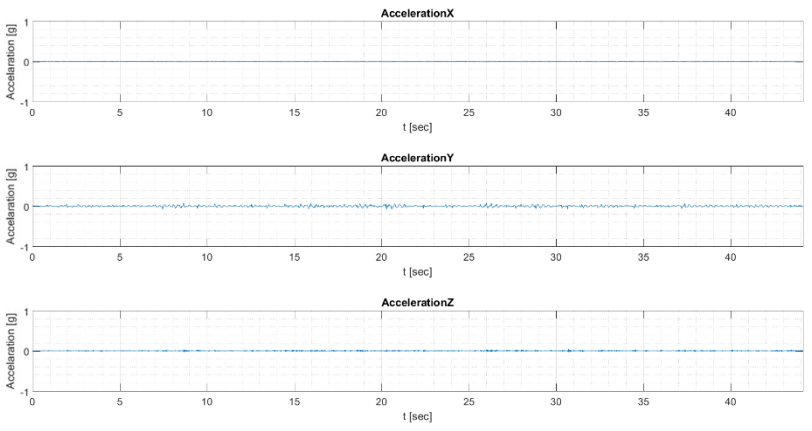

Acceleration UUT1 Cabint RP475 L1 ISO LAT

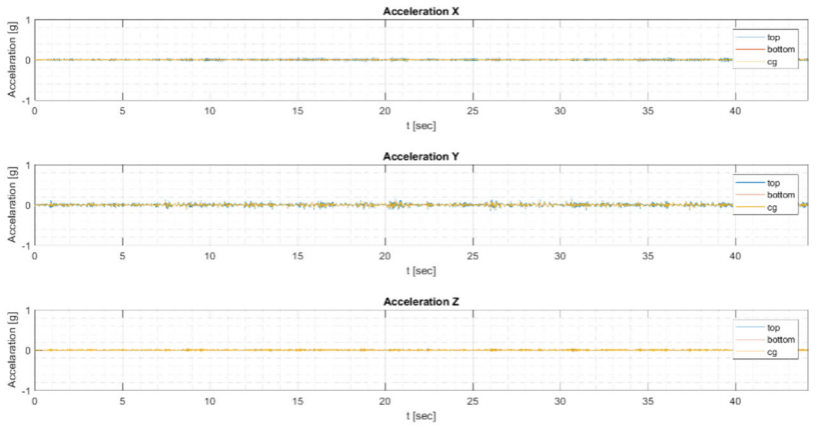

Acceleration UUT2 Cabint RP475 L1 ISO LAT

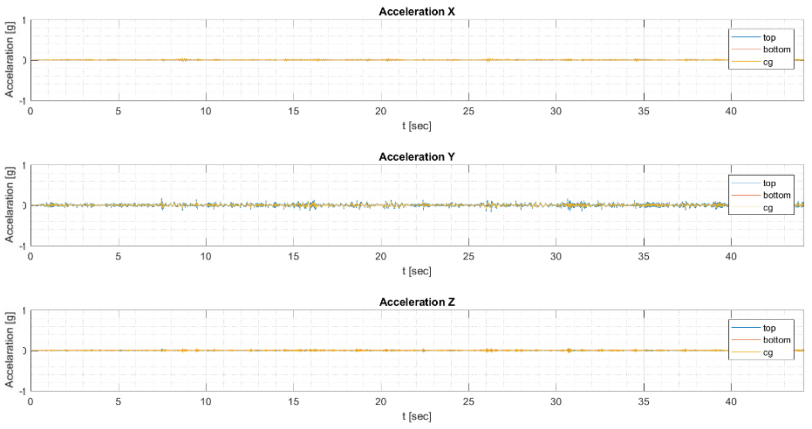

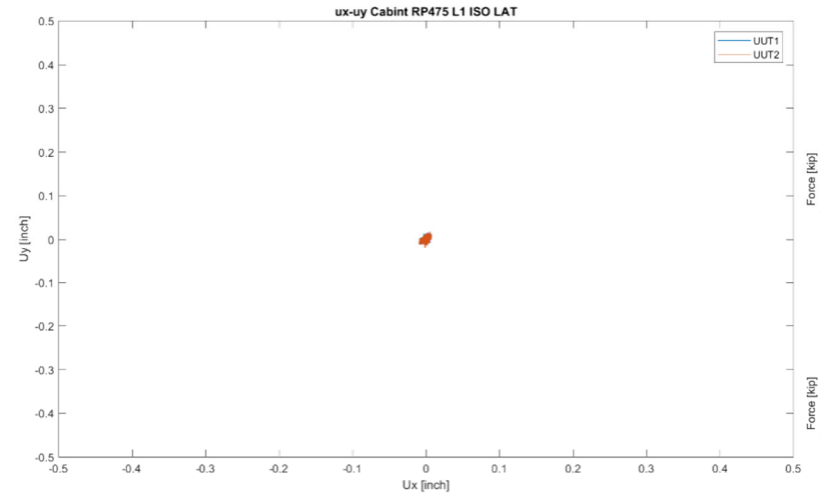

Anchor Forces Cabint RP475 L1 ISO LAT

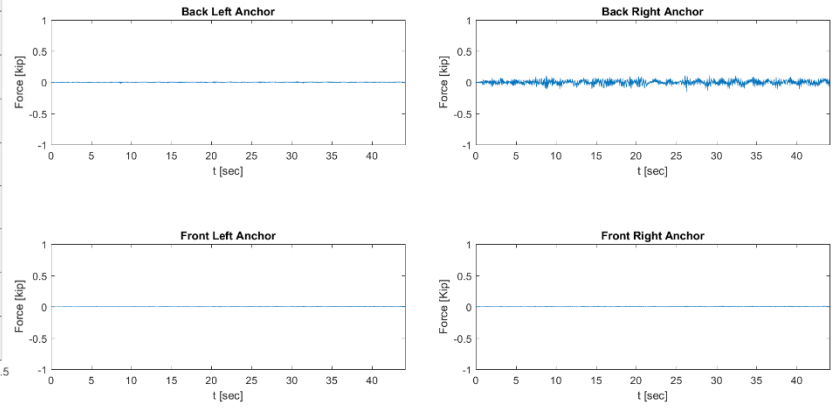

Testing Phase 2 – (21) Level 1 RP 475 Y direction – Isolated

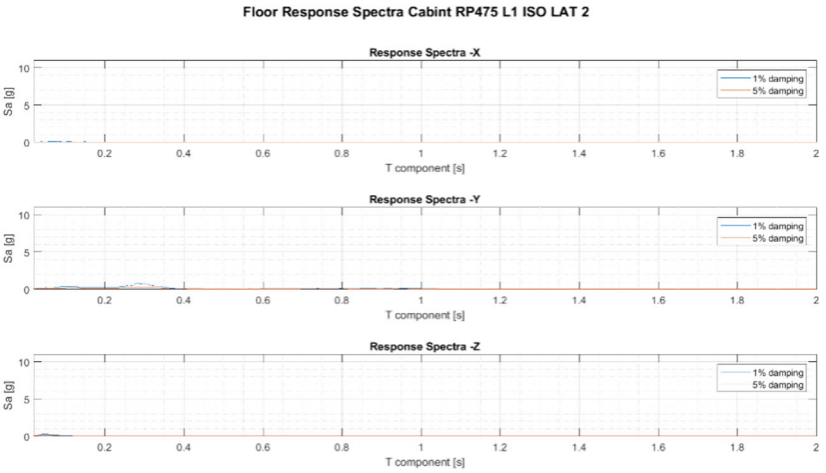

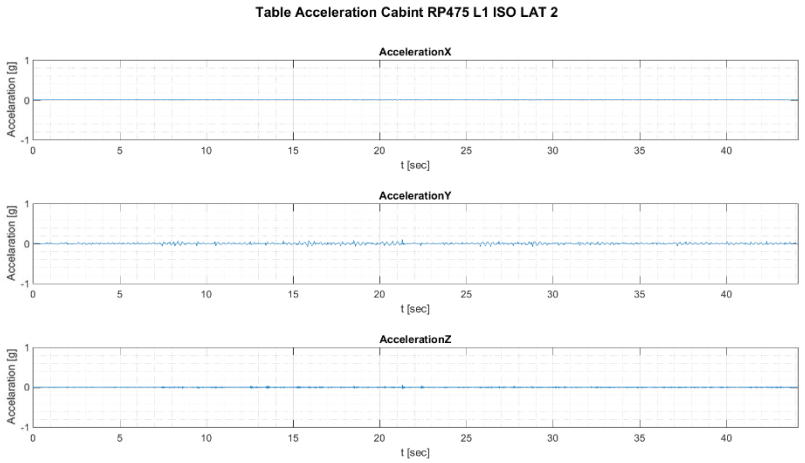

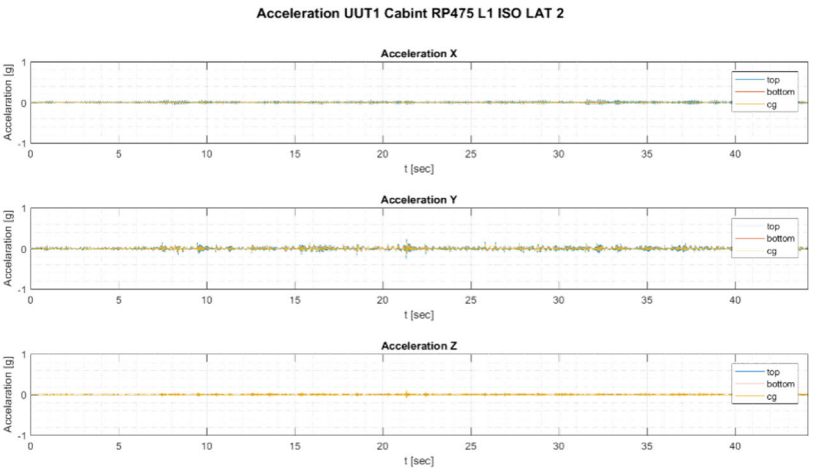

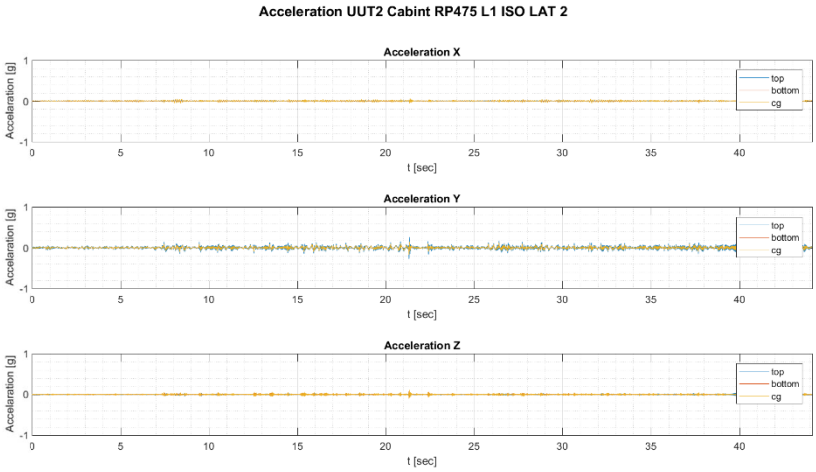

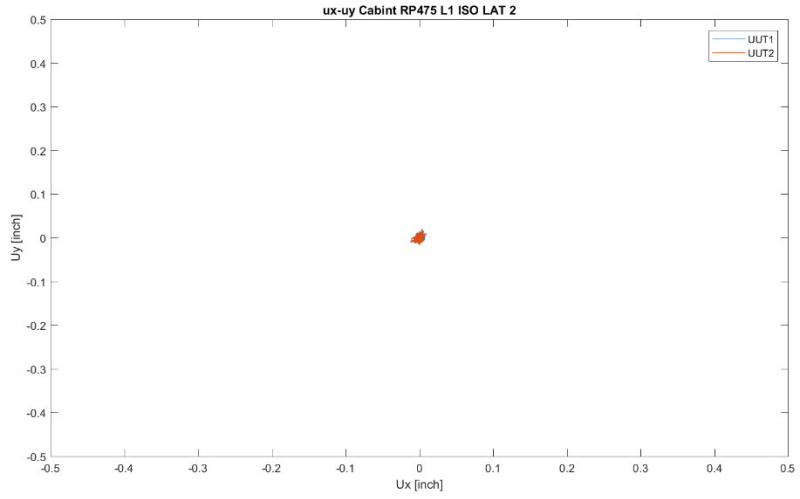

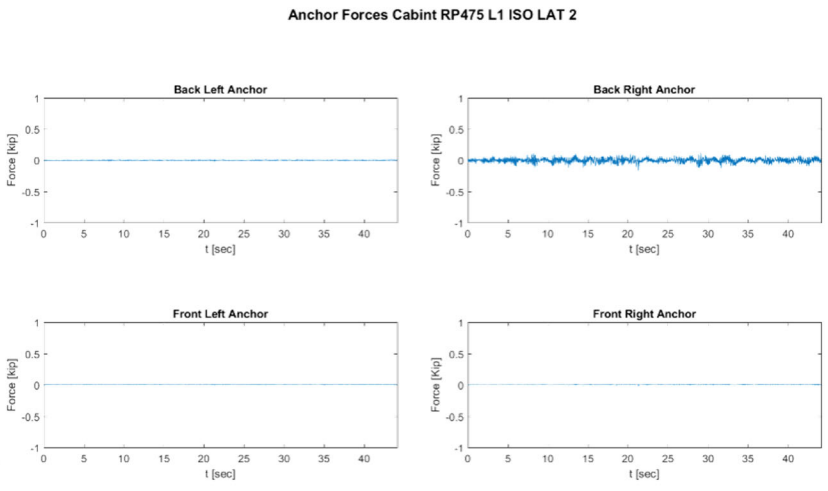

Testing Phase 2 – (22) Roof RP 475 Y direction – Isolated

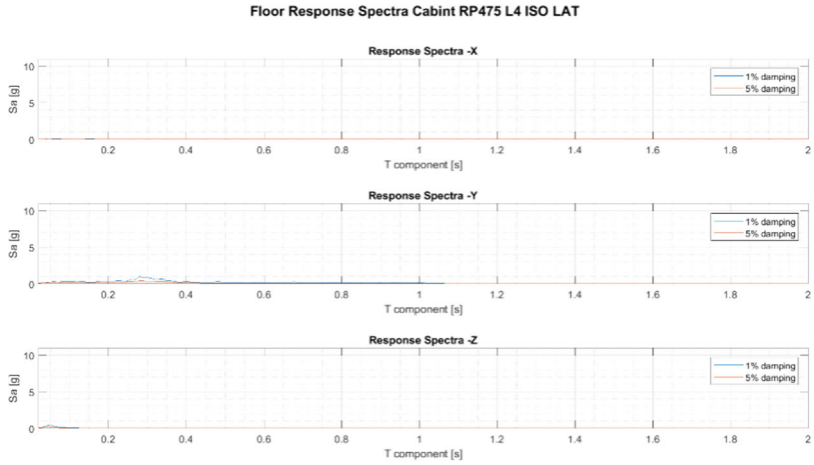

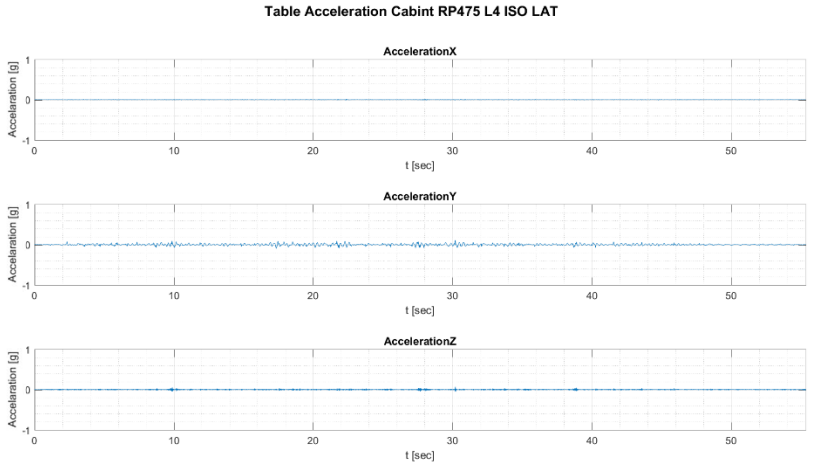

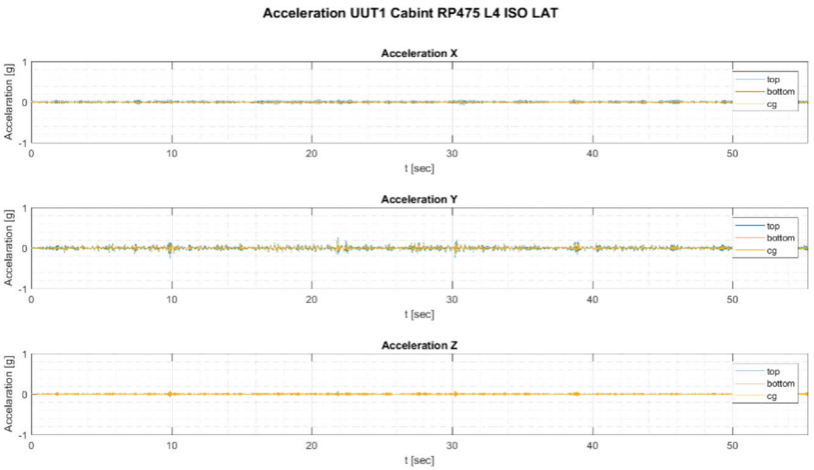

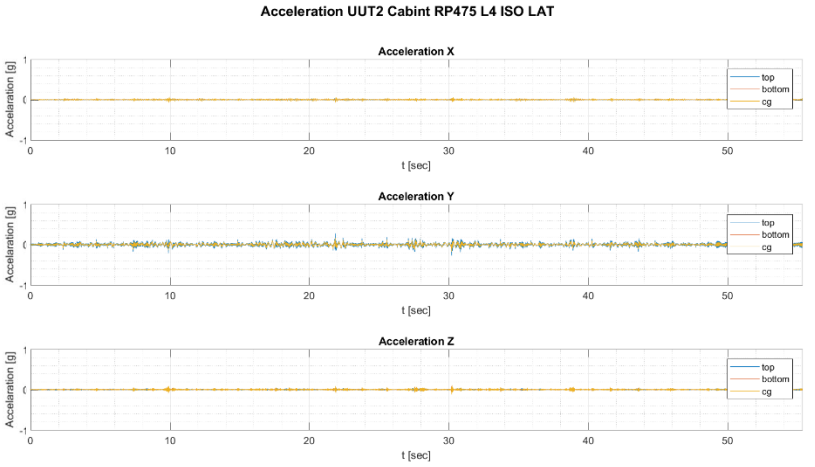

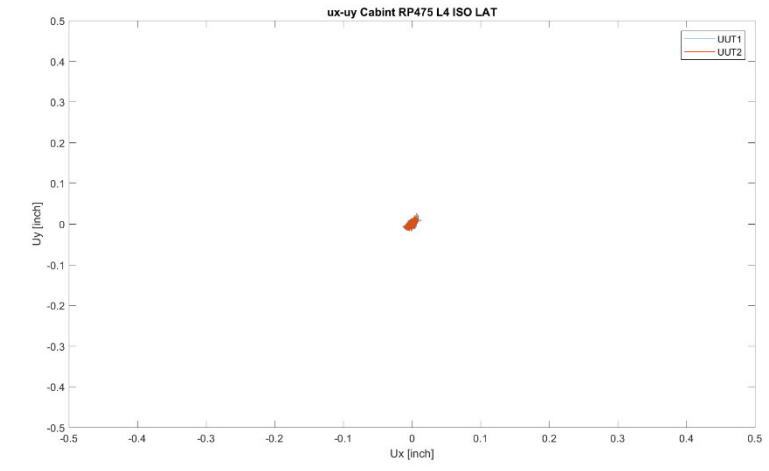

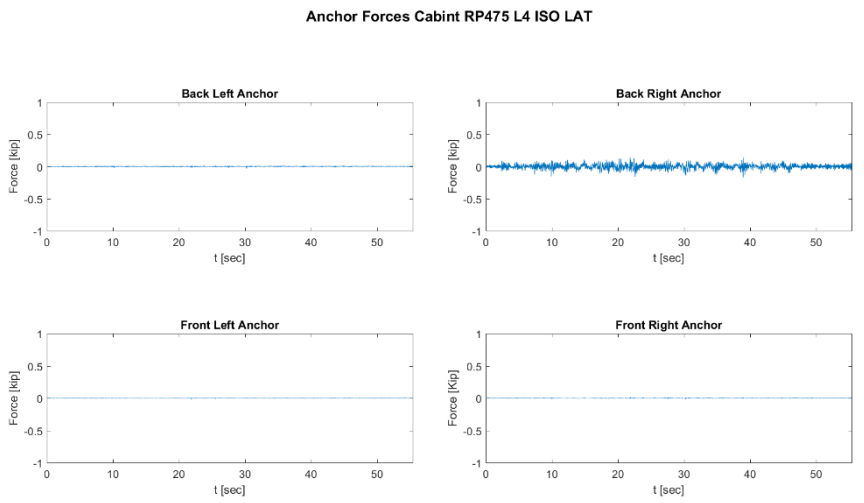

Testing Phase 2 – (23) Level 1 RP 475 Y direction – Low rise

Floor Response Spectra Cabint RP475 L1 FIX LAT

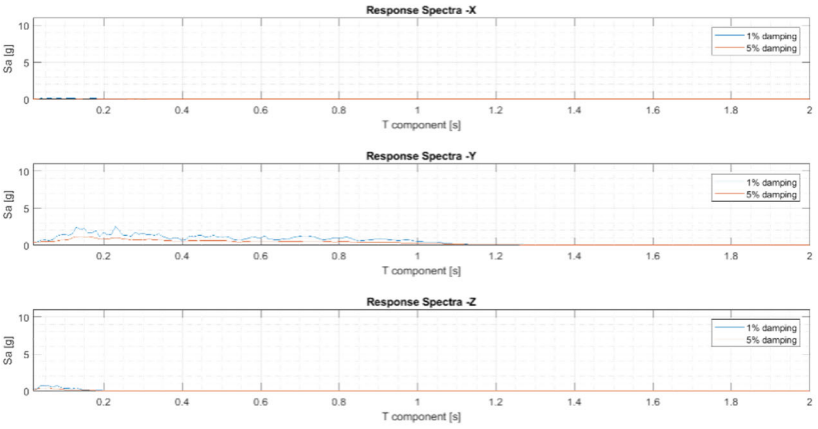

Table Acceleration Cabint RP475 L1 FIX LAT

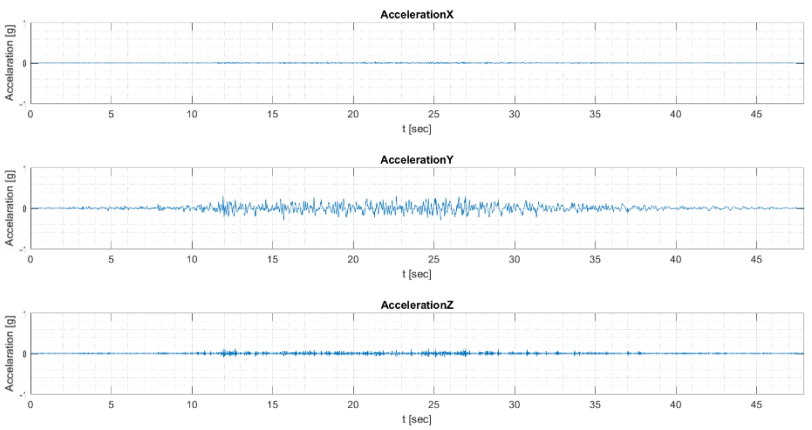

Acceleration UUT1 Cabint RP475 L1 FIX LAT

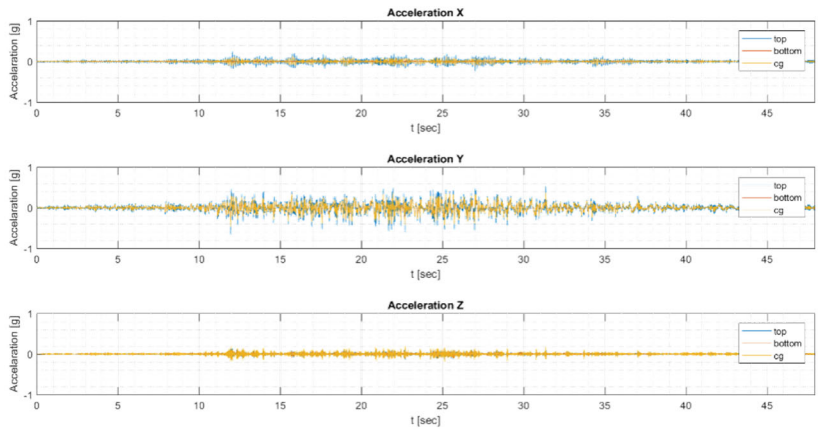

Acceleration UUT2 Cabint RP475 L1 FIX LAT

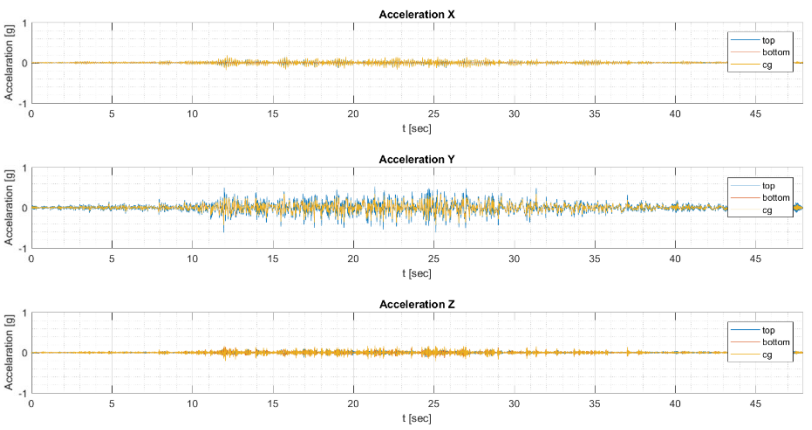

ux-uy Cabint RP475 L1 FIX LAT

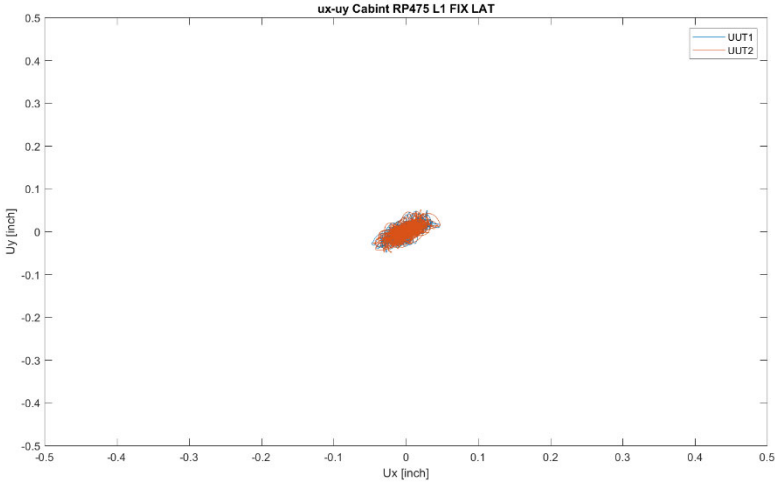

Anchor Forces Cabint RP475 L1 FIX LAT

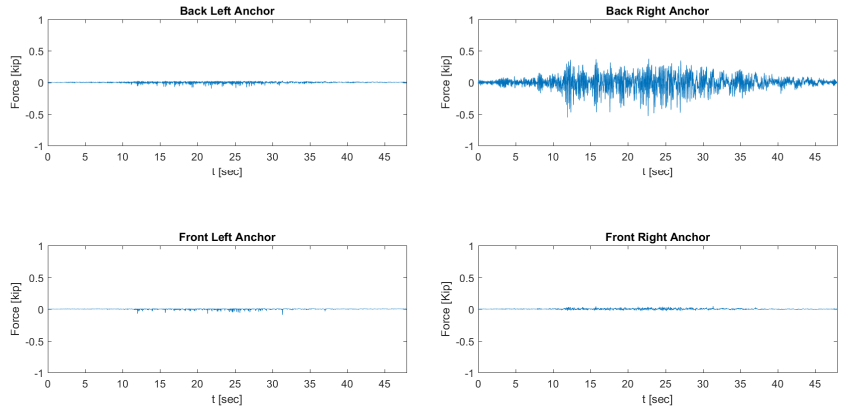

Testing Phase 2 – (24) Roof RP 475 Y direction – Low rise

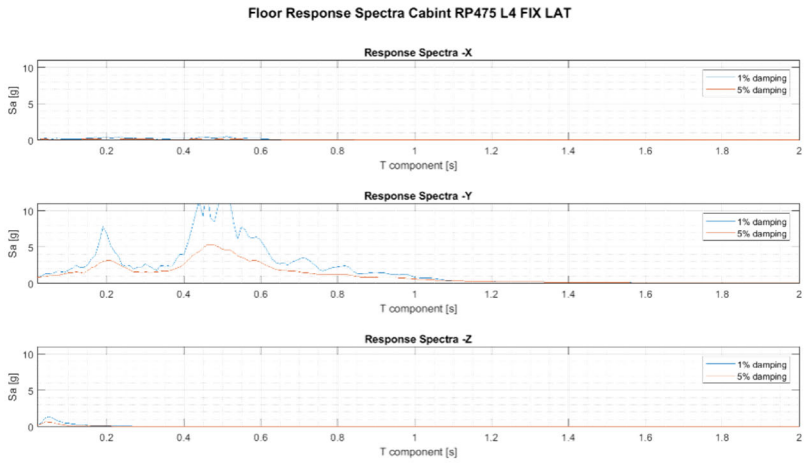

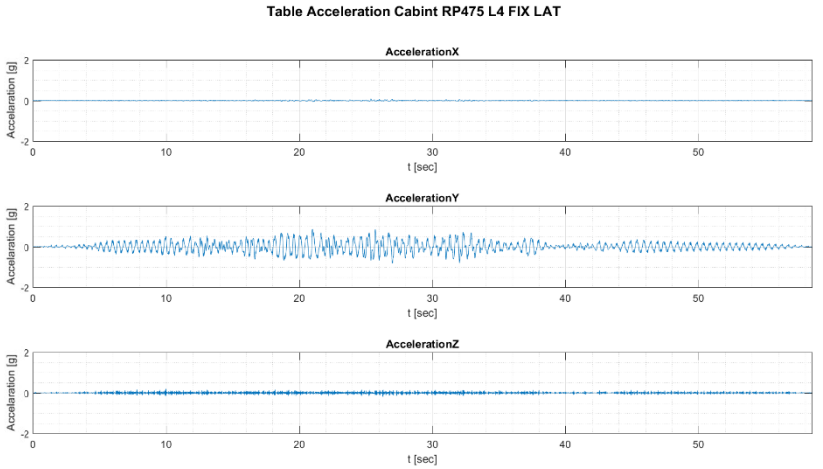

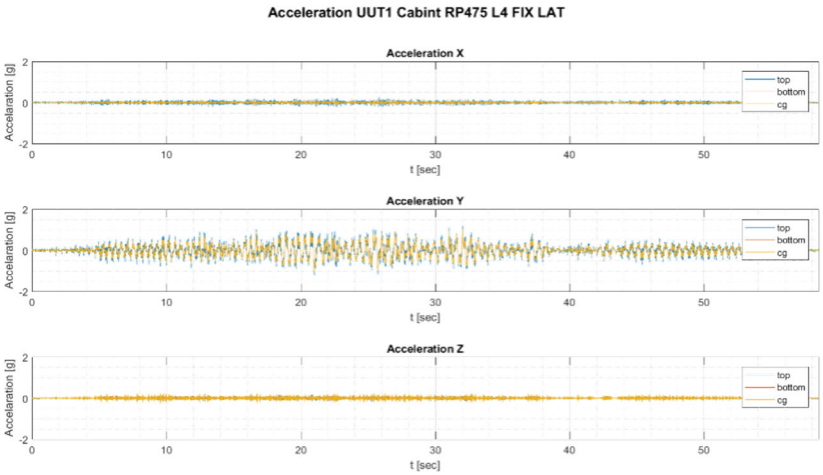

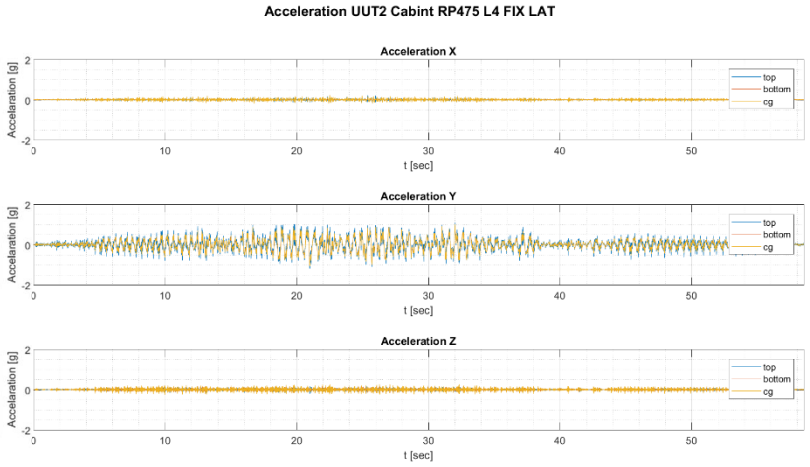

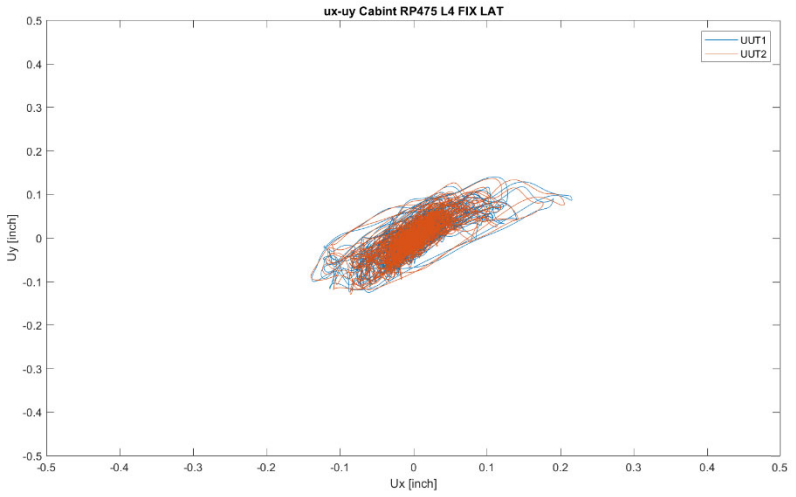

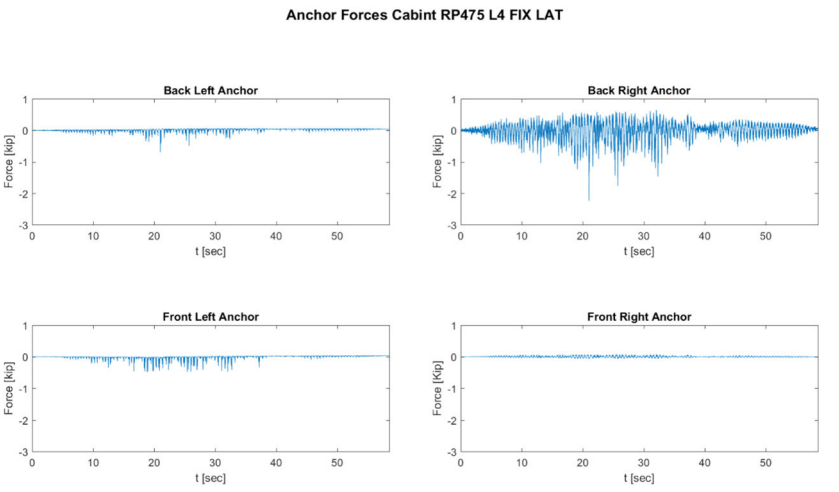

Testing Phase 2 – (25) Level 1 RP 475 X direction – Isolated

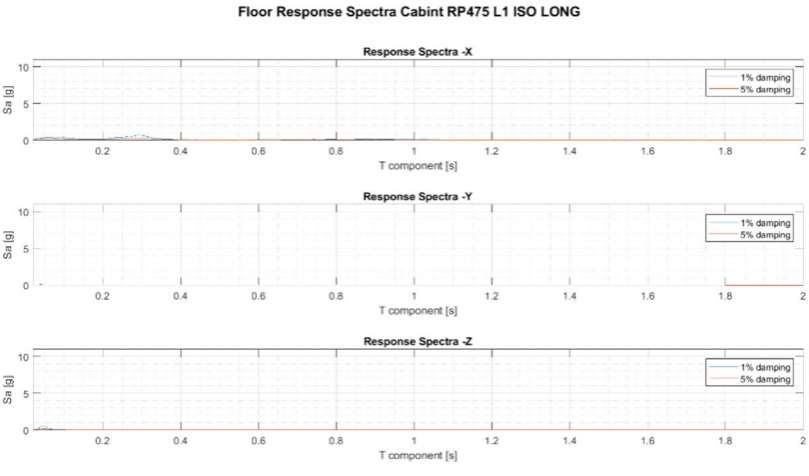

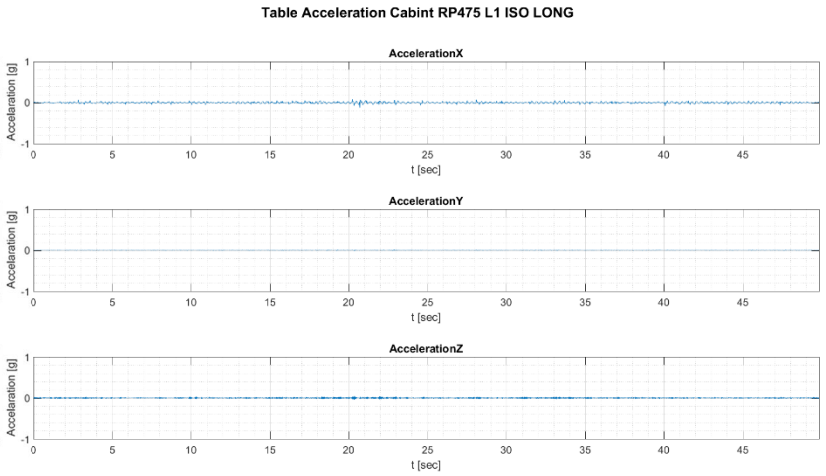

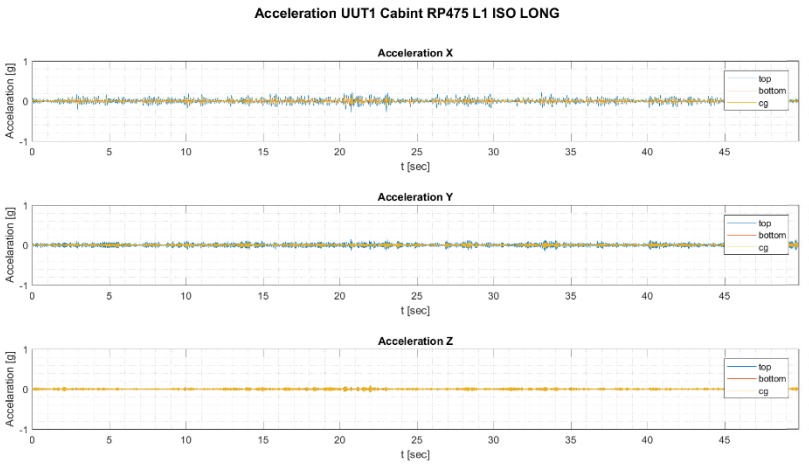

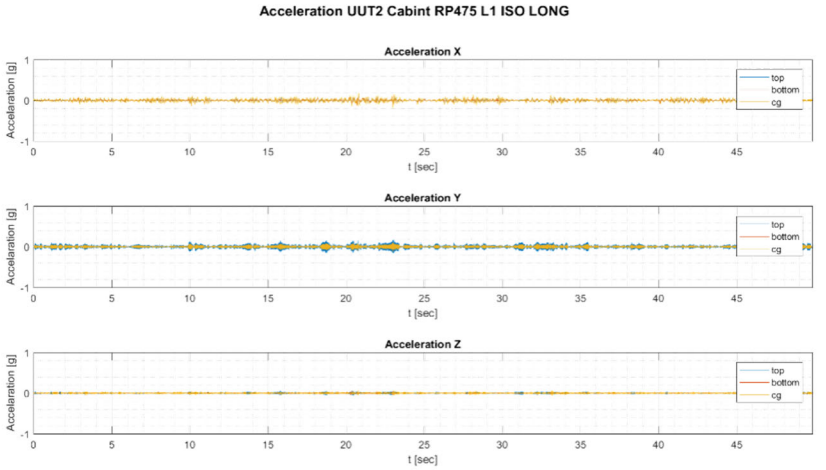

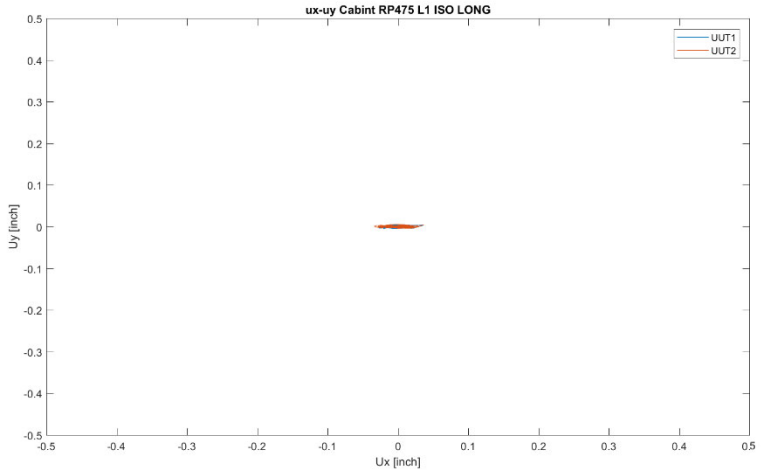

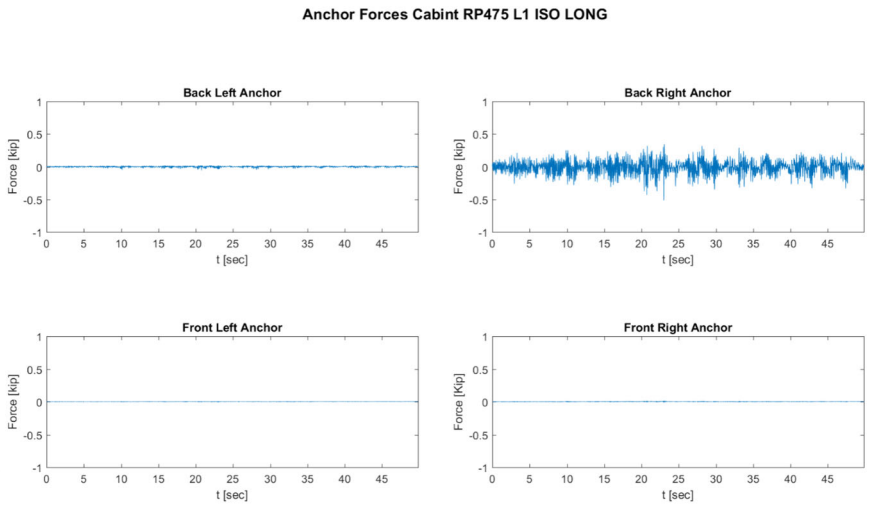

Testing Phase 2 – (26) Roof RP 475 X direction – Isolated

Floor Response Spectra Cabint RP475 L4 ISO LONG

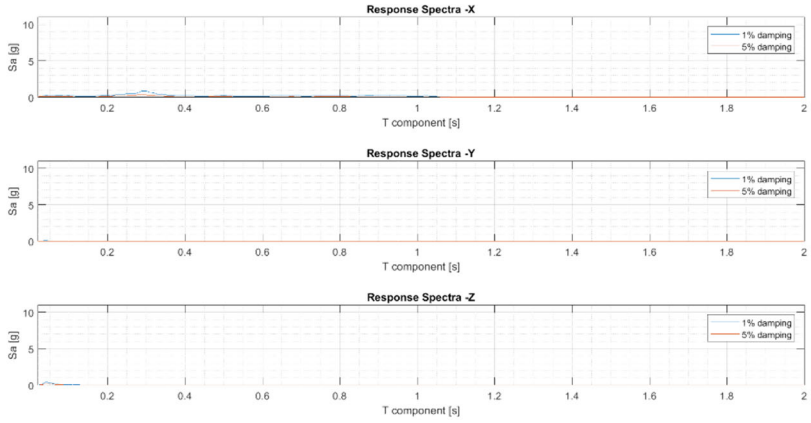

Table Acceleration Cabint RP475 L4 ISO LONG

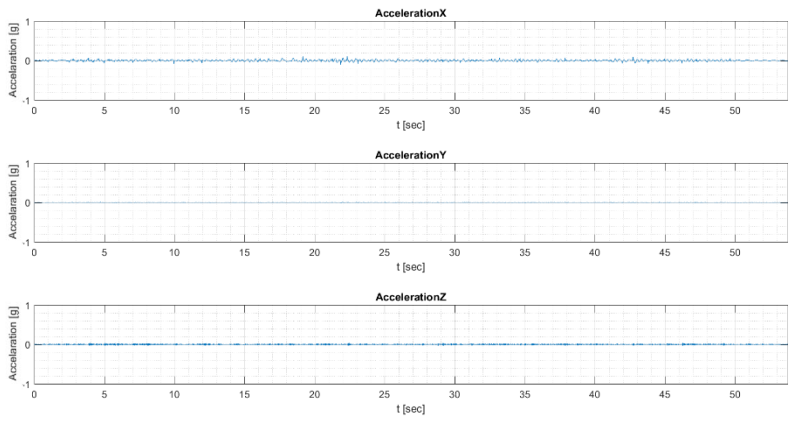

Acceleration UUT1 Cabint RP475 L4 ISO LONG

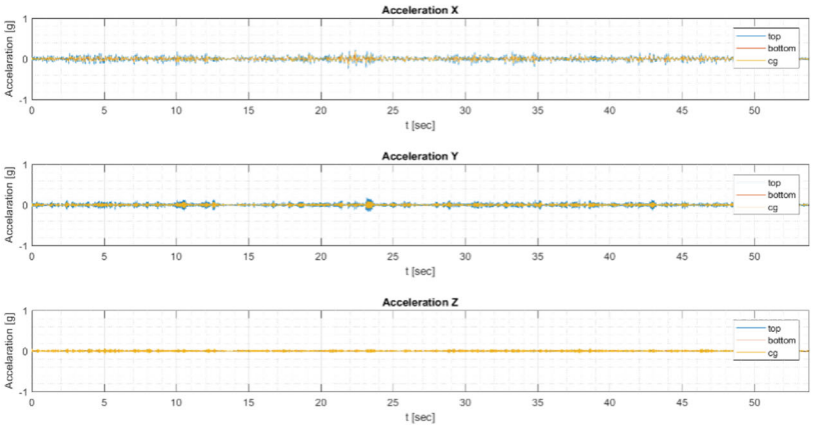

Acceleration UUT2 Cabint RP475 L4 ISO LONG

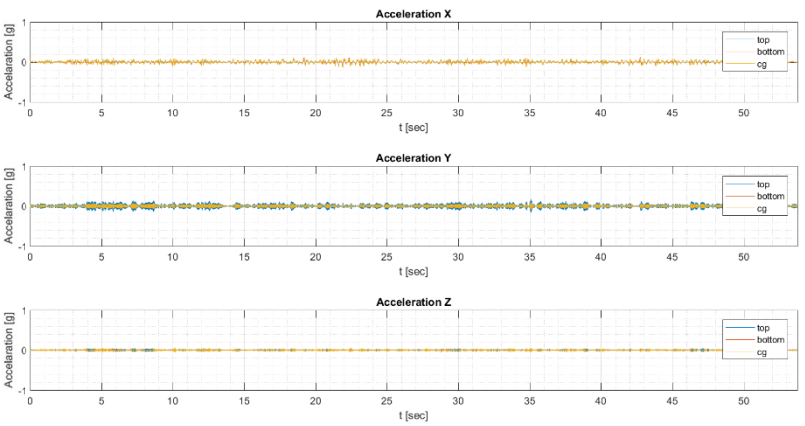

ux-uy Cabint RP475 L4 ISO LONG

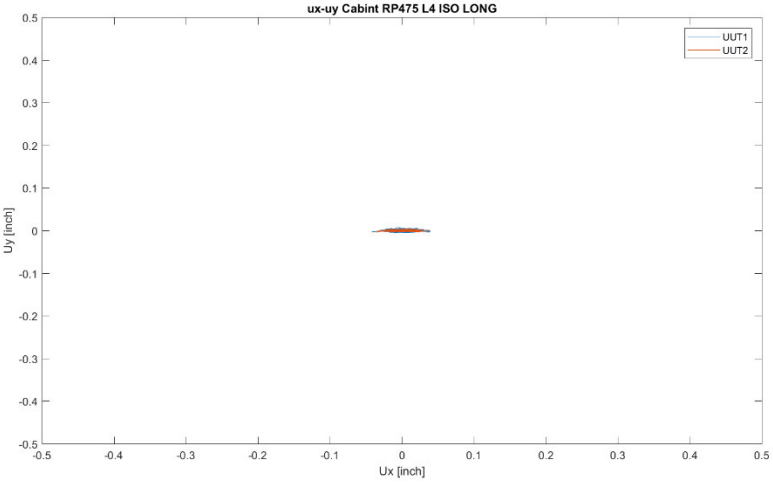

Anchor Forces Cabint RP475 L4 ISO LONG

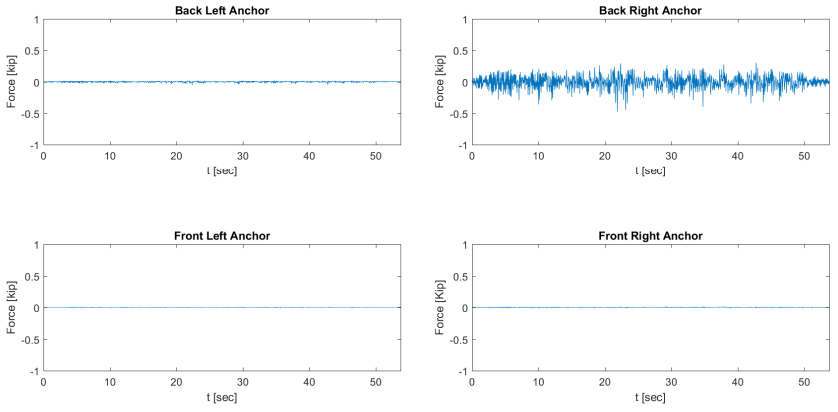

Testing Phase 2 – (27) Level 1 RP 475 X direction – Low rise

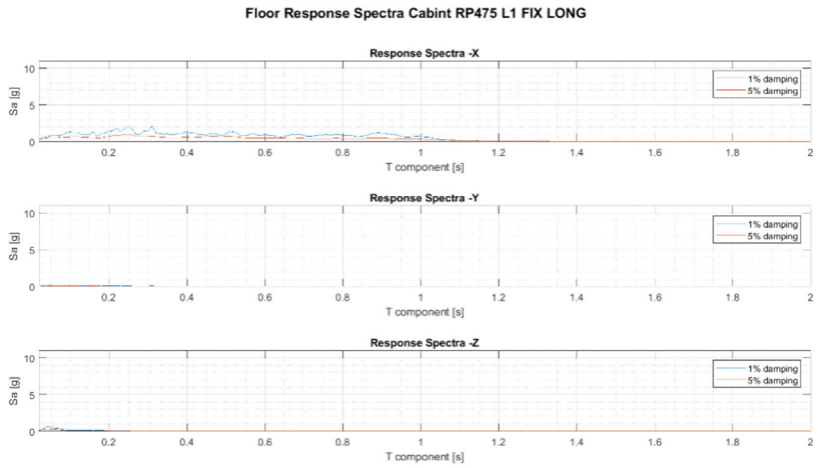

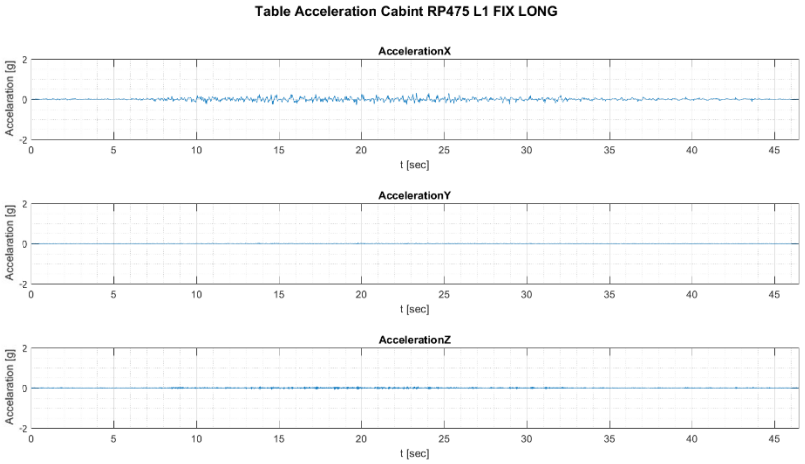

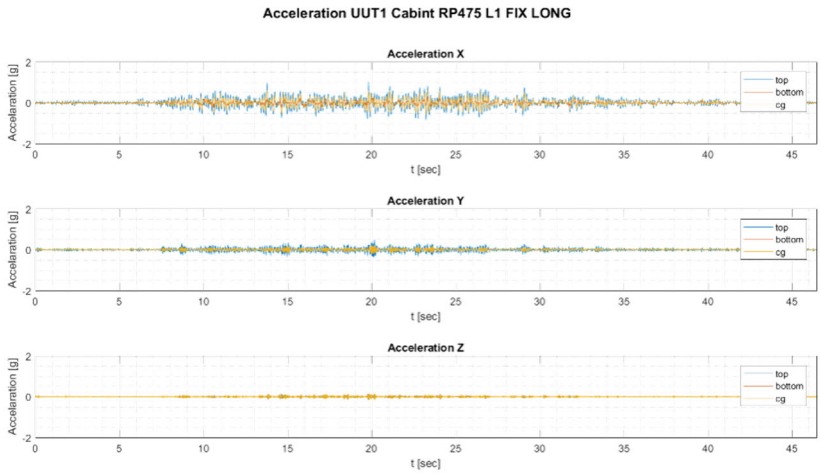

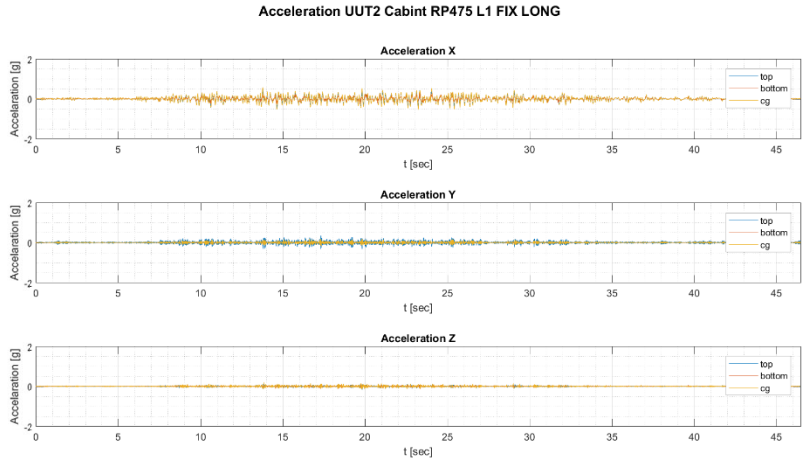

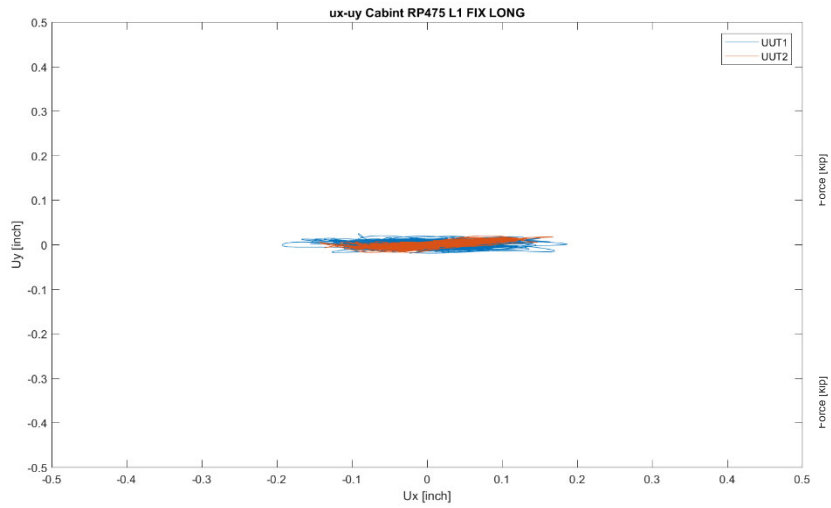

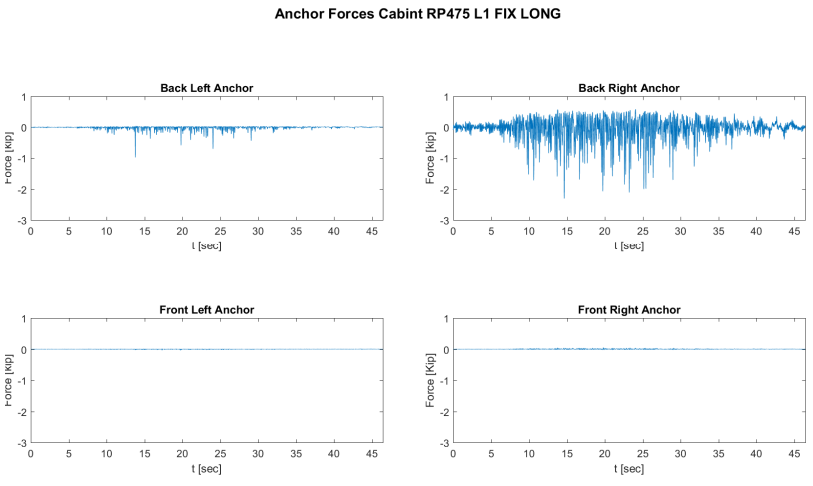

Testing Phase 2 – (28) Roof 1 RP 475 X direction – Low rise

Floor Response Spectra Cabint RP475 L4 FIX LONG

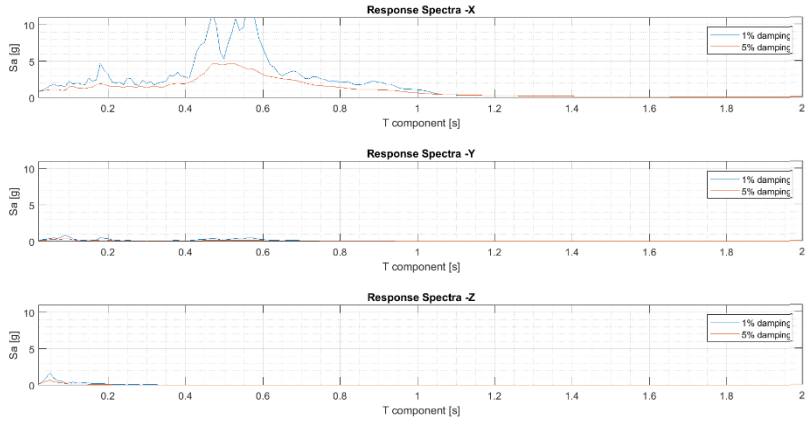

Table Acceleration Cabint RP475 L4 FIX LONG

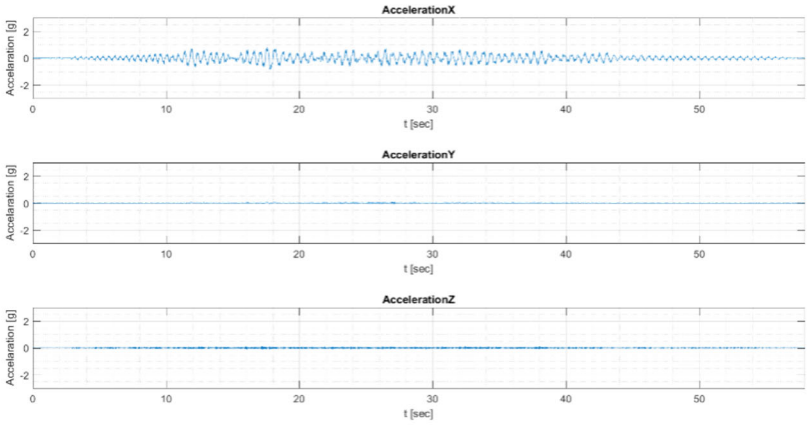

Acceleration UUT1 Cabint RP475 L4 FIX LONG

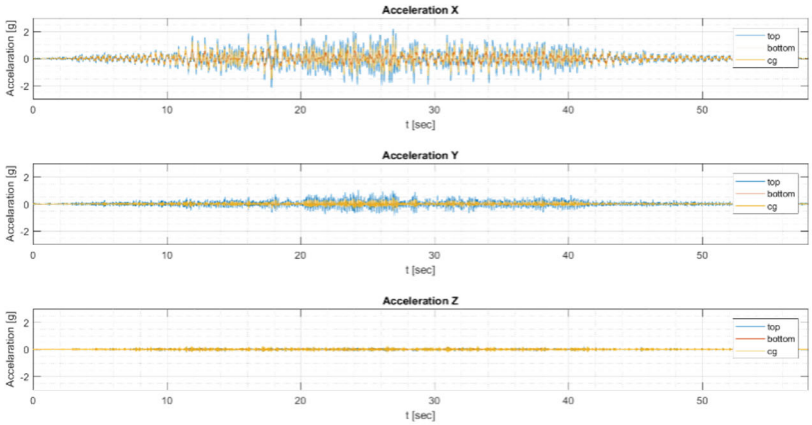

Acceleration UUT2 Cabint RP475 L4 FIX LONG

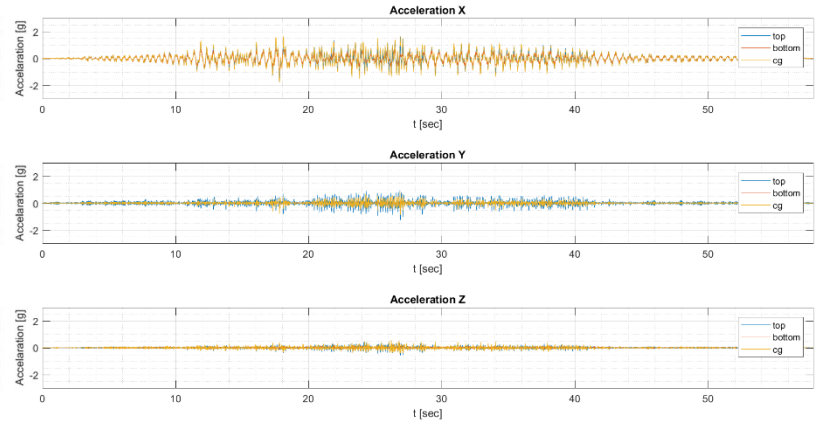

ux-uy Cabint RP475 L4 FIX LONG

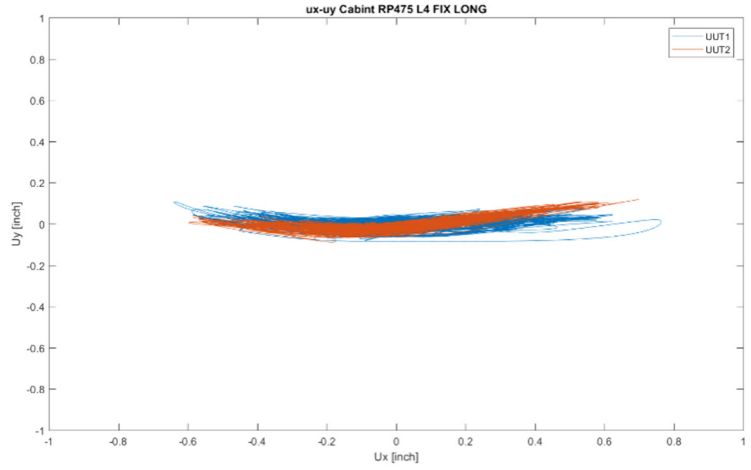

Anchor Forces Cabint RP475 L4 FIX LONG

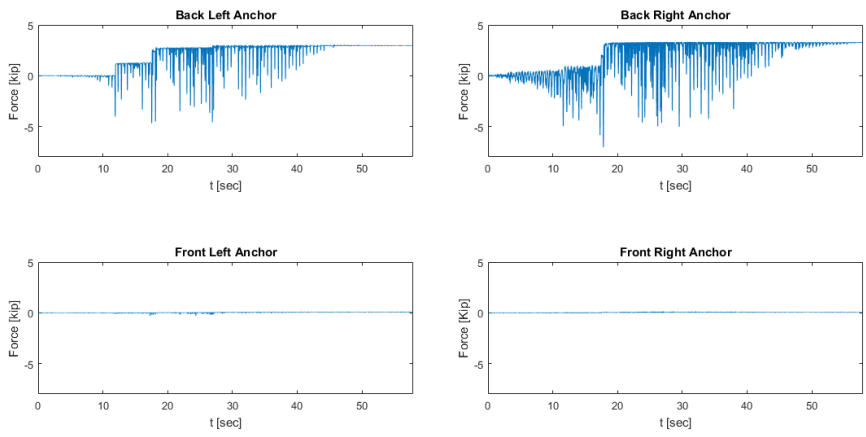

Testing Phase 2 – (29) IEEE X direction

Floor Response Spectra Cabint OSHPD IEEE LONG

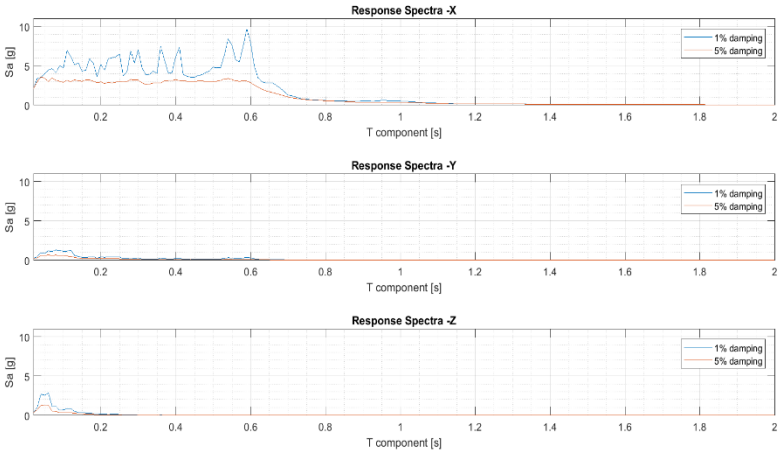

Table Acceleration Cabint OSHPD IEEE LONG

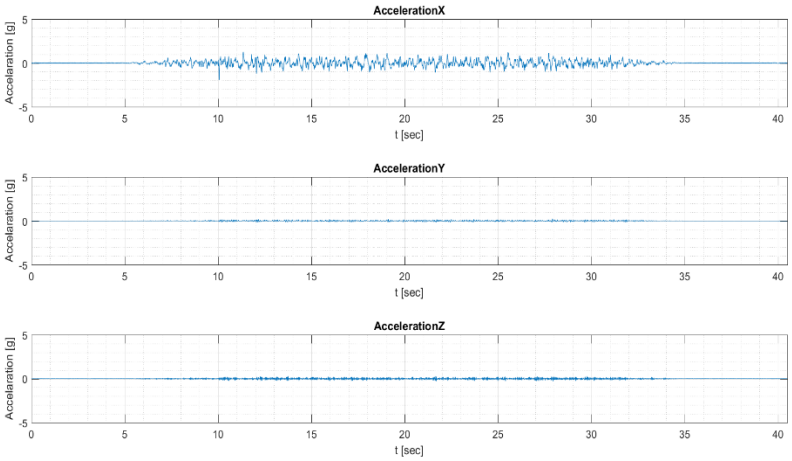

Acceleration UUT1 Cabint OSHPD IEEE LONG

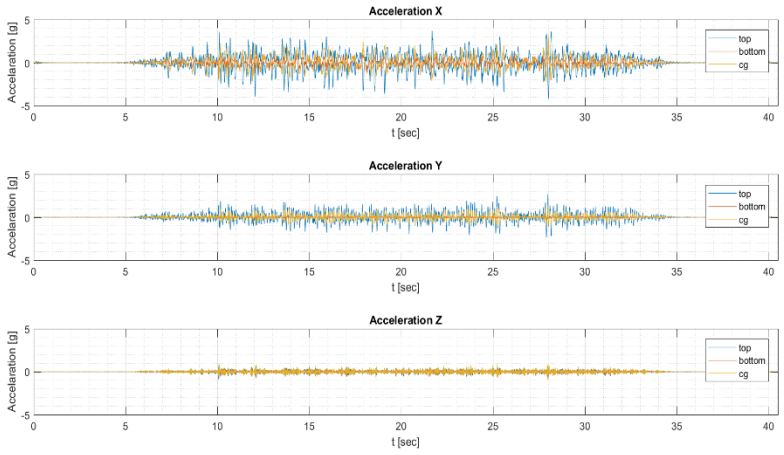

Acceleration UUT2 Cabint OSHPD IEEE LONG

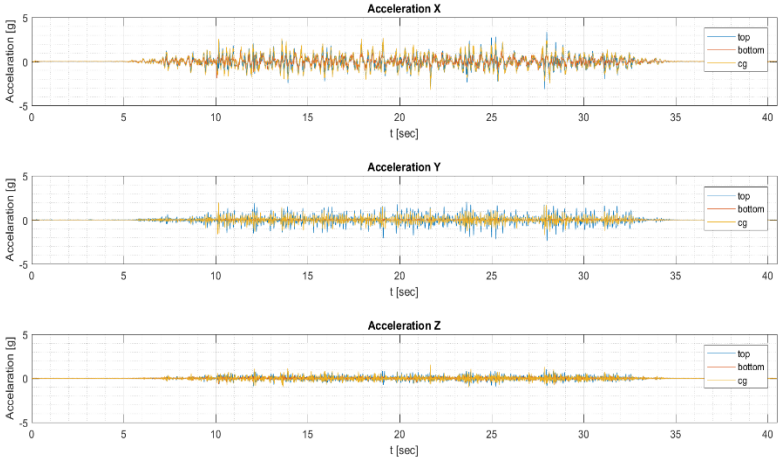

ux-uy Cabint OSHPD IEEE LONG

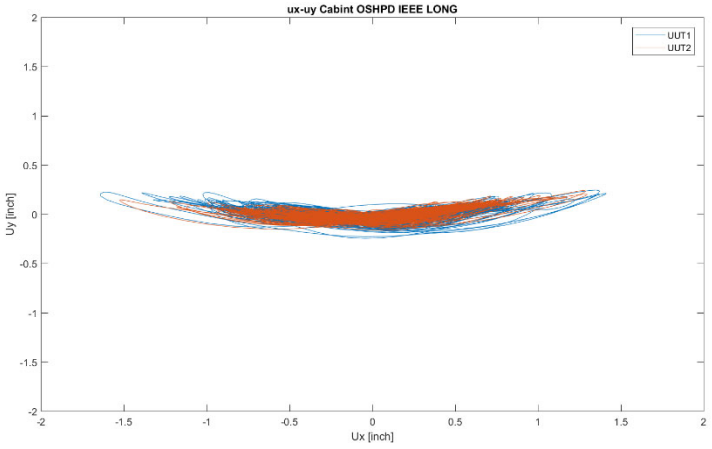

Anchor Forces Cabint OSHPD IEEE LONG

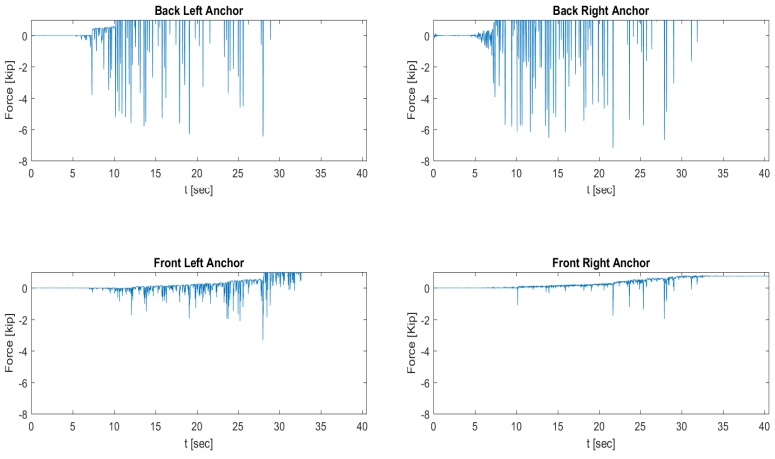

Testing Phase 2 – (30) IEEE XY direction

Floor Response Spectra Cabint OSHPD IEEE LAT LONG

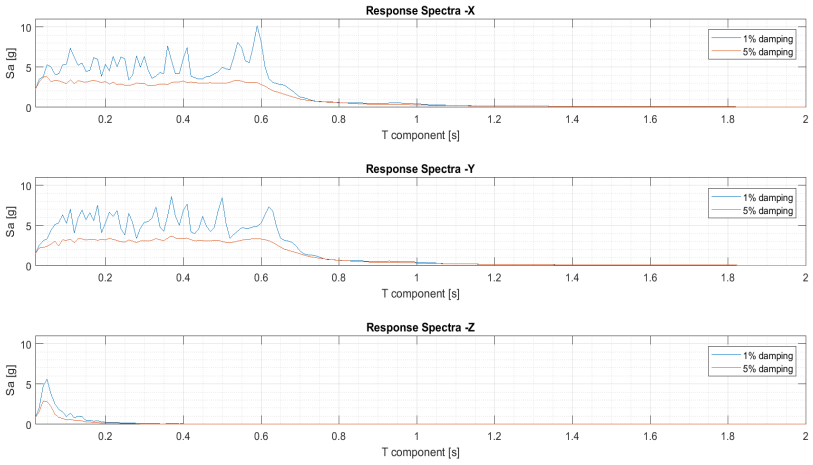

Table Acceleration Cabint OSHPD IEEE LAT LONG

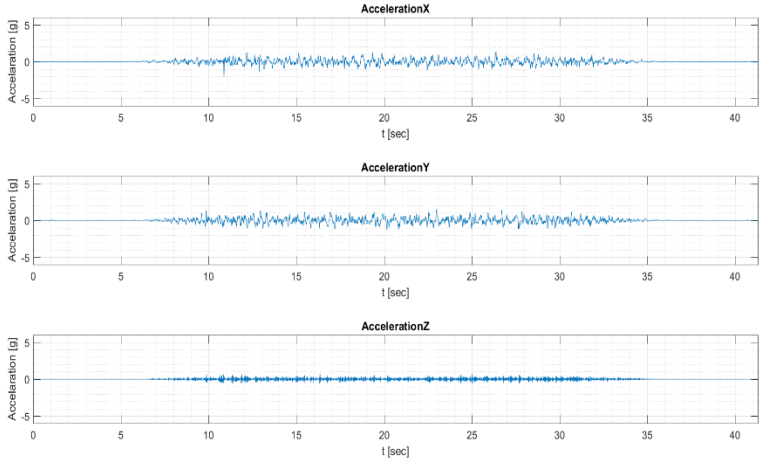

Acceleration UUT1 Cabint OSHPD IEEE LAT LONG

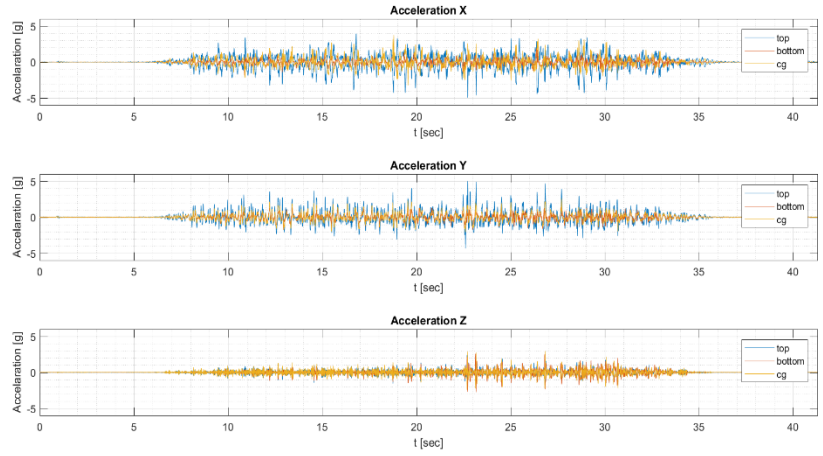

Acceleration UUT2 Cabint OSHPD IEEE LAT LONG

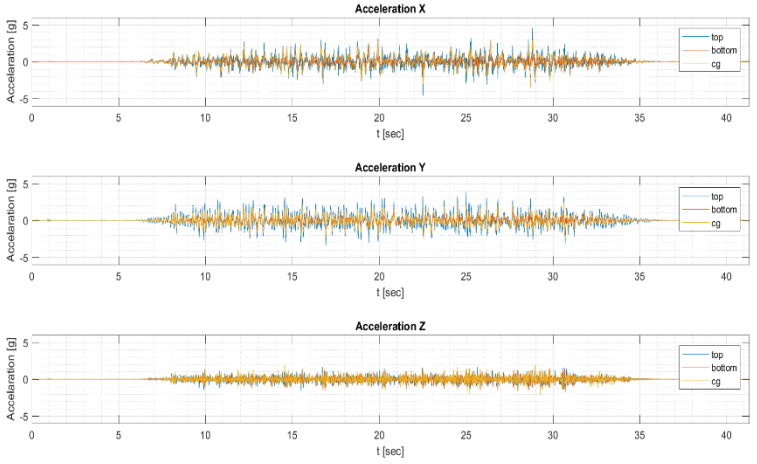

ux-uy Cabint OSHPD IEEE LAT LONG

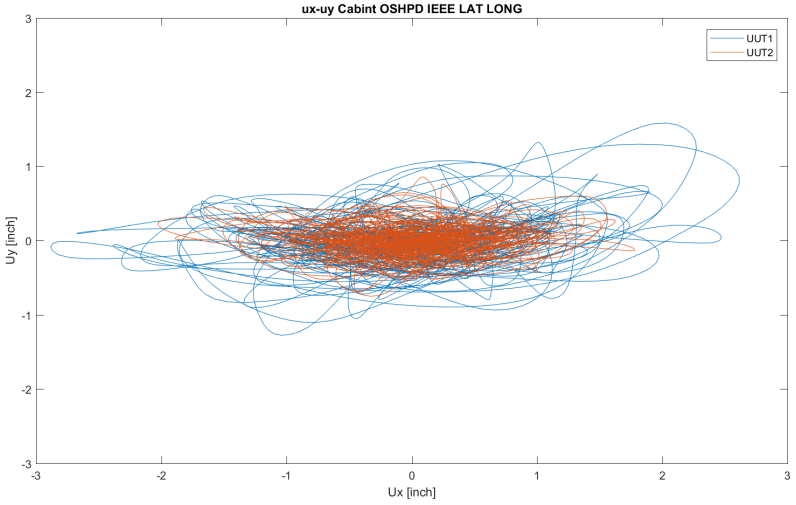

Anchor Forces Cabint OSHPD IEEE LAT LONG

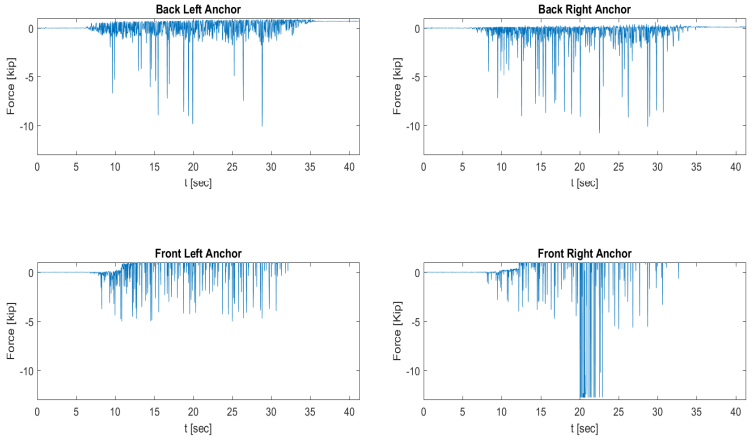

Testing Phase 2 – (31) Level 9 RP 475 XYZ direction - Aftershock

Floor Response Spectra Cabint RP475 L9 R LAT LONG VERT

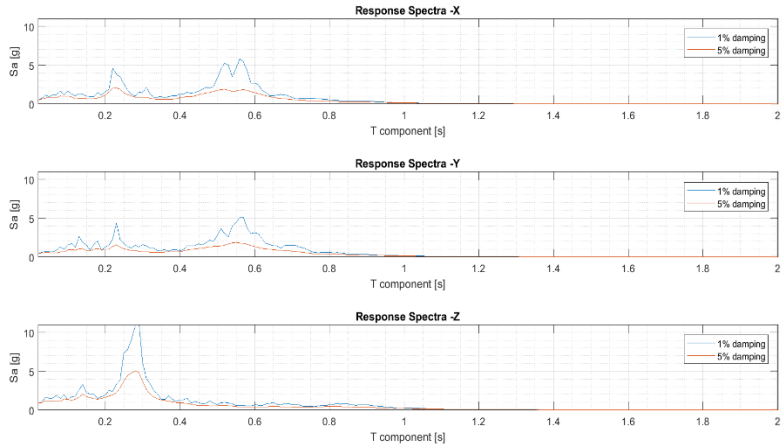

Table Acceleration Cabint RP475 L9 R LAT LONG VERT after shock

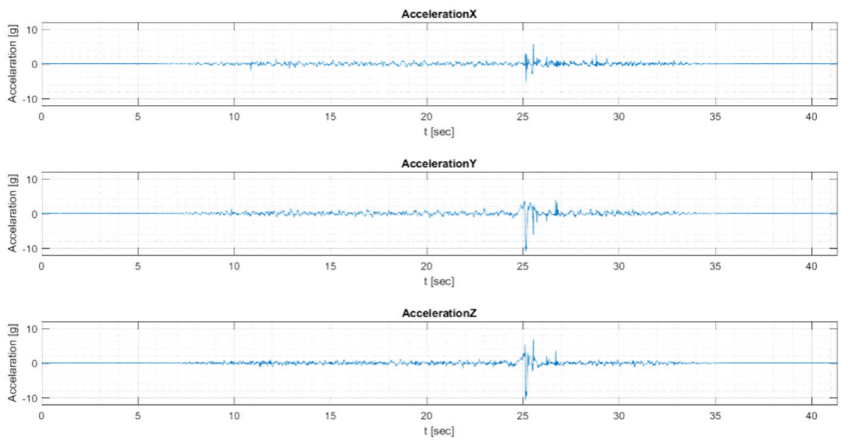

Acceleration UUT1 Cabint RP475 L9 R LAT LONG VERT after shock

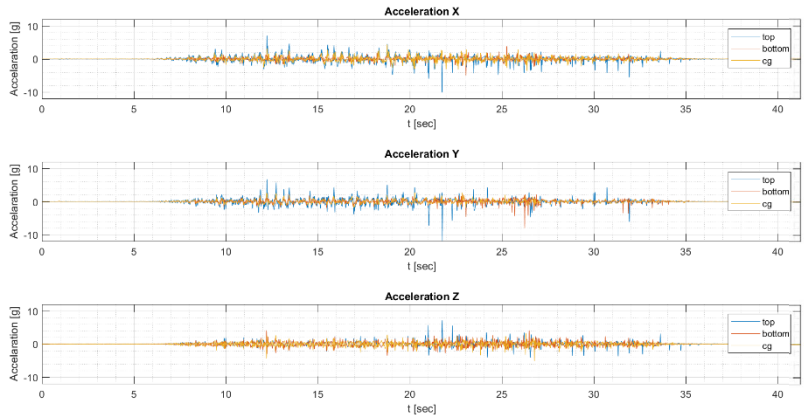

Acceleration UUT2 Cabint RP475 L9 R LAT LONG VERT after shock

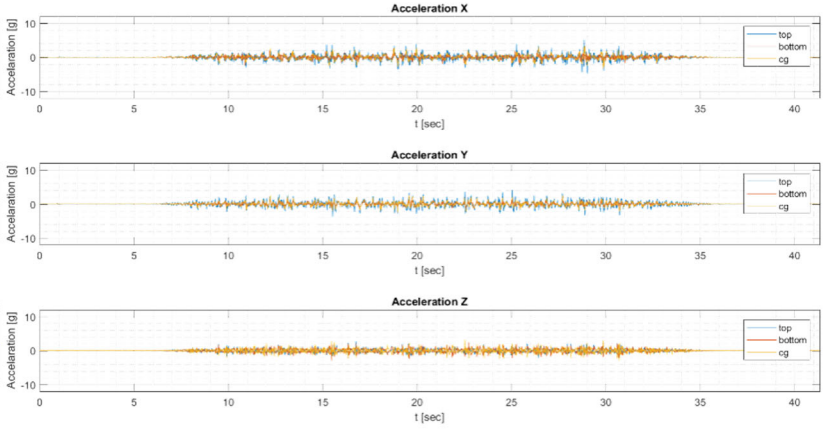

ux-uy Cabint RP475 L9 R LAT LONG VERT after shock

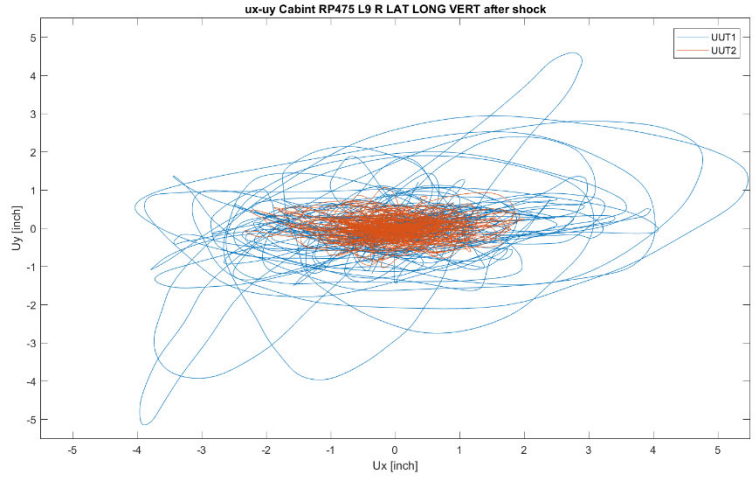

Anchor Forces Cabint RP475 L9 R LAT LONG VERT after shock

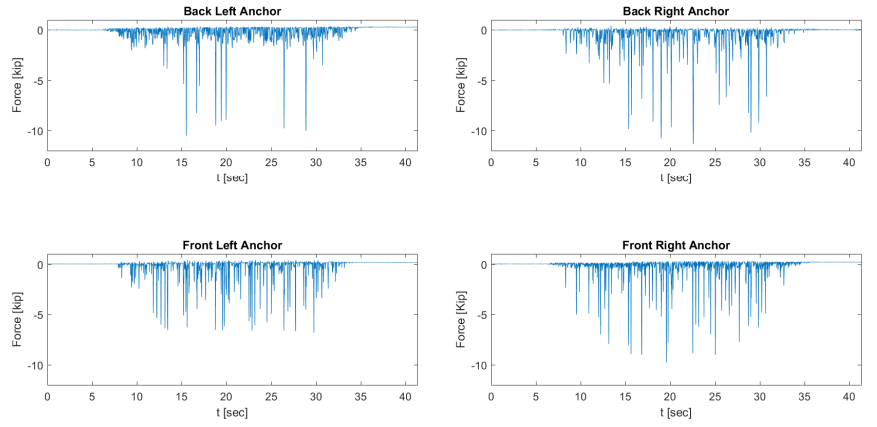

Testing Phase 2 – (32) Level 2 RP 475 X direction - Freezer

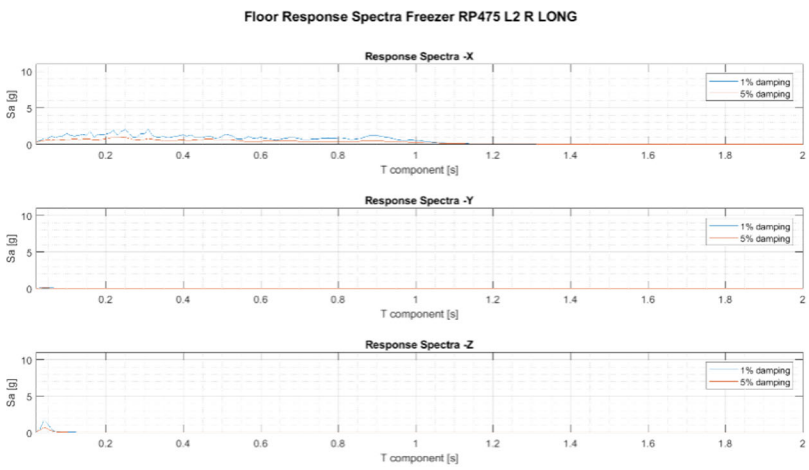

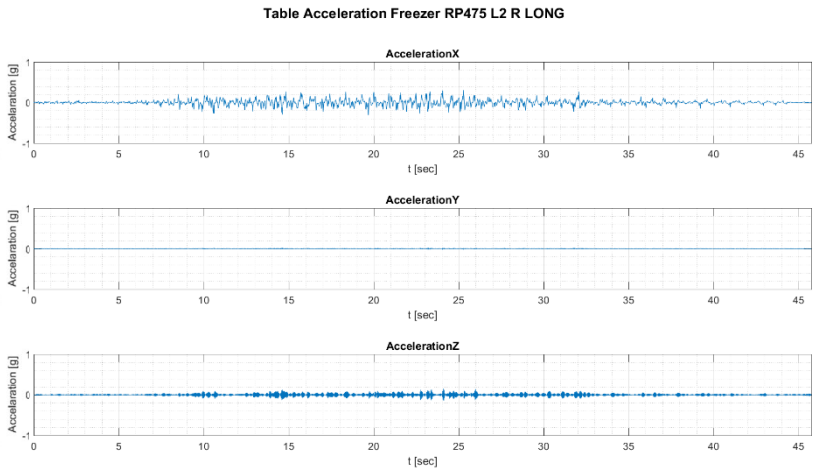

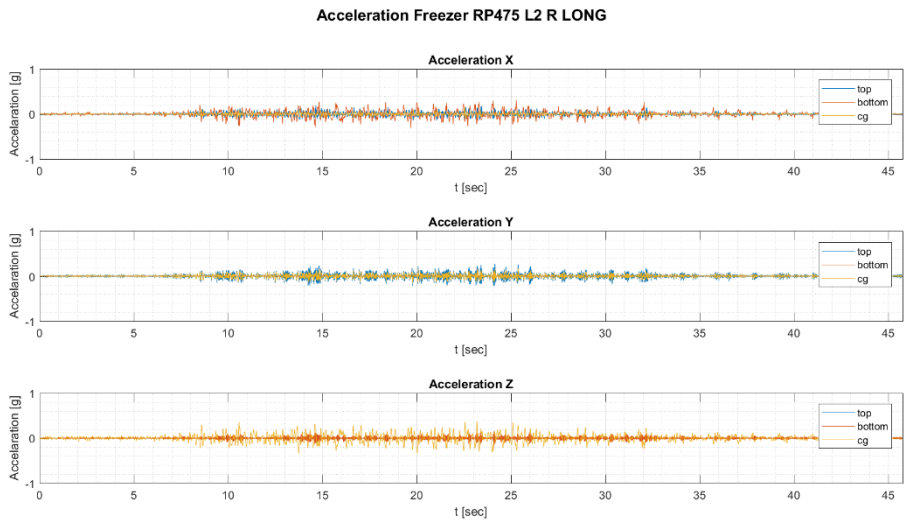

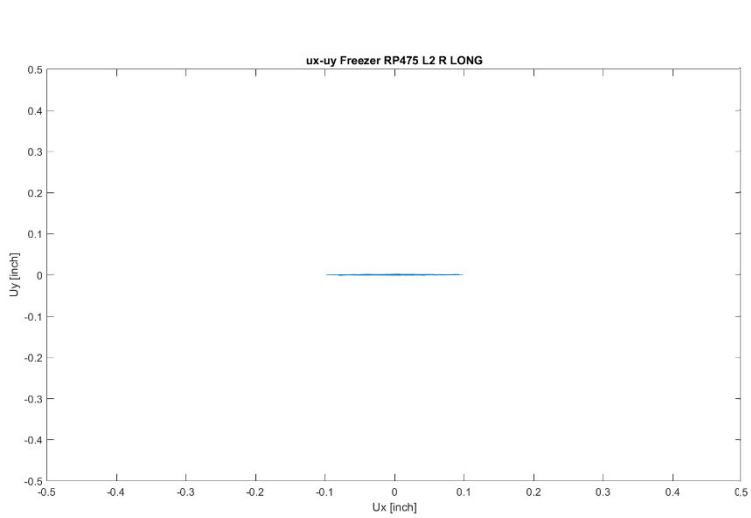

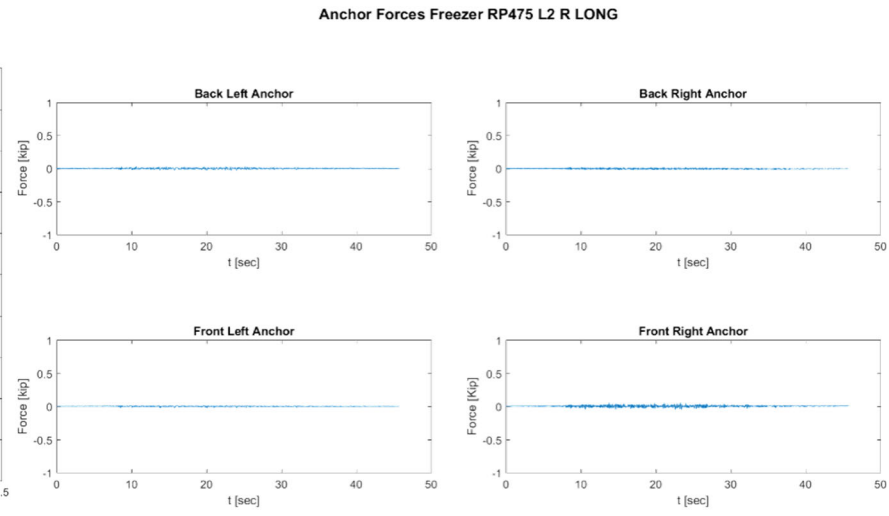

Testing Phase 2 – (33) Level 2 RP 475 Y direction - Freezer

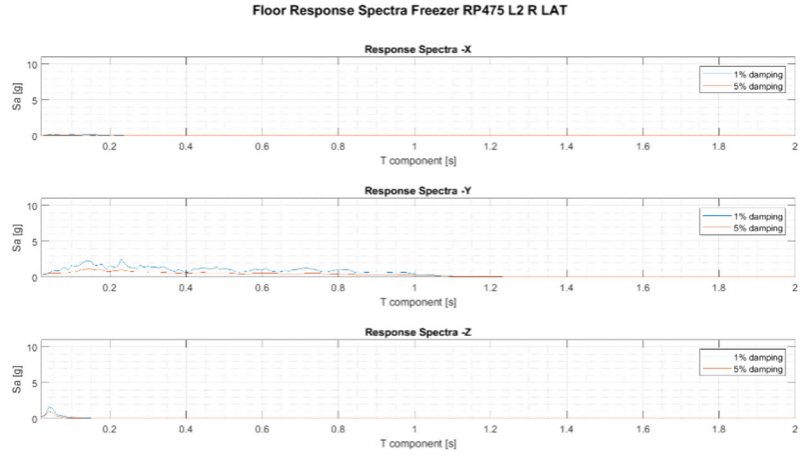

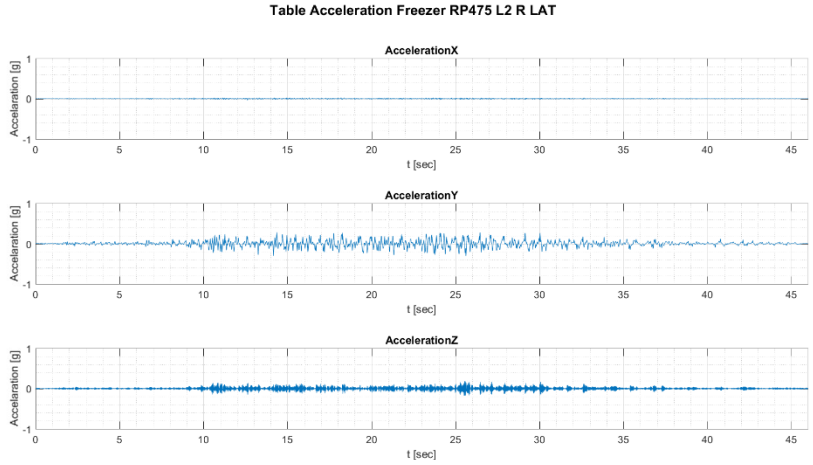

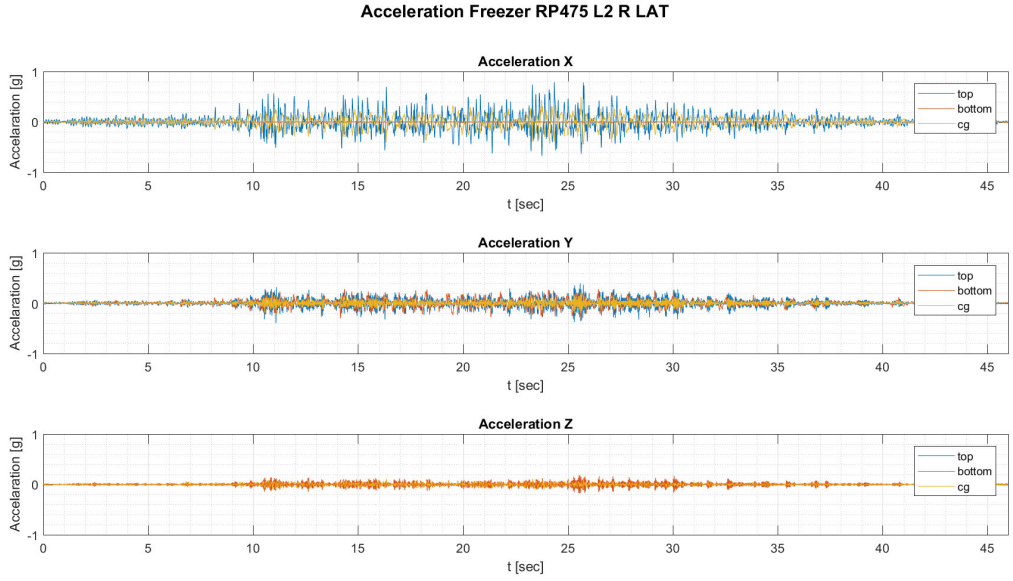

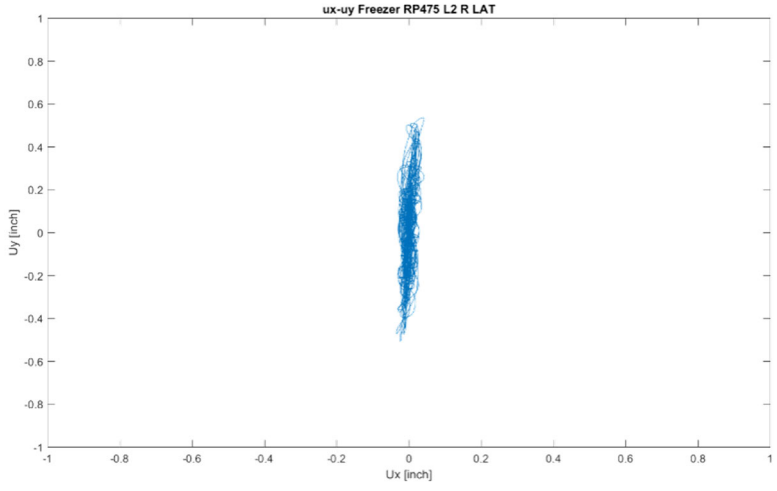

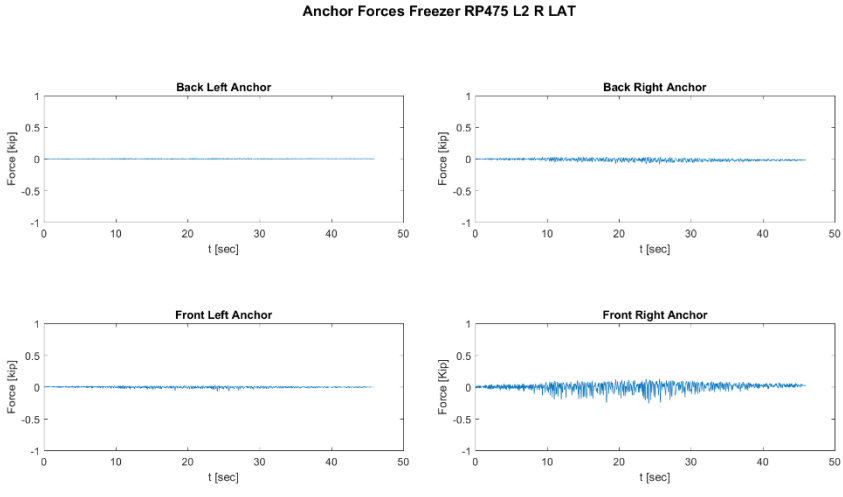

Testing Phase 2 – (34) Level 2 RP 475 XY direction - Freezer

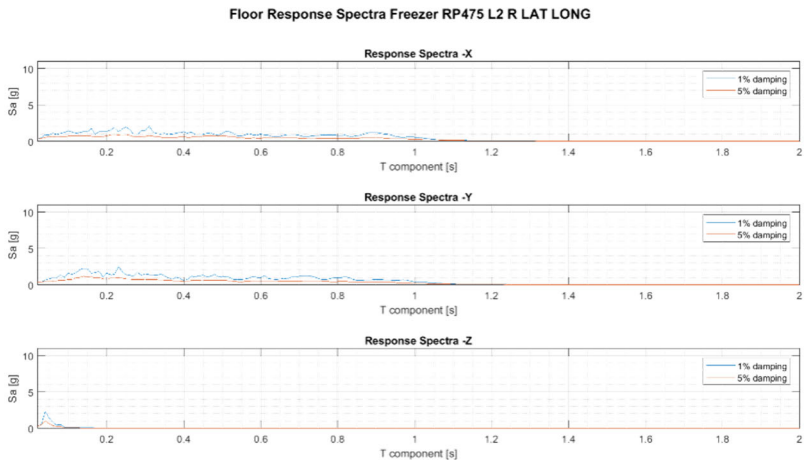

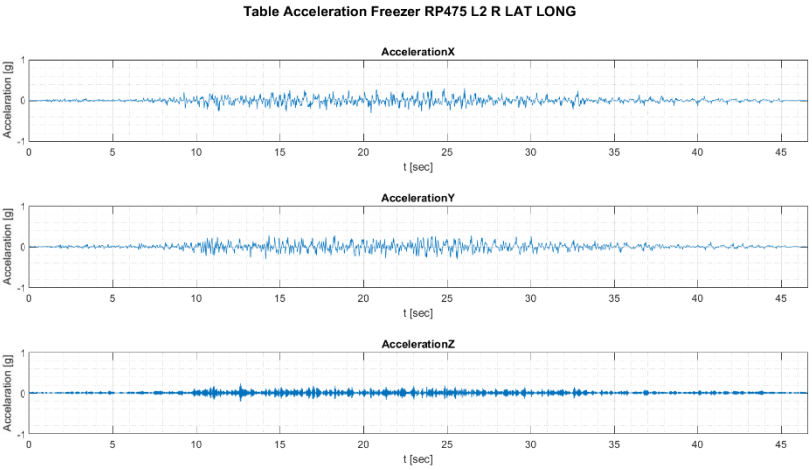

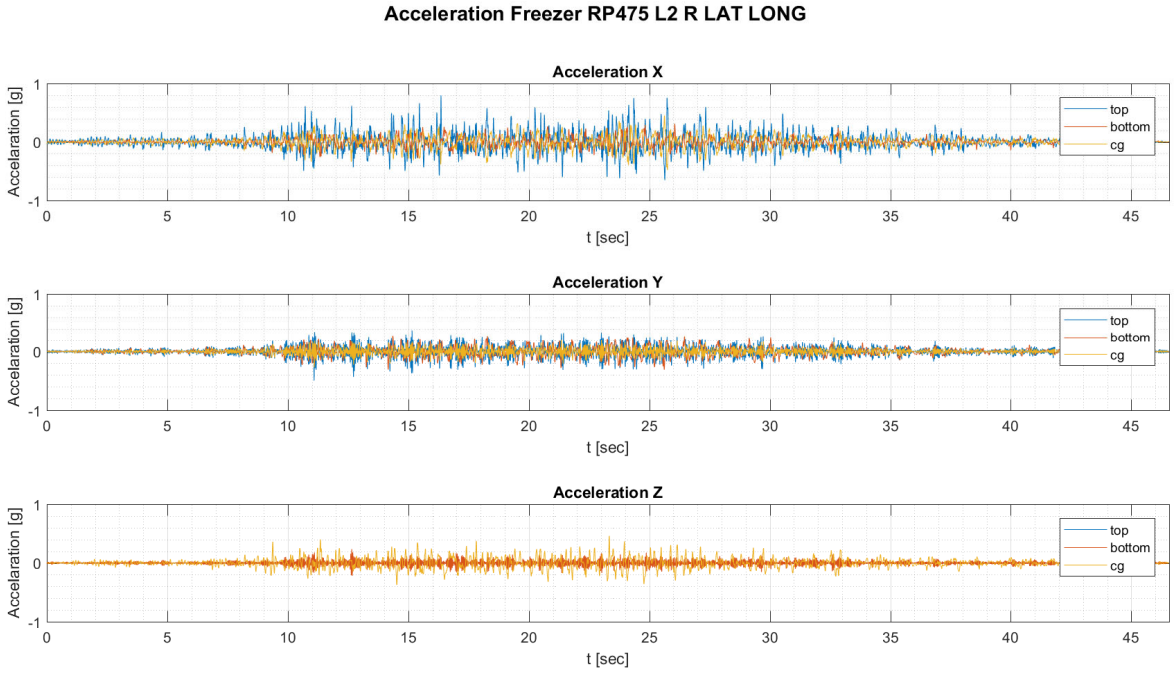

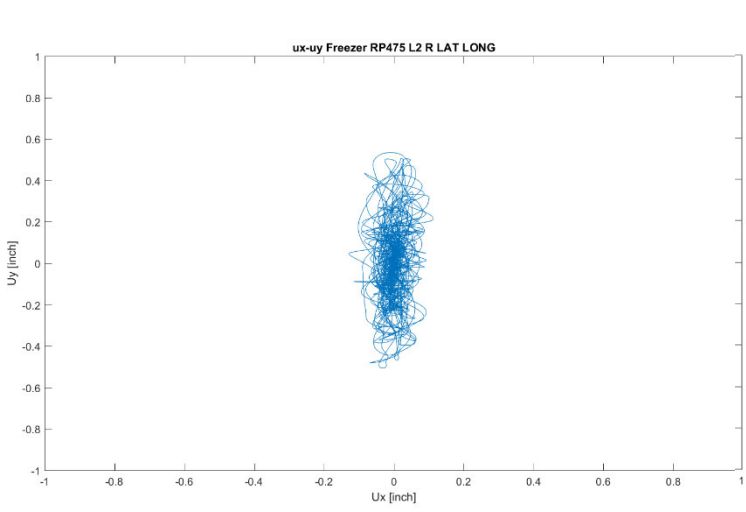

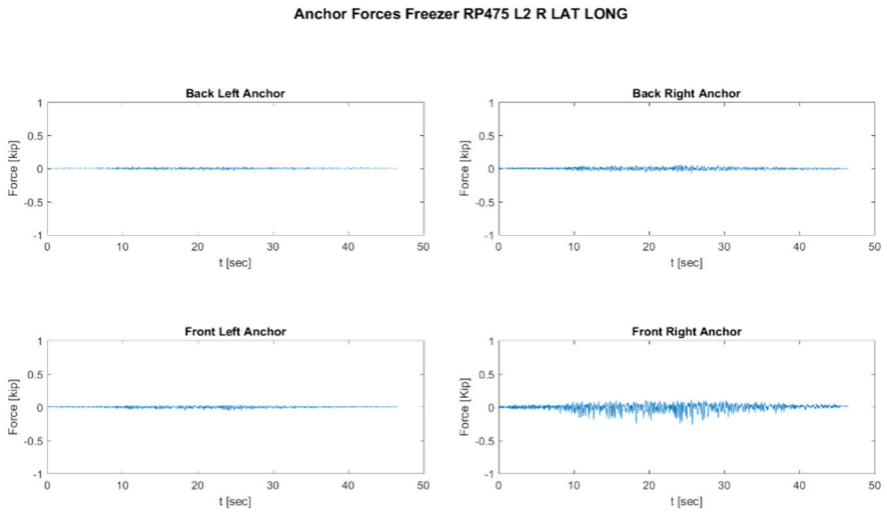

Testing Phase 2 – (35) Level 2 RP 475 XYZ direction - Freezer

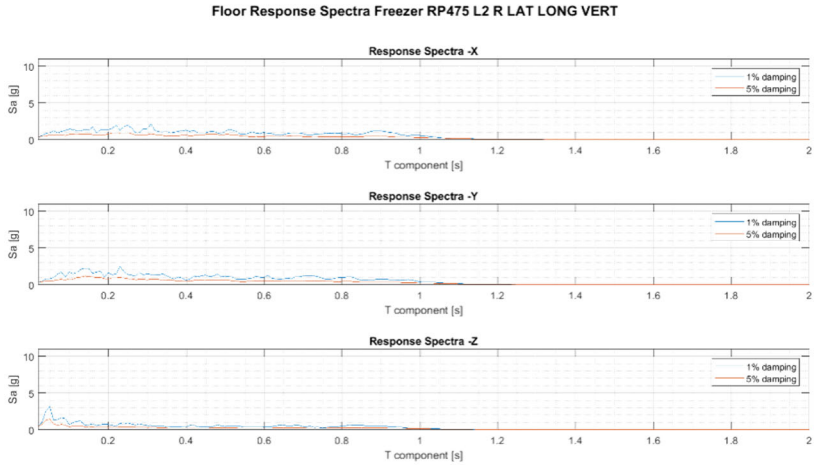

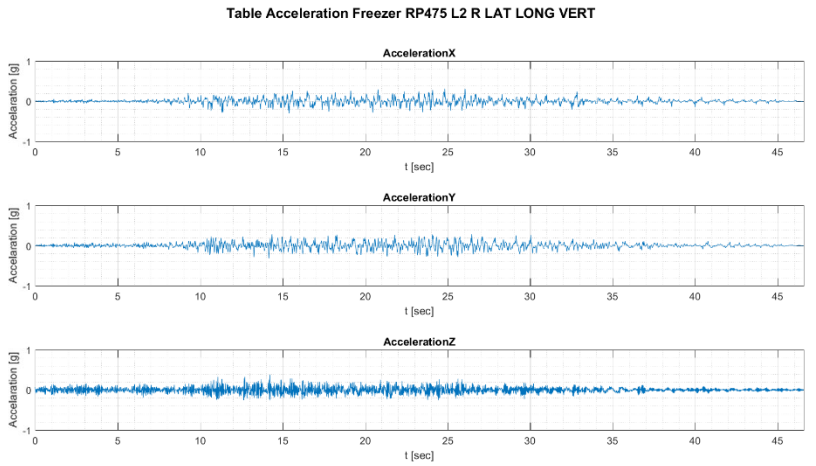

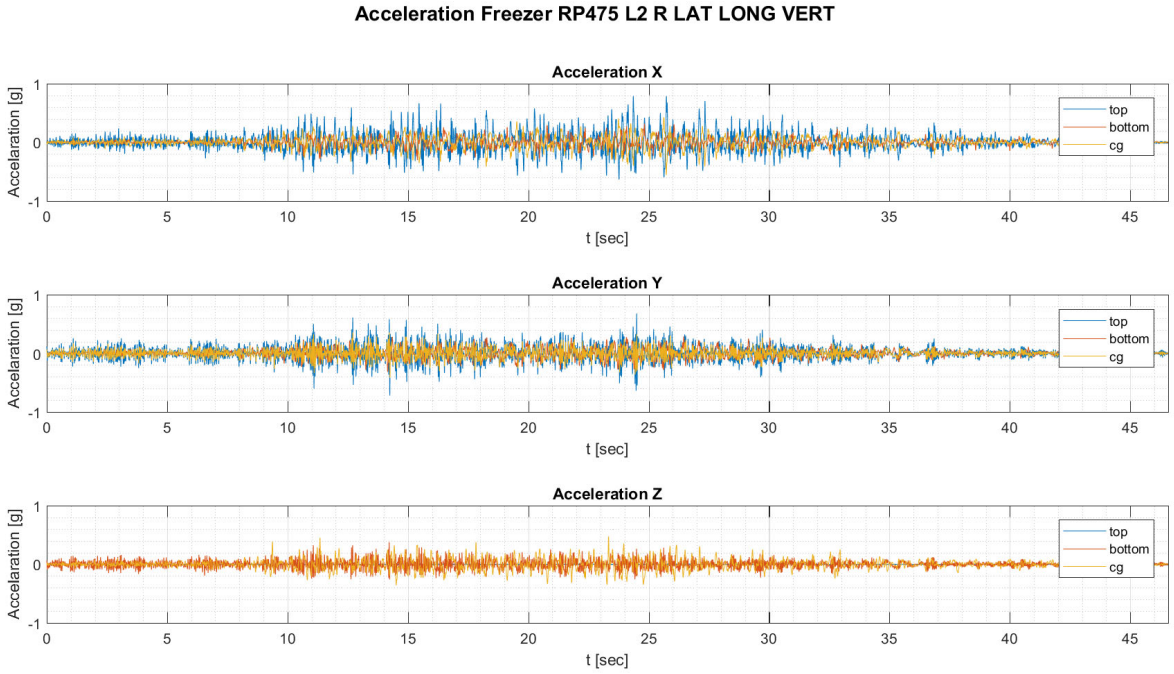

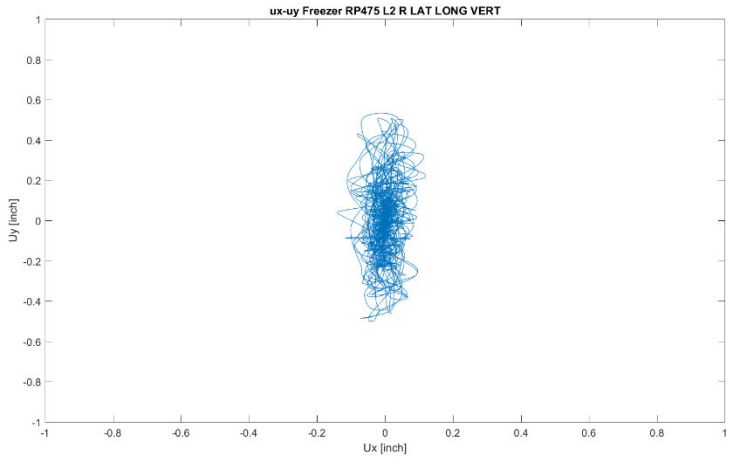

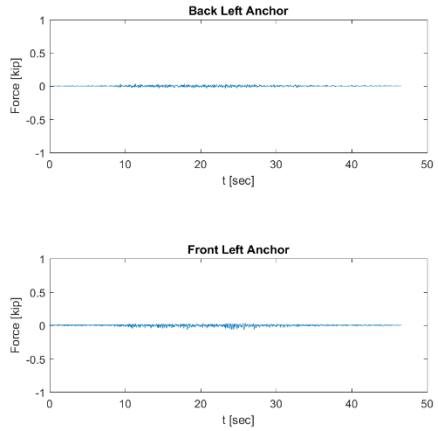

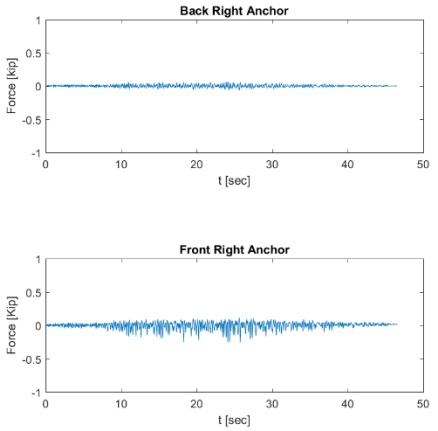

Testing Phase 2 – (36) Level 9 RP 475 X direction - Freezer

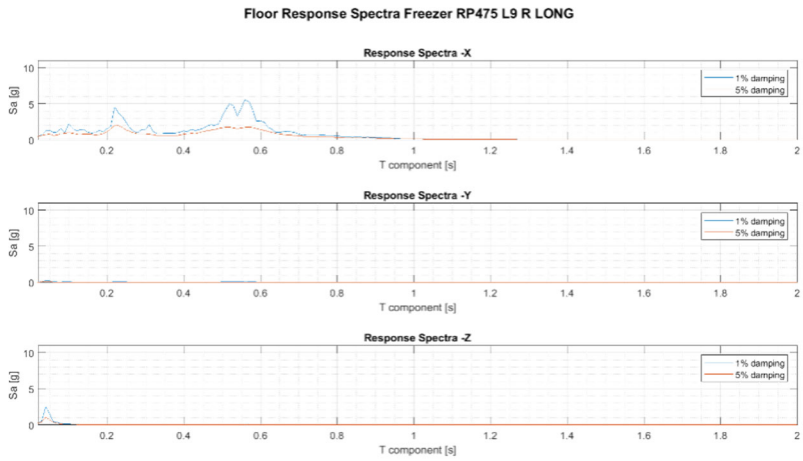

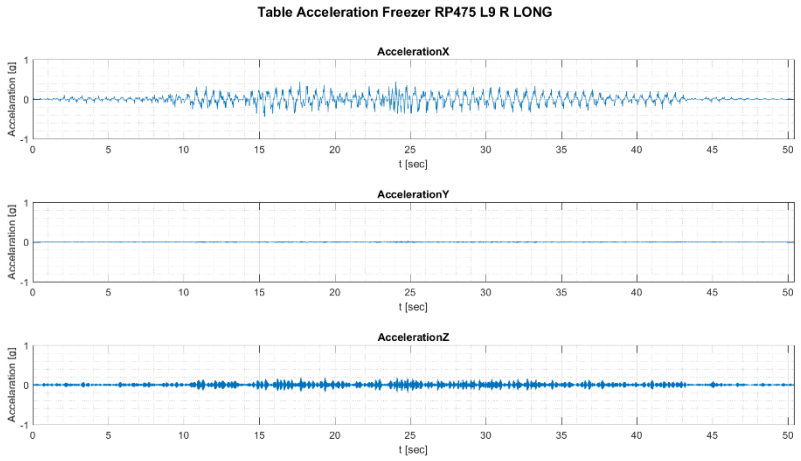

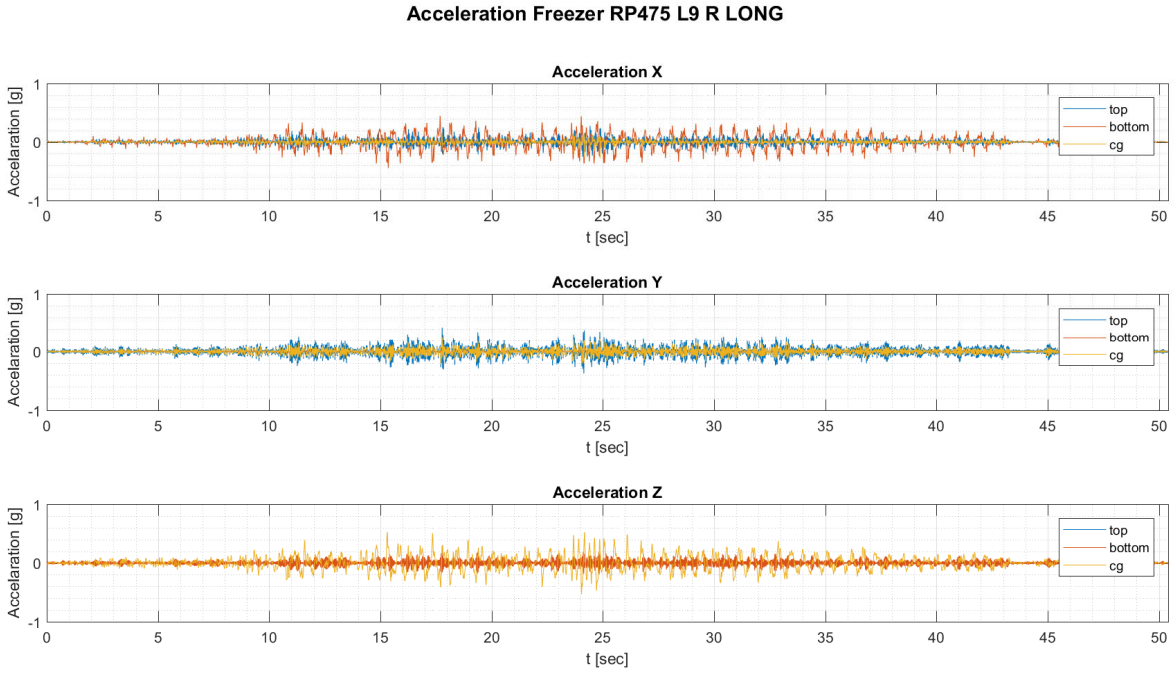

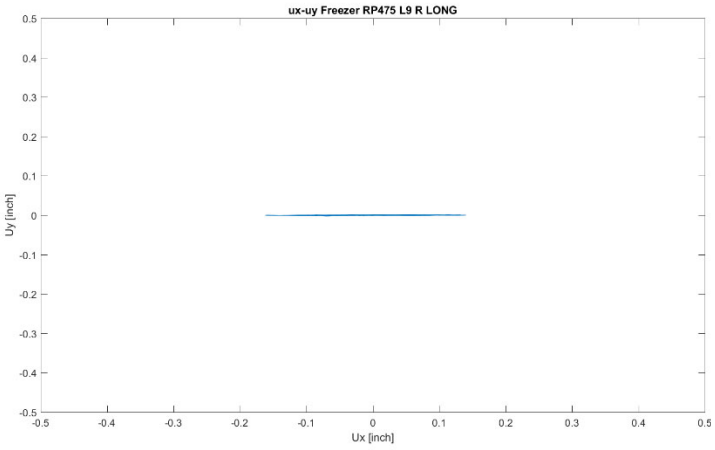

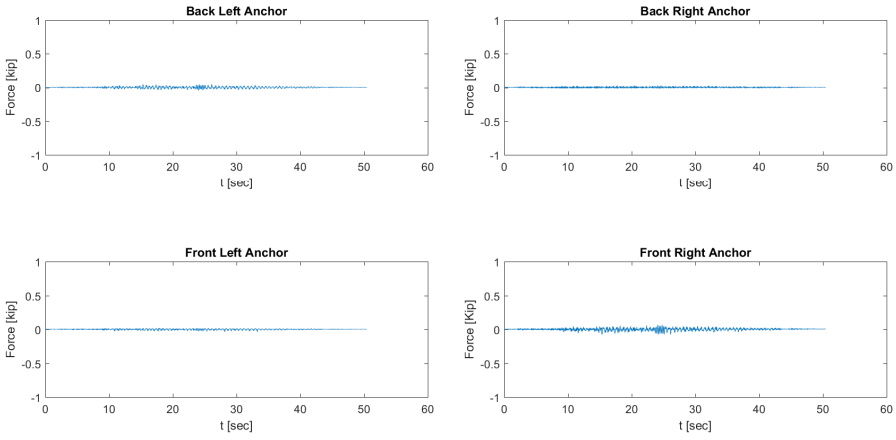

Testing Phase 2 – (37) Level 9 RP 475 Y direction - Freezer

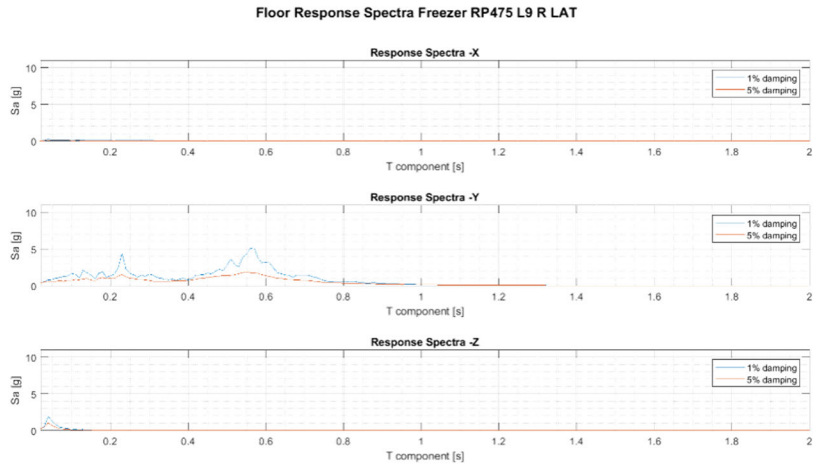

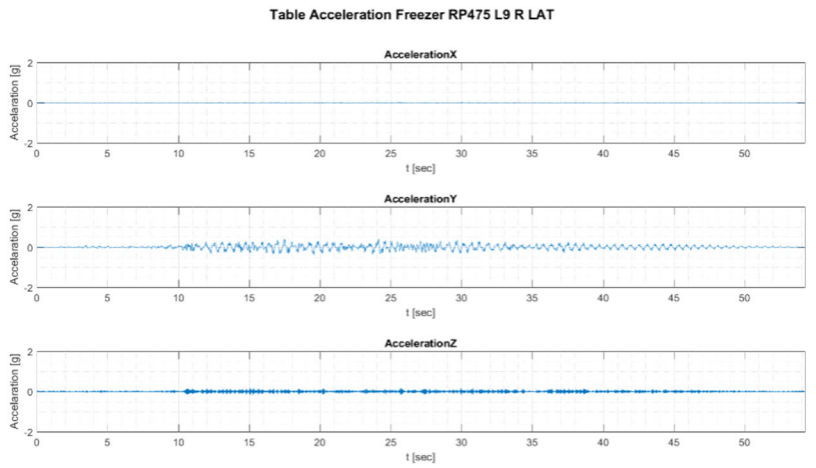

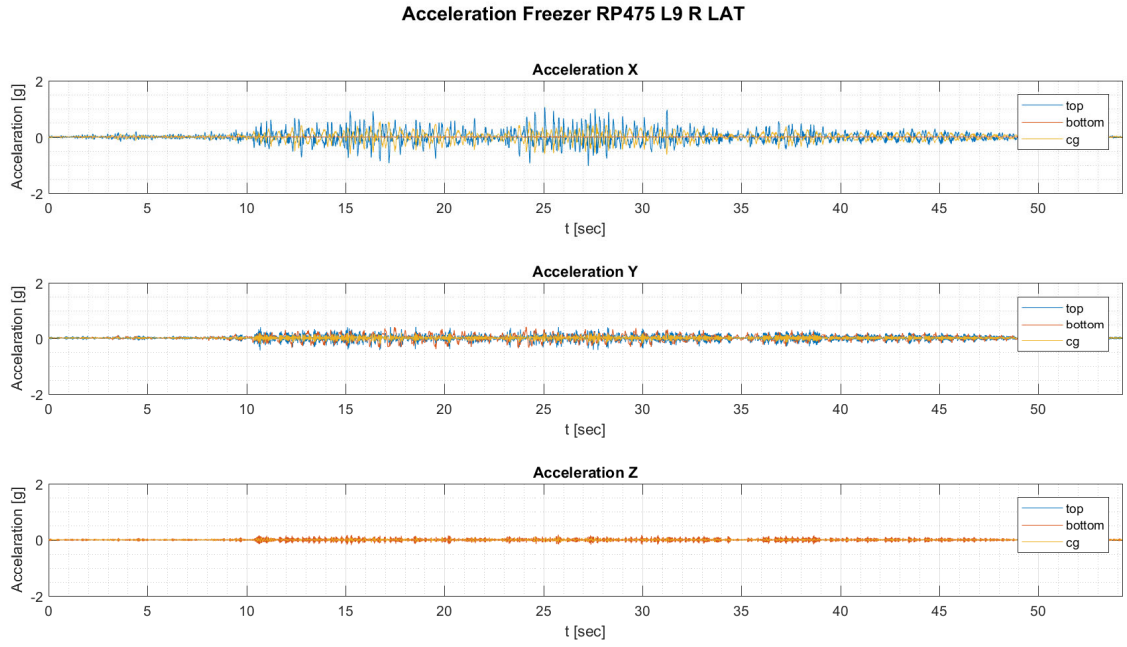

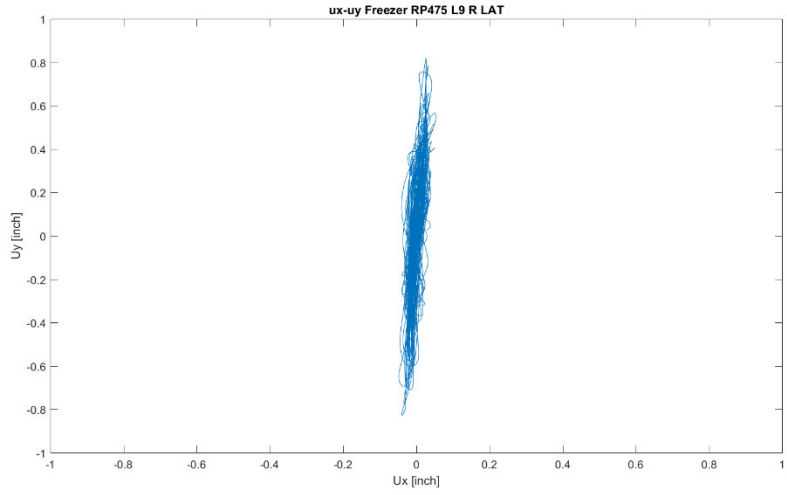

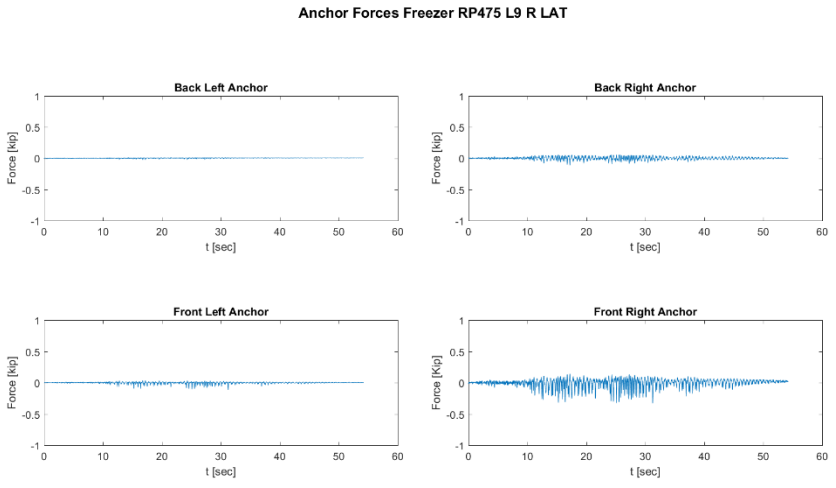

Testing Phase 2 – (38) Level 9 RP 475 XY direction - Freezer

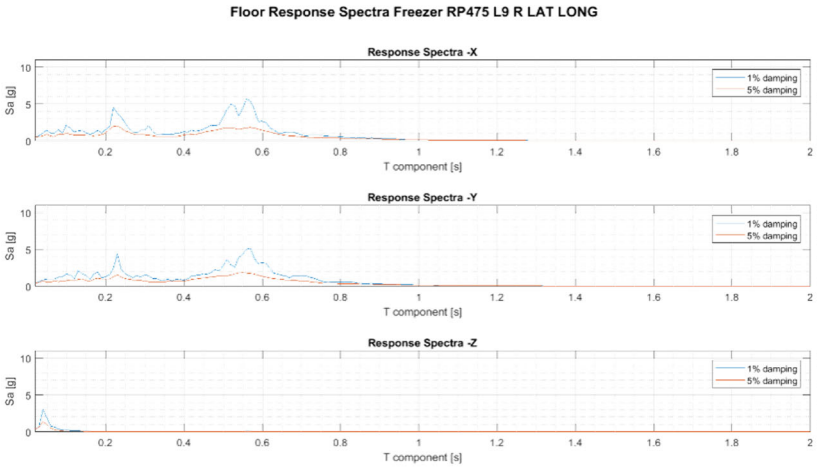

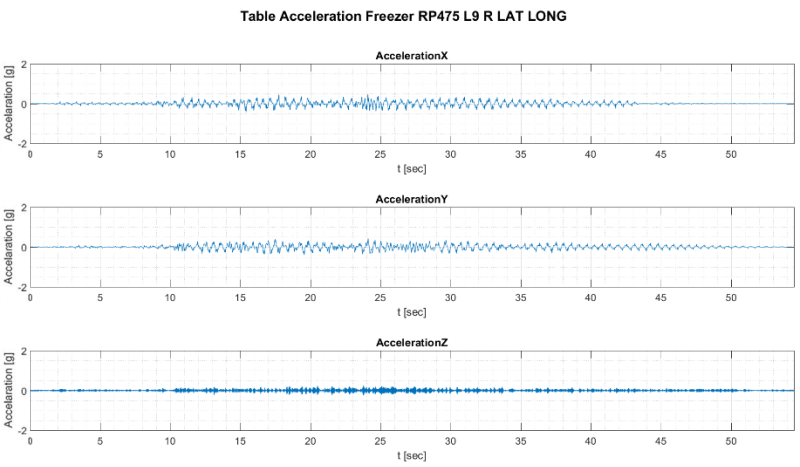

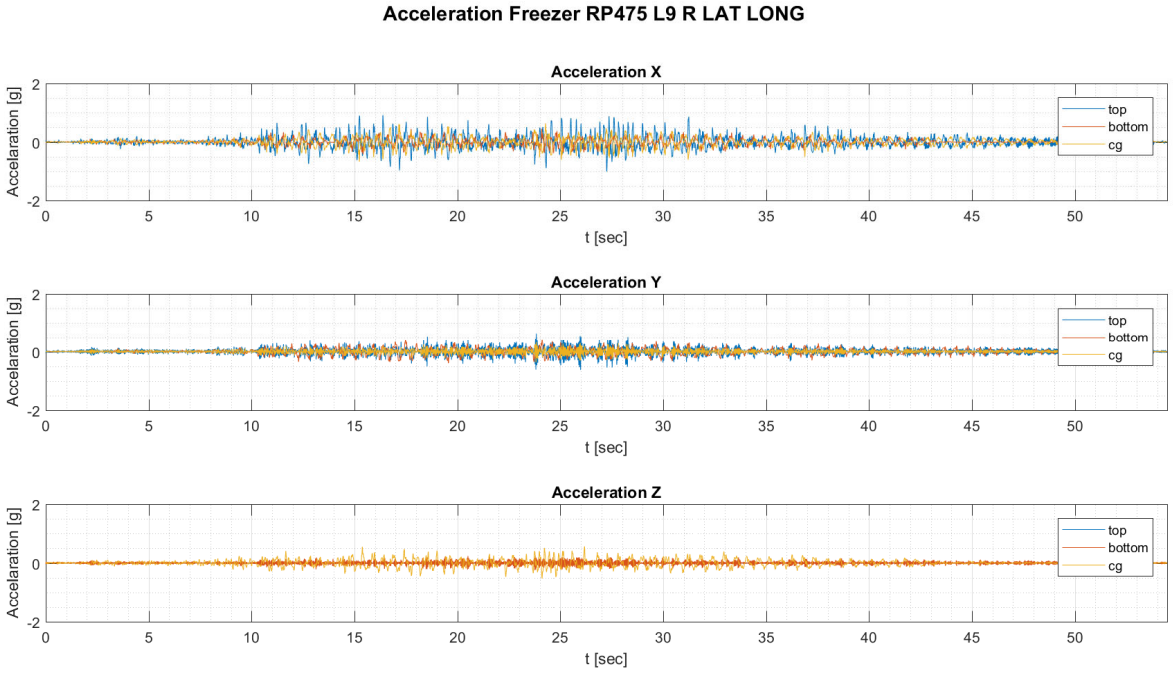

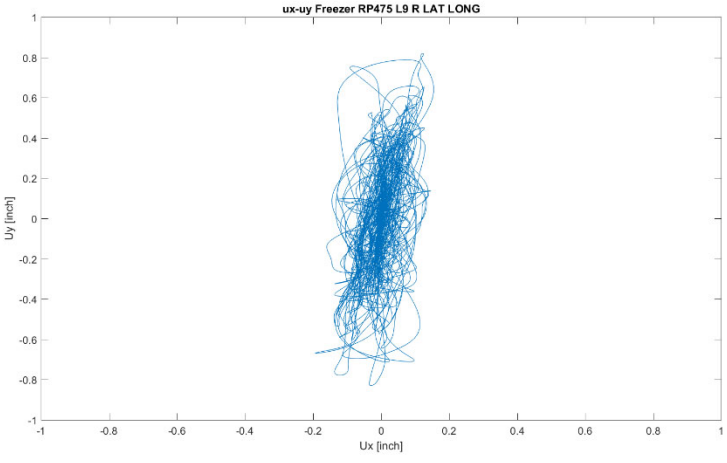

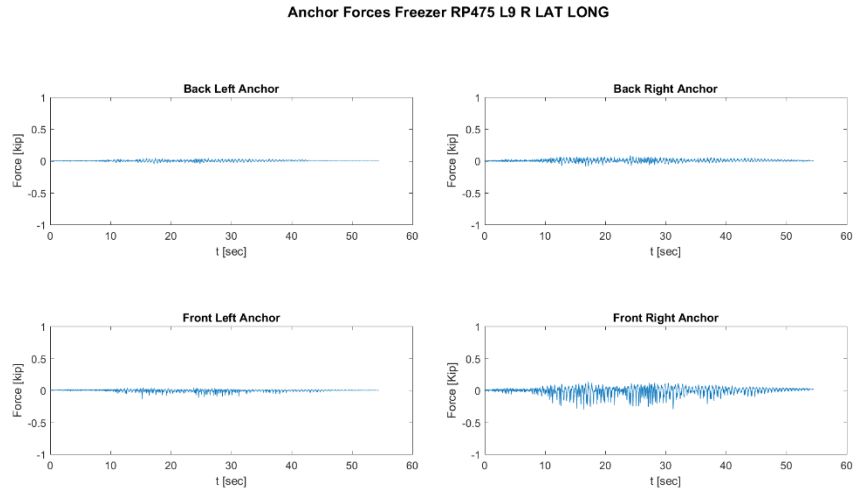

Testing Phase 2 – (39) Level 9 RP 475 XYZ direction - Freezer

Floor Response Spectra Freezer RP475 L9 R LAT LONG VERT

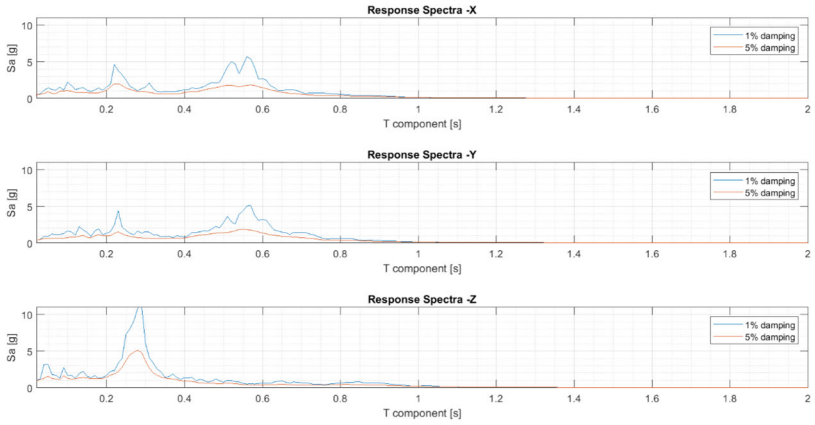

Table Acceleration Freezer RP475 L9 R LAT LONG VERT

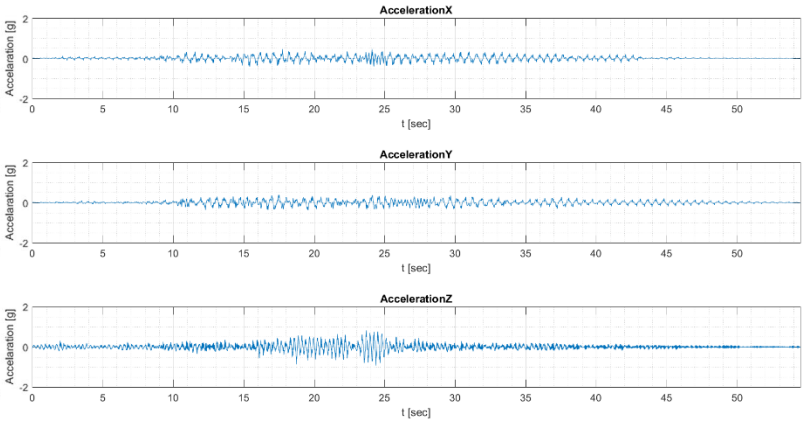

Acceleration Freezer RP475 L9 R LAT LONG VERT

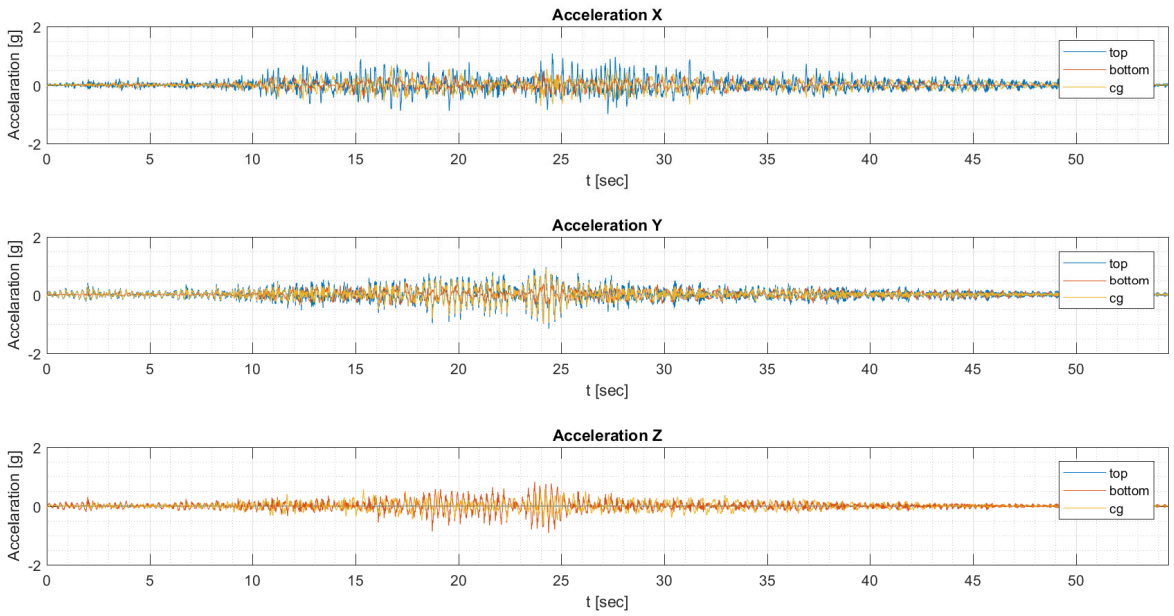

ux-uy Freezer RP475 L9 R LAT LONG VERT

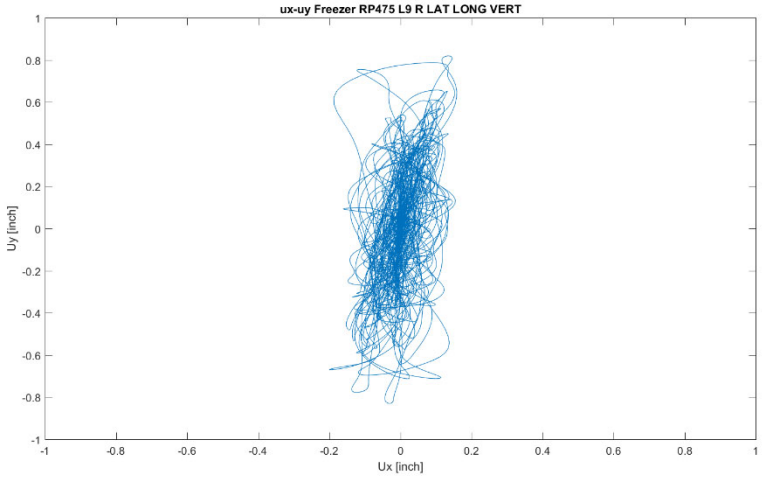

Anchor Forces Freezer RP475 L9 R LAT LONG VERT

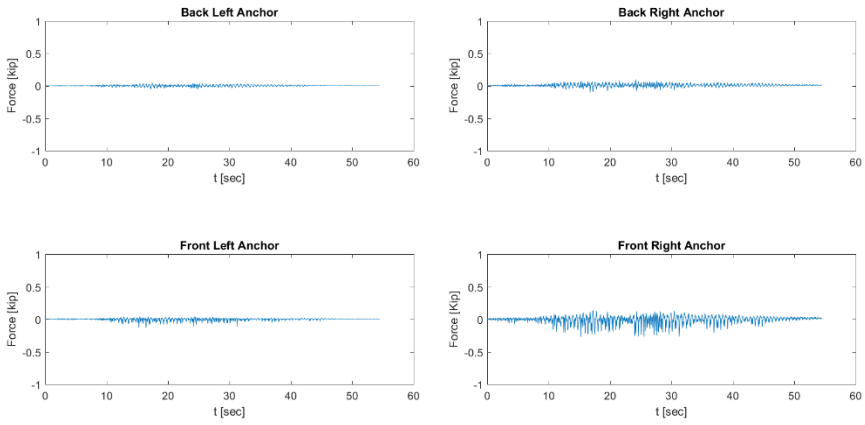

Testing Phase 2 – (40) Roof RP 475 X direction - Freezer

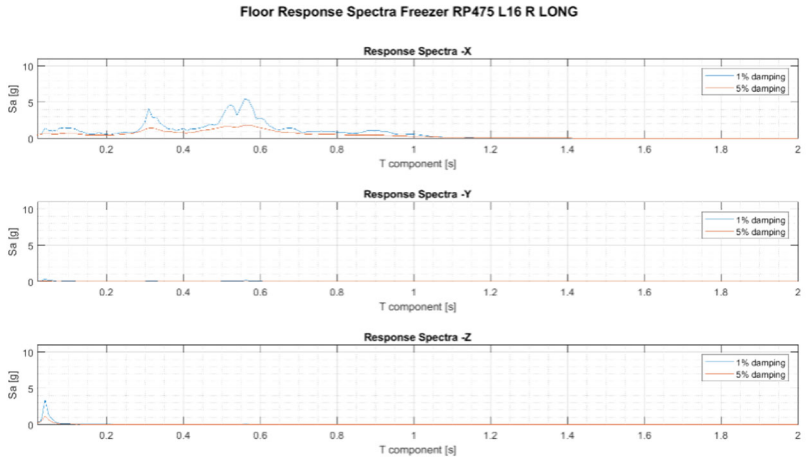

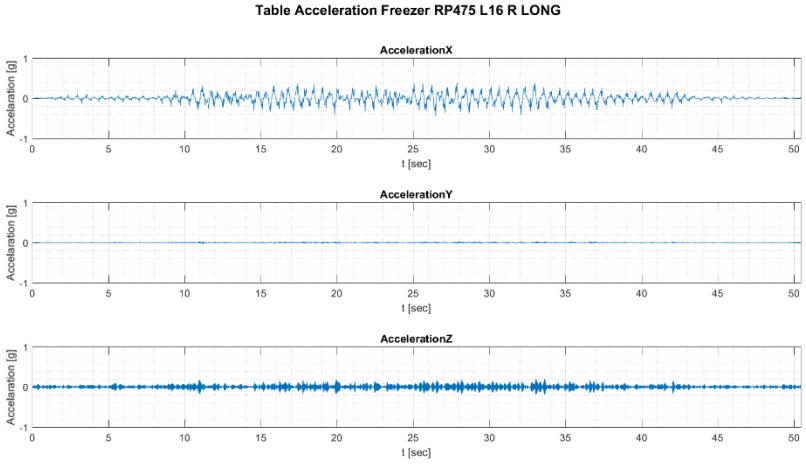

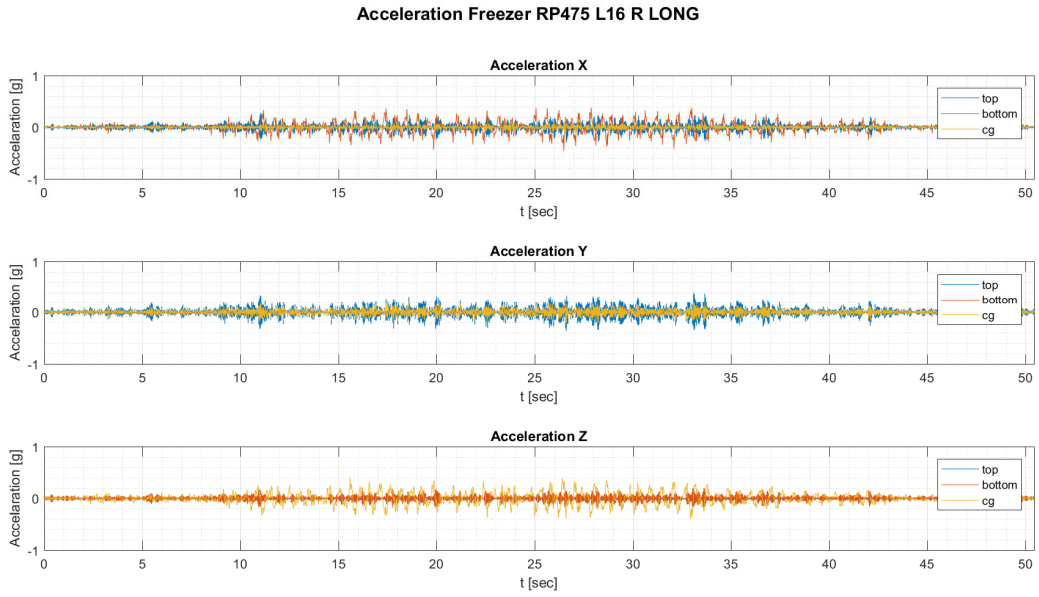

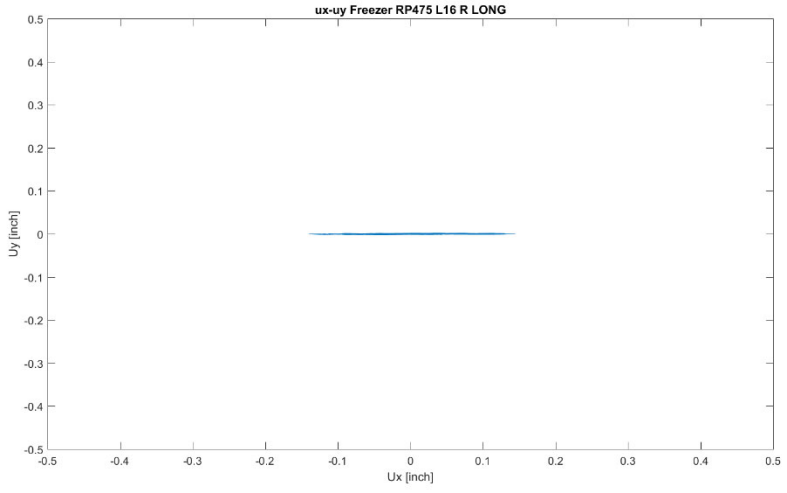

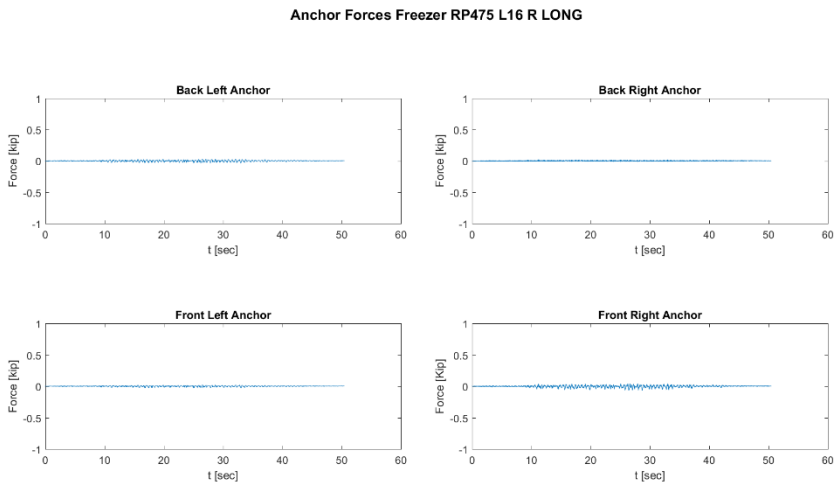

Testing Phase 2 – (41) Roof RP 475 Y direction - Freezer

Floor Response Spectra Freezer RP475 L16 R LAT

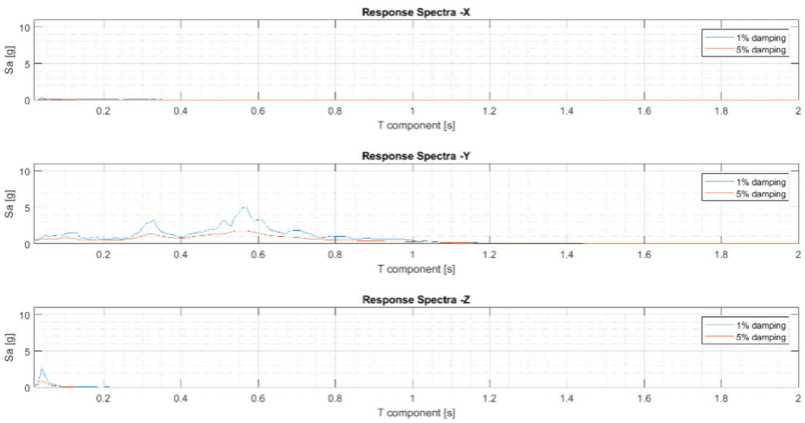

Table Acceleration Freezer RP475 L16 R LAT

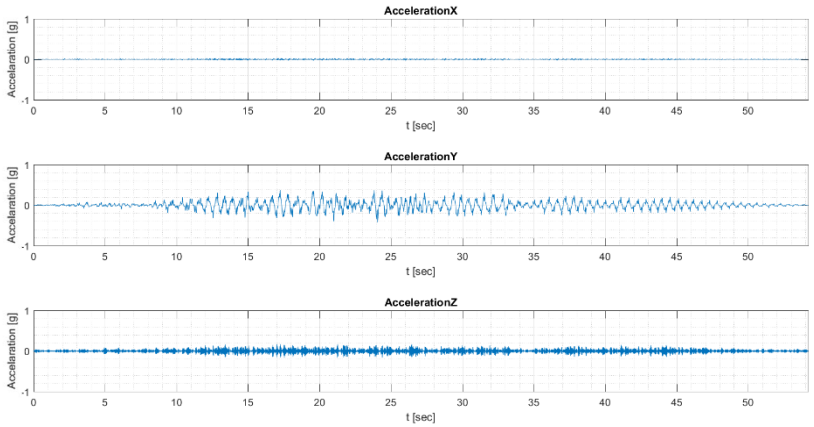

Acceleration Freezer RP475 L16 R LAT

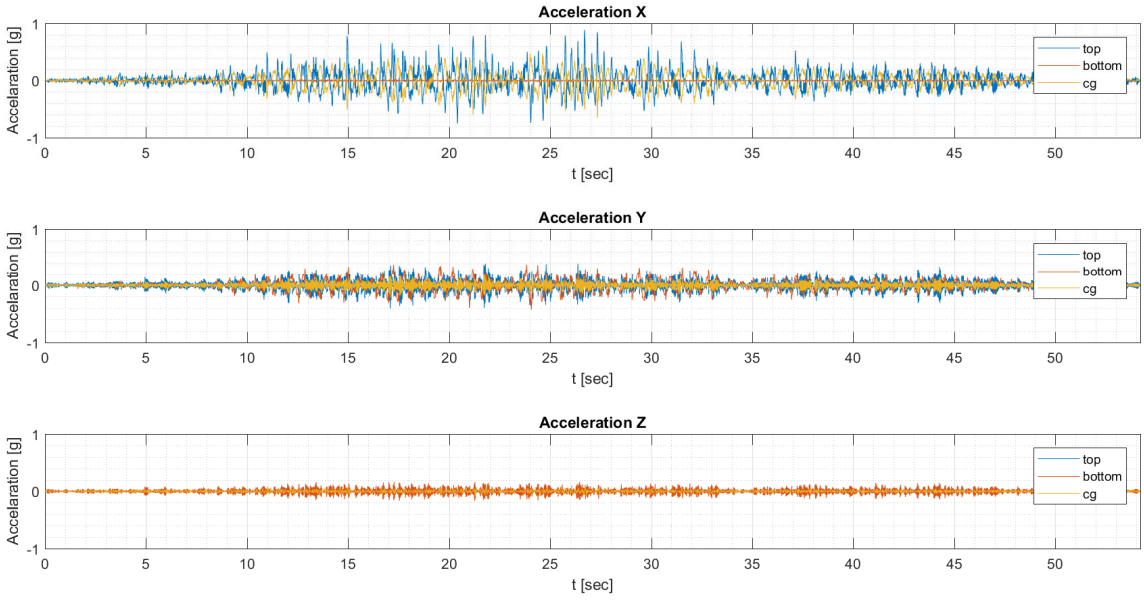

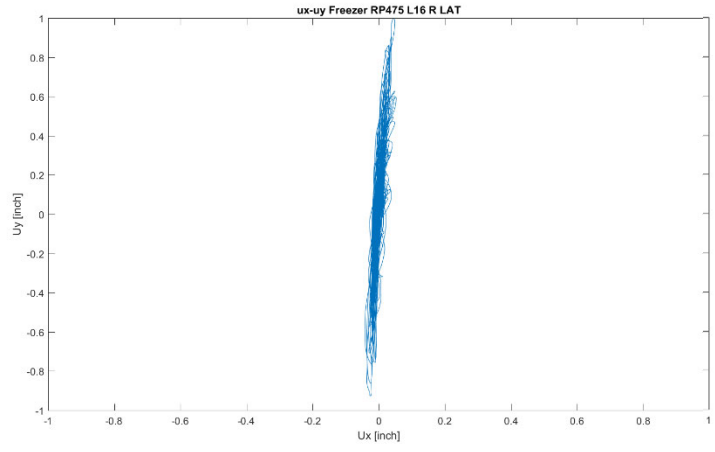

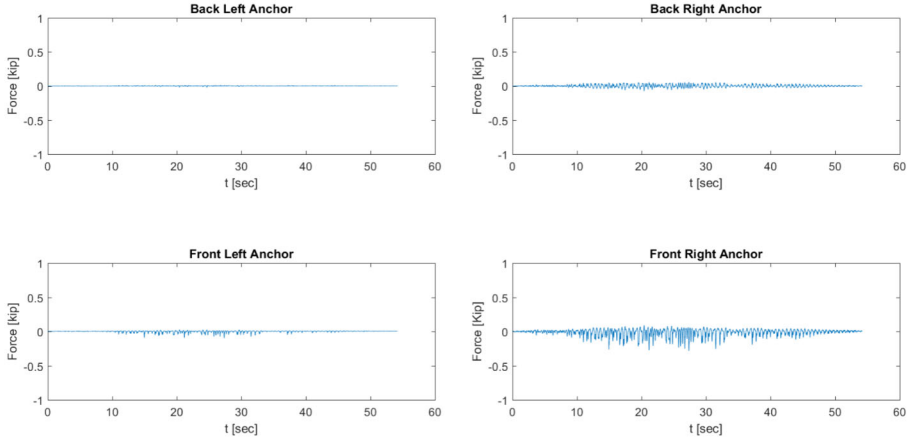

Testing Phase 2 – (42) Roof RP 475 XY direction - Freezer

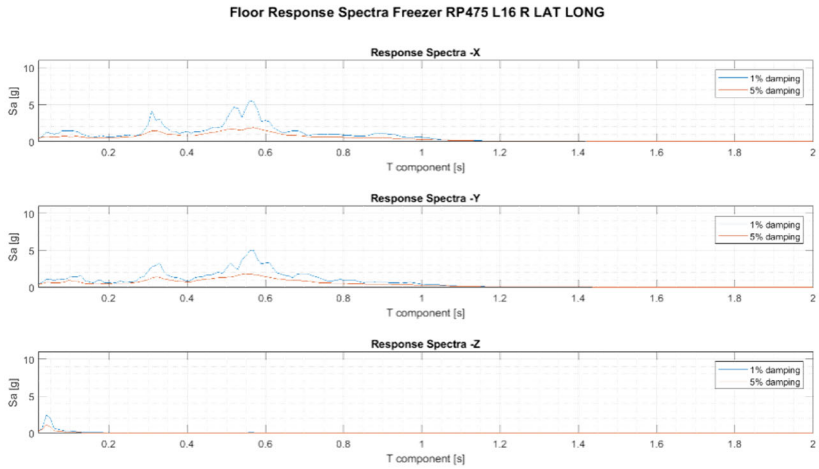

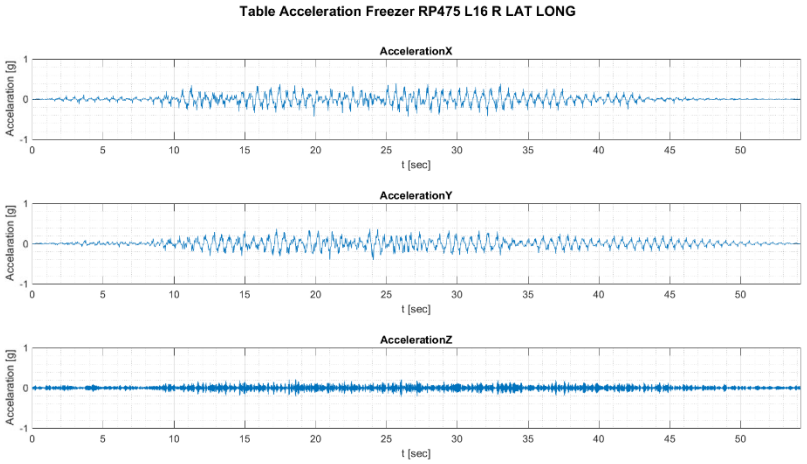

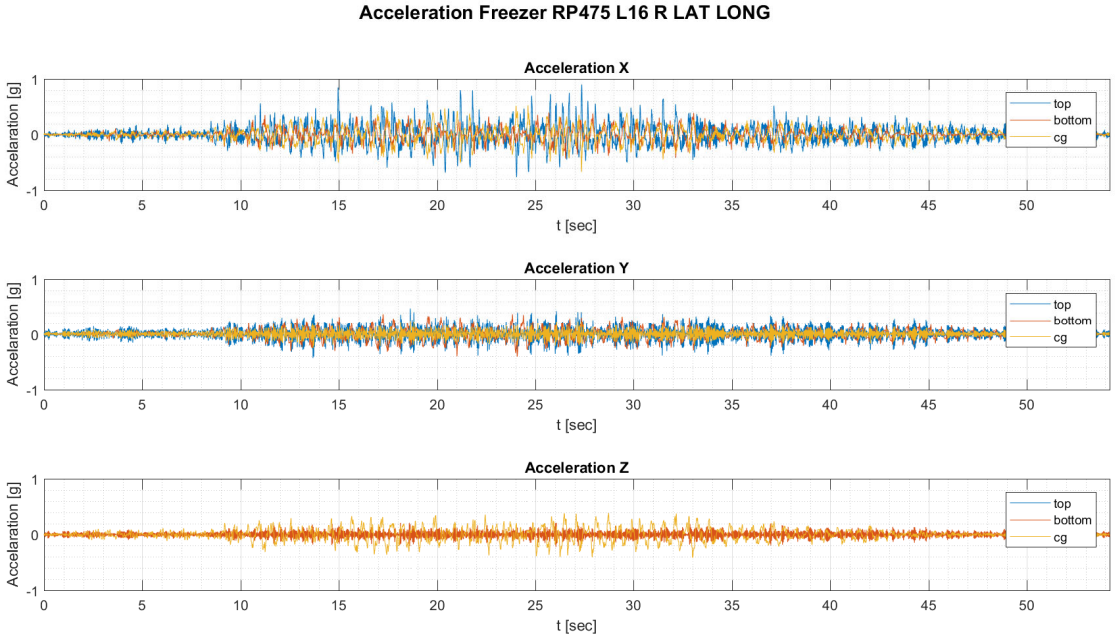

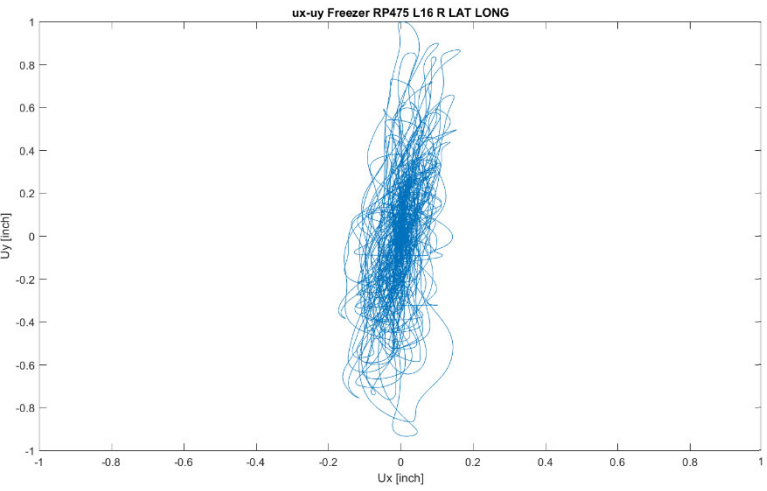

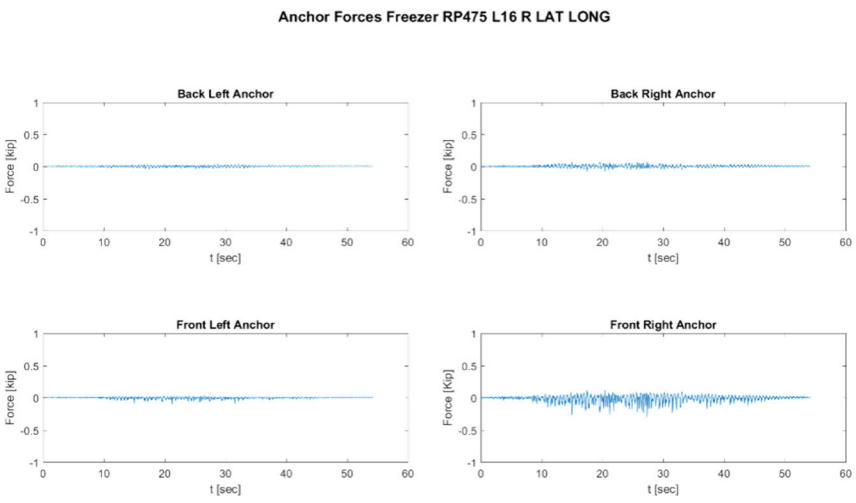

Testing Phase 2 – (43) Roof RP 475 XYZ direction - Freezer

Floor Response Spectra Freezer RP475 L16 R LAT LONG VERT

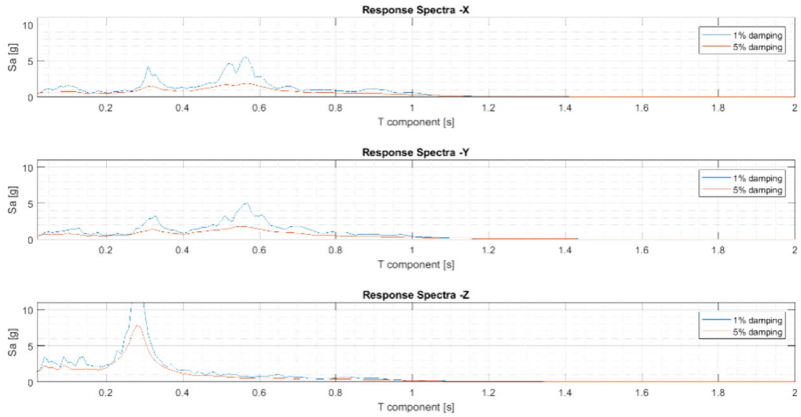

Table Acceleration Freezer RP475 L16 R LAT LONG VERT

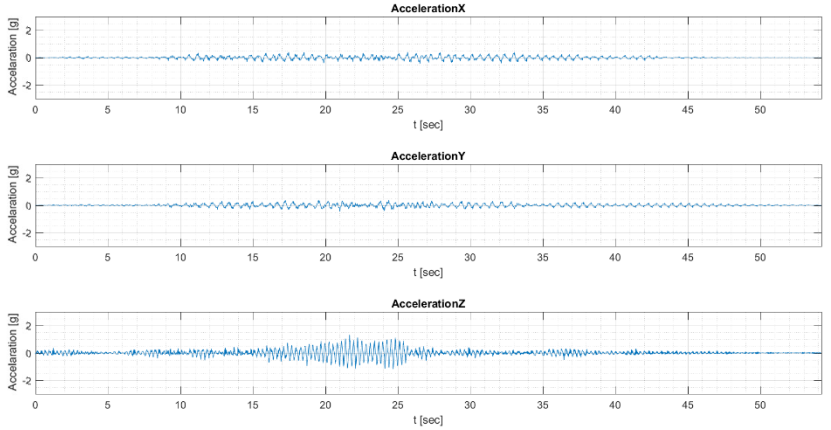

Acceleration Freezer RP475 L16 R LAT LONG VERT

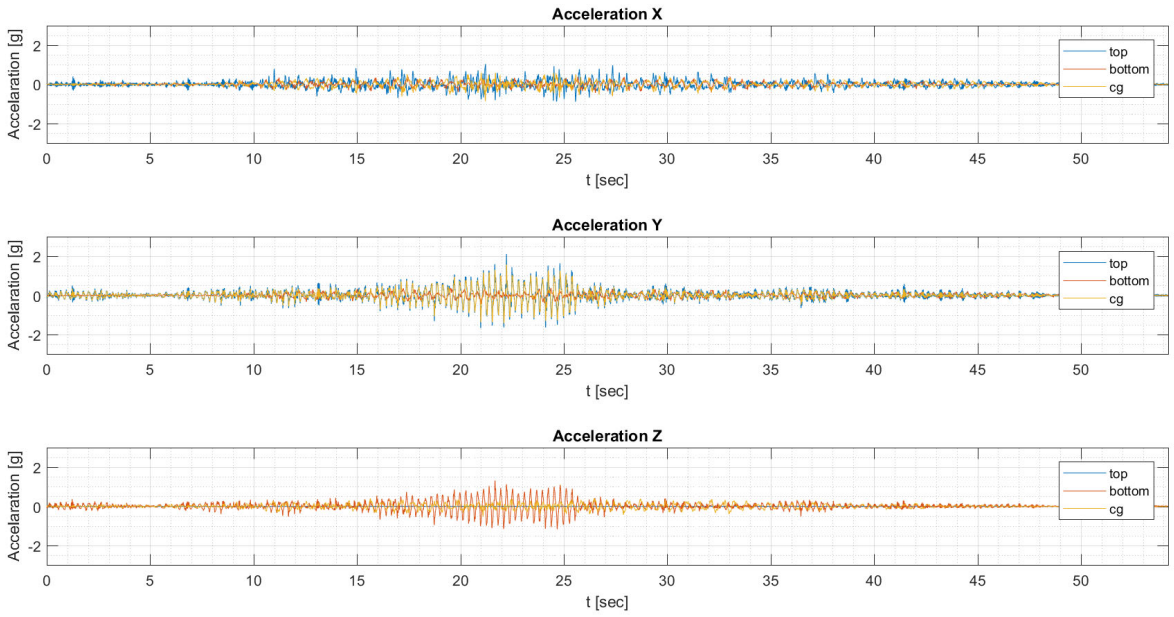

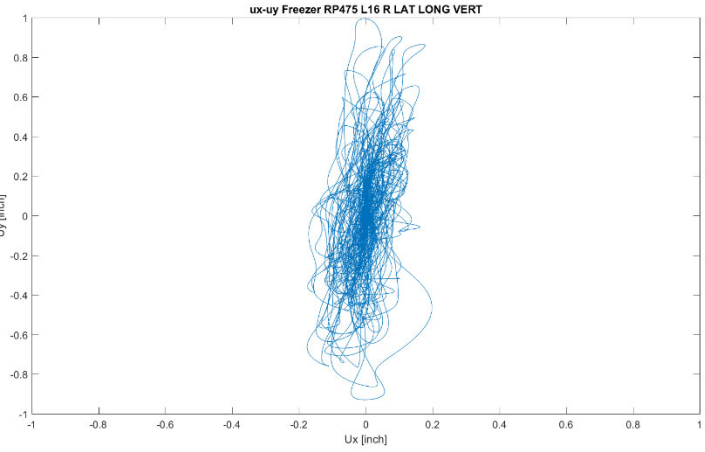

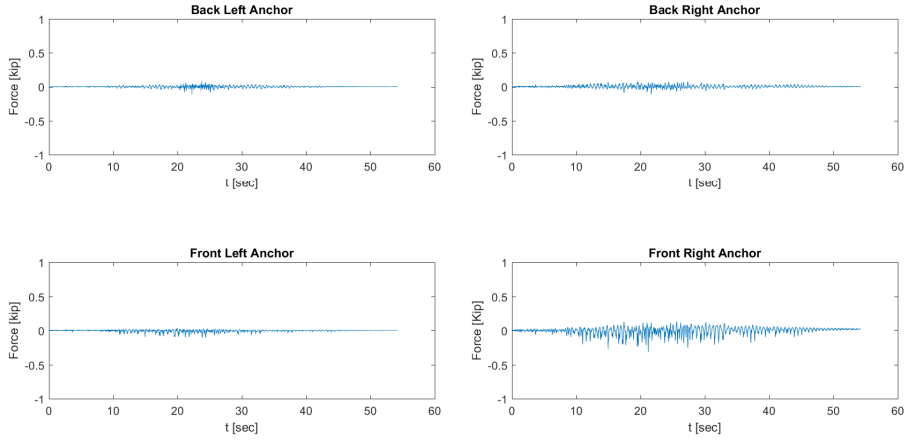

Testing Phase 2 – (44) Level 2 RP 475 X direction – Freezer SM

Floor Response Spectra Freezer RP475 L2 SM LONG

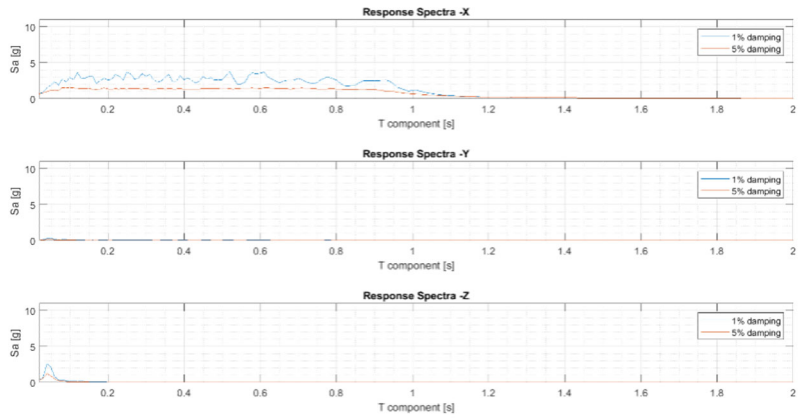

Table Acceleration Freezer RP475 L2 SM LONG

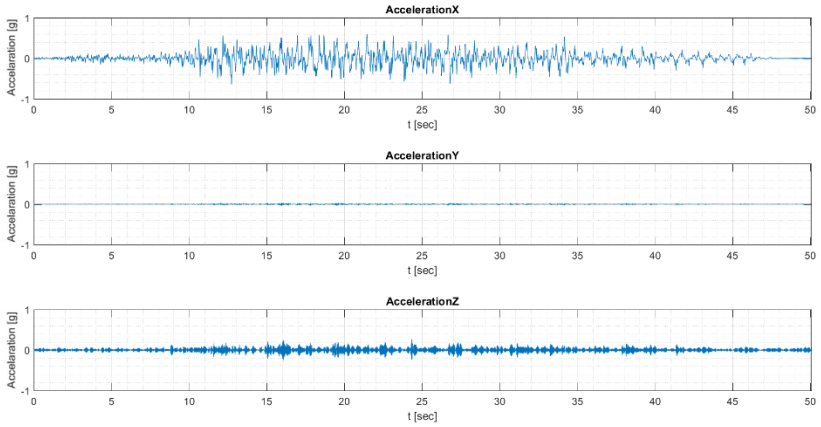

Acceleration Freezer RP475 L2 SM LONG

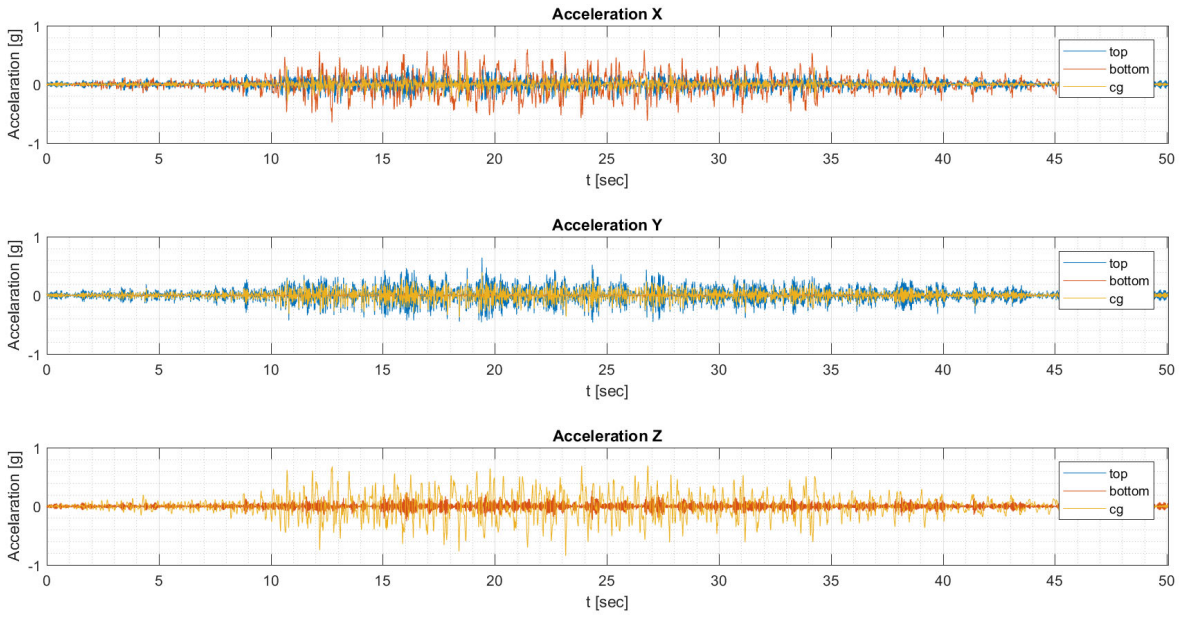

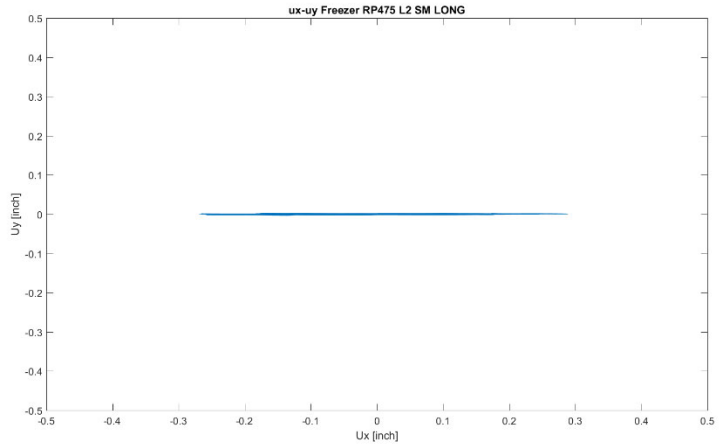

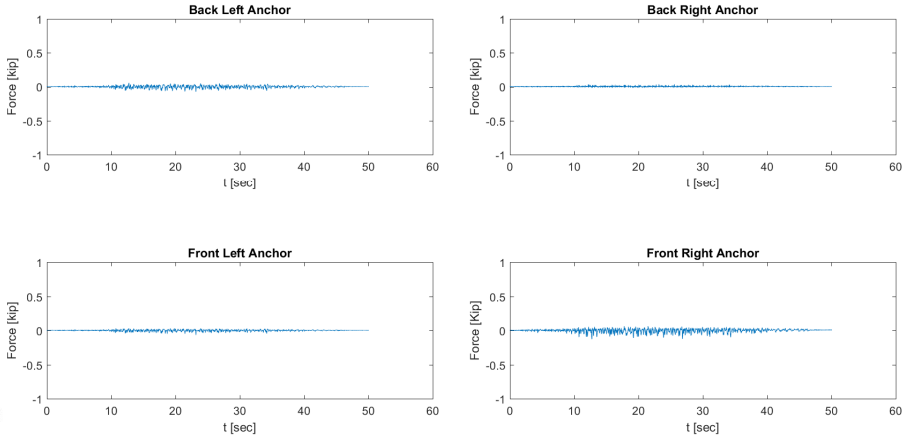

Testing Phase 2 – (45) Level 2 RP 475 Y direction – Freezer SM

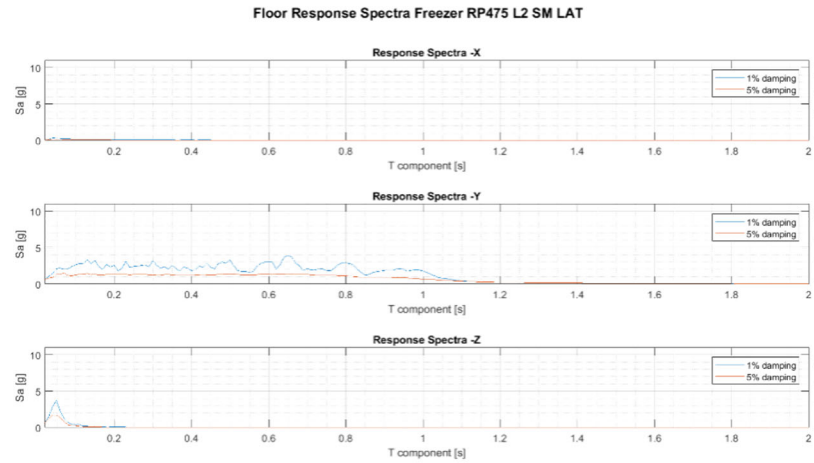

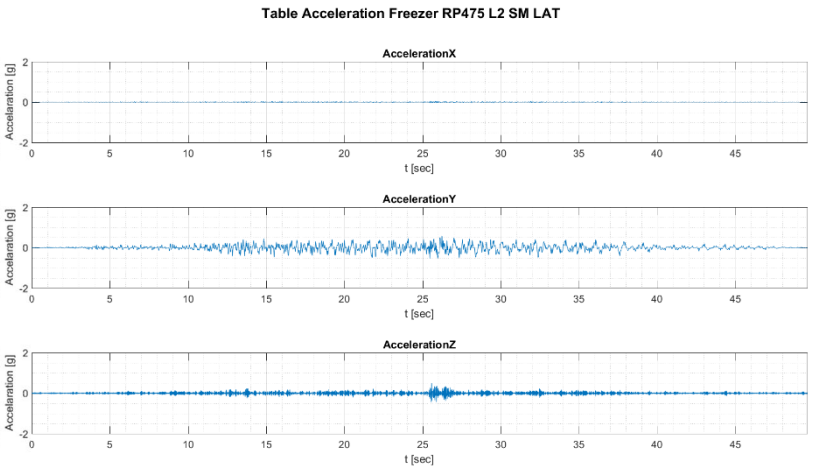

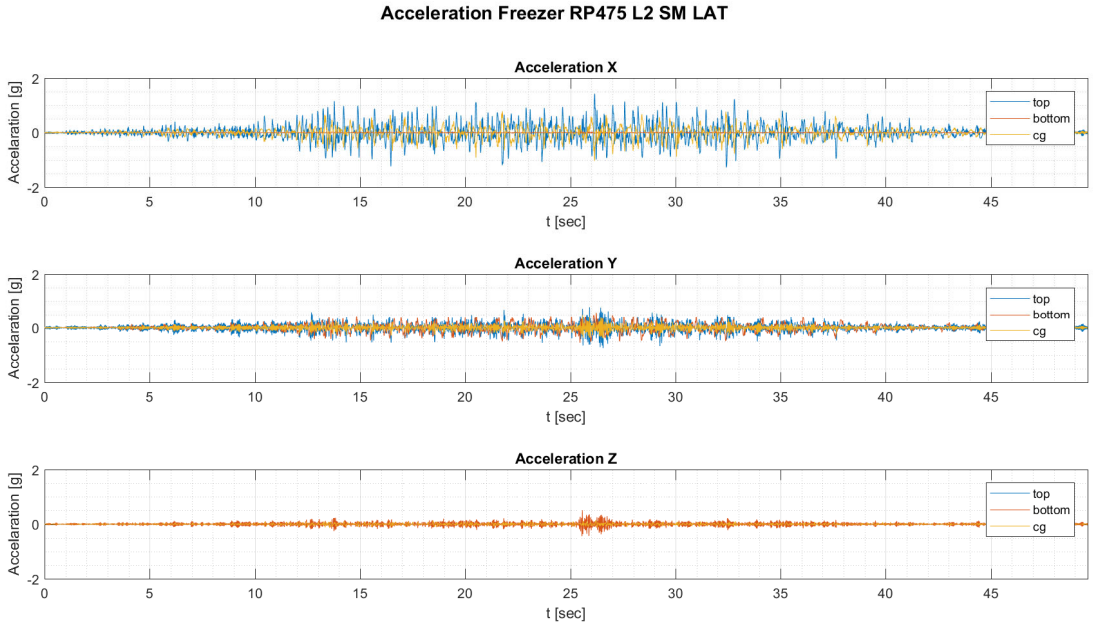

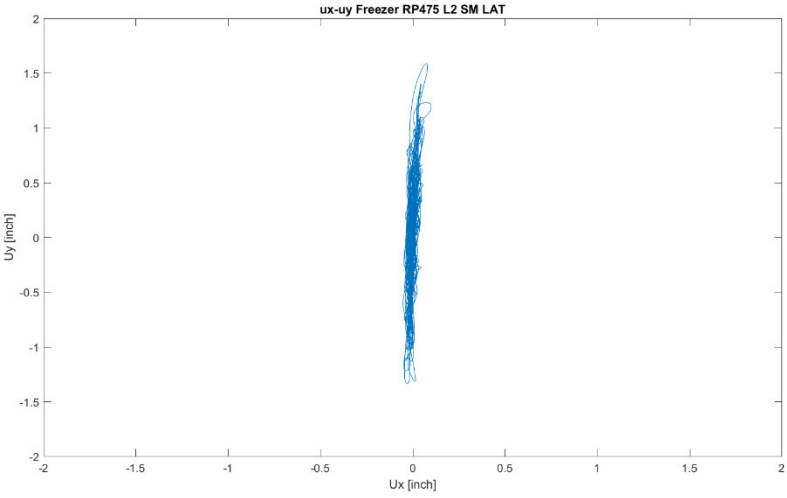

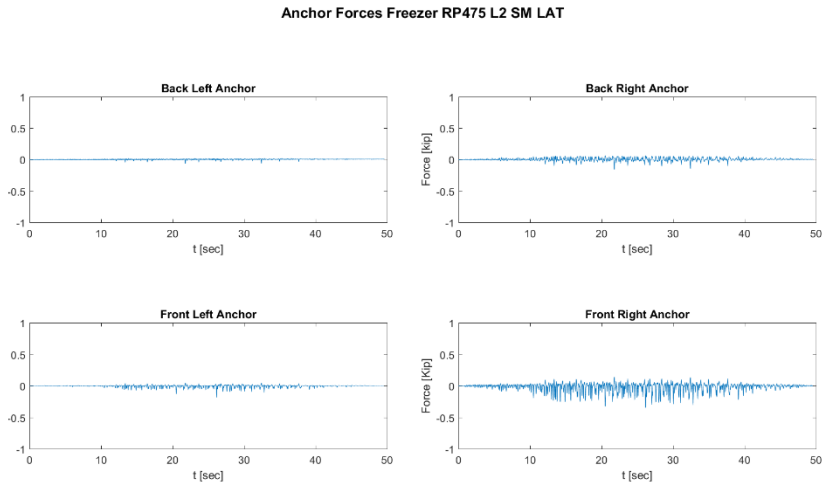

Testing Phase 2 – (46) Level 2 RP 475 XY direction – Freezer SM

Floor Response Spectra Freezer RP475 L2 SM LONG LAT

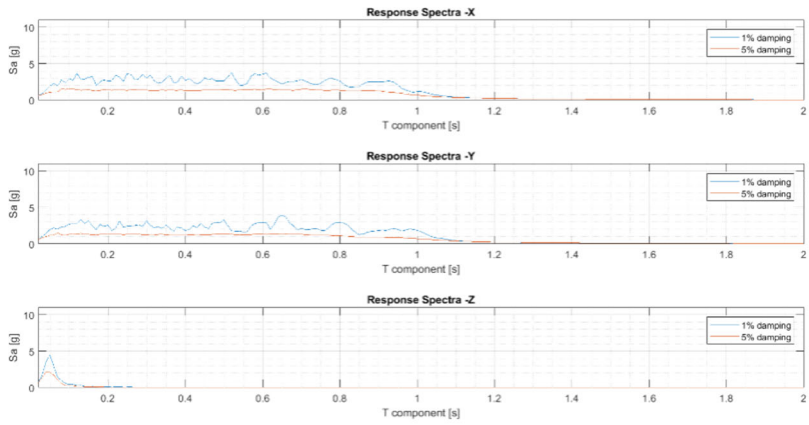

Table Acceleration Freezer RP475 L2 SM LONG LAT

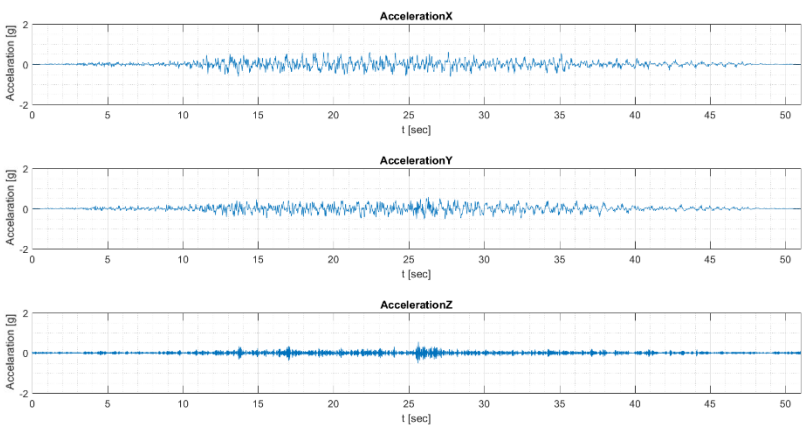

Acceleration Freezer RP475 L2 SM LONG LAT

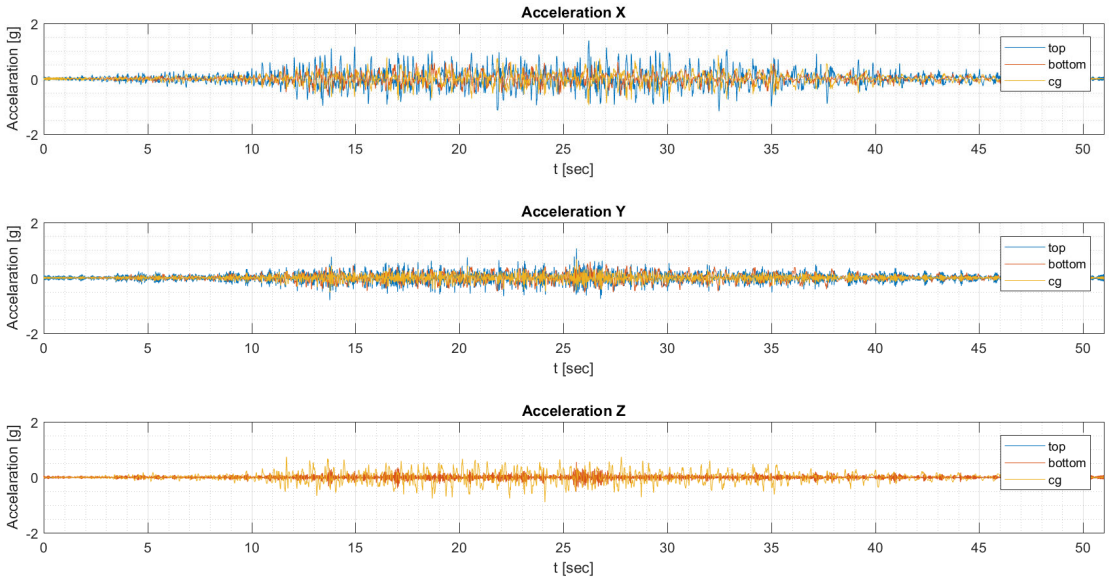

ux-uy Freezer RP475 L2 SM LONG LAT

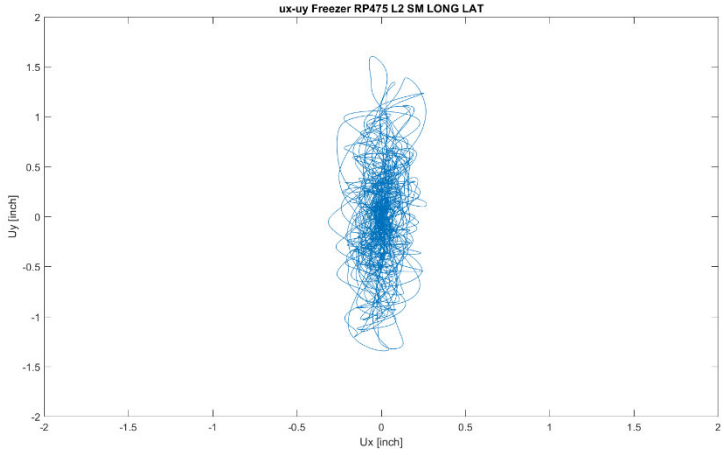

Anchor Forces Freezer RP475 L2 SM LONG LAT

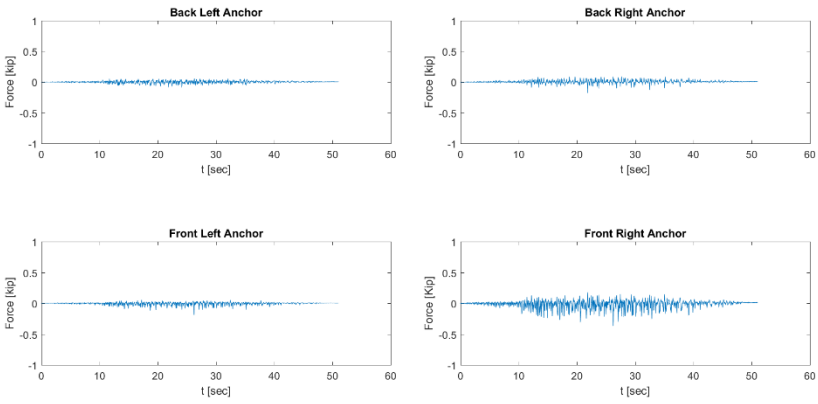

Testing Phase 2 – (47) Level 9 RP 475 X direction – Freezer SM

Floor Response Spectra Freezer RP475 L9$_S$M LONG

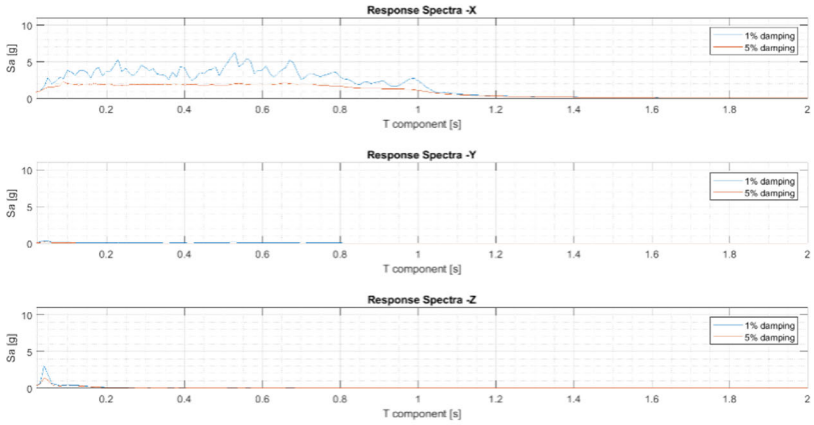

Table Acceleration Freezer RP475 L9$_S$M LONG

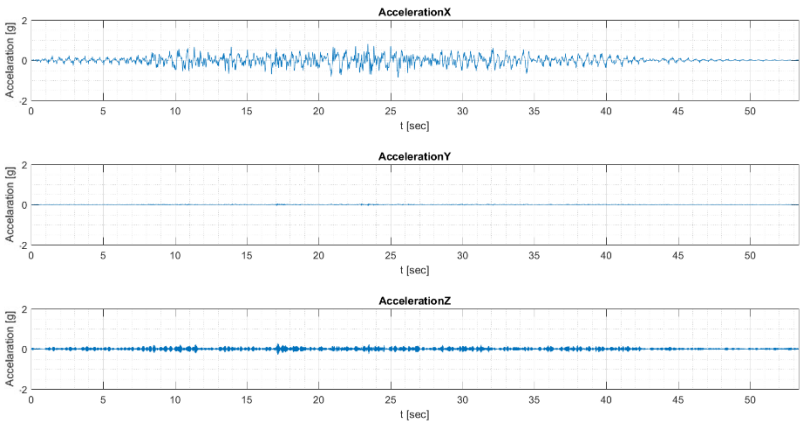

Acceleration Freezer RP475 L9$_S$M LONG

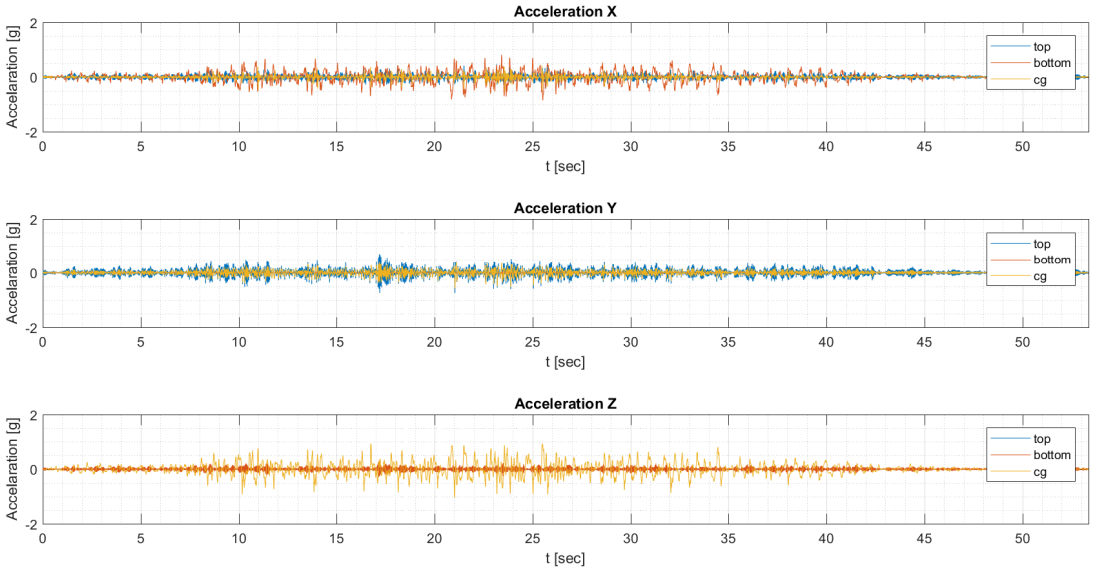

ux-uy Freezer RP475 L9$_S$M LONG

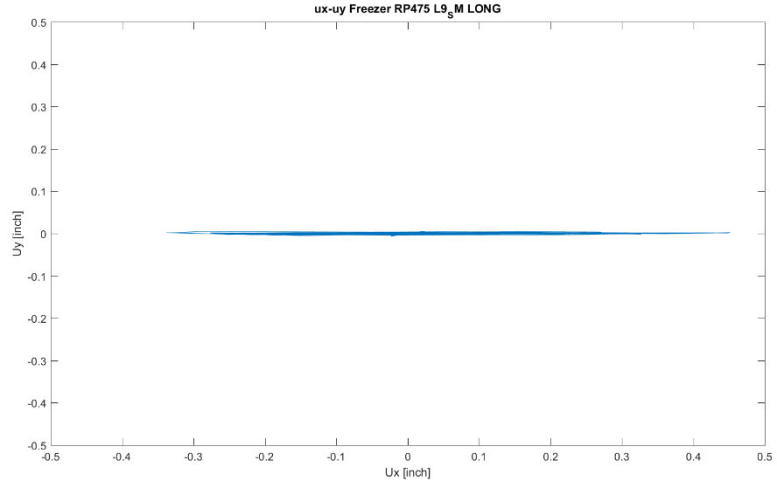

Anchor Forces Freezer RP475 L9$_S$M LONG

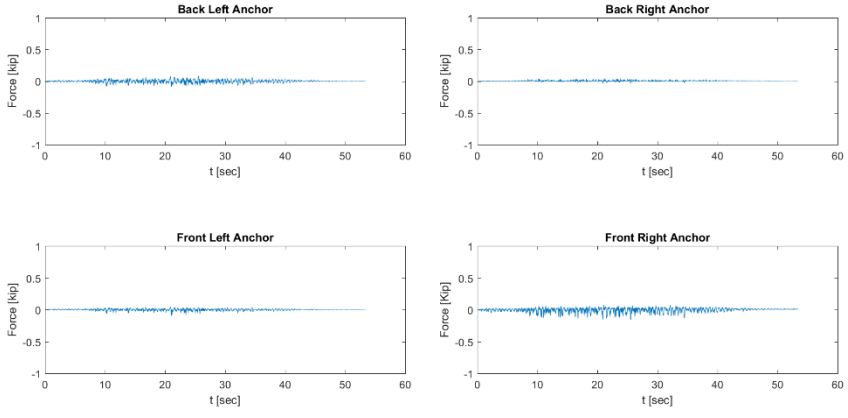

Testing Phase 2 – (48) Level 9 RP 475 Y direction – Freezer SM

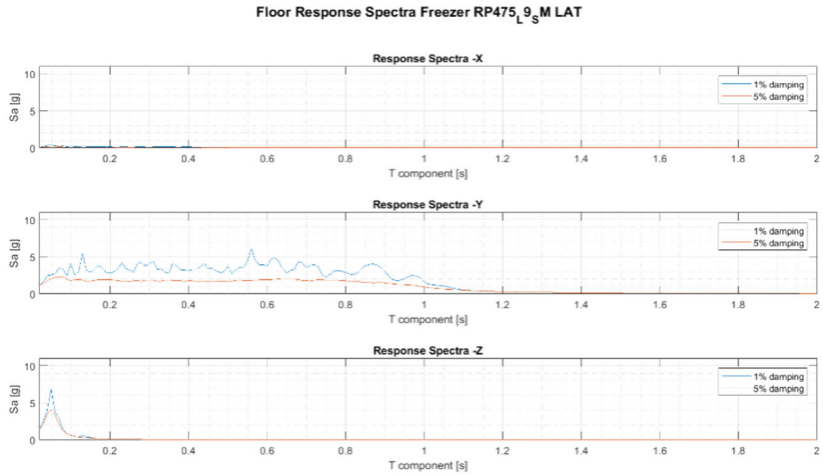

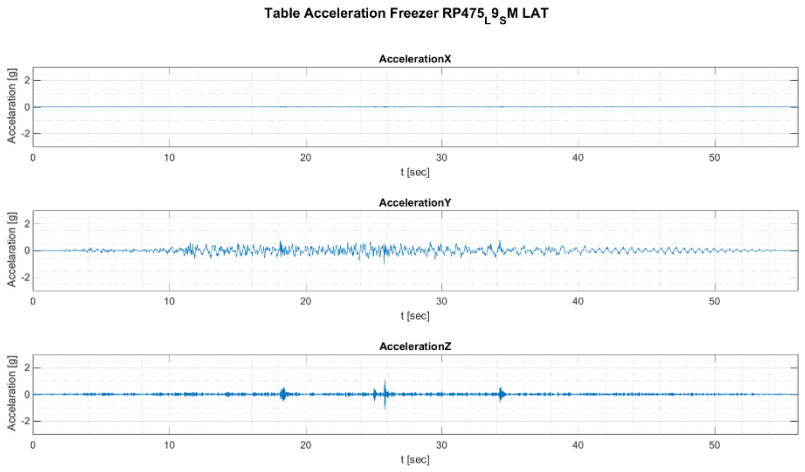

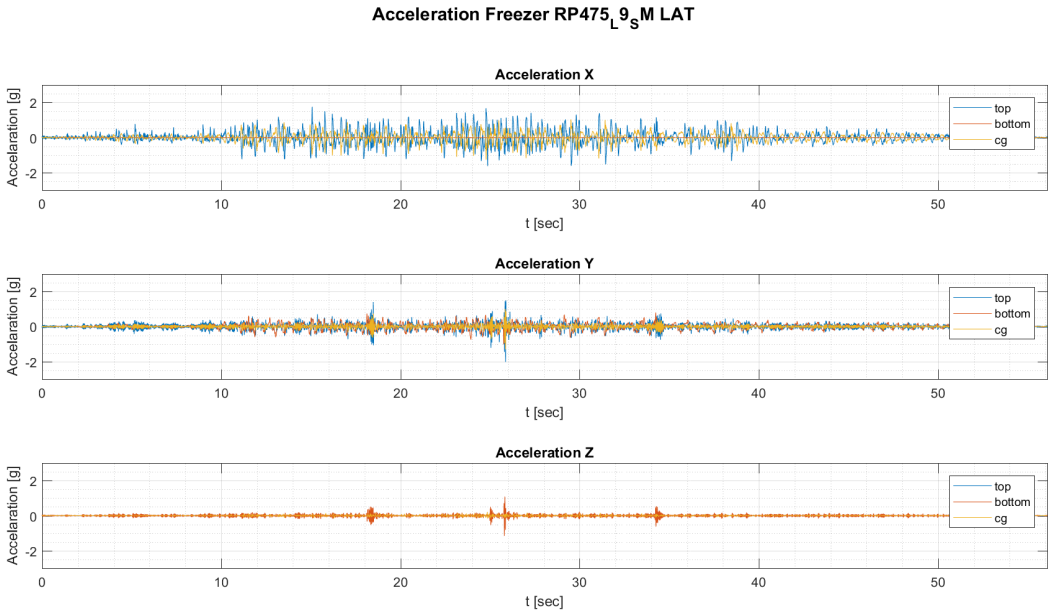

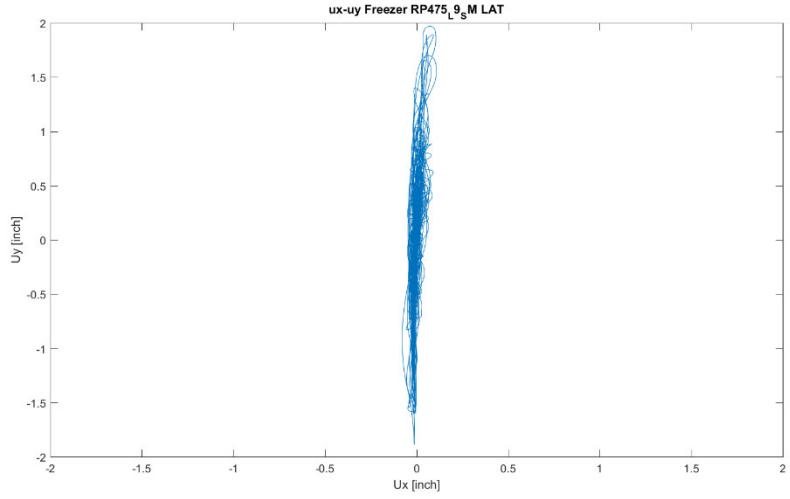

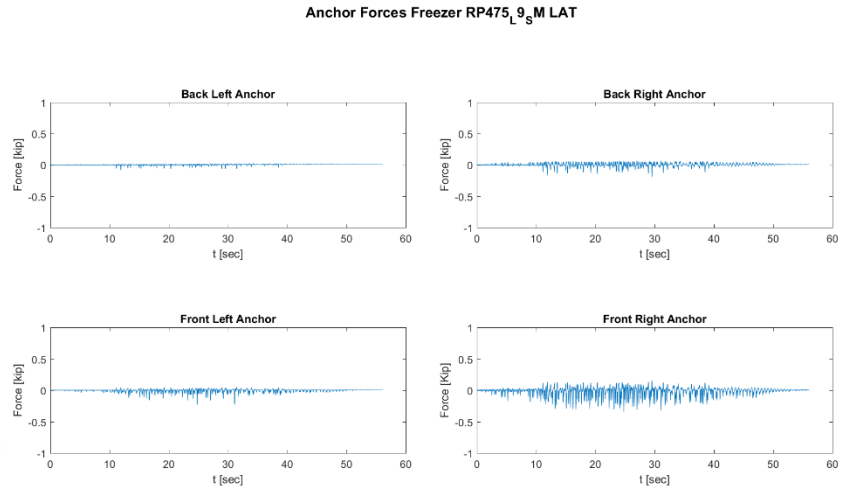

Testing Phase 2 – (49) Level 9 RP 475 XY direction – Freezer SM

Floor Response Spectra Freezer RP475 L9 SM LONG LAT

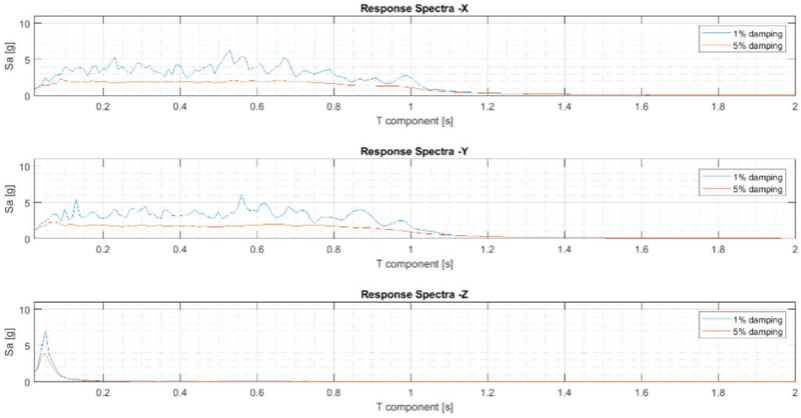

Table Acceleration Freezer RP475 L9 SM LONG LAT

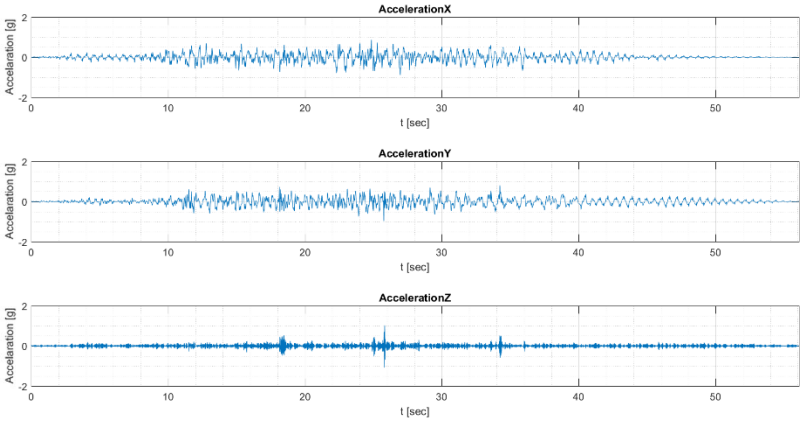

Acceleration Freezer RP475 L9 SM LONG LAT

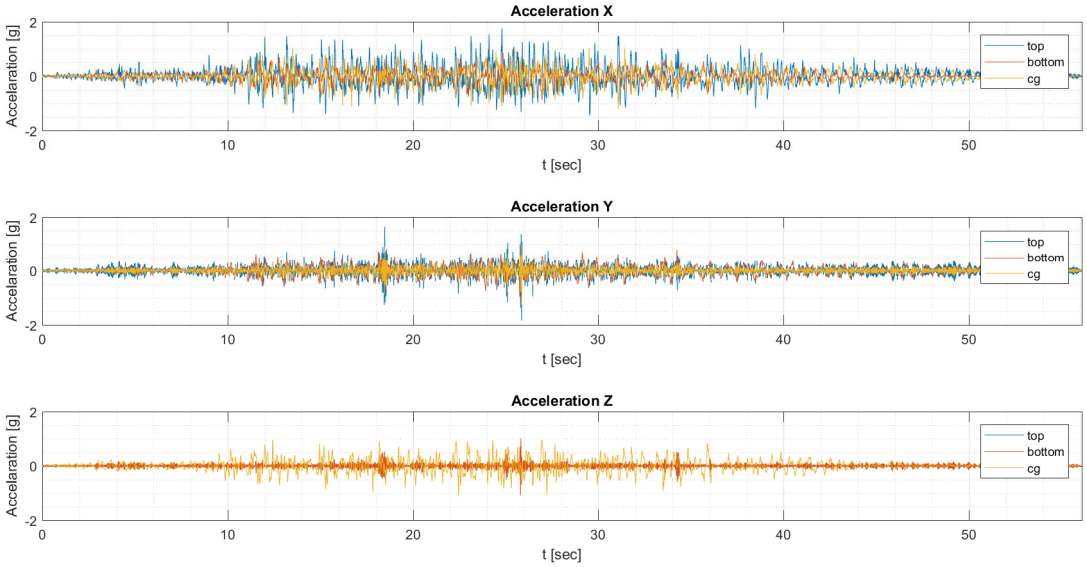

ux-uy Freezer RP475 L9 SM LONG LAT

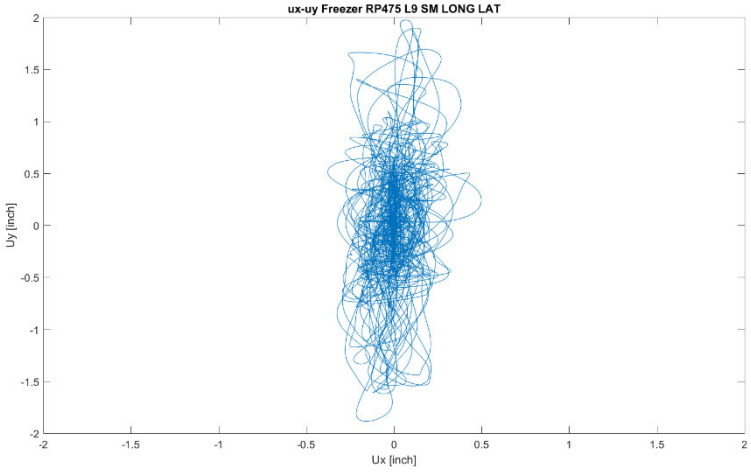

Anchor Forces Freezer RP475 L9 SM LONG LAT

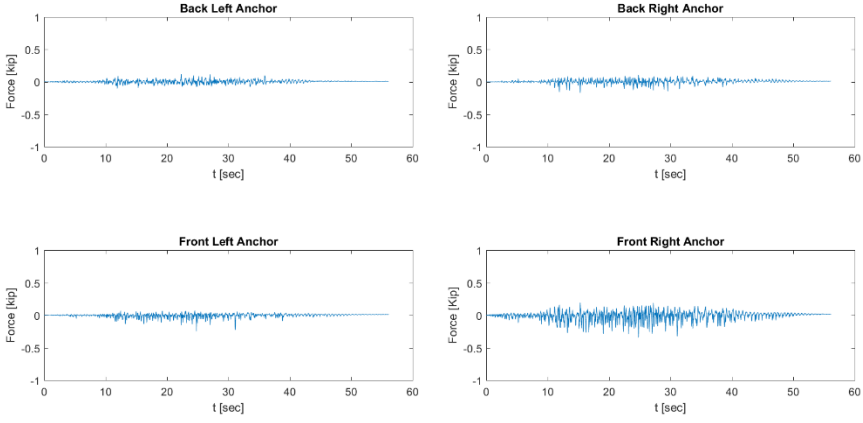

Testing Phase 2 – (50) Ground RP 475 X direction – Freezer Isolated

Floor Response Spectra Freezer RP475 L1 ISO LONG

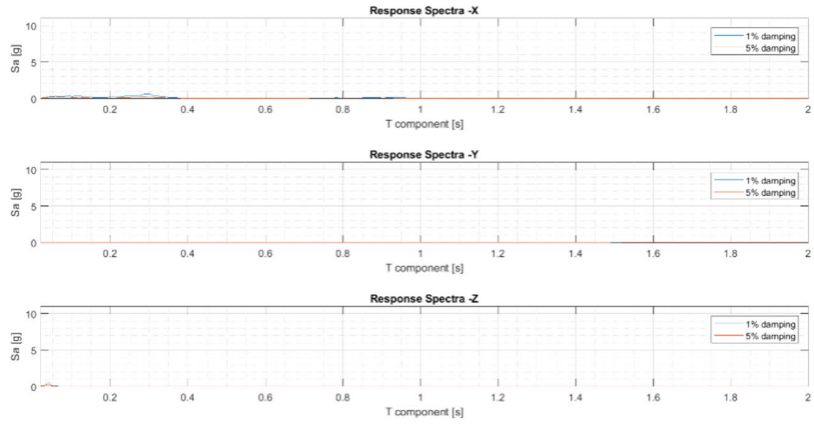

Table Acceleration Freezer RP475 L1 ISO LONG

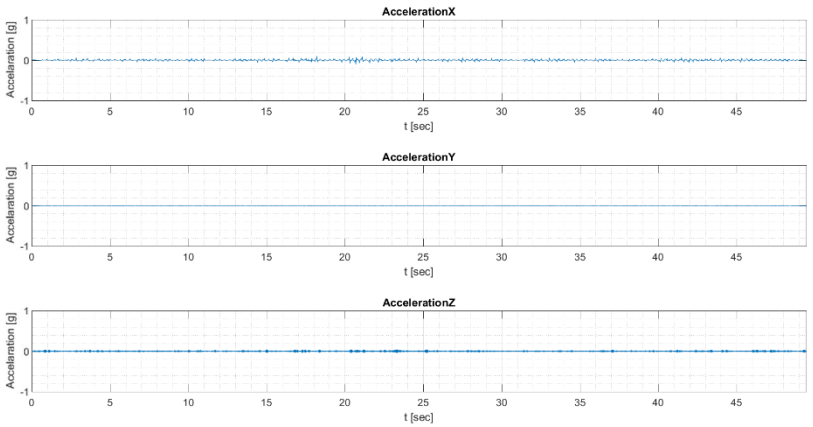

Acceleration Freezer RP475 L1 ISO LONG

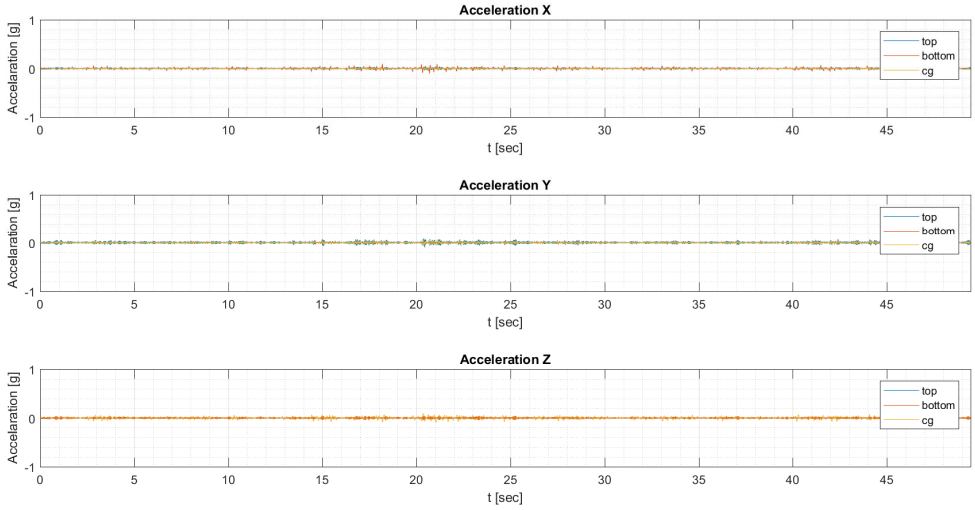

ux-uy Freezer RP475 L1 ISO LONG

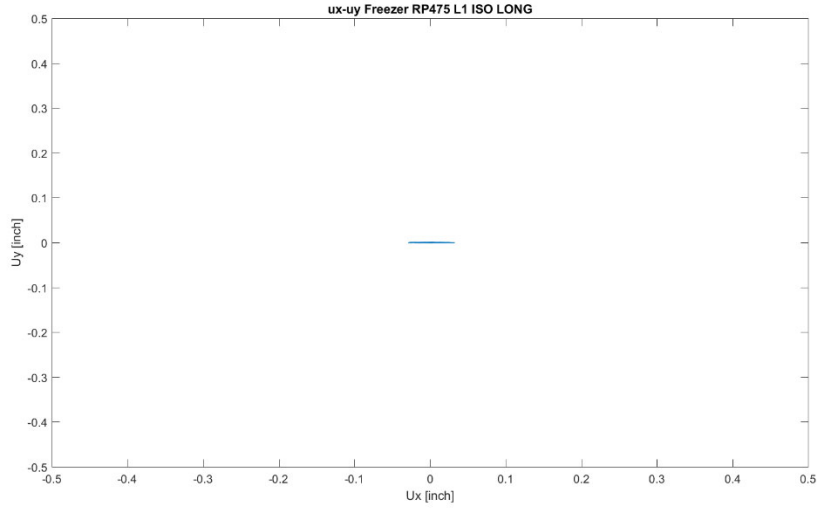

Anchor Forces Freezer RP475 L1 ISO LONG

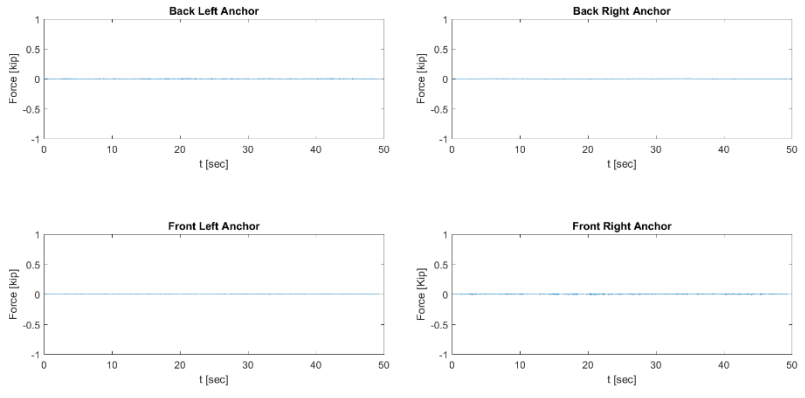

Testing Phase 2 – (51) Roof RP 475 X direction – Freezer Low rise

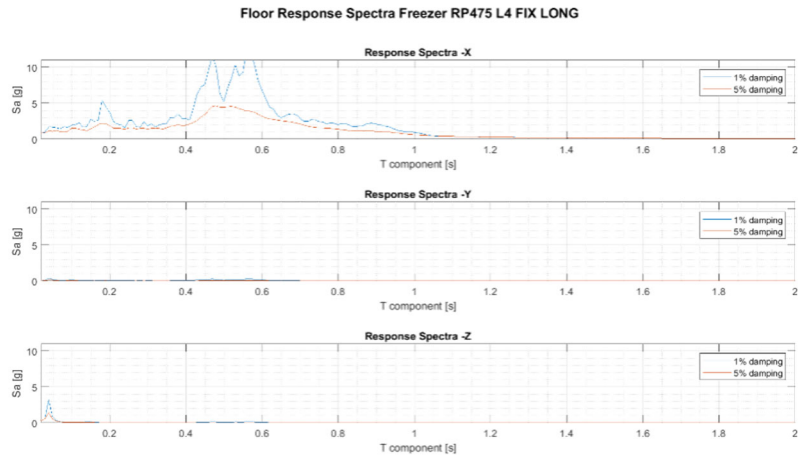

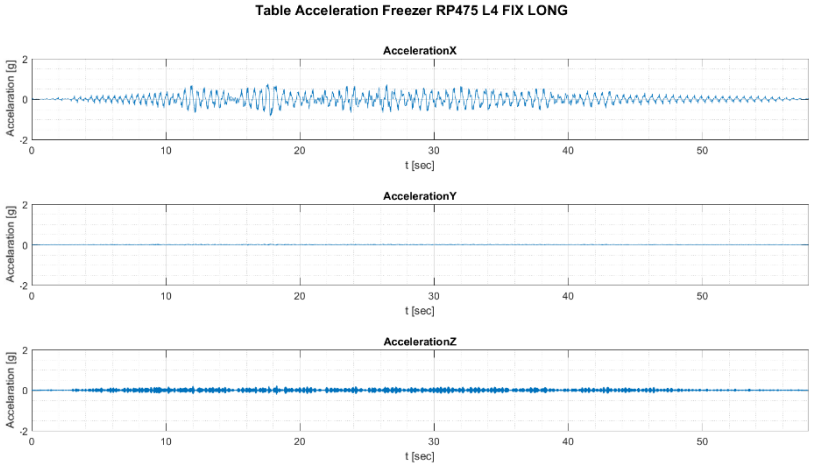

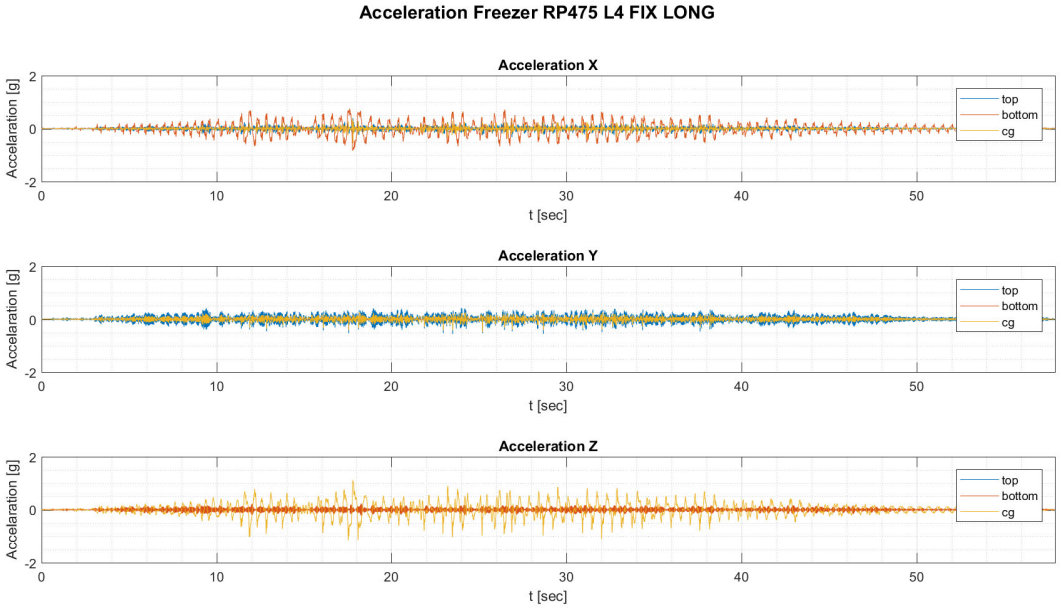

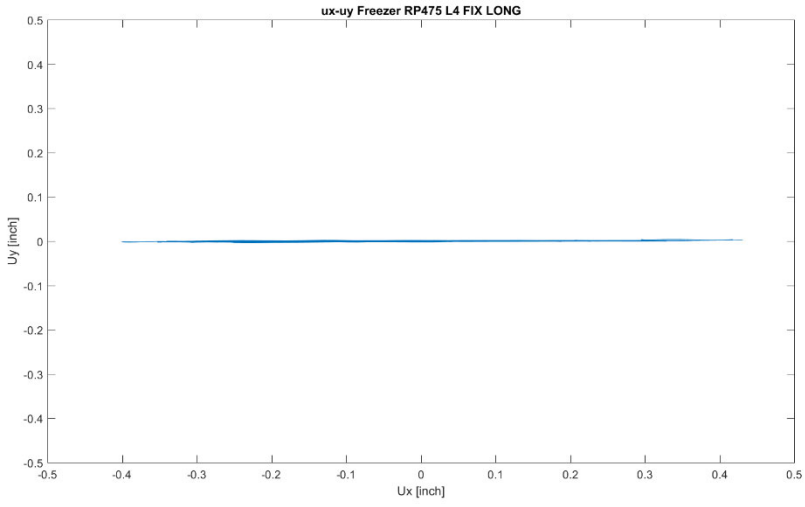

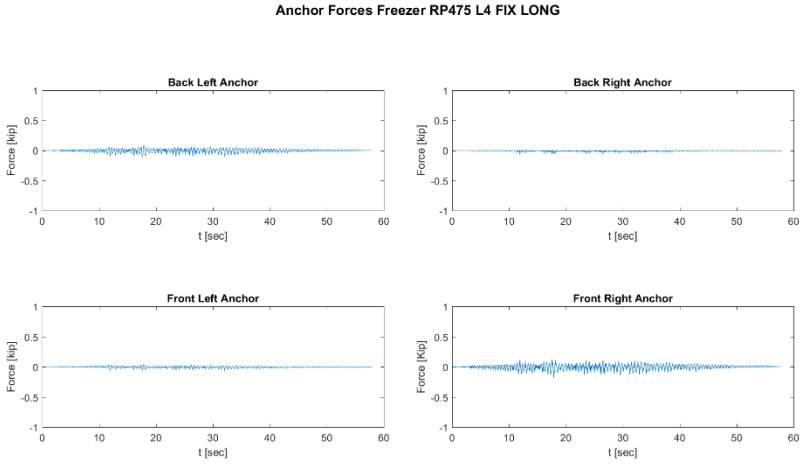

Testing Phase 2 – (52) Roof RP 475 Y direction – Freezer Low rise

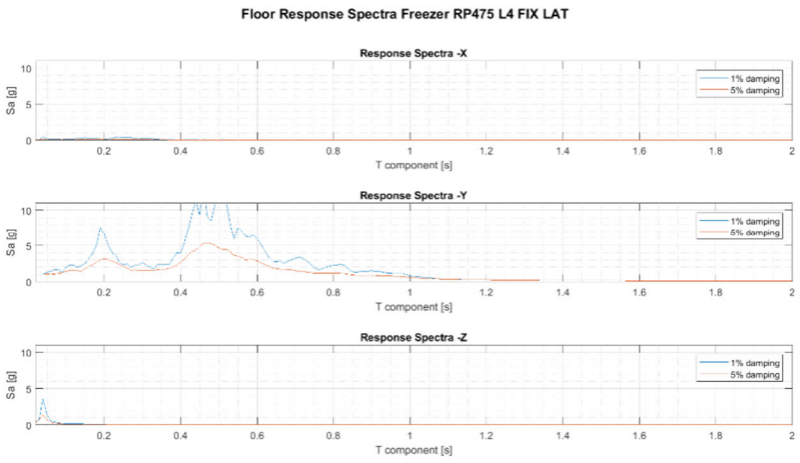

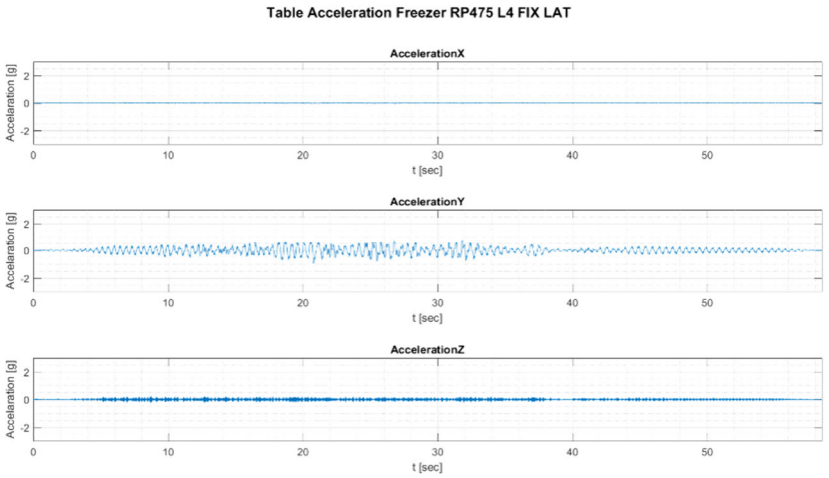

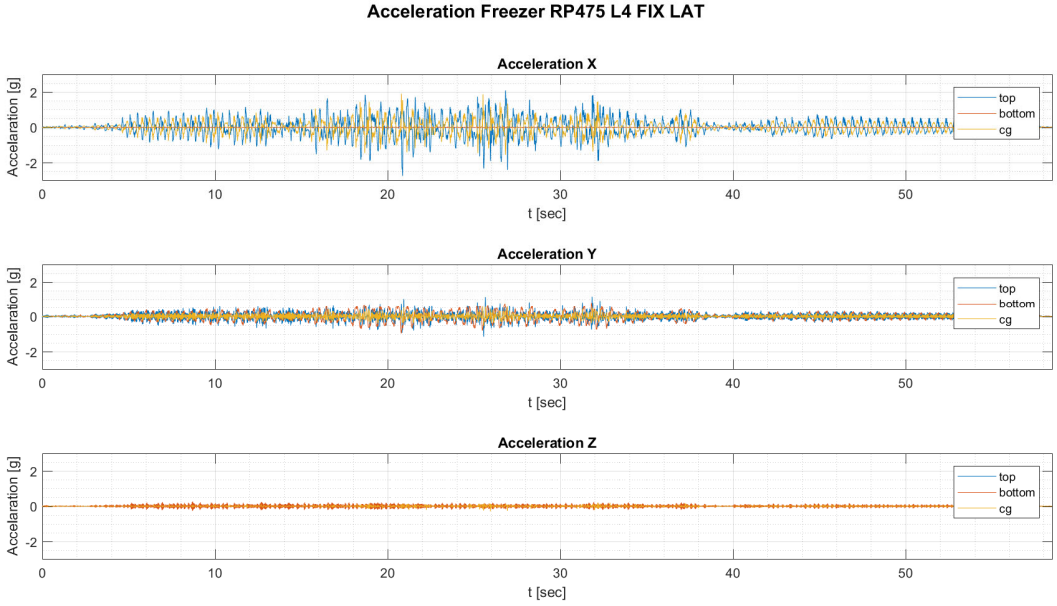

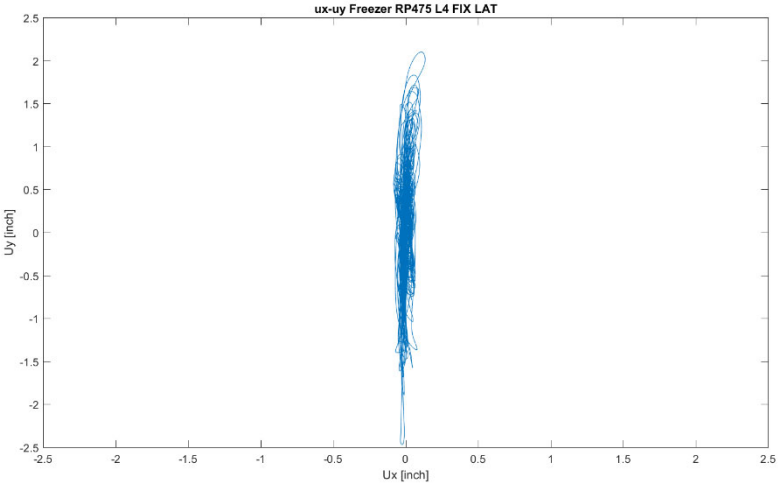

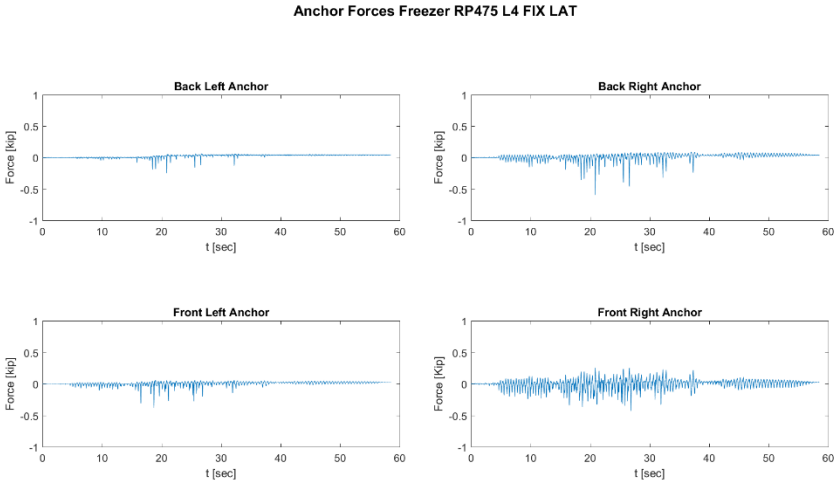

Testing Phase 2 – (53) IEEE XY direction – Freezer

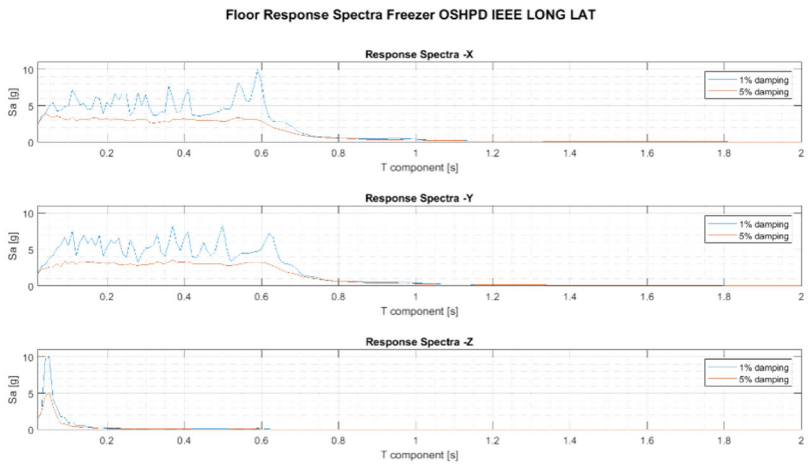

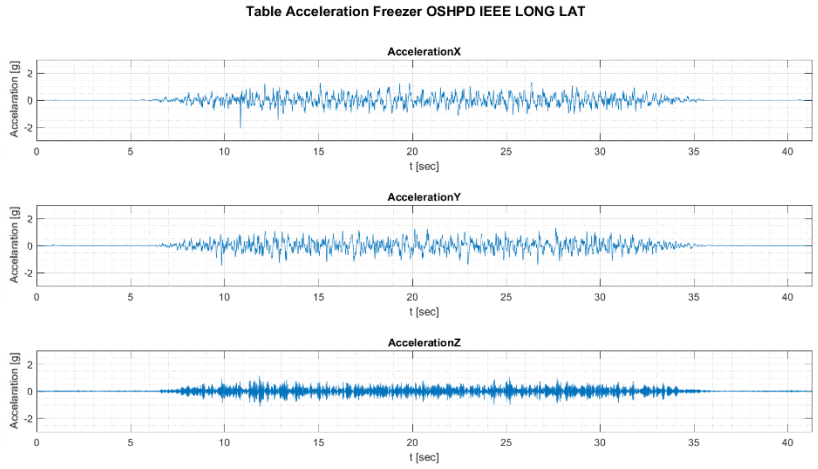

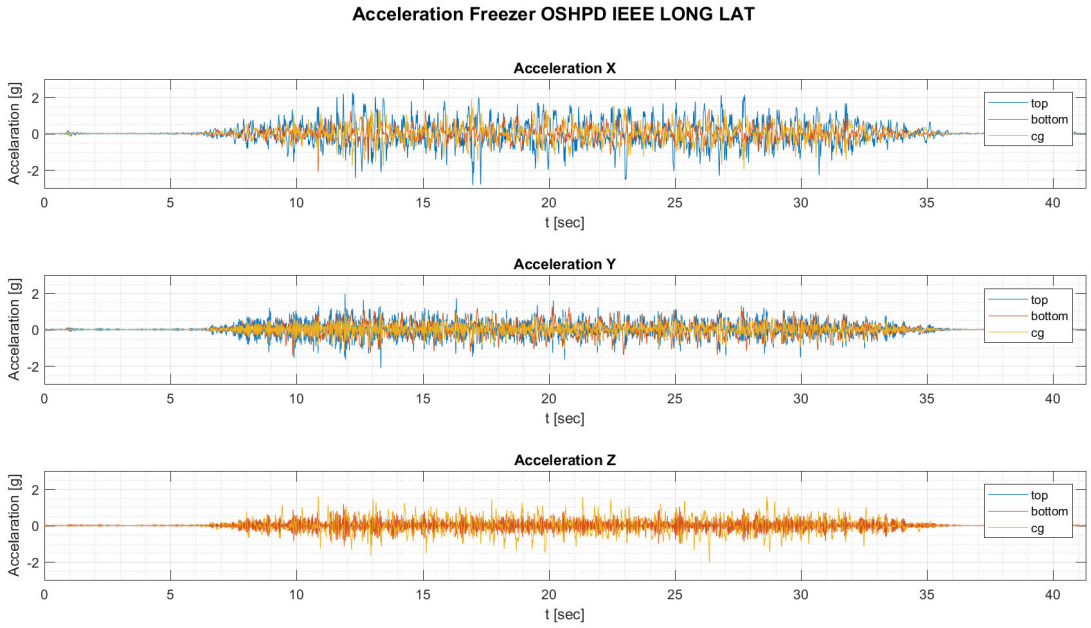

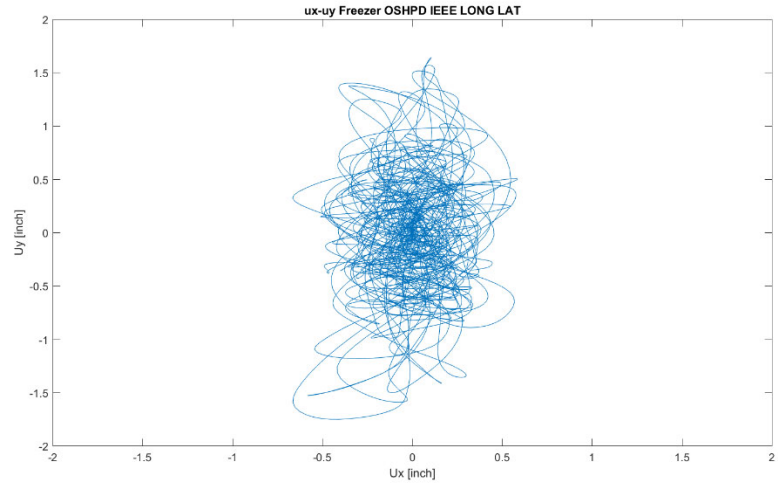

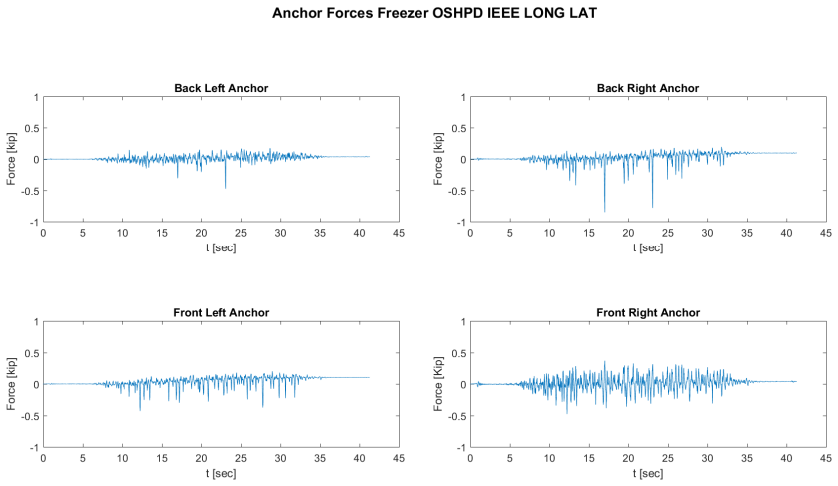

Testing Phase 2 – (54) IEEE XYZ direction – Freezer

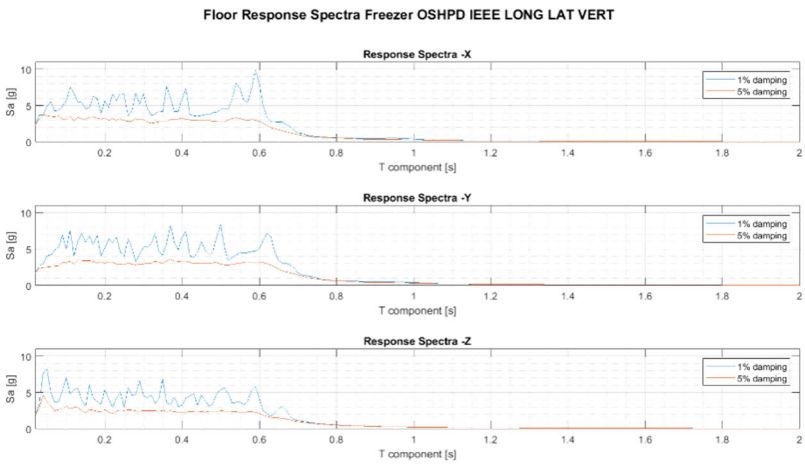

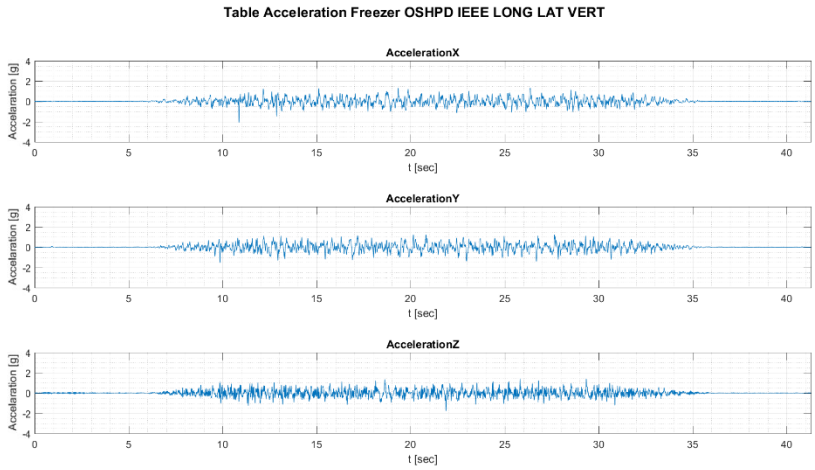

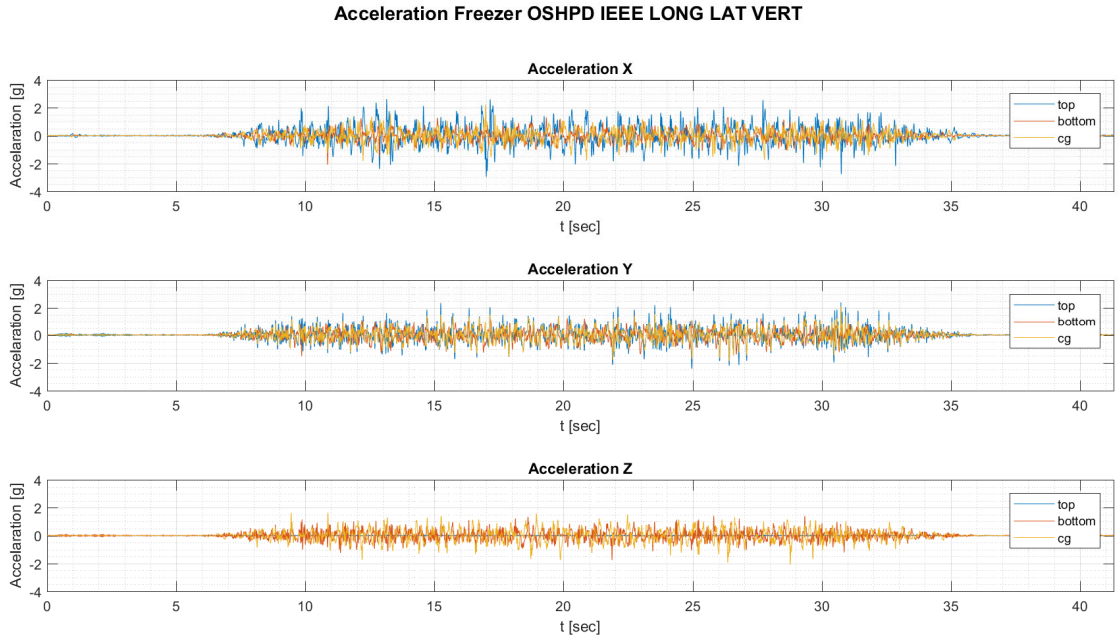

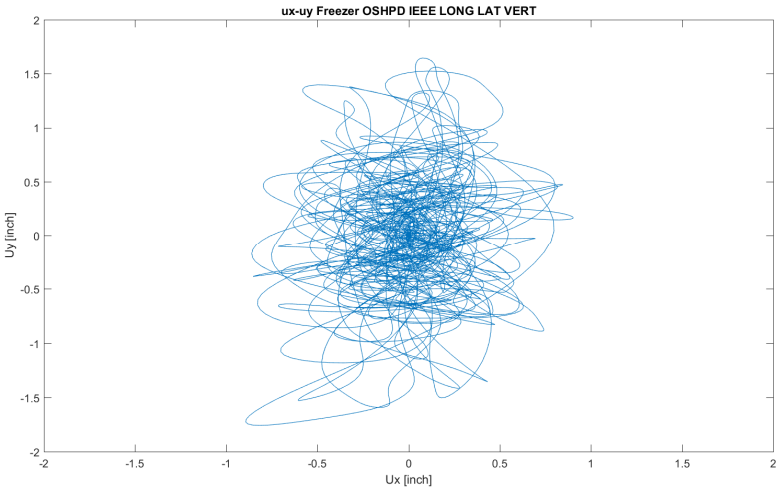

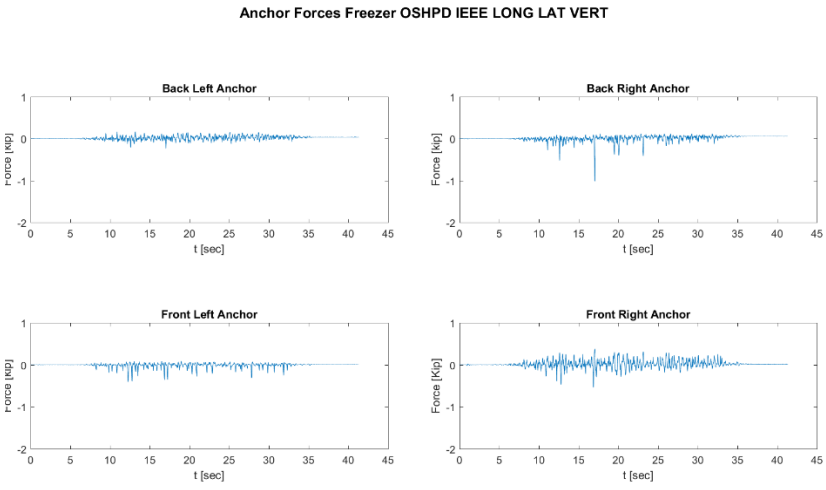

Testing Phase 2 – (55) Level 9 RP 475 X direction – Freezer Thin

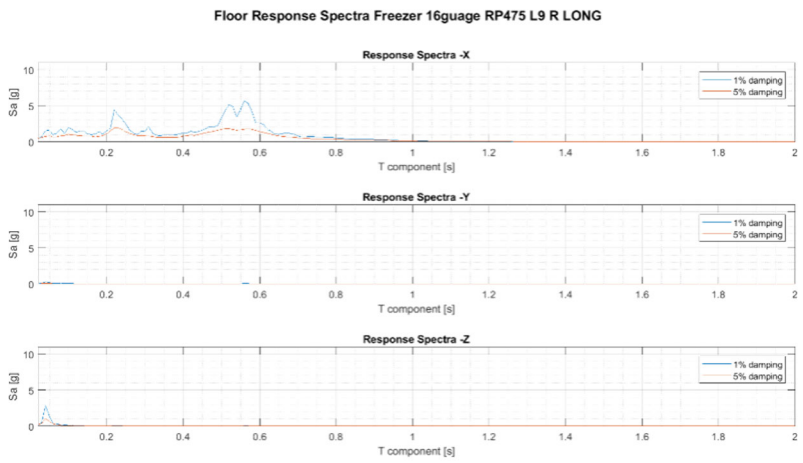

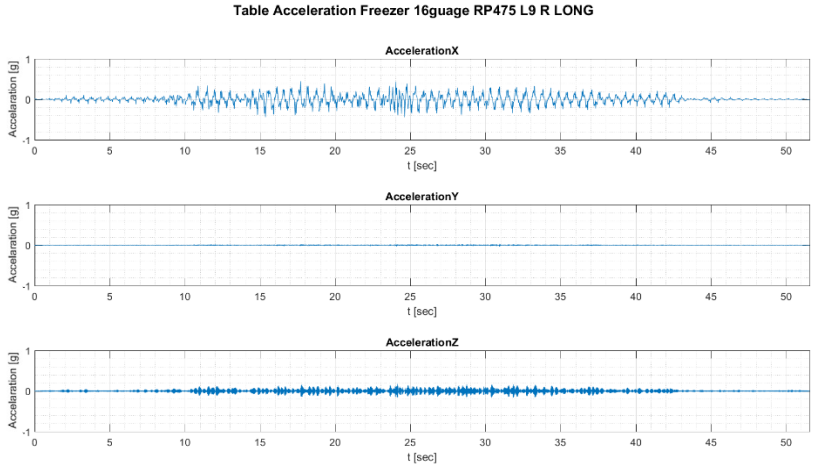

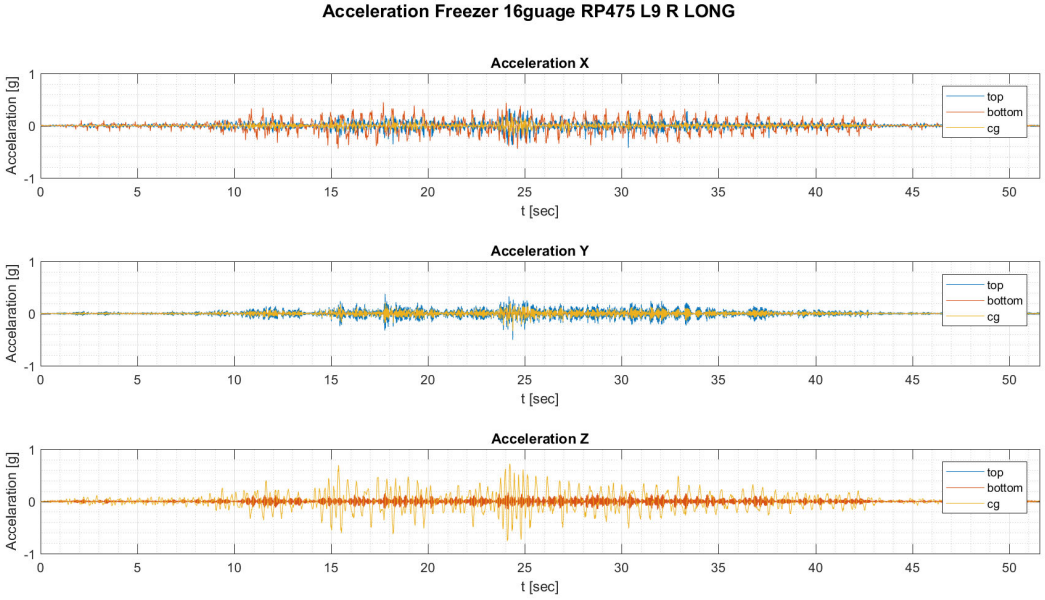

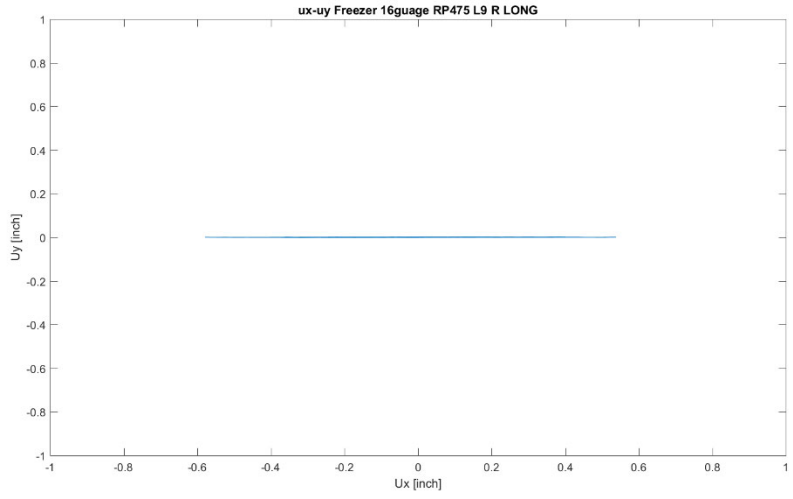

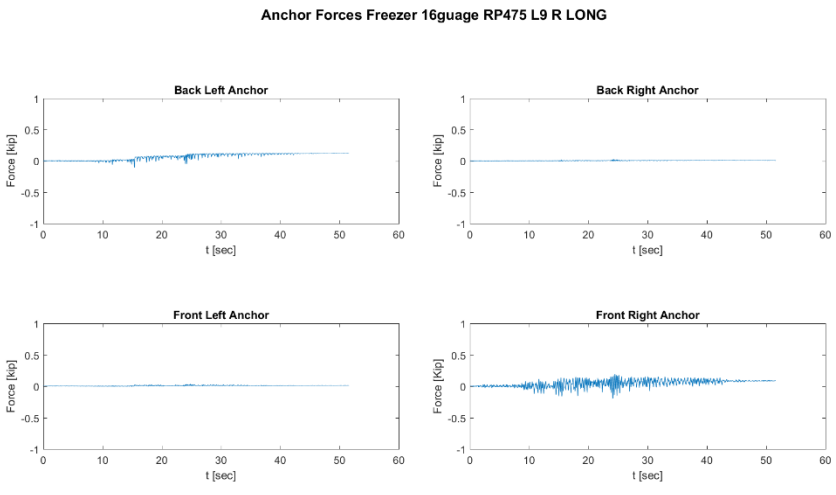

Testing Phase 2 – (56) Level 9 RP 475 Y direction – Freezer Thin

Floor Response Spectra Freezer 16guage RP475 L9 R LAT

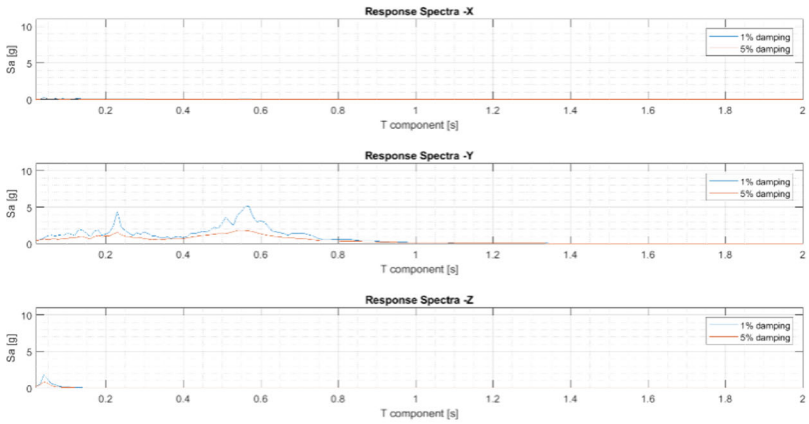

Table Acceleration Freezer 16guage RP475 L9 R LAT

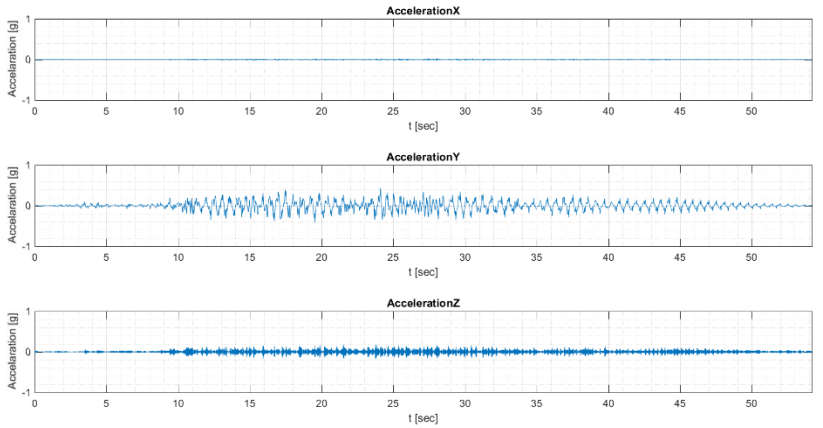

Acceleration Freezer 16guage RP475 L9 R LAT

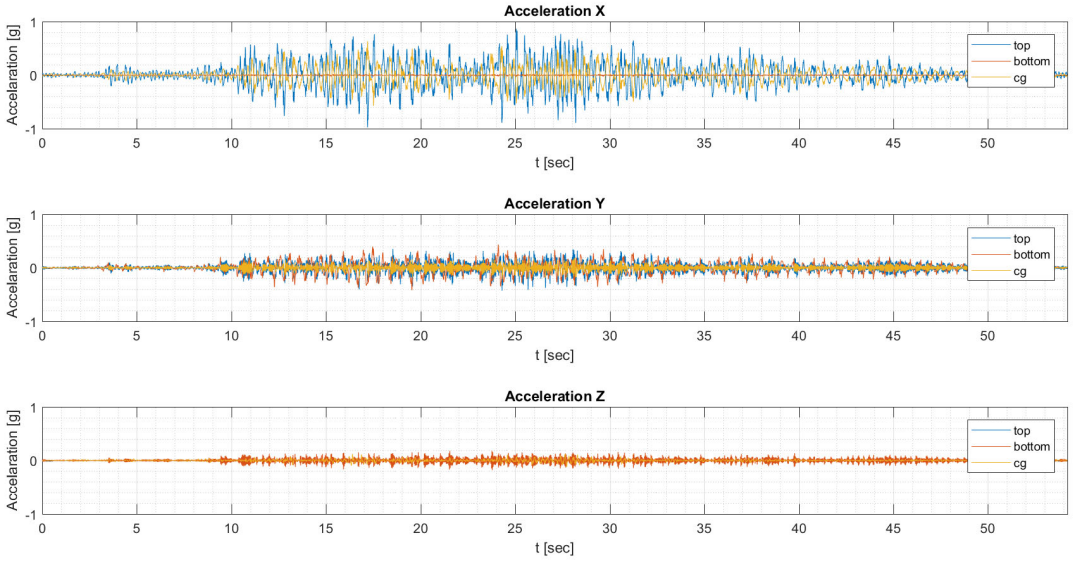

ux-uy Freezer 16guage RP475 L9 R LAT

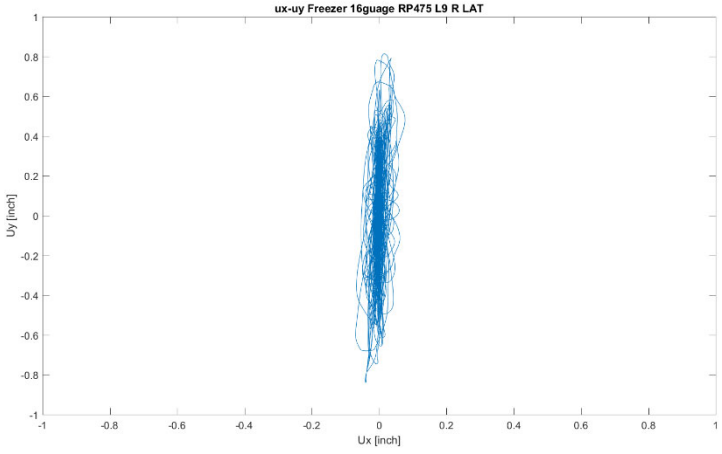

Anchor Forces Freezer 16guage RP475 L9 R LAT

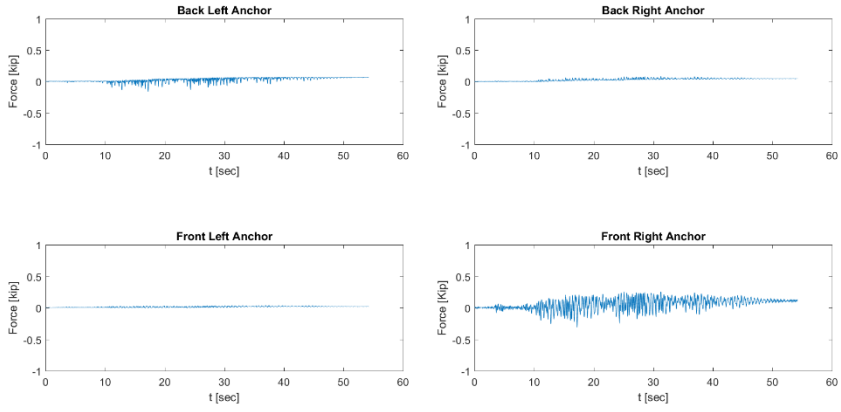

Testing Phase 2 – (57) Level 9 RP 475 XYZ direction – Freezer Thin

Floor Response Spectra Freezer 16guage RP475 L9 R LAT LONG VERT

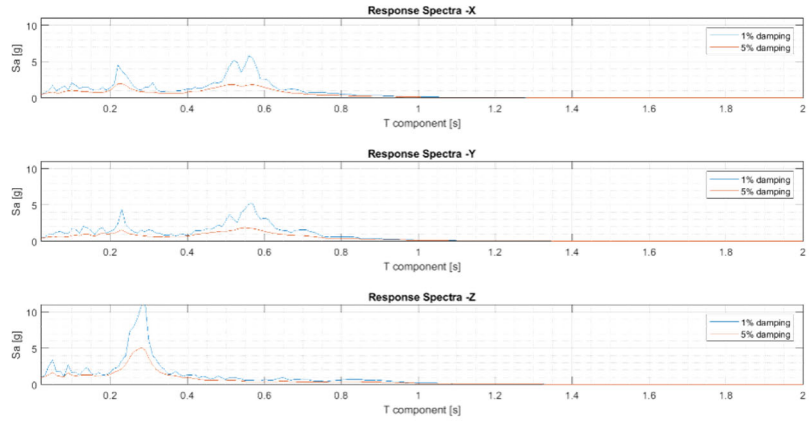

Table Acceleration Freezer 16guage RP475 L9 R LAT LONG VERT

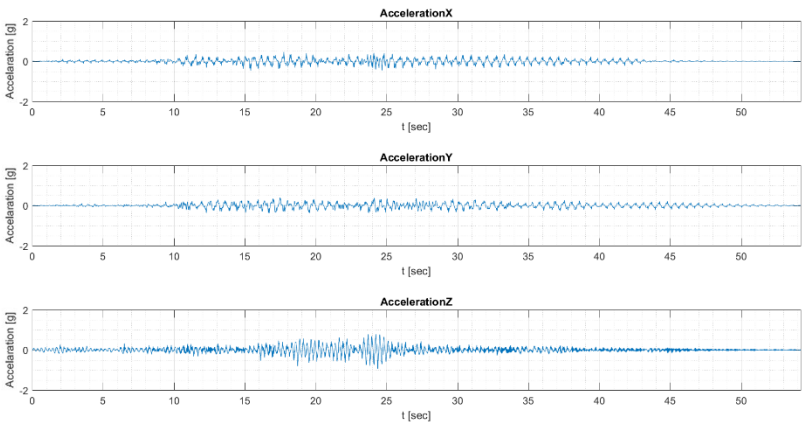

Acceleration Freezer 16guage RP475 L9 R LAT LONG VERT

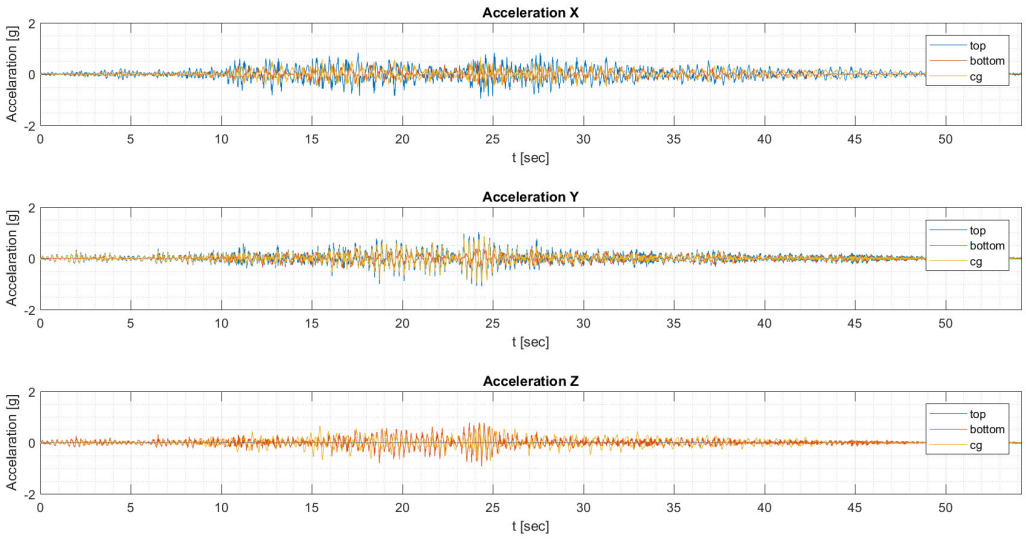

ux-uy Freezer 16guage RP475 L9 R LAT LONG VERT

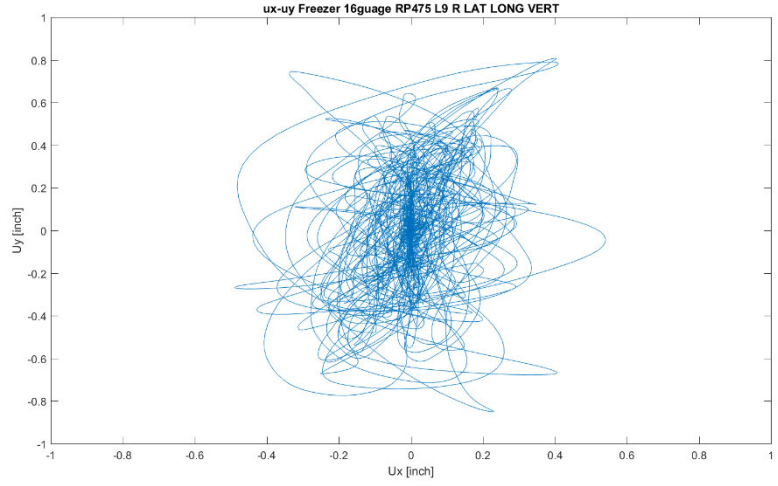

Anchor Forces Freezer 16guage RP475 L9 R LAT LONG VERT

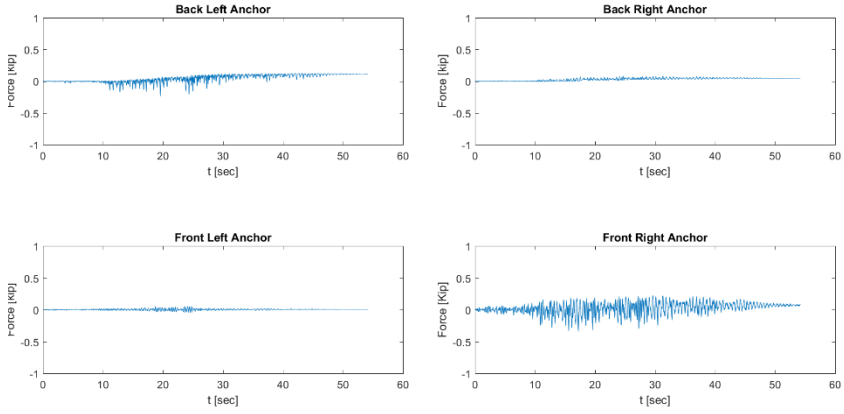

Testing Phase 2 – (58) IEEE XYZ direction - Freezer

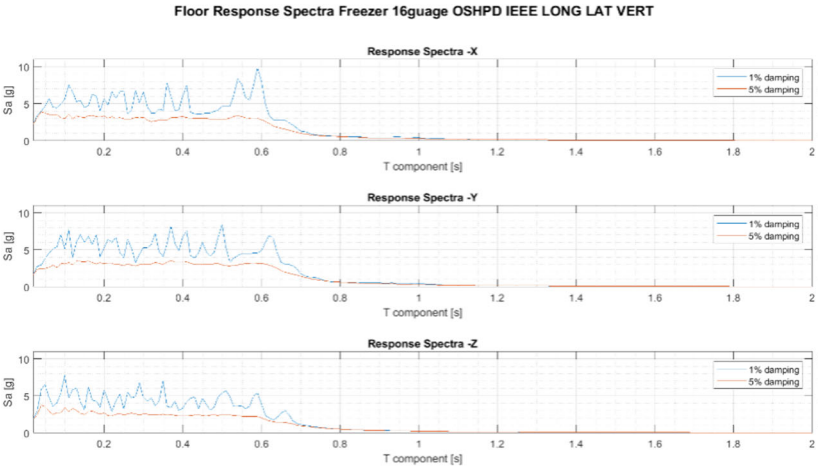

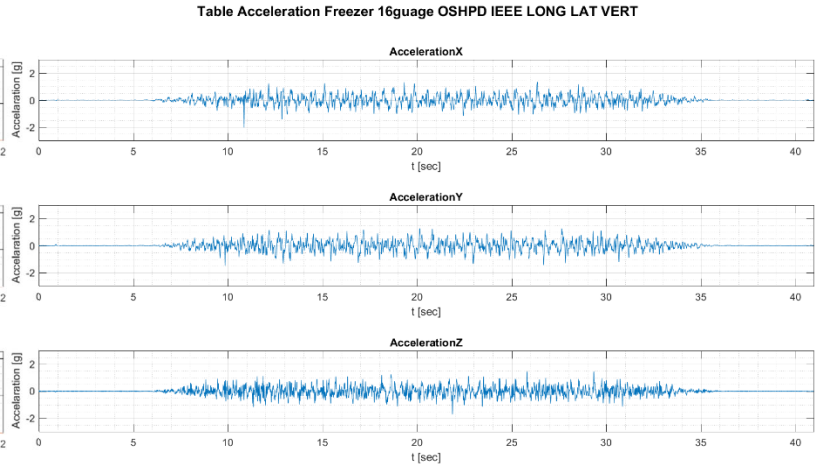

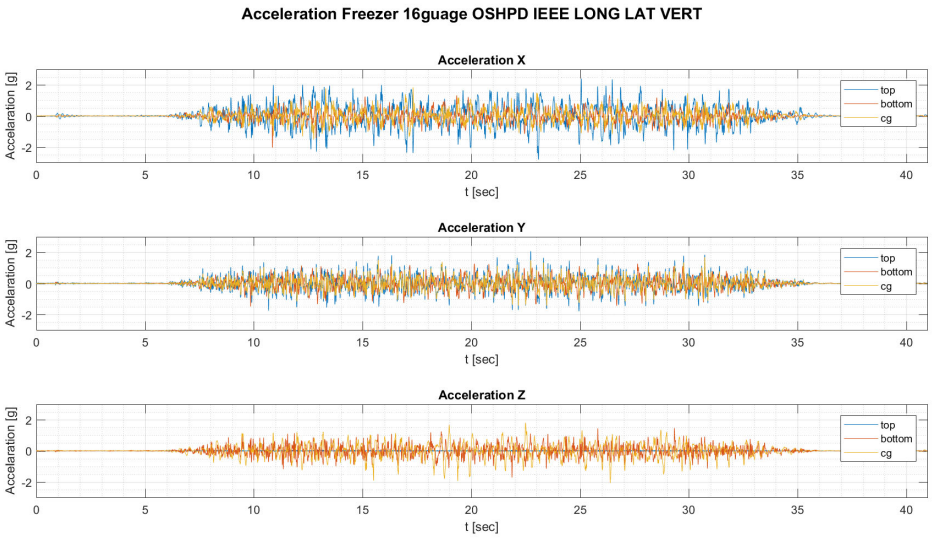

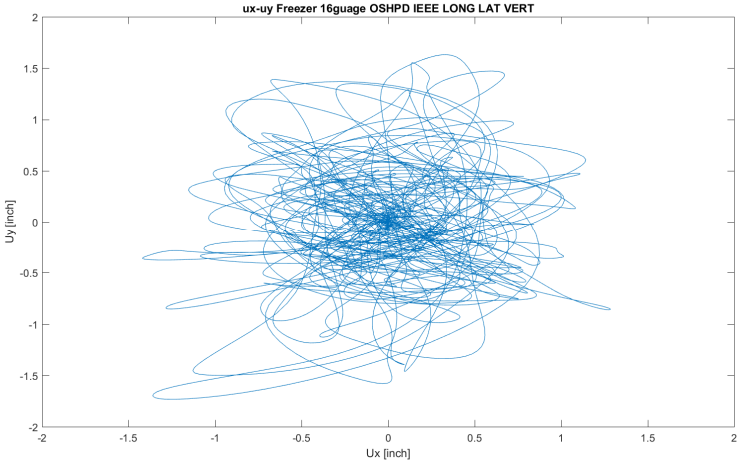

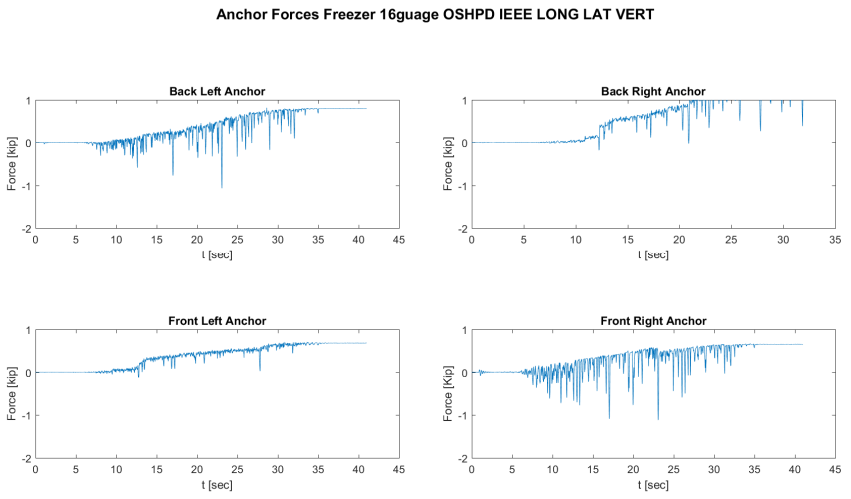

Testing Phase 1 – (59) IEEE XYZ direction

Floor Response Spectra IEEE LAT LONG VERT

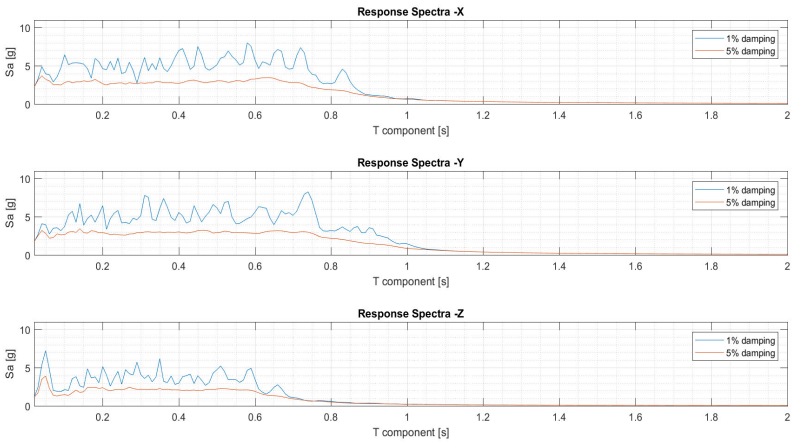

Table Acceleration IEEE LAT LONG VERT

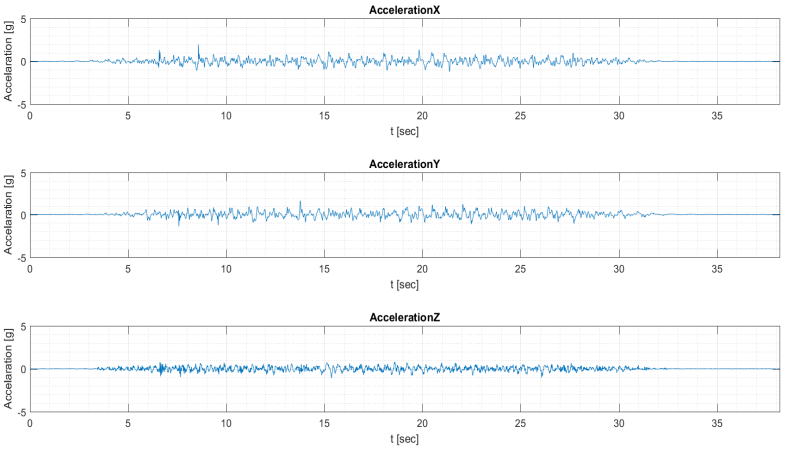

Acceleration IEEE LAT LONG VERT

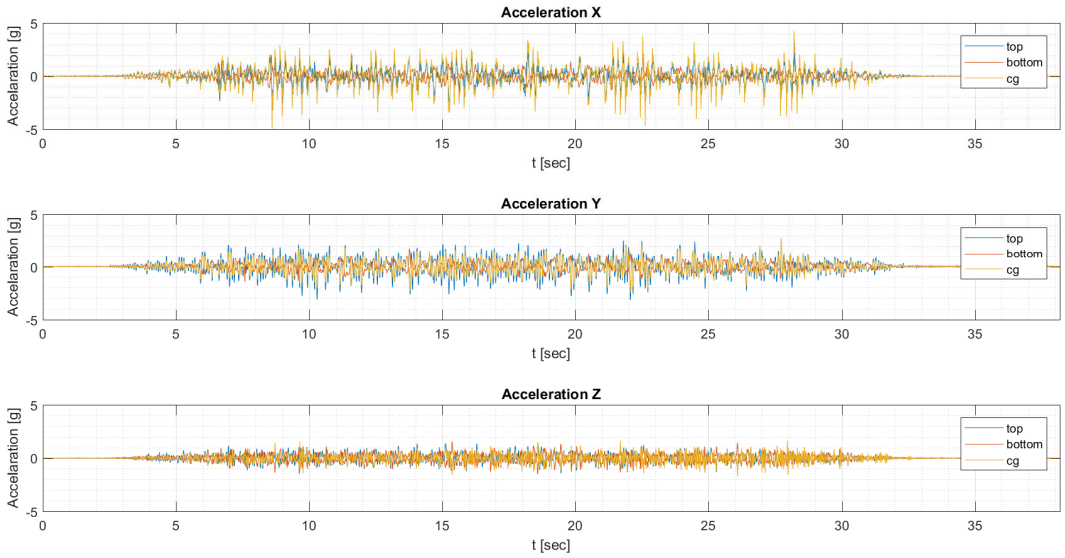

Anchor Forces IEEE LAT LONG VERT

ux-uy IEEE LAT LONG VERT

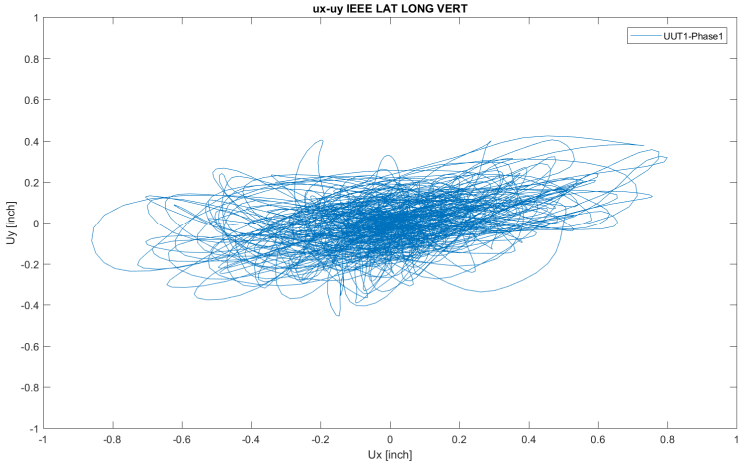

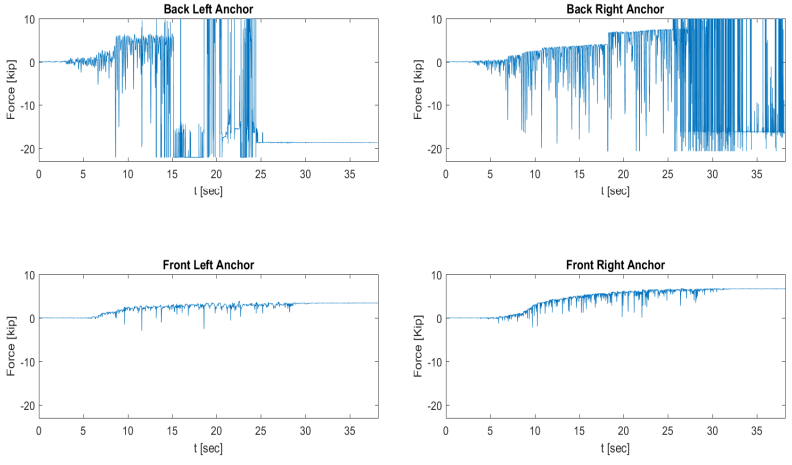

Testing Phase 1 – (60) IEEE Y direction

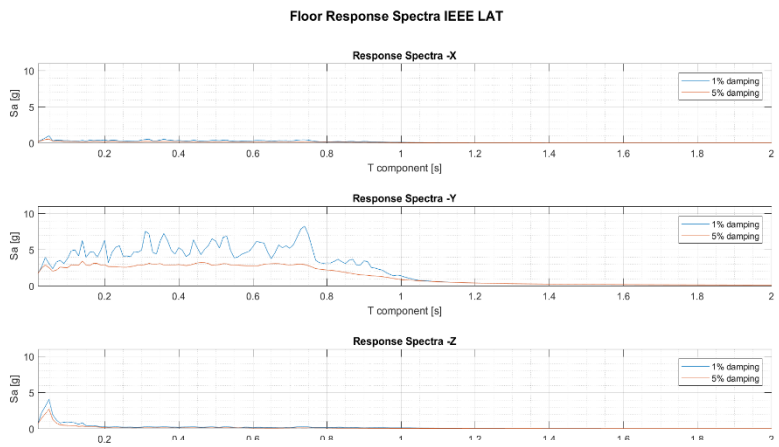

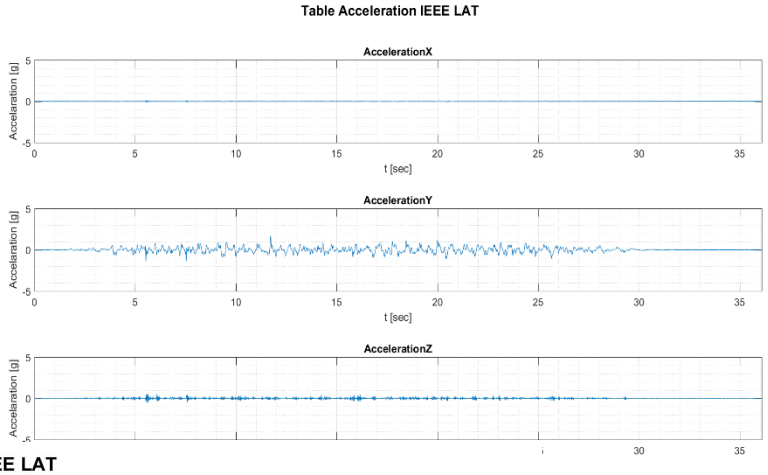

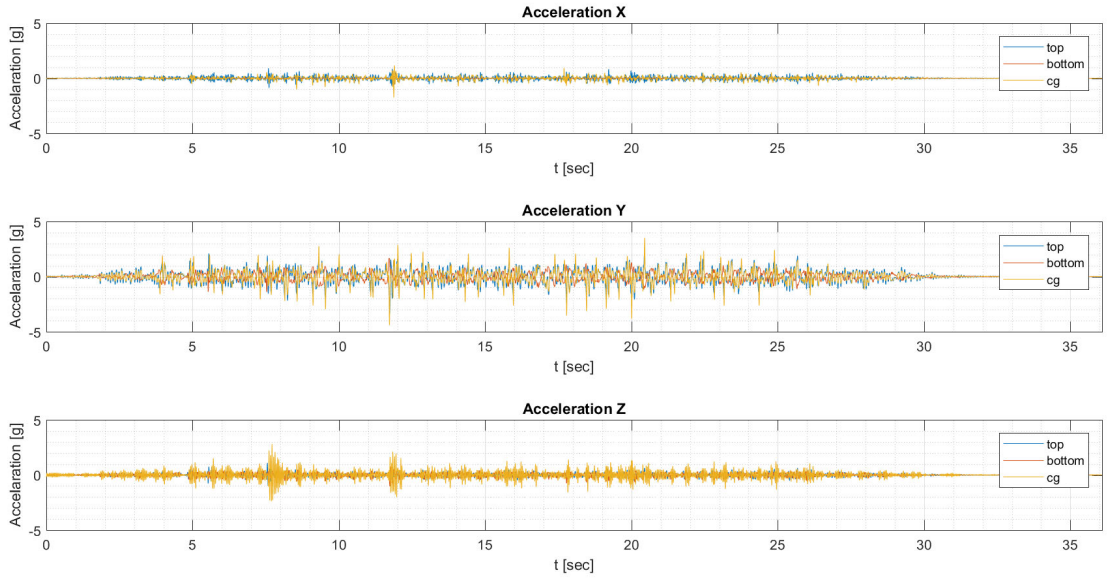

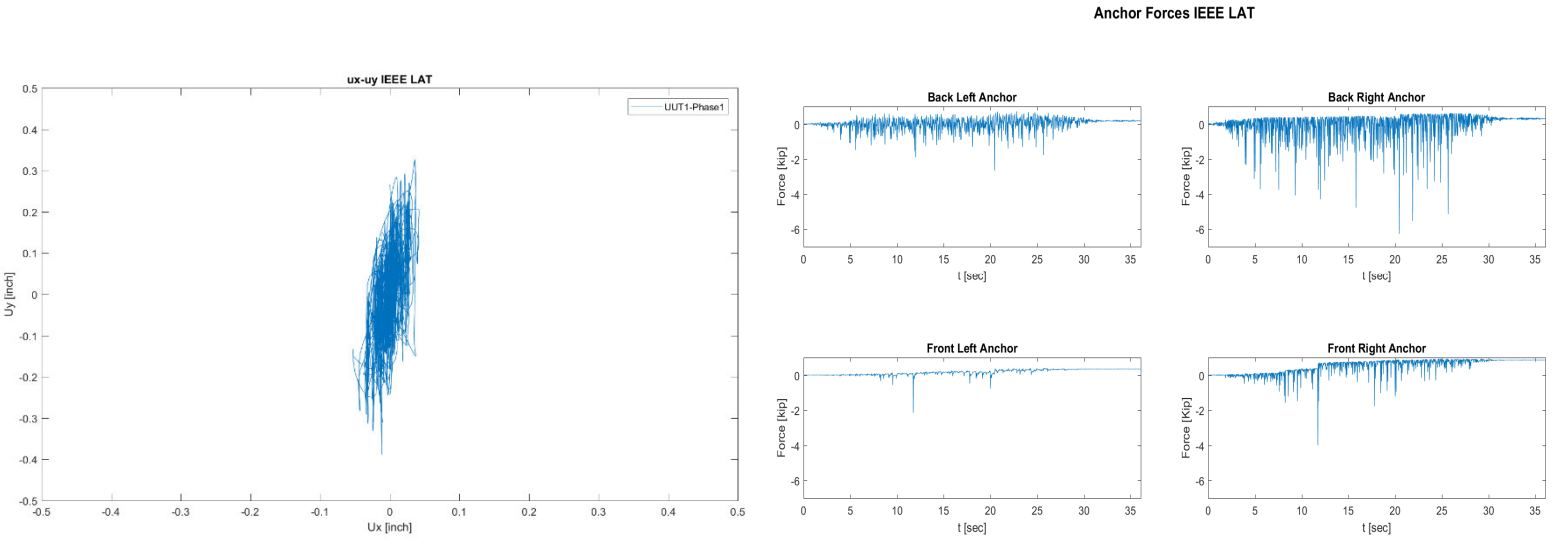

Testing Phase 1 – (61) IEEE X direction

Floor Response Spectra IEEE LONG

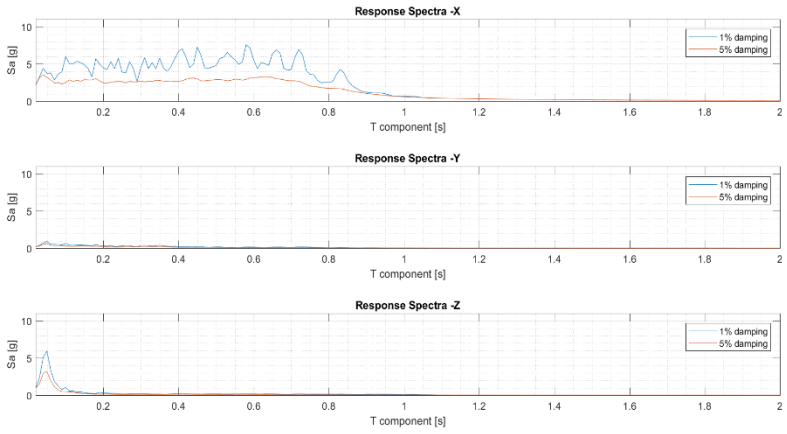

Table Acceleration IEEE LONG

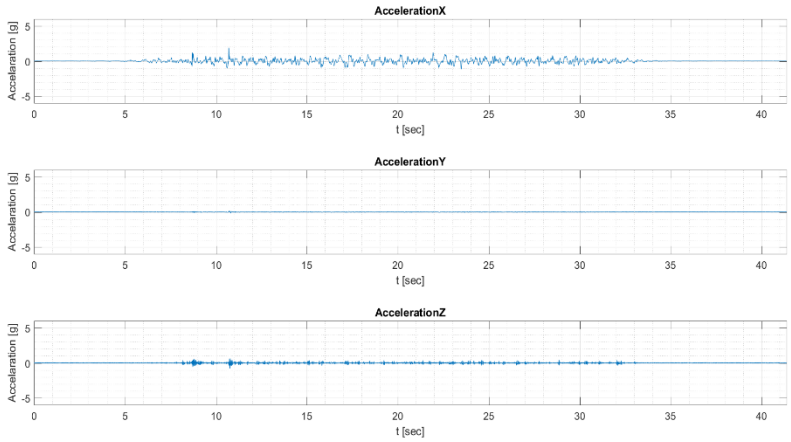

Acceleration IEEE LONG

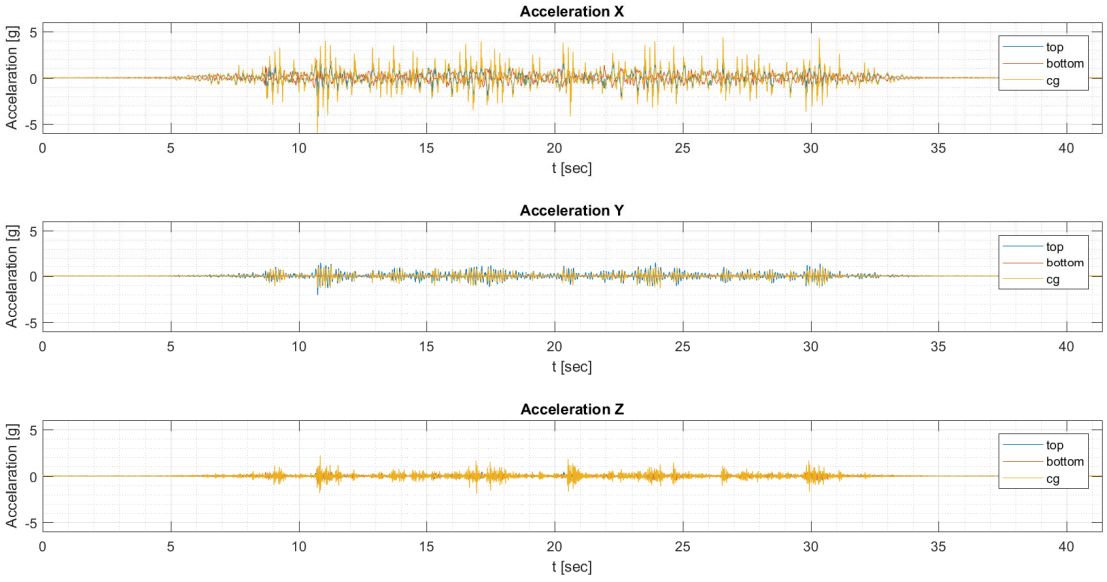

Anchor Forces IEEE LONG

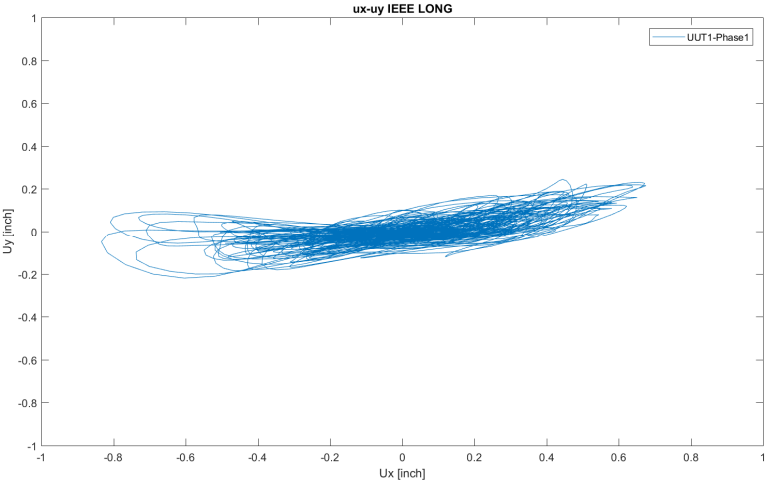

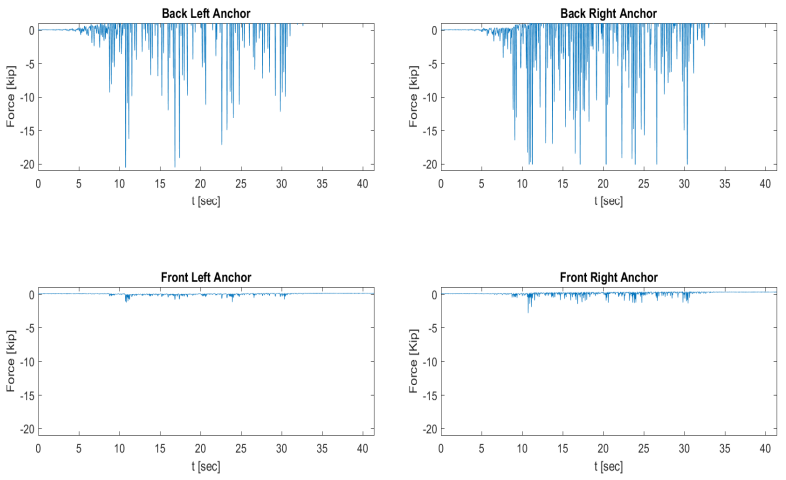

Testing Phase 1 – (62) IEEE XY direction

Floor Response Spectra IEEE LAT LONG

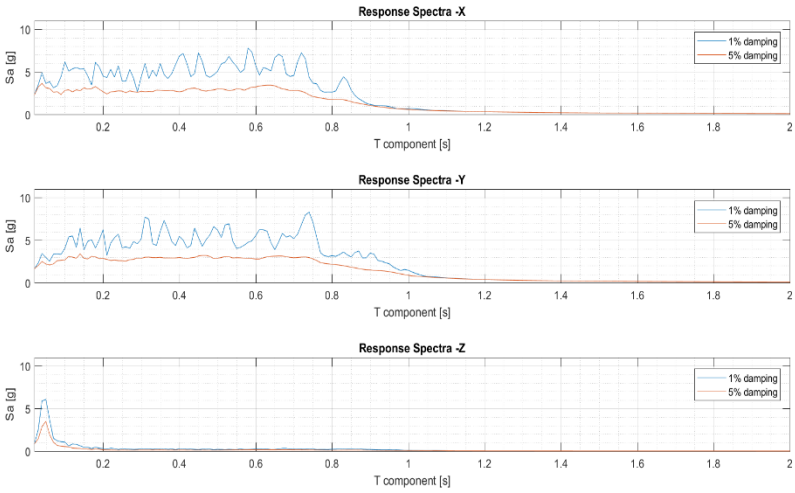

Table Acceleration IEEE LAT LONG

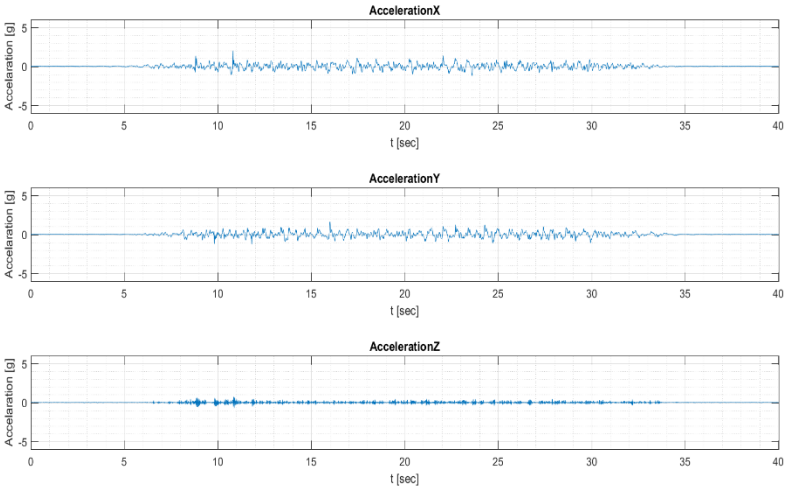

Acceleration IEEE LAT LONG

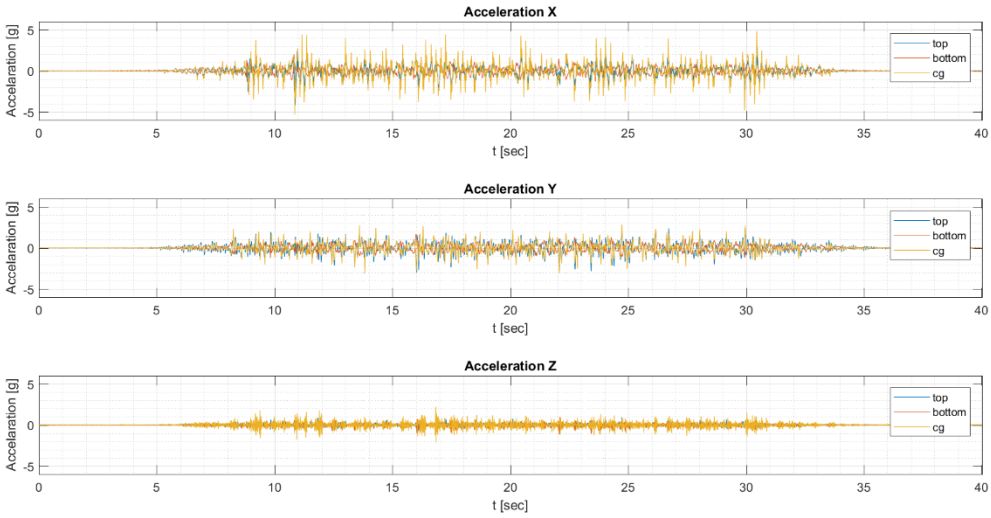

Anchor Forces IEEE LAT LONG